

DESTRUCTION OF ANALGESIC AND ANTI-INFLAMMATORY
PHARMACEUTICALS IN WATER BY CATALYTIC AND ADVANCED OXIDATION
PROCESSES

by

ASU ZİYLAN YAVAŞ

BS. in Env. E., Yıldız Technical University, 2005

MS. in Env. Tech., Boğaziçi University, 2009

Submitted to the Institute of Environmental Sciences in partial fulfillment of
the requirements for the degree of

Doctor

of

Philosophy

Boğaziçi University

2017

DESTRUCTION OF ANALGESIC AND ANTI-INFLAMMATORY
PHARMACEUTICALS IN WATER BY CATALYTIC AND ADVANCED
OXIDATION PROCESSES

APPROVED BY:

Prof. Dr. Nilsun H. İnce
(Thesis Supervisor)



Prof. Dr. İdil Arslan Alaton



Prof. Dr. Işıl Balcıoğlu



Prof. Dr. Ayşen Erdinçler



Doç. Dr. Rana Kıdak



DATE OF APPROVAL. (14/02/2017)

*dedicated to my dear husband, Ahmet Kerem Yavaş,
to my niece the little angel, Mercan Ege Baş*

ACKNOWLEDGEMENTS

I would like to express my deep and sincere gratitude to my thesis supervisor Prof. Dr. Nilsun H. İnce for her insightful guidance, friendly approach and encouragement throughout this study and beyond. I consider myself immensely fortunate and privileged to be able to work with her. She has always supported me both in academic and personal terms, being much more than a supervisor. I would like to thank her for her cognitive and constructive criticisms that motivated me to delve deeper into my research. Her contributions has finally turned me into an independent thinker and researcher. I cannot forget her unconditional support in and out of the laboratory as a philosopher, mentor and scientific artist.

I would like to express my appreciation to the members of my committee Prof. Dr. İdil Arslan Alaton, Prof. Dr. Işıl Balcıoğlu, Prof. Dr. Ayşen Erdinçler and Assoc. Prof. Rana Kıdak for their valuable and supportive comments.

The financial support provided by Boğaziçi University Research Fund to the projects 10Y00D6, 12Y00D8, 15Y00D5 and 14Y00P7 is greatly acknowledged.

I would like to express my sincere gratitude to Prof. Yasuaki Maeda for the unique opportunity to work in his laboratory for getting the experience in sonochemical synthesis of metallic nanoparticles. The research scholarship provided through the SATREPS project supported by JST and JICA via the International Cooperation Program of Osaka Prefecture University is appreciated. I am also grateful to Prof. Yoshiteru Mizukoshi for his valuable support and comments during my stay in Japan.

I wish to express my special thanks to Assoc. Prof. Rana Kıdak for her permission and support to the analysis of the byproducts of some of my processes in her laboratory. I am also thankful to Dr. Şifa Doğan for her help in the use of GC/MS equipment, to Dr. Bilge Gedik Uluocak for her assistance in nanoparticle image analysis, and to Prof. Dr. Ayşe Neren Ökte for her support in the analysis of band gaps. I would also like to thank Prof. Aharon Gedanken for this collaboration in providing us with Fe-modified nanoparticles to be used in some of the catalytic experiments. I wish to express my sincere gratitude to Prof. Victoria

Aviyente for her valuable support and collaboration in the computational modelling and assessment of oxidation byproducts.

Special thanks to my dear friends Ayşe Gül Geyik, Sibel Şen Kavurmacı, Serpil Sarıoğlu, Çağrı Akyol, Şükriye Çelikkol, Cemre Birben, Moris Abolafya, Burcu Doğu, Uğur Doğu, Elif Hot, Başak Savun, Neşe Işık Aşık, Enis Aşık, Ayfer Yabaaksu, İsmail Yabaaksu, Duygu Pişkin, Ali Pişkin, Nazile Demirkılıç, Bahadır Demirkılıç and Neda Soydan for their friendship, endless support and encouragement throughout my study. I would also like to thank Filiz Ayılmaz and Gülhan Özkösemen for their help in the laboratory.

Last but definitely not least, I would like to express my most sincere appreciation to my family Emine Ziylan, Mustafa Ziylan, Aslı Ziylan Baş, Engin Baş, Neval Yavaş, Mustafa Yavaş, Didem Yavaş and to a special person who completely understood and encouraged me in the most difficult times of my study, my dear husband and precious friend- Ahmet Kerem Yavaş. He spent a considerable time at the laboratory to motivate me with patience, without which I could not complete my experiments. Finally, I am thankful to my little niece Mercan Ege Baş, who taught me how to capture happiness in everyday life, which is so much easier than grabbing it from the challenges in a professional life.

DESTRUCTION OF ANALGESIC AND ANTI-INFLAMMATORY PHARMACEUTICALS IN WATER BY CATALYTIC AND ADVANCED OXIDATION PROCESSES

The present study aims to emphasize the occurrence of pharmaceutical residues in water and their treatability in homogeneous and heterogeneous solutions by advanced oxidation processes utilizing ultrasound and a variety of solid catalysts. Hence, an important part of the study is the synthesis of metallic nanoparticles/nanocomposites and the assessment of their catalytic activity in the destruction of pharmaceuticals in water.

One of the main highlights of the study is the higher efficiency of heterogeneous processes that were assisted by ultrasound than homogeneous systems due to the properties of ultrasound accelerating the transfer of organic solutes to the solid surfaces, where they adsorbed and reacted with many different reactive species. A second highlight of the research is the utility of ultrasound in modification of conventional catalysts such as titanium dioxide and alumina to enable the synthesis of platinum, gold and palladium-supported nanocomposites. The method was demonstrated to enhance the catalytic activity of the catalysts via the electron-trapping ability of the co-catalyst, the massive surface area, increased number of adsorption sites and e^- transfer from co-catalyst for enhanced rate of $\bullet\text{OH}$ production. Finally, hybrid processes (e.g. sono-ozonation, sono-photolysis, sono-photo-ozonation) was more efficient than singles leading to the generation of excess radical species.

AĞRI KESİCİ VE ÖDEM SÖKÜCÜ İLAÇLARIN KATALİTİK VE İLERİ OKSİDASYON YÖNTEMLERİ İLE GİDERİMİ

Bu çalışma ilaç kalıntılarının sudaki varlığının vurgulanması ve bu kirleticilerin homojen veya heterojen ortamlarda çeşitli katalist ilavesi ile ultrases dalgalarının da eşlik ettiği ileri oksidasyon yöntemleri kullanılarak artırılabilirliklerinin araştırılmasını amaçlanmaktadır. Çalışmanın önemli bölümlerinden birini de metalik nano-parçacık/kompozitlerin sentezlenmesi ve bu katalizörlerin ilaçların parçalanması üzerindeki katalitik aktivitelerinin değerlendirilmesi oluşturmaktadır.

Çalışmanın en önemli bulgularından birisi sesüstü dalgaların çeşitli reaktif maddelerle reaksiyonların gerçekleştiği katı yüzeylere adsorbsiyon veya kütle transfer hızını artırma hususundaki etkinlikleri nedeni ile heterojen oksidasyon sistemlerinde homojen sistemlere göre çok daha etkili olduğunun gözlemlenmesidir. Diğer bir bulgu ise geleneksel titanyum dioksit ve alüminyum oksit gibi katalizör yüzeylerine ses üstü dalgalar kullanılarak platin, altın veya paladyum gibi asal metal nano-parçacıklarının tutundurulması yöntemi ile yeni yarı iletken kompozitlerin üretilebilmesidir. Bu metot yüzeye tutundurulan metal nano-parçacıkların elektronları alıkoyma özellikleri, artan yüzey alanı ve adsorpsiyon bölgeleri, eş katalistten elektron transferinin gerçekleşmesi sayesinde hidroksil radikali üretiminin artması sonucu yarı iletken kompozitlerin katalitik etkinliklerinin arttırılabileceğini göstermektedir. Son olarak, çalışmanın bir diğer önemli bulgusu ise tekli uygulamalar ile kıyaslandığında ses üstü dalgalar eşliğinde uygulanan bütünleşik proseslerin (ses üstü dalgalar/ozon, ses üstü dalgalar/ultraviyole ışık ve ses üstü dalgalar/ultraviyole ışık/ozon) fazla radikal üretimine neden olması sebebi ile daha yüksek verime sahip oldukları belirlenmiştir.

TABLE OF CONTENTS

ACKNOWLEDGEMENTS	iv
SUMMARY	vi
ÖZET	vii
TABLE OF CONTENTS	viii
LIST OF TABLES	xiv
LIST OF FIGURES	xvii
LIST OF SYMBOLS/ABBREVIATIONS	xxiv
1. INTRODUCTION	1
2. BACKGROUND AND LITERATURE REVIEW	7
2.1. Principles and Tools of Advanced Oxidation Processes	7
2.1.1. UV/H ₂ O ₂	7
2.1.2. Fenton, UV/Fenton and Advanced Fenton	8
2.1.3. Ozonation	11
2.1.4. Ionizing Radiation	12
2.2. Principles of Sonochemistry	12
2.2.1. Types of Cavitation	15
2.2.2. Parameters Effecting the Sonochemical Reactions	17
2.2.3. US-assisted AOPs	28
2.2.4. Ultrasonic Production of Nanoparticles	31
2.3. Catalytic Processes	34
2.3.1. Sonocatalysis	34
2.3.2. Catalytic Ozonation	35
2.3.3. Heterogeneous Fenton, Photo-Fenton and Fenton-like Processes	38
2.3.4. Photocatalysis	40
2.4. Occurrence, Fate and Elimination of Analgesic and Anti-inflammatory Pharmaceuticals	46
2.4.1. Emerging Pollutants in the Environment: Analgesic and Anti- inflammatories	46
2.4.2. Occurrence and Fate of Analgesics and Anti-inflammatory in the Aquatic Environment	50

2.4.3. Elimination of Analgesic and Anti-inflammatory Pharmaceuticals in WWTPs	52
2.4.4. Overview of the Treatability of Some Common a-PhACs in in WWTPs	53
2.4.5. The Principles of Advanced Oxidation Processes on Organic Compound Elimination	55
2.4.6. Elimination of AIs and ANs in Wastewater Treatment Plants (WWTPs) Integrated with Advanced Processes	56
2.4.7. Overview of AN and AI Elimination in Drinking Water Treatment Plants (DWTPs)	57
2.4.8. Advanced Oxidation Processes (AOPs) as Viable Options for Destroying PhAC Residues in WWTP and DWTP Effluents	58
3. MATERIALS AND METHODS	69
3.1. Materials	69
3.1.1. Test Compounds	69
3.1.2. Reagents	70
3.1.3. Catalysts	70
3.2. Methods	71
3.2.1. Experimental Set-ups	71
3.2.2. Experimental Procedures	75
3.2.3. Analytical Methods	77
3.2.4. Adsorption	82
3.3. Synthesis Of Nanoparticles	82
3.4. System Parameters of Ultrasonic Systems	84
4. SONOLYTIC AND SONOCATALYTIC DECOMPOSITION OF DICLOFENAC USING ZERO-VALENT IRON	88
4.1. Introduction	88
4.2. Materials and Methods	89
4.2.1. Analytical	90
4.2.2. Experimental	90
4.2.3. Procedure	90
4.3. Results and Discussion	92
4.3.1. Optimization of the Reaction Parameters	92
4.3.2. Conversion and Degradation of DCF by Sonolysis	96

4.3.3. Sonocatalysis	97
4.3.4. Mineralization	99
4.3.5. Comparison of Nano-and Micro-ZVI for the Efficiency of DCF Elimination	101
4.4. Conclusions	102
5. SONOCHEMICAL DEGRADATION OF DICLOFENAC: BY-PRODUCT ASSESSMENT, REACTION MECHANISMS AND ENVIRONMENTAL CONSIDERATIONS	103
5.1. Introduction	103
5.2. Materials and Methods	104
5.2.1. Experimental	104
5.2.2. Analytical	105
5.3. Results and Discussion	105
5.3.1. A Synopsis of the Overall Degradation Process	105
5.3.2. Byproduct Analysis	109
5.3.3. Environmental Considerations	114
5.4. Conclusions	117
6. OZONATION-BASED ADVANCED OXIDATION FOR PRE-TREATMENT OF WATER WITH RESIDUALS OF ANTI-INFLAMMATORY MEDICATION	119
6.1. Introduction	119
6.2. Materials and Methods	120
6.2.1. Experimental	120
6.2.2. Analytical	120
6.2.3. Procedure	121
6.3. Results and Discussion	124
6.3.1. Are Hydrolysis and Adsorption Potential Pathways in the Observed Decay of DCF in Raw Water?	124
6.3.2. Selection of the Effective Operation Parameters and Comparison of Process Efficiencies	124
6.3.3. Treatability of AOP- pretreated Samples by Coagulation	132
6.4. Conclusions	134
7. CATALYTIC OZONATION OF IBUPROFEN WITH ULTRASOUND AND Fe- BASED CATALYSTS	136

7.1.	Introduction	136
7.2.	Materials and Methods	137
7.2.1.	Experimental	137
7.2.2.	Analytical	138
7.3.	Results and Discussion	138
7.3.1.	Prediction of the Ozone Mass Transfer Rate Coefficient	138
7.3.2.	Selection of the Ozone Dose, pH and IBP Concentration	140
7.3.3.	Catalytic Ozonation with Ultrasound	142
7.3.4.	Catalytic Ozonation with Fe-bearing Species	143
7.3.5.	Catalytic Ozonation with US and Fe-bearing Solids	146
7.4.	Conclusions	148
8.	SINGLE, SIMULTANEOUS AND SEQUENTIAL APPLICATIONS OF ULTRASONIC FREQUENCIES FOR THE ELIMINATION OF IBUPROFEN IN WATER	149
8.1.	Introduction	149
8.2.	Materials and Methods	150
8.2.1.	Experimental	151
8.2.2.	Procedure	152
8.2.3.	Analytical	152
8.3.	Results and Discussion	152
8.3.1.	Power Efficiencies of the Reactor Systems	152
8.3.2.	Silent Absorption of IBP on ZVI	153
8.3.3.	Control Experiments: Sonolysis without ZVI	154
8.3.4.	Sonolysis with ZVI	156
8.3.5.	The Effect of H ₂ O ₂	159
8.4.	Conclusions	161
9.	SUPPORTING OF PRISTINE TiO ₂ WITH NOBLE METALS TO ENHANCE THE OXIDATION AND MINERALIZATION OF PARACETAMOL BY SONOLYSIS AND SONOPHOTOLYSIS	162
9.1.	Introduction	162
9.2.	Materials and Methods	163
9.2.1.	Experimental	164
9.2.2.	Analytical	165

9.3. Results and Discussion	166
9.3.1. Characterization of Nanocomposites	166
9.3.2. Silent Adsorption of PCT on TiO ₂ and/or Its Nanocomposites	167
9.3.3. Sonolysis and Sonocatalysis	169
9.3.4. The effect of Persulfate Addition	173
9.3.5. Stability of the Catalysts	176
9.3.6. Photo- and Sono-photocatalysis	178
9.4. Conclusions	182
10. ENHANCED PHOTO-DEGRADATION OF PARACETAMOL ON n-PLATINUM-MODIFIED TiO ₂ : THE EFFECT OF ULTRASOUND AND •OH/HOLE SCAVENGERS	183
10.1. Introduction	183
10.2. Materials and Methods	184
10.2.1. Procedure	185
10.2.2. Analytical	185
10.3. Results and Discussion	186
10.3.1. Characterization of the Catalysts	186
10.3.2. Control Experiments	186
10.3.3. Catalytic Experiments with US, UV and TiO ₂	190
10.3.4. The Effect of •OH/h ⁺ _{vb} Scavengers	194
10.4. Conclusions	199
11. CATALYTIC OZONATION OF PARACETAMOL USING COMMERCIAL AND Pt-SUPPORTED NANOCOMPOSITES OF Al ₂ O ₃ : THE IMPACT OF ULTRASOUND	201
11.1. Introduction	201
11.2. Materials and Methods	202
11.2.1. Experimental	203
11.2.2. Analytical	203
11.3. Results and Discussion	204
11.3.1. Characterization of the Catalysts	204
11.3.2. Adsorption of PCT on Al ₂ O ₃ and Pt-Al ₂ O ₃ : The Effect of Catalyst Dose and HA	205
11.3.3. Ozonation: Selection of the Operating Parameters	206

11.3.4. Catalytic Ozonation with γ - and nPt-supported Al_2O_3	208
11.3.5. The Effect of Water Matrix and/or $\bullet\text{OH}$ Scavengers	211
11.3.6. Can Ultrasound Improve the Activity of the Catalysts and the Efficiency of the Process?	214
11.4. Conclusions	216
12. CONCLUSIONS AND RECOMMENDATIONS	218
13. REFERENCES	220
APPENDIX A: Supporting of pristine TiO_2 with noble metals to enhance the oxidation and mineralization of paracetamol by sonolysis and sonophotolysis	260
APPENDIX B: Enhanced photo-degradation of paracetamol on n-platinum-modified TiO_2 : the effect of ultrasound and $\bullet\text{OH}$ /hole scavengers	266

LIST OF TABLES

Table 2.1. Physical and chemical properties of some common analgesic and anti-inflammatory pharmaceuticals	47
Table 2.2. Physical/chemical and aquatic toxicity properties of some common analgesic and anti-inflammatory pharmaceuticals.	47
Table 2.3. Country-wise occurrence of analgesic and anti-inflammatory pharmaceuticals in surface water, and influents/ effluents of WWTPs	51
Table 2.4. Metabolic forms and natural degradation pathways of AIs and ANs in water	52
Table 2.5. Relative fractions of ANs and AIs removal in conventional and tertiary treatment units of WWTPs	57
Table 2.6. The fate of most common ANs/AIs in unit processes of DWTPs (1-4); further elimination in effluents or fresh water surface by photolysis (5)	59
Table 2.7. Most common AOPs for water and wastewater treatment	60
Table 2.8. Efficiency of lab-scale AOPs for the degradation and mineralization of AI/AN chemicals.	61
Table 3.1. Molecular structures, chemical and physical properties of diclofenac, ibuprofen and paracetamol.	69
Table 3.2. The catalysts and their properties.	70
Table 3.3. The operation conditions of HPLC for analysis of DCF, PCT and IBP.	77
Table 3.4. The operation parameters of ultrasonic reactors.	84
Table 4.1. Characteristics of the catalyst.	89
Table 4.2. The release of TOC and Fe from 0.2 g L ⁻¹ ZVI during sonication at pH 3.0	97

Table 4.3. Initial reaction rate constants at the applied catalyst concentrations and Fe doses	98
Table 5.1. The absorption maxima of some selected chromophores, functional groups and substituents that are potential components of the oxidation byproducts	107
Table 5.2. The oxidation byproducts and their octanol-water partition coefficients	110
Table 5.3. Relative occurrence of DCF and its oxidation byproducts	112
Table 5.4. Microtox toxicity of the reactor during 300-min sonication	115
Table 5.5. Calculated algal toxicities and classification of the oxidation byproducts	116
Table 6.1. Properties of the influent water in WTP after aeration	121
Table 6.2. Chemical/physical properties of the test samples	122
Table 6.3. Experimental conditions	123
Table 6.4. The role of solution matrix on 5-min reaction rate constants and 5/10-min oxidation efficiencies of the test processes at $8 \text{ mg L}^{-1} \text{ O}_3$ ($C_0=30 \text{ } \mu\text{M}$)	128
Table 6.5. Relative conversion and mineralization efficiencies of 10-min sonication with H_2O_2 , O_3 , UV and combinations in pure (S1) and raw water (S2) samples spiked with $30 \text{ } \mu\text{M}$ DCF	131
Table 7.1. The catalysts	137
Table 7.2. Adsorption of IBP on surfaces of solid catalysts after 24 h contact of $50 \text{ } \mu\text{M}$ IBP with 5 mg L^{-1} Fe-equivalent of the catalysts at pH 6.5, and leaching of Fe^{II} from the catalysts in pure water at the same conditions	144
Table 8.1. Results of calorimetric analyses	153
Table 8.2. Comparison of system performances in terms of the apparent reaction rate constants and percentages of IBP and TOC decay	158

Table 8.3. Comparison of ZVI-added operations for sonochemical yields, reaction rate constants and mineralization efficiencies	160
Table 9.1. The apparent reaction rate constants of PCT decay (min^{-1}) by sonolysis, photolysis and sono-photolysis and the corresponding synergy indices	180
Table 10.1. Estimated reaction rate constants and the efficiency of photocatalysis for decomposing PCT ($C_0=40 \mu\text{M}$) and its oxidation byproducts	192
Table 10.2. Estimated concentrations of HQ and BQ, and the corresponding mineralization efficiency of the sonophoto process in the presence and absence of 8.75 mM KI and PR	199
Table 11.1. Relative effectiveness of $\gamma\text{-Al}_2\text{O}_3$ and nPt- Al_2O_3 in catalytic ozonation of PCT at various pH	209
Table 11.2. The effect of ultrasound on the efficiency of PCT degradation by catalytic ozonation with alumina and Pt-supported alumina	215

LIST OF FIGURES

Figure 2.1. The core-shell model of zero valent iron (ZVI) depicting potential mechanisms for the removal of metals and chlorinated compounds	10
Figure 2.2. The frequency spectrum from infrasound to ultrasound	13
Figure 2.3. Growth and implosion of cavitation bubbles in aqueous solution under ultrasonic irradiation	14
Figure 2.4. Possible chemical reaction sites of cavitation event in homogeneous reaction media	16
Figure 2.5. Illustration of the effects of acoustic fields of identical frequency (a) low-intensity ultrasound, (b) high-intensity ultrasound	17
Figure 2.6. The nature of rarefaction and compression cycles at low and high frequency with varying amplitudes	20
Figure 2.7. The reactions of sonolytic ozonation in an ultrasonic reactor	29
Figure 2.8. The possible pathways of contaminant degradation and the interaction between ozone and ultrasound	30
Figure 2.9. Sonochemical synthesis of various nanostructured inorganic materials	33
Figure 2.10. The physical and chemical effects of heterogeneous cavitation	35
Figure 2.11. The possible mechanism for HO• or other radical species generation by reaction of ozone with reduced metal of catalyst	37
Figure 2.12. The mechanism of catalytic ozonation over alumina	38
Figure 2.13. The classification of photo catalysis	42
Figure 2.14. Schematic diagram of the mechanism of semiconductor photo catalysis	42

Figure 2.15. The general mechanism of photocatalytic process of metal supported TiO ₂	46
Figure 3.1. The schematic view of 20 kHz (R1) and 40 kHz (R2) type reactors	72
Figure 3.2. The schematic view of 200 kHz ultrasonic bath reactor	73
Figure 3.3. The schematic view of multi-frequency plate type reactor	73
Figure 3.4. The schematic view of sono-photo reactor (R7).	74
Figure 3.5. The procedure of nanocomposite preparation by sonochemical method	83
Figure 3.6. The temperature increase in R4 reactor (frequency (f)=861 kHz) in the presence and absence of air bubbling	85
Figure 3.7. The effect of water impurities on temperature increase (a) and formation of H ₂ O ₂ during sonolysis of water at (R4), f=861 kHz	86
Figure 3.8. The image of sonochemiluminescence in luminol solution (250 mL) at R4 reactor (f=861 kHz)	87
Figure 4.1. Nanoparticle separation system	92
Figure 4.2. Sonochemical rate of DCF degradation at low and high frequency ultrasound (C ₀ = 30 μM, pH=2.8-3.0, P=0.20±0.04 W mL ⁻¹)	93
Figure 4.3. The effect of pH and temperature on the UV spectrum of DCF	94
Figure 4.4. Relative degradation of DCF under air, argon and oxygen atmospheres (C ₀ =30 μM, pH _i =3.0, gas flow rate=0.5 L min ⁻¹)	95
Figure 4.5. The effect of ultrasonic power or dose on the fraction of DCF elimination (C ₀ =30 μM, pH _i =3.0, at 861 kHz)	95
Figure 4.6. Relative conversion, degradation and mineralization of DCF at 861 kHz (C ₀ =420 μM, pH=3.0, air flow rate=0.5 L min ⁻¹)	96
Figure 4.7. Accumulation of H ₂ O ₂ during sonolysis of DCF in the presence of 0.1 g L ⁻¹ (“ZVI1”), 0.2 g L ⁻¹ (“ZVI2”) and 0.3 g L ⁻¹ (“ZVI3”) ZVI at 861 kHz	100

Figure 4.8. Relative rates of chlorine (a) and nitrogen (b) mineralization by sonocatalysis ($C_0=30 \mu\text{M}$, $\text{pH}=3.0$, $\text{ZVI}=0.2 \text{ g L}^{-1}$)	101
Figure 4.9. Relative efficacies of ZVI-nano and ZVI-micro as a function of the Fe dose	102
Figure 5.1. Time rates of concentration and intensity decay during 90-min sonication of DCF ($15.7 \mu\text{M}$) at $\text{pH} 6.5$.	106
Figure 5.2. Relative impacts of sonication time and absorption wavelength on the optical density of DCF test solution ($C_0=5 \text{ mg L}^{-1}$).	108
Figure 5.3. Relative rates of carbon, chlorine and nitrogen mineralization and the accompanied alterations in UV absorption of a test solution during 90-min sonication ($C_0=5 \text{ mg L}^{-1}$, $\text{pH}_0=6.5$) at 861 kHz.	109
Figure 5.4. Relative distribution of DCF and its oxidation byproducts during 90-min sonication ($C_0=5 \text{ mg L}^{-1}$) at 861 kHz.	113
Figure 6.1. The experimental scheme.	123
Figure 6.2. Relative impacts of the applied ozone test concentration and contact time on fractions of DCF conversion and mineralization in Milli-Q and raw	125
Figure 6.3. Relative effectiveness of single and combined ozonation processes (AOPs) for converting and mineralizing DCF ($30 \mu\text{M}$) in pure (MQW) and raw water samples (RW)	127
Figure 6.4. Relative rates of DCF transformation during 5-min exposure of S1 and S2 ($C_0=30 \mu\text{M}$) to ozone-combined AOPs	129
Figure 6.5. Relative mineralization in sample (S2) and control (S3) after 10-min contact with the test AOPs at $8 \text{ mg L}^{-1} \text{ O}_3$	130
Figure 6.6. Variations in the UV-vis spectra of S1 and S2 during 10-min exposure to US-combined processes	133

Figure 6.7. The impact of AOP-pretreatment on the efficiency of DOC elimination by coagulation	134
Figure 6.8. The modified WTP flow chart.	134
Figure 7.1. Estimation of O ₃ mass transfer rate coefficient using the unsteady-state concentration data at varying O ₃ flow rates (a) and pH levels (b)	140
Figure 7.2. Variations in the rate of IBP degradation with the initial solute concentration (a) and the applied pH (b)	141
Figure 7.3. Interactive effects of concentration, pH and gas flow rate on mineralization of IBP by 1-h ozonation (O ₃ = 2, 4, 8 mg L ⁻¹)	142
Figure 7.4. pH-related degradation and mineralization of IBP by singly and simultaneously applied ozonation and sonication	143
Figure 7.5. Relative degradation and mineralization of IBP (C ₀ =50 μM) by 1-h ozonation at pH 6.5 and a gas flow rate of 12 mg min ⁻¹ (O ₃ =8 mg L ⁻¹) in the presence of 5 mg L ⁻¹ of the catalysts (as Fe)	145
Figure 7.6. Degradation IBP by 40-min sono-catalytic ozonation with Fe-based solids at optimized conditions (C ₀ =50 μM, O ₃ flow=12 mg min ⁻¹ (O ₃ =8 mg L ⁻¹), specific US _{power} = 0.23 W L ⁻¹ , pH = 6.5)	147
Figure 7.7. Mineralization of IBP by 40-min sono-catalytic ozonation in the presence of 5 mg L ⁻¹ Fe-equivalent of Goethite, Magnetite and ZVI-graphite at optimized conditions	147
Figure 8.1. The experimental Scheme	151
Figure 8.2. The effect of ZVI dose on the adsorption of IBP	154
Figure 8.3. Time-rate of elimination (a) and mineralization of IBP (b) by single frequency irradiation at pH 3.0 (C ₀ =50 μM)	155

- Figure 8.4. Time-rate of IBP elimination (a) and H₂O₂ formation (b) during single-frequency operations with ZVI 157
- Figure 8.5. Interactive relations between the reactor systems, the yield coefficient and total TOC decay 160
- Figure 9.1. HAADF-STEM images of (a) Pd-TiO₂, (b) Au-TiO₂, (c) and Pd/Au-TiO₂ 167
- Figure 9.2. Relative adsorption of PCT (C₀=35 M) on 5 mg L⁻¹ of commercial and immobilized TiO₂ during silent shaking: (a) the effect of pH; (b) the effect of increasing the adsorbent concentration 168
- Figure 9.3 The impact of pH, frequency, and concentration on the rate of PCT degradation (a, b, c) and C-mineralization (d) by ultrasound 170
- Figure 9.4. The impact of pH on sonocatalytic degradation and mineralization of (35 μM, 861 kHz) in the presence of 5 mg L⁻¹ of commercial and Pd-supported TiO₂ (a, b, c); the effect of catalyst (Pd-TiO₂) concentration at pH 6.5 (d) 171
- Figure 9.5. Relative rate of PCT degradation during 30 min sonocatalysis at pH 6.5. The insert shows the decay of TOC in 1-h reaction under the same conditions: C₀= 35 μM PCT, f= 861 kHz, cat= 5 mg L⁻¹ 173
- Figure 9.6. Oxidation decay of PCT (C₀= 35 μM) by 15 min reaction with persulfate (2.5 Mm) under silent conditions at pH 3.0, 6.5 and 10 175
- Figure 9.7. The impact of PS addition (2.5 Mm) on the initial rate of degradation (a) and 1-h mineralization of PCT (b) in the presence of ultrasound and 5 mg L⁻¹ of commercial and immobilized TiO₂ at pH 6.5 176
- Figure 9.8. The loss in the efficiency of Pd-TiO₂ upon recovery and reuse of the spent catalyst successively in sonocatalytic degradation of PCT 177
- Figure 9.9. Initial rate of PCT decay by photolysis (254 nm) in the presence of 5 mg L⁻¹ of commercial and metal-supported TiO₂ 179

- Figure 9.10. Relative mineralization of PCT after 60-min exposure to the test processes in the presence of commercial and immobilized TiO_2 (5 mgL^{-1}) at pH 6.5 181
- Figure 10.1. ESEM images (500000x) of P1- TiO_2 , P2- TiO_2 , P4- TiO_2 and spent P4- TiO_2 187
- Figure 10.2. Sorption of PCT ($40 \text{ }\mu\text{M}$) on 5 mg L^{-1} P1, P2 and P4 at pH 6.5 during 3-h shaking 187
- Figure 10.3. Relative rate of H_2O_2 formation during 15-min sonication of ultrapure water with 572 kHz, 856 kHz and 1130 kHz at non-buffered natural pH 6.5 189
- Figure 10.4. The impact of frequency on C-mineralization (a) and the relative rate of H_2O_2 formation by sonolysis of pure water and the sample solution at 572 kHz (b) 189
- Figure 10.5. Relative effectiveness of “control” processes (US, UV, US/UV) for the decomposition and mineralization of PCT 191
- Figure 10.6. Sonocatalytic decay of PCT in the presence of TiO_2 , P1, P2 and P4 191
- Figure 10.7. Photocatalytic elimination and mineralization of PCT ($C_0=40 \text{ }\mu\text{M}$) in the presence of 5 mg L^{-1} TiO_2 and Pt/ TiO_2 containing 1 mM, 2 mM and 4 mM Pt (P1, P2, P4), respectively 193
- Figure 10.8. Sono-photocatalytic elimination and mineralization of PCT in the presence of pristine and Pt-loaded TiO_2 195
- Figure 10.9. Relative rate of PCT elimination during sono-photocatalysis with Pt- TiO_2 (P4) in the presence of 2-propanol and potassium iodide. “Control” refers to the absence of scavengers 196
- Figure 10.10. The impact of PR and two different doses of KI on the decomposition and carbon mineralization of PCT by sono-photocatalysis with P4. Control refers to the absence of scavengers. 198

- Figure 11.1. ESEM-EDX images of γ - Al_2O_3 (a) and nPt- Al_2O_3 (b) with multi elemental mapping. 204
- Figure 11.2. Adsorption isotherms of PCT (a) and adsorptive (or chemical) elimination of PCT in relation to humic acid concentration (b) 206
- Figure 11.3. The impact of gas flow rate on the rate of PCT ($C_0=35 \mu\text{M}$) decay (a) and C-mineralization (b) by ozonation at pH 7.0 207
- Figure 11.4. Variations in the rate of PCT decay ($C_0=35 \mu\text{M}$) (a), H_2O_2 formation and C-mineralization (b) with the solution pH during ozonation without catalysts at 6 mg min^{-1} ($\text{O}_3= 4 \text{ mg L}^{-1}$) 208
- Figure 11.5. Accumulation/depletion of aqueous ozone with time in the presence of Al_2O_3 , nPt- Al_2O_3 and PCT ($\text{O}_3 \text{ flow}=6 \text{ mg min}^{-1}$ ($\text{O}_3= 4 \text{ mg L}^{-1}$), pH=7, catalyst dose= 5 mg L^{-1} , $\text{PCT}_0=35 \mu\text{M}$) 209
- Figure 11.6. The impact of HA (5 mgL^{-1}) on the rate of oxidation and mineralization of PCT during and after catalytic ozonation with pristine and nPt- Al_2O_3 (a); the effect of HA dose on mineralization and H_2O_2 formation in the presence of nPt- Al_2O_3 (b) 212
- Figure 11.7. Impacts of HA and bicarbonate on the rate of decomposition/mineralization of PCT during ozonation with pristine and Pt-supported alumina (a-b); the rate of absorbance decay during ozonation of PCT with Pt- Al_2O_3 (c-d) 213

LIST OF SYMBOLS/ABBREVIATIONS

A	Absorbance
AOP	Advanced oxidation process
AN	Analgesic drug
AI	Anti-inflammatory drug
Au-TiO ₂	Gold nanoparticle supported TiO ₂ nanocomposite
BOD	Biochemical oxygen demand
BQ	Benzoquinone
C	Concentration
COD	Chemical oxygen demand
C _p /C _v	Ratio of specific heats
cps	Count per second
DCF	Diclofenac
DOC	Dissolved organic carbon
E	Efficacy, as a function of degradation rate coefficient and catalyst dose
EC	European Commission
e ⁻ /h ⁺	Electron/hole pair
ESEM	Environmental scanning electron microscope
EU	European Union
G	Sonochemical product yield
HA	Humic acid
HQ	Hydroquinone
h ⁺ _{vb}	Hole
IBP	Ibuprofen
k	Degradation rate coefficient
k'	Pseudo-first order degradation rate coefficient
K _{La}	Ozone mass transfer rate coefficient
Log K _{ow}	Octanol-water partition coefficient
MQW	Mili-Q water (synthetic water)
NC	Nanocomposite

NOM	Natural organic matter
NP	Nanoparticle
nPt	Platinum nanoparticle
nZVI	Nano- zero valent iron
NSAIDs	Non- steroidal anti-inflammatory drugs
•OH	Hydroxyl radical
P	Ultrasonic power
P-25	Commercial TiO ₂
PCT	Paracetamol
P _d	Power dissipated in the system
Pd-TiO ₂	Palladium nanoparticle supported TiO ₂ nanocomposite
Pd/Au-TiO ₂	Palladium/Gold supported TiO ₂ nanocomposite
PhAC	Pharmaceutically active compound
PEG-MS	Polyethylene-glycol monostarate
PR	Propanol
PS	Persulfate
Pt-TiO ₂	Platinum nanoparticle supported TiO ₂ nanocomposite
RW	Raw water
S1	Ultrapure water sample spiked with diclofenac
S2	Raw water sample spiked with diclofenac
S3	Control sample of raw water
SEM	Scanning electron microscope
STEM	Scanning-transmission electron microscopy
TOC	Total organic carbon
US	Ultrasonic irradiation
UV	Ultraviolet irradiation
W	Watt
WTP	Water treatment plant
WWTP	Waste water treatment plant
ZVI	Zero valent iron
ZVI-1	Carbide coated zero valent iron
ZVI-2	Zero valent iron micropowder
ZVI-graphite	Graphite coated zero valent iron

γ	Polytropic gas ratio
κ	Thermal conductivity

1. INTRODUCTION

The presence of pharmaceutically active compounds (PhACs) including analgesic and anti-inflammatory chemicals (e.g. codeine, ibuprofen, paracetamol, acetylsalicylic acid, diclofenac, fenoprofen) in the water environment has become an emerging issue due to their classification as “emerging pollutants” under EC Water Directive 2000/60/EC and EU decision No. 2455/2001/EC. A significant fraction of pharmaceutical wastes in water and wastewater is composed of anti-inflammatory and analgesic compounds, which are used without prescription as pain relievers and inflammation reducers with an estimated annual consumption of several hundred tons in developed countries. The removal of these compounds in sewage treatment plants or other biological systems is a major challenge due to their low biodegradability. Hence, they are disposed to receiving water bodies with the effluent of bio-systems and ultimately end up in natural waters, where natural elimination by hydrolysis, sorption, biodegradation and photolysis is unlikely. Knowledge on the impacts of anti-inflammatory and analgesic chemicals on human health is currently insufficient. Nevertheless, there is evidence that even trace concentrations of these compounds may lead to dysfunction of the reproductive organs in fish, damage of the liver and kidney cell functions in birds and livestock, and acute and chronic liver and kidney damage in humans and wildlife (Triebkorn et al., 2004; Ziylan and Ince, 2011).

Advanced oxidation refers to those chemical oxidation processes initiated by the in-situ generated free radicals such as the hydroxyl ($\text{HO}\bullet$), which is non-selective and highly reactive with a wide range of organic compounds (Gültekin and Ince, 2006; Tezcanli-Güyer and Ince, 2004a). In addition to a wide variety of $\text{HO}\bullet$ generation methods in water (e.g. UV/peroxide, ozonation, TiO_2 photocatalysis, ionizing radiation) ultrasonic irradiation has lately emerged as a promising one, due to the unique properties of ultrasound to pyrolyzed water molecules, to enhance the rate of mass transfer and to improve surface properties. Hence, the use of ultrasound to generate hydroxyl radicals in advanced oxidation processes (AOPs) is particularly effective when the method is combined with another advanced oxidation tool (e.g. TiO_2 photocatalysis, ozonation) as it provides additional benefits. Ultrasound also reduces particle size and can be used as a tool in nanotechnology, which is an emerging science used in the development of innovative methods for the design, synthesis,

characterization and application of nanoscale materials to reduce the harm to the environment and to enhance the capability for environmental remediation (Mansoori et al., 2008).

Hence, it is believed that ultrasound-assisted AOPs in nanoparticle-loaded heterogeneous solutions are promising options for the elimination of recalcitrant compounds in water such as analgesic and anti-inflammatory pharmaceuticals. The presence of such particles provides a massive surface and in the presence of ultrasound particles will remain in a uniform distribution. This Ph.D. research has aimed to investigate the degradability of three analgesic/anti-inflammatory pharmaceuticals in water by sonication, ozonation, Fenton oxidation, photolysis and various combinations thereof. Moreover, the study aimed to demonstrate the effect of ultrasound in heterogeneous catalysis using zero-valent iron and other iron species, TiO_2 , Al_2O_3 and their metal-loaded nanocomposites synthesized sonolytically in the lab.

The first part of the study (Chapter 2) presents a thorough and critical review of the most common analgesic and anti-inflammatory compounds, their occurrence and fate in the water environment and treatability in sewage and drinking water treatment plants. Hence, the objective of the first part is to overview and interpret the existing literature on the degradability of analgesic and anti-inflammatory pharmaceuticals in water and/or in effluents of water/wastewater treatment plants by advanced oxidation processes.

In the second part, three model compounds- ibuprofen, diclofenac and paracetamol were exposed to ultrasonication, ozonation, photolysis and various combinations thereof in the presence and absence of heterogeneous and homogeneous catalysts (e.g. graphite-coated carbide, zero valent iron (ZVI), hematite, goethite, magnetite, $\text{Fe}^{+2}/\text{Fe}^{+3}$, TiO_2 and its metal-supported nanocomposites, alumina and Pt-supported alumina. Sonolytic synthesis of the nanocomposites is also covered in this part to shed light on the applicability of the method and the effect of the particles in decontamination of water from pharmaceutical residues. In the following is a summary of the dissertation, its components and outputs as publications and presentations:

- **2. Background and Literature Review.** The section covers an extensive review of the principles of Advanced Oxidation Processes (AOPs), sonochemistry and catalysis; the occurrence, fate and elimination of analgesic and anti-inflammatory chemicals in water and wastewater. The review of analgesic and anti-inflammatory pharmaceuticals, their environmental significance and treatability by AOPs has been published in *Journal of Hazardous Materials* 187 (2011) 24–36.
- **3. Materials and Methods.** The section covers a thorough description of materials, methods and reactors used throughout the study including methods of optimization.
- **4. Sonolytic and Sonocatalytic Decomposition of Diclofenac with ZVI.** The section covers an investigation of the degradability of diclofenac by sonolytic and sonocatalytic processes using commercial zero valent iron (ZVI) and carbide-coated ZVI. The aim was to determine the operational parameters and to assess the contribution of a lab-made, cost effective nano-size catalyst with magnetic properties in improving the efficiency of the processes. The effectiveness of each process was evaluated by the rate of DCF elimination at optimized conditions, and by the reduction in COD, BOD, TOC, Cl⁻ and N-content of the solutions. The section also covers an assessment of HO• production and a comparison of catalyst efficacies with those of commercial ZVI. The content of this section has been published in *Ultrasonic Sonochemistry* 20 (2013) 580–586 and was partially presented in the “17th International Conference on Advanced Oxidation Technologies for Treatment of Water, Air and Soil”, San Diego USA, 16-20 Nov, 2011 and the “4th National Catalyst Conference”, Kocaeli, Turkey, 2012.
- **5. Sonochemical Degradation of Diclofenac: By-Product Assessment, Reaction Mechanisms and Environmental Considerations.** The section covers an evaluation of the environmental friendliness/safety of a sonochemical process by identification of the reaction byproducts and determination of their relative toxicity. The objective was to present a novel approach to the overall degradation of diclofenac under high frequency ultrasound to highlight: i) the formation, identification, and characterization of the oxidation byproducts and their reaction mechanism, ii) the assessment of the environmental safety of the applied process via changes in the acute toxicity and biodegradability of the reactor aliquots. The results of the study have been published in *Environmental Science and Pollution Research* 21 (2014) 5929–5939 and partially presented in the “18th International Conference on Advanced Oxidation Technologies for Treatment of Water, Air and Soil”, Jacksonville, USA, 16-20 Nov, 2012 and the “14th

Meeting of the European Society of Sonochemistry”, Avignon University, France, 2-6 June, 2014.

- **6. Ozonation-Based Advanced Oxidation for Pre-Treatment of Water with Residuals of Anti-Inflammatory Medication.** The section covers a pre-treatment option for drinking water treatment by ozonation with ultrasound or $\text{Fe}^{2+}/\text{Fe}^{3+}$ species to eliminate residuals of anti-inflammatory pharmaceuticals. The contents include evaluation of the following AOPs for partial or complete destruction of ibuprofen: i) ozonation with H_2O_2 , UV; ultrasound, UV/ultrasound and FeSO_4 /ultrasound; ii) sonication with H_2O_2 , UV, O_3 and O_3/UV . The study also includes an investigation of the treatability of the effluents of the above processes in a coagulation/flocculation basin using $\text{Al}_2(\text{SO}_4)_3$ or no coagulant. The contents of this section have been published in *Chemical Engineering Journal* 220 (2013) 151–160 and partially presented in the “18th International Conference on Advanced Oxidation Technologies for Treatment of Water, Air and Soil” Jacksonville, USA, 11-15 Nov, 2012.
- **7. Catalytic Ozonation of Ibuprofen with Ultrasound and Fe-Based Catalysts.** The section covers the evaluation of a novel method of decomposing and mineralizing the emerging contaminant ibuprofen by catalytic ozonation with high-frequency ultrasound (US) and Fe-bearing catalysts. This study has been published in *Catalysis Today* 240 (2015) 2-8 and presented in the “3rd European Conference on Environmental Applications of Advanced Oxidation Processes”, Almeria, Spain, 25 October, 2013.
- **8. Single, Simultaneous and Sequential Applications of Ultrasonic Frequencies for the Elimination of Ibuprofen in Water.** The section covers an evaluation of single, simultaneous and sequential applications of different ultrasonic frequencies in the decomposition of ibuprofen. The work also covers evaluation of the effect of ZVI on the efficiency of the applied reaction systems. The contents of this section have been recently accepted for publication in *Ultrasonic Sonochemistry*. A different part of the research has also been presented in the “252th ACS National Meeting & Exposition”, Philadelphia, USA, 21-25 August, 2016, the “15th Meeting of European Society of Sonochemistry, Istanbul, Turkey, 2016 and the “22nd International Conference on Advanced Oxidation Technologies for Treatment of Water, Air and Soil”, Atlanta, USA, 13-17 Nov, 2016.
- **9. Supporting of Pristine TiO_2 with Noble Metals to Enhance the Oxidation and Mineralization of Paracetamol by Sonolysis and Sonophotolysis.** The section is about the elimination and degradation of paracetamol in water by catalytic oxidation with high-

frequency ultrasound, UV-254 and both using lab-made nanocomposites of TiO₂. The study also covers the effect of persulfate addition and evaluation of a synergy index for each of the hybrid processes. The content of this section has been published in *Applied Catalysis B: Environmental* 172 (2015) 7–17 and partially presented in the “20th International Conference on Advanced Oxidation Technologies for Treatment of Water, Air and Soil,” San Diego, USA, 17-20 Nov, 2014 and the “250th ACS National Meeting & Exposition,” Boston, USA, 16-20 August 2015. Early work with the suspensions of the catalysts was presented in “14th Meeting of the European Society of Sonochemistry”, Avignon University, France, 2-6 June, 2014.

- **10. Enhanced Photo-Degradation of Paracetamol on n-Platinum-Modified TiO₂: The Effect of Ultrasound and •OH/Hole Scavengers.** The section covers elimination and mineralization of paracetamol by catalytic oxidation with lab-made nanocomposites of Pt-TiO₂ by sonolysis, photolysis and both. The objective was to assess the potential of Pt-support in separation of e⁻/h⁺ pairs and facilitating the charge transfer process. The study further aimed to assess the mineralization of the compound, the major reaction sites and the relative significance of •OH and h_{vb}⁺ on the overall degradation process. The content of the section has been published in *Chemosphere* 162 (2016) 324-332 and partially presented in the “4th European Conference on Environmental Applications of Advanced Oxidation Processes”, Athens, Greece, 21-24 October, 2015, the “15th Meeting of European Society of Sonochemistry”, Istanbul, Turkey, 2016 and the “22th International Conference on Advanced Oxidation Technologies for Treatment of Water, Air and Soil, Atlanta, GA, USA, 13-17 Nov, 2016.
- **11. Catalytic Ozonation of Paracetamol Using Commercial and Pt-Supported Nanocomposites of Al₂O₃: The Impact of Ultrasound.** The section covers an investigation of paracetamol degradation by catalytic ozonation in the presence of a lab-made nanocomposite of alumina (Pt-Al₂O₃) and comparison of the process efficiency with that catalyzed with commercial alumina. The objective was to select and optimize the operation parameters, the role of •OH and the impact of ultrasonic irradiation that was expected to improve the process efficiency via enhanced rate of mass transfer and excess •OH production. The study has been recently accepted for publication in *Ultrasonic Sonochemistry* and partially presented in the “4th European Conference on Environmental Applications of Advanced Oxidation Processes, Athens, Greece, 21-24

October, 2015 and the “15th Meeting of European Society of Sonochemistry, Istanbul, Turkey, 2016, which was awarded as the “Best Poster Presentation”.

- **12. Conclusions and Recommendations.** The section comprises of a summary of all findings, concluding remarks and suggestions for future work.

2. BACKGROUND AND LITERATURE REVIEW

2.1. Principles and Tools of Advanced Oxidation Processes

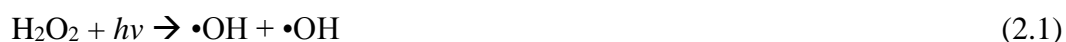
Over the past 30 year, research on AOPs has received significant attention and found applications in water and wastewater treatment, groundwater and soil remediation, sludge conditioning, production of ultrapure water, volatile organic compound and odor control (Klavarioti et al., 2009). AOPs are defined as the aqueous phase oxidation processes that generate highly reactive species such as hydroxyl radicals in sufficient quantity to degrade a number of organic and inorganic contaminants including volatile, semi-volatile, and non-volatile compounds (Ince, 1999).

There are two major routes that have been proceeded by AOPs: i) oxidation with O_2 in temperature ranges of 200–300°C and 1–20 MPa and ii) the use of high energy oxidants such as ozone and H_2O_2 and/or photons that are able to generate highly reactive intermediates $\bullet OH$ radicals which is a powerful, non-selective chemical oxidant (Munter, 2001). Once generated, $\bullet OH$ rapidly attack almost all organic compounds. Hydroxyl radicals attack organic pollutants through four basic pathways: radical addition, hydrogen abstraction, electron transfer, and radical combination producing carbon centered radicals ($R\bullet$ or $R\bullet-OH$) that may be transformed organic peroxy radicals ($ROO\bullet$) in the presence of oxygen (Deng and Zhao, 2015). Thus, all these radicals lead to the formation of more reactive species such as H_2O_2 and super oxide ($O_2\bullet$) resulting in chemical degradation and even mineralization of these organic compounds. By the fact that hydroxyl radicals have a very short lifetime, they are only in situ generated during application through different methods, including a combination of oxidizing agents (such as H_2O_2 and O_3), irradiation (such as ultraviolet light or ultrasound), and catalysts (such as Fe^{2+}). These processes are briefly described below:

2.1.1. UV/ H_2O_2

UV/ H_2O_2 systems involves the generation of $\bullet OH$ radical through photolysis of hydrogen peroxide by a direct process with a yield of two radical per photon absorbed by

254 nm ($\epsilon_{254\text{nm}} = 18.6 \text{ M}^{-1} \text{ cm}^{-1}$) (Parsons and William, 2004). UV/H₂O₂ is one of the most viable AOP technique via its potential for photolytic cleavage of all H₂O₂ to OH• at a stoichiometric ratio of 1:2, provided that the light source has sufficient emission at 190-200 nm. Besides, the anion of hydrogen peroxide, H₂O⁻ absorb UV radiation at 254 nm to generate •OH ($\epsilon_{254\text{nm}} = 240 \text{ M}^{-1} \text{ cm}^{-1}$) (Landi and Naddeo, 2011; Parsons and William, 2004):

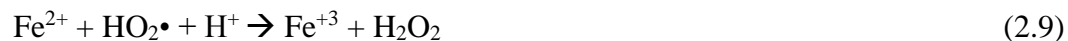
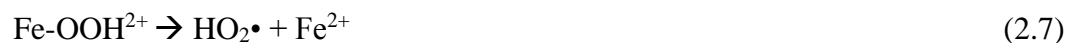


The mechanism of UV/H₂O₂ is based on direct photolysis and hydroxyl attack, however the concentration of hydrogen peroxide may limit the beneficial effects of the system due to its scavenging effect on •OH (Parsons and William, 2004). The maximum absorbance of H₂O₂ occurs at 220 nm and hence, the high concentrations of hydrogen peroxide is required to generate sufficient amount of hydroxyl radical at 254 nm.

2.1.2. Fenton, UV/Fenton and Advanced Fenton

Fenton's reagent, a mixture of soluble ferrous iron and hydrogen peroxide is a powerful oxidant for the destruction of organic compounds (Landi and Naddeo, 2011). If ferrous iron is replaced by ferric iron, then the mixture is called as Fenton-like reagent (Rodriguez et al., 2013). When Fe²⁺ and Fe³⁺ dissolved, they may exist in the form of a range of hydrolysis species or inorganic complexes (Fe²⁺, Fe³⁺, FeOH²⁺, Fe(OH)₂⁺) depending on the pH, the concentration of iron or other inorganic ligands (Parsons and William, 2004). The rate of ferrous iron reaction with hydrogen peroxide is very high at acidic pH and Fe²⁺ is oxidized to Fe³⁺ in a few minutes to seconds and then H₂O₂ is decomposed to •OH by Fe³⁺ as follow (Landi and Naddeo, 2011; Parsons and William, 2004):





Fenton's reaction alone is not capable of destroying organic compounds completely and the process is limited by the redox cycle between Fe^{2+} and Fe^{3+} (Ameta et al., 2013). The photo-Fenton process is less limited, because at 180-400 nm irradiation the metal complex decomposes to form $\bullet\text{OH}$ and Fe^{2+} (Ameta et al., 2013; Landi and Naddeo, 2011; Parsons and William, 2004):

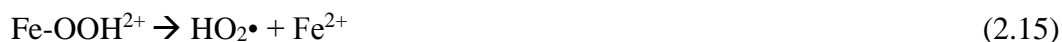


Photo-Fenton reaction is beneficial also because it may utilize a large portion of solar radiation and Fe^{3+} ions are not accumulated so that more the rate of $\bullet\text{OH}$ generation is not limited (Ameta et al., 2013). The most crucial experimental parameter is pH, because the most active ferric water complex ($[\text{Fe}(\text{OH})]^{+2}$) that hinders precipitation forms at pH 2.8-3.0 (Rodriguez et al., 2013).

Another mode of the Fenton reaction is called the "Advanced Fenton", which utilizes zero-valent iron as the Fe source. If the particles are < 100 nm, (ZVI) exhibits a typical core-shell structure as illustrated in Figure 2.1. The core consists metallic iron that provides the reducing power, while the shell is largely composed of mixed valent ($\text{Fe}^{2+}/\text{Fe}^{3+}$) oxides/hydroxides formed via oxidation of ZVI (Li et al., 2006).

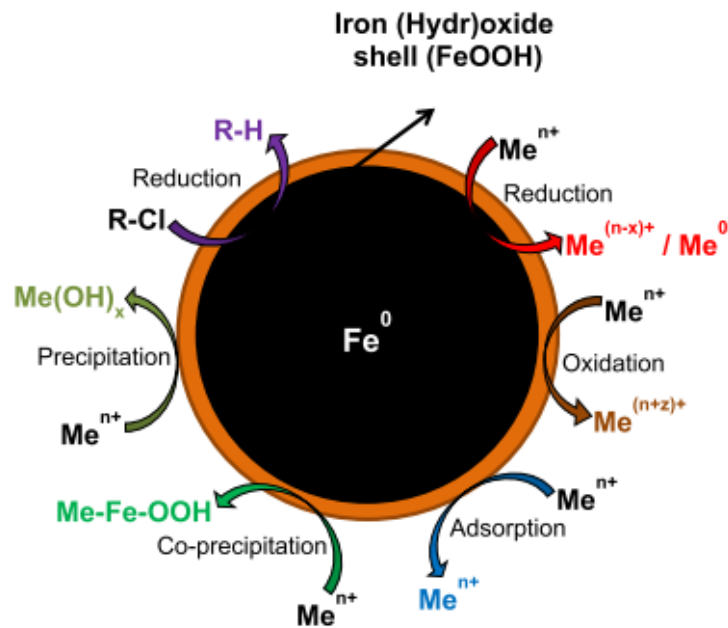
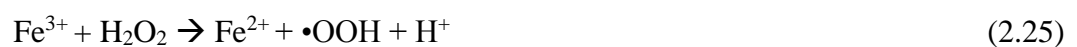
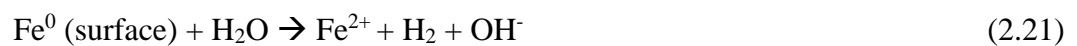
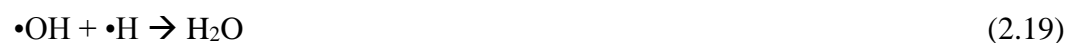
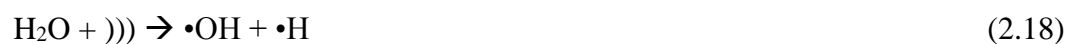
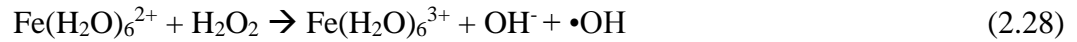


Figure 2.1. The core-shell model of zero valent iron (ZVI) depicting potential mechanisms for the removal of metals and chlorinated compounds (O'Carroll et al., 2013).

Application of ZVI together with ultrasonic irradiation leads to accelerated mass transfer of reactants to the metal surface with enriched reactive sites and a continuously cleaned surface (Tezcanlı-Güyer and Ince, 2011). The reaction scheme in sonicated water is as the following (Hung et al., 1998; Tezcanlı-Güyer and Ince, 2011):





2.1.3. Ozonation

Ozone is a powerful but selective oxidant and is an unstable gas that is decomposed by a complex mechanism to generate $\bullet\text{OH}$ (Landi and Naddeo, 2011). Organic compounds react either directly with it or indirectly with its decomposition products (Gottschalk et al., 2000).

Direct ozonation is crucial when the radical reaction is inhibited either by the absence of initiators or the excess of scavengers (Gottschalk et al., 2000). Under acidic conditions (below pH 4.0) the direct pathway dominates, while the indirect pathway is dominant at alkaline conditions. Ozone decomposition follows the following reactions (Beltran, 2004; Kasprzyk-Hordern, 2003):



The disadvantages of ozonation are the selectivity, low solubility and instability of the reagent so that in most cases it is incapable of providing complete oxidation. The efficiency of the process is commonly improved by the addition of H₂O₂, UV, US, Fenton's reagents or a solid catalyst (catalytic ozonation) to enhance the decomposition of O₃ and the production of •OH.

2.1.4. Ionizing Radiation

Radiation chemistry is the study of the chemical changes produced by the adsorption of radiation to produce ionization (Cooper et. al 1998). In Ionizing radiation, reaction is initiated by ionized and excited atoms and molecules reacting rapidly with organic compounds via free radicals generated by excited molecules (Cooper et. al 1998).

2.1.5. Ultrasonic Irradiation

Ultrasonic cavitation is a tool in AOPs that results in very unique and extreme conditions generated by ultrasonic waves in liquid media, leading to a remarkably suitable medium for high energy chemistry, which is called "sonochemistry". The extreme conditions generated from sonochemistry, do not only promote the oxidative destruction of target contaminants via free radical reactions, but also provide an excellent medium for their thermal decomposition in the gas phase. Therefore, the production of free radical species encompasses the objectives of AOP beyond aqueous phase oxidative destruction to gaseous decomposition (Ince et al., 2001). In Section 2.2, more detailed information on ultrasonic irradiation is given.

2.2. Principles of Sonochemistry

An emerging field in AOPs is the use of cavitation in environmental remediation which could be categorized under three main purposes: i) to put into practice a clean energy source; ii) to improve the efficiency of other treatment methods; and iii) to reduce the amounts of chemicals required for conventional treatments (Adewuyi, 2005). Furthermore, it has been becoming a mostly applied laboratory technique because it has been found to enhance reaction rates, increase conversion, improve yields, initiate the reactions on biological or

chemical systems (Thompson and Doraiswamy, 1999). Therefore, it has been recently attracted attention and appeared to be a promising alternative either as a sole or as an assisted process.

Ultrasound occurs at a frequency above 16 kHz which is higher than the audible frequency of the human ear, and is typically associated with the frequency range of 20 kHz to 1 MHz (Thompson and Doraiswamy, 1999) as depicted in Figure 2.2. The sonic spectrum can be divided into three main regions: i) low frequency or conventional power ultrasound (20-100 kHz); ii) medium frequency or ultrasound with sonochemical effects (300 kHz-1 MHz); and iii) high frequency of diagnostic ultrasound (2-10 MHz) (Ince et al., 2001). Sonochemical oxidation techniques involve the use of ultrasonic waves to produce an oxidative environment through cavitation that yields microbubbles and supercritical regions in the liquid phase (Adewuyi, 2001). The choice of ultrasonic frequency determines the physical and chemical effects to be occurred which caused by the phenomenon of acoustic cavitation: the creation, expansion, and implosive collapse of bubbles in ultrasonically irradiated during compression and rarefaction period of sound waves (Adewuyi, 2005; Mason et al., 2011; Thompson and Doraiswamy, 1999).

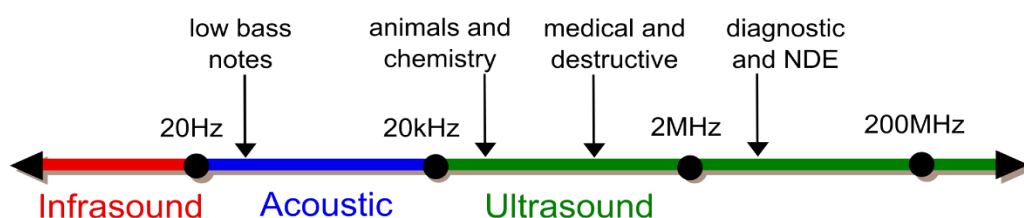


Figure 2.2. The frequency spectrum from infrasound to ultrasound.

During the irradiation of a liquid medium with high intensity sound or ultrasound, it is transmitted through the medium via pressure waves and induces vibrational motion of the molecules which alternately compress and stretch the molecular structure of the medium due to a time-varying pressure (Mason and Peter, 2002). Compression and rarefaction cycles exert a positive and negative pressure on the liquid pushing or pulling the molecules together or away from one another, respectively (Suslick, 1990). In case of the ultrasonic intensity in a liquid is exceeded, a point is reached where the applied pressure equals to the negative pressure developed in the rarefaction cycle of the wave. Therefore, the critical distance

between the molecules exceeds the critical molar distance to hold it together resulting in the disintegration of the liquid to form cavities, made of vapor and gas filled microbubbles (Suslick, 1990). This cavity is called “cavitation bubble” and the phenomenon of acoustic cavitation can be considered to involve at least three stages: i) nucleation; ii) bubble growth (expansion); and iii) implosive collapse as depicted in Figure 2.3. The first stage-cavity formation- is a nucleated process, by which cavitation nuclei are generated from negative pressure of an expansion wave at weak point in the liquid such as microbubbles trapped in micro-crevices of suspended particulate matter within the liquid (Suslick, 1990). In the second stage - bubble growth stage-, the bubbles grow and expand in a manner restricted by the intensity of the applied sound wave. The third stage- cavitation collapse- occurs at the intensity of the ultrasound wave exceeding that of the “acoustic cavitation threshold” (Mason and Peter, 2002). At this condition, the microbubbles overgrow to the extent where they can no longer efficiently absorb energy from the sound environment to sustain them and implode violently (Suslick, 1990).

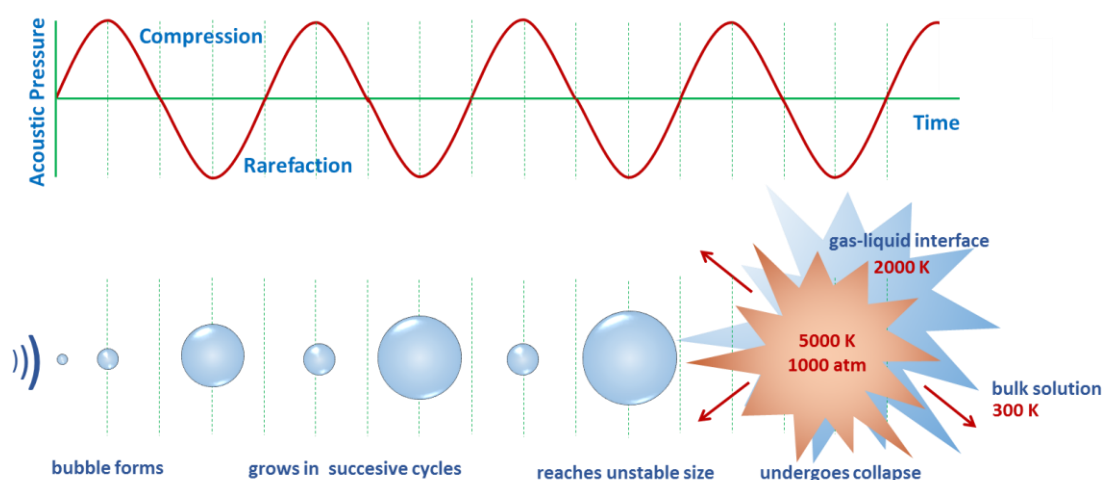


Figure 2.3. Growth and implosion of cavitation bubbles in aqueous solution under ultrasonic irradiation (adapted from Adewuyi, 2005; Suslick et al., 1999).

The chemical effects of ultrasound can be considered in three main areas: i) homogeneous sonochemistry of liquids, ii) heterogeneous sonochemistry of liquid-liquid or liquid-solid systems, and iii) sonocatalysis overlapping the first two (Suslick and Price, 1999). In general, most studies involving the sonochemical degradation of chemical contaminants have adopted the “hot spot theory” which assumes that the collapse of bubbles

near a adiabatic process produces extreme conditions such as intense, localized and transient temperatures (~ 5000 K) and high pressures (~ 1000 atm), with very short lifetimes of the order of microseconds, heating and cooling rates above 10^9 K s^{-1} (Adewuyi, 2005; Suslick et al., 1999) and these bubbles are also referred to as micro-reactors or hot spots (Ashokkumar et al., 2007).

A sonochemical reaction produces highly reactive species including hydroxyl ($\bullet\text{OH}$), hydrogen ($\text{H}\bullet$), and hydroperoxy ($\text{HO}_2\bullet$) radicals, hydrogen peroxide (H_2O_2), H_2 , perhaps $e^-_{(\text{aq})}$ and heat from a well-defined micro-reactor which is comprised of three chemical reaction regions: i) the inside of the cavitation bubble known as the hot gaseous nucleus; ii) the interfacial region between the gaseous bubble and surrounding liquid, a region with radial gradient in temperature and local radical density; and iii) the bulk solution at ambient temperature (Adewuyi, 2005; Mason, 2003; Suslick et al., 1999). The radicals are generated either react with each other to form new molecules and radicals or diffuse into the bulk liquid to serve as oxidants (Mason, 2003). Reactions involving free radicals can occur within the collapsing bubble, at the interface of the bubble, and in the surrounding liquid. The formation of $\bullet\text{H}$ and $\bullet\text{OH}$ is attributed to the thermal dissociation of water vapor present in the cavities during the compression phase (Adewuyi, 2005) and hence, the cavitation activity is found to be proportional to the amount of gaseous impurity acting as nucleation site (Adewuyi, 2005; Thompson and Doraiswamy, 1999). The potential reaction sites of a cavitation event for chemical reactions are shown in Figure 2.4.

2.2.1. Types of Cavitation

The microbubbles can be either stable at their average size for many cycles or transient when they grow to certain size and violently collapse or implode during compression of the waves as illustrated in Figure 2.5 (Adewuyi, 2001). The implosions are the outstanding part of the sonochemistry (Adewuyi, 2001) and the critical size depends on the liquid and the frequency of sound (Suslick, 1990). Stable bubbles are considered to be weakly and symmetrically oscillating bubbles, whereas transient bubbles are considered to be “active cavitation” bubbles (Ashokkumar, 2011). According to experimental evidences, it was found that transient bubbles exist only for one or a few acoustic cycles whereas stable bubbles exist for hundreds of acoustic cycles (Tronson et al., 2002).

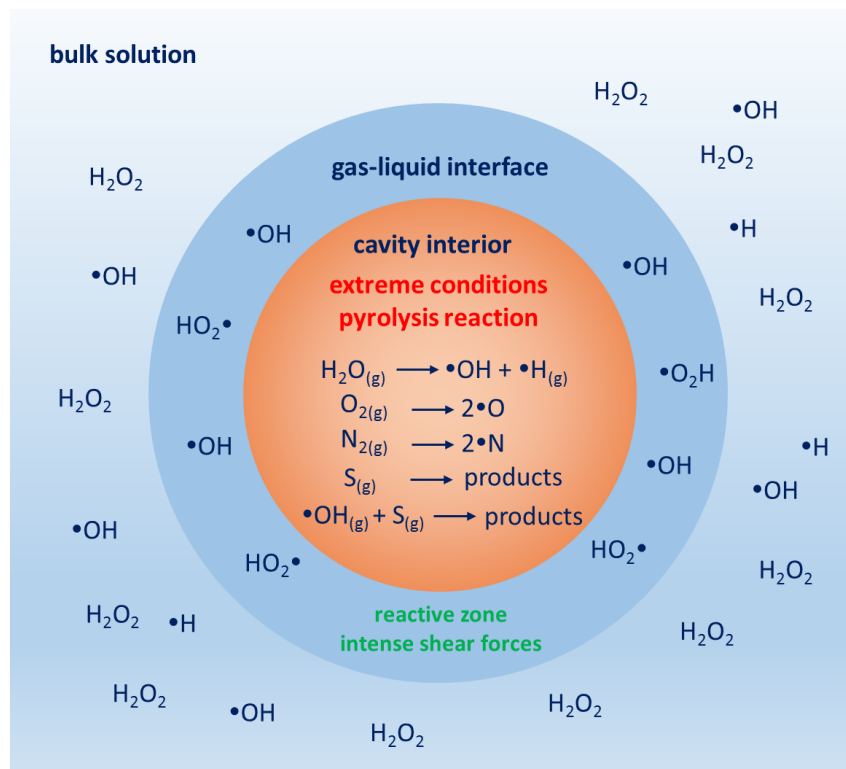


Figure 2.4. Possible chemical reaction sites of cavitation event in homogeneous reaction media (Adewuyi, 2001; Ince et al., 2001).

Hence, the large number of oscillations of stable bubbles which is formed by power ultrasound cause their existence for a sufficient time for surface active solutes to adsorb on the bubble/solution interface, to accumulate gaseous decomposition products, and to allow a significant amount of the gases solubilized in solution to enter the bubble (Ashokkumar, 2011). However, these events can be considerably suppressed for transient bubbles which is formed by the application of medium frequency. In contrast to stable cavitation, the pressures and temperatures developed in transient cavitations are much higher than that of stable cavitations because in stable cavitation phenomena there are lots of time for the diffusion of dissolved gases and vapors into the bubble, therefore this collapse has a “cushion effect” (Ince et al., 2001).

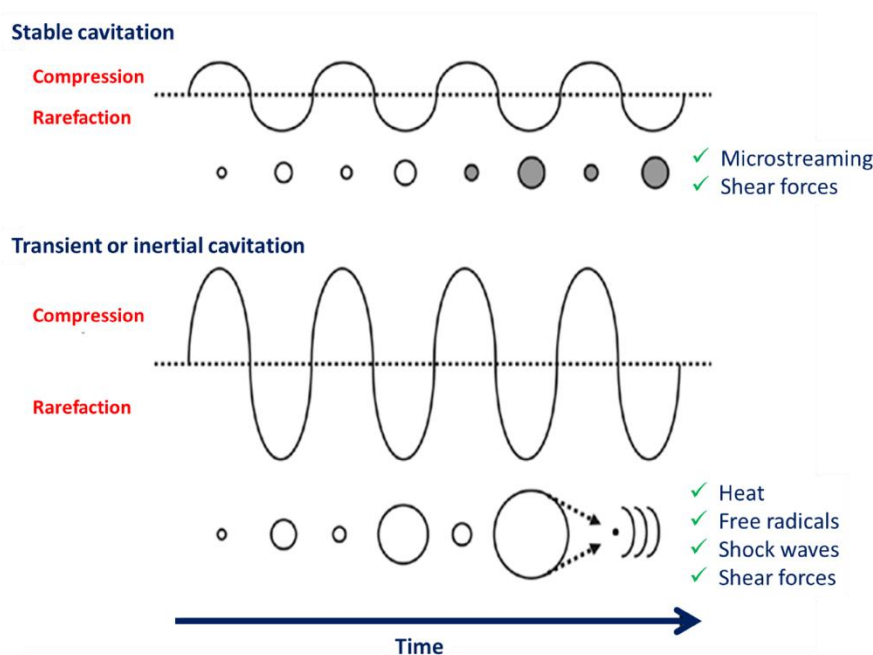


Figure 2.5. Illustration of the effects of acoustic fields of identical frequency (a) low-intensity ultrasound, (b) high-intensity ultrasound (Newman and Bettinger, 2007).

2.2.2. Parameters Effecting the Sonochemical Reactions

Sonochemistry is complicated by the fact that the nature or the physicochemical properties of the solvent, solute (i.e. viscosity, vapor pressure, surface tension), external factors (i.e. dissolved gas in the bubble, system temperature and hydrostatic pressure) and acoustic factors (i.e. frequency, intensity) show dramatic effects on the stages cavitation collapse (Lorimer and Mason, 1987; Mason and Peter, 2002). There are two main strategies to maximize the reaction efficiency in sonochemical reactions: i) optimization of power and reactor configuration and/or ii) enhancement of cavitation. The former is a mechanistic approach which grounds on the selection of the transducer (i.e. piezoelectric or magnetic material) and generator (i.e. probe type for low frequency or plate types for high frequency), the configuration of the reaction cell, and the optimization of the most effective power density (Ince et al., 2001). Hence, the frequency, applied pressure, power intensity and bulk solution temperature may be considered as the most crucial parameters to optimize mechanistic effects whereas, the physicochemical properties of the pollutant and the solute, bubbled gas, and the solid addition are essential to enhance cavitation via maximized chemical reactions for the latter strategy (Ince et al., 2001).

Frequency. The effect of frequency as one of the most important factors to specify the efficiency of sonochemical reactions has been widely investigated from a fundamental point of view ranging from 20 to 1200 kHz (Beckett and Hua, 2001; Entezari and Kruus, 1996; Petrier et al., 1992; Petrier and Francony, 1997; Sato et al., 2000). It was found that sonochemical reaction efficiency at different frequencies is complicated to compare because the formation and behavior of the bubble is directly associated with frequency, emitting area, cavitation threshold, bubble population, lifetime of bubbles etc. (Asakura et al., 2008; Petrier and Francony, 1997).

It was found that the higher ultrasonic frequencies generally cause to increase the cavitation threshold and require significantly more power as a result of the higher rates of molecular motion which results in greater power losses due to insufficient disruption of liquid through very short cycles of rarefaction and compression (Lorimer and Mason, 1987). Therefore, at a constant input power, less cavitation bubble collapses are produced at a low frequency with higher energy of each bubble while more cavitation bubble implosions occur at a higher frequency with lower energy (Fuchs and Puskas, 2005). The additional effects of high frequency irradiation is the occurrence of more events per time and smaller size of cavitation bubbles. It was found that the sonochemical efficiency increases with the logarithm of the frequency but it is generally expected to decrease above a certain frequency in the higher region (Asakura et al., 2008). On the other hand, the micro jetting and streaming caused by cavity disruption is more likely to occur at lower frequencies and larger resonant bubble radii (Beckett and Hua, 2001). The size of cavitation bubbles is inversely related to frequency producing a stronger shock wave with larger cavitation bubbles (Fuchs and Puskas, 2005). Cavitation bubbles reach to an unstable size (resonant size) just before they implode violently and the resonant size of the bubbles is as shown in the following equation (Leighton, 1995):

$$R_r^2 = \frac{3\kappa P_0}{\rho \omega_r^2} \quad (\text{Eq. 2.1})$$

where: R_r is the resonant bubble radius, κ is the polytropic index (C_p/C_v), P_0 is the hydrostatic pressure, ρ is the density of the solution and ω_r is the resonant frequency. At low frequencies, the number of cavitation events per second is lower than that of high frequency

with higher resonant radius which have longer lifetimes resulting in more violent collapse due to the build-up of more energy (Lorimer and Mason, 1987; Petrier and Francony, 1997). For example, when pure water is sonicated at 20 kHz, the size of the bubbles are 164 μm whereas the bubble are of radiuses 19 μm , 11 μm , and 7.5 μm at 176 kHz, 300 kHz, and 446 kHz, respectively (Wayment, 1997). This means that “stable” or long-lived bubble formed at low frequency with average life times of $\sim 10 \mu\text{s}$ allow radical scavenging and recombination reactions at the interfacial sheath due to delayed growth and long collapse duration of gas-filled bubbles, thus inhibiting the mass transfer of hydroxyl radicals into the solution bulk (Barbier and Petrier, 1996; Mason and Peter, 2002). Therefore, at low frequency ultrasound, the reactions with hydrophobic solutes are more likely to occur which allows to easily diffusion into the cavity bubbles to undergo pyrolysis inside the bubble, or hydroxylation and thermal decomposition at the interfacial region, where pressure gradients and temperatures are still high enough to induce thermolytic fragmentation (Ince et al., 2001). On the other hand, at medium frequency (200-1000 kHz), cavitation bubbles are extremely small (4.6 μm at 500 kHz), short-lived with average life times of 0.4 μs and comprised of mainly vapor-filled “transient” cavitations releasing larger energies into the surrounding liquid (Ince et al., 2001; Suslick, 1990). Hence, there is no sufficient time for radical recombination reactions in the hot bubble or at the interfacial region and as a consequence, medium frequency waves are highly effective for oxidation reactions in the liquid bulk (Barbier and Petrier, 1996; Ince et al., 2001).

Moreover, the attenuation and reflection of ultrasound waves and resonance of liquid samples may be responsible for the formation of standing waves. The increase in ultrasonic intensity means a rise in the acoustic amplitude at which more violent bubble collapse occurs as illustrated in Figure 2.6 (Asakura et al., 2008; Entezari et al., 1997). The increase in hydroxyl radical formation at high frequencies may be due to shorter collapse times resulting in hindering of the radical recombination as well as the generation of more violent bubble collapse inducing the formation of $\bullet\text{OH}$ compared to the situation at low frequency (Wayment, 1997). Additionally, it was found that surfaces with small surface details are more likely to be reacted and/or cleaned successfully using higher ultrasonic frequencies due to production of smaller cavitation bubbles at higher frequencies at which the penetration and production of bubble implosions closer to a surface is enabled compared to a lower frequency (Fuchs and Puskas, 2005).

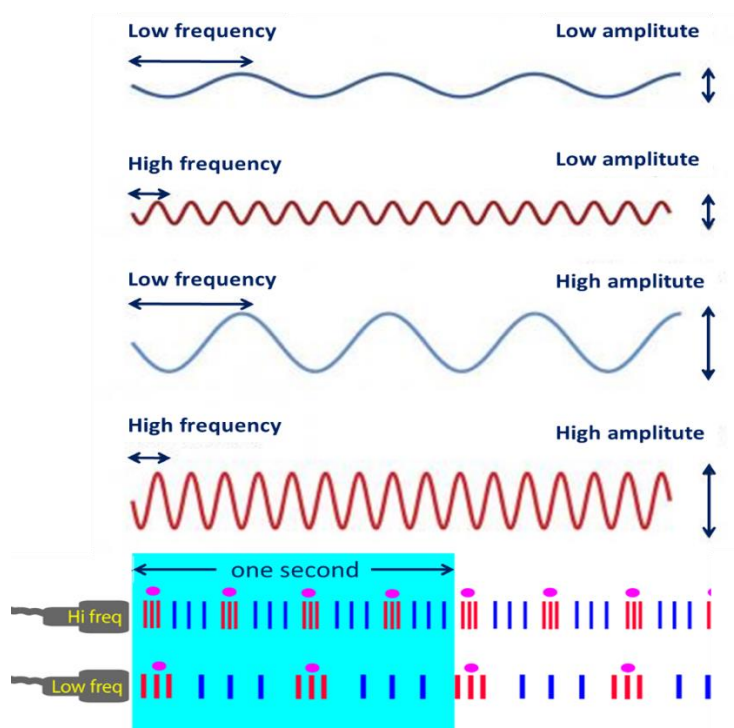


Figure 2.6. The nature of rarefaction and compression cycles at low and high frequency with varying amplitudes.

Power Intensity. One of the most important parameter in sonochemistry playing a major role is the ultrasound power (Sathishkumar et al., 2016). Sonochemical power is commonly stated as the electrical input or output power from the generator in which the electrical power is transformed into ultrasonic energy depending not only on the devices but also on the conditions of oscillators (Kimura et al., 1996).

It was found that the rate of sonochemical reaction increases with increase in power continuously up to a certain limit which results in increased number of active cavitation bubbles and hence, increased amount of $\bullet\text{OH}$ formation and acceleration in reaction (Villaroel et al., 2014; Zhang et al., 2006). However, a further increase in the acoustic power may lead to decrease in the rate of reaction (Sathishkumar et al., 2016). This may be attributed to the fact that the cavitation bubble size, the bubble collapse time, the transient temperature, and the internal pressure in the cavitation bubble during collapse are all dependent on the power intensity (Kang et al., 1999).

The power intensity is directly proportional to the square of the amplitude and a function of the acoustic amplitude as follows (Kang et al., 1999; Mason, 1999):

$$I = \frac{P_A^2}{2\rho c} \quad (\text{Eq. 2.2})$$

where: I is the sound intensity (amount of energy flowing per unit area per unit time), ρ is the density of the medium, and c is the velocity of sound in the medium.

The maximum bubble size of a cavitation bubble is contingent on the density of the liquid, frequency, the hydrostatic pressure, and the acoustic pressure as follows (Kang et al., 1999):

$$R_{max} = \frac{4}{3\omega_a} (P_A - P_h) \left(\frac{2}{\rho P_A}\right)^{1/2} \left[1 + \frac{2}{3P_h} (P_A - P_h)\right]^{1/3} \quad (\text{Eq. 2.3})$$

where: ω_a is the applied acoustic frequency and P_h is the external (hydrostatic) pressure, which is 1 atm under our experimental conditions (Kang et al., 1999). Moreover, the bubble collapse time, τ , is proportional to the maximum bubble size, R_{max} (Kang et al., 1999; Mason and Lorimer, 2002):

$$\tau = 0.915R_m \left(\rho/P_m\right)^{1/2} \left(1 + P_{vg}/P_m\right) \quad (\text{Eq. 2.4})$$

where: P_m is the pressure in the liquid (i.e., $P_m = P_h + P_a$) and P_{vg} is the vapor pressure in the bubble (Kang et al., 1999). Therefore, at high acoustic intensity with large P_A values, the cavitation bubbles are more likely to grow larger in size during a rarefaction cycle which results in incomplete collapse during a single compression cycle due to insufficient time (Kang et al., 1999). There is an optimum power density which can be applied during sonochemical irradiation in order to obtain maximum reaction rates because there are some limitations to the ultrasonic energy input to the system (Kang et al., 1999; Mason, 1999):

- i. A minimum intensity, which is depending upon the frequency, is required to reach cavitation threshold.
- ii. The introduction of a large amount of ultrasonic power into a sonochemical system leads to generation of a great number of cavitation many of which will coalesce to form larger size and longer lived bubbles.
- iii. High vibrational amplitudes suppress the contact of ultrasound and liquid which is known as decoupling that results in a significant loss of power transfer from source to liquid medium.

It is also known that the intensity of sound is decreased as it progresses through the medium and some of the energy is dissipated as heat and the extend of attenuation is inversely related to the frequency (Mason, 1999). This indicates that a higher initial power is required to obtain an identical intensity in a medium at a given distance from an ultrasonic source (Mason, 1999).

There are several methods to estimate the ultrasonic power dissipated into a sonochemical reaction (Mason and Peter, 2002). The most common method is calorimetry, which involves measurement of the initial rate of a temperature rise produced per time in a sonochemical reactor and the method assumes that almost all energy is transformed to heat and the output power can be determined via calorimetry (Kimura et al., 1996).

Dissolved Gases. Dissolved gas or small gas bubbles in a liquid may act as nuclei for cavitation to promote a uniform cavitation lowering the cavitation threshold (Mason, 1999; Mason and Lorimer, 2002). The heat capacity ratio (C_p/C_v) or polytrophic ratio (γ) of the gas in the bubble affects the amount of heat released and, hence the final temperature produced in an adiabatic compression (Mason and Peter, 2002). Therefore, the large values of polytrophic ratio will provide larger sonochemical effects of gas filled bubbles. Furthermore, the thermal conductivity of the gas affects cavitation collapse and the energy developed on the collapse of gas filled bubbles will increase with larger ratio of specific heats (Adewuyi, 2001; Mason, 1999). A gas with low thermal conductivity reduces heat dissipation following adiabatic collapse in which small amounts of heat are transferred to the bulk liquid (Adewuyi, 2001). Hence, monoatomic gases such as He, Ar and Ne are preferred to diatomic gasses such as N_2 , air, O_2 but less favorable gas is CO_2 (Mason and Peter, 2002). It was found that

halogenic compounds are more efficiently broken down under argon, and the others (without halogens) are more efficiently degraded under air (Rooze et al., 2013). In case of the sonication of oxygen saturated solution, additional H_2O_2 formation occurs due to formation of peroxy and hydroxyl radicals via homolytic cleavage inside the bubble and their recombination at the cooler sites (interface or the solution bulk) produces additional hydrogen peroxide as follows (Mason and Lorimer, 2002; Tezcanli-Güyer and Ince, 2004a) :



However, although oxygen can increase radical production, the hot spot temperature may be lowered by this addition, i.e. the maximum in radical production does not necessarily coincide with the maximum hot spot temperature (Rooze et al., 2013).

When sonication occurs in air saturated solution, H_2O_2 generation is accompanied by the formation of nitrous and nitrogenous ion (Mason and Lorimer, 2002). Despite the low polytrophic gas ratio of air, larger yields are obtained in the presence of air due to the reaction of nitrogen with molecular oxygen to form nitric acid and radical species such as $\bullet\text{OH}$, $\bullet\text{NO}_2$, and $\bullet\text{NO}_3$ accelerating the oxidation process (Kidak and Ince, 2006). Sonochemical reactions in the presence of air are as follows (Ullerstam et al., 2000):



Although the formation of nitrous and nitric acids favor the decomposition process via pH reduction, generation of excess strong oxidants such as $\bullet\text{OH}$, nitrite and nitrate radicals, ($k_{\bullet\text{NOX}} = 10^7 \text{ molL}^{-1} \text{ s}^{-1}$; $k_{\bullet\text{OH}} = 10^{12} \text{ molL}^{-1} \text{ s}^{-1}$) further accelerates the oxidation reactions (Kidak and Ince, 2006; Petrier and Casadonte, 2001).

In addition, the solubility of the gas in the liquid is also an important aspect; the more soluble gases are more likely to diffuse into the cavitation bubble to form excessive nuclei for cavitation (Adewuyi, 2001). The increase in the gas content of the medium lowers both the cavitation threshold and the intensity of the shock wave released on the collapse of the bubble as a result of the greater “cushioning” effect (Mason and Lorimer, 2002). Furthermore, it is important to note that sonication of water containing organic compounds results in thermal or chemical decomposition either in the gas phase (hydrophobic compounds), or in the liquid and the interfacial layers depending on the degree of solutes’ partitioning between gaseous and aqueous interfaces.

Temperature. In sonochemical reactions, the rate of reaction was found to be strongly depend on temperature. When the temperature increases, viscosity and surface tension decreases lowering cavitation threshold, as well as increasing vapor pressure and producing a large number of cavitation which act as a barrier to sound transmission (Mason, 1999; Mason and Peter, 2002) and hence make the implosions less violent and damp the effective ultrasonic energy (Adewuyi, 2001; Mason, 1999). Overall then, it can be concluded that cavitation bubbles are more easily produced as the temperature increases, however the effects resulting from cavitation collapse are reduced (Mason and Lorimer, 2002).

Environmental Use of Ultrasound. Ultrasonic irradiation of aqueous solutions results in the formation of free radicals due to the sonolysis of water which are able to attack essentially all organic compounds (including halocarbons, pesticides, and nitro-aromatics) and through a series of reactions oxidize them completely (Suslick, 2001). The cavitation bubble behaves as a micro reactor which discharges radical species and free electrons into the bulk solution as well as thermal reactions inside the bubble (Petrier and Casadonte, 2001). In environmental remediation, there are essential research areas of interest including the destruction/transformation of organic pollutants, the removal of biological contamination

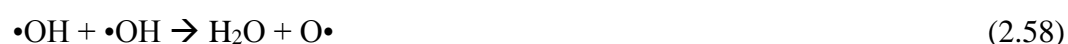
(disinfection), acoustic deliquoring and ultrasonic dispersion (Crum et al., 1999; Mason, 2003).

The degradation of chemical pollutants is possible through the effects of cavitation created by ultrasound (Mason, 2003). The reaction rate and the mode of sonochemical elimination is a function of the physical and chemical properties of the target compounds such as its hydrophobicity and vapor pressure (Mason, 2003; Mason and Lorimer, 2002; Petrier and Casadonte, 2001). In case of volatile contaminants, degradation process may occur in the gas bubble where extreme conditions are generated during the bubble collapse by thermal reactions in the “hot spot” of the cavitation bubble (Crum et al., 1999). A compound with a high vapor pressure or hydrophobic character is more likely to capture hydroxyl radicals at the bubble-liquid interface more efficiently than more solubilized compounds whereas hydrophilic compounds are decomposed in the bulk liquid by hydroxyl radicals released from cavitation bubble (Mason, 2003). Therefore, the most important physical parameters of a solute to identify its degradability by sonication is i) the Henry’s Law constant, H ($\text{Pa m}^3 \text{ mol}^{-1}$) -the equilibrium air-water distribution-, which determines the relative amount of a solute entering the vapor bubble that increases the degradation rate as H increases and ii) the octanol-water partitioning coefficient, K_{ow} , which approximates the hydrophobicity of a compound and gives insight into the amount of surface excess at the cavitation bubble interface resulting in increased degradation rates as K_{ow} increases (Weavers, 2001).

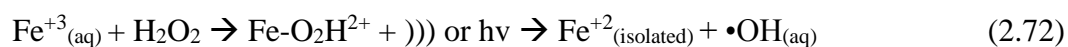
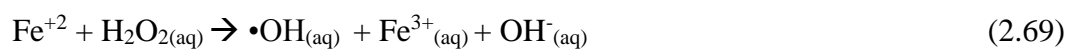
The desirability of sonolysis for environmental remediation lies in its low maintenance requirements and the low energy efficiency of alternative methods (e.g., ozonolysis, UV photolysis) (Suslick, 2001). However, it may sometimes ineffective for the remediation of water which contains refractory or a mixture of organic compounds. Depending on the pollutants to be eliminated, the combination of advanced oxidation processes such as ozonation with ultrasound or an integrated ultrasonic/biological treatment can significantly improve process efficiency and economy (Mason, 2003). It was found that there is a great synergistic improvements in the combined application of ultrasound with ozonolysis, ultraviolet light and/or homogeneous Fenton Reaction for the destruction of organic contaminants (Barik and Gogate, 2016; Crum et al., 1999; Gültekin and Ince, 2006; Song et al., 2007; Tezcanli-Güyer and Ince, 2004b). The combination of oxidizing agents with

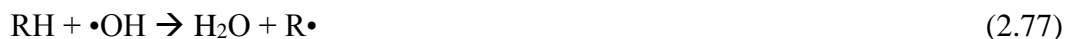
ultrasound is expected to yield synergistic results due to the common underlying mechanism of oxidation generating excess reactive species whose activation energy of the reaction with compounds are typically low (Chand et al., 2009). The chain reactions occurring during sonication, sono-Fenton, sonophoto-Fenton, sono-ozonation, sono-photo and sono-peroxide oxidation of pure water are as follows:

Sonolysis

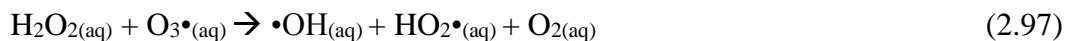
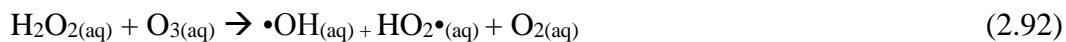
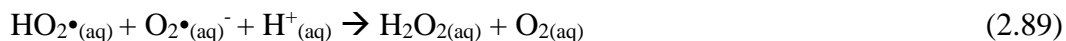


Sono-Fenton, Sonophoto-Fenton





Sono-ozonation, Sono-photolysis, Sono-peroxide





2.2.3. US-assisted AOPs

US/O₃. Ozonation in the presence of ultrasonic irradiation provides a synergy via: excess $\bullet\text{OH}$, higher mass transfer and diffusion of O₃ that improves its dissolution and the generation of secondary oxidative species as illustrated in Figure 2.7 (Landi and Naddeo, 2011; Mason and Lorimer, 2002).

The overall rate of contaminant (C) degradation in US-assisted ozonation is represented as follows (Laugier et al., 2008):

$$-\frac{dC}{dt} = k_{US}[C] + k_{O_3}[C] + k_{US-O_3}[C] \quad (\text{Eq. 2.5})$$

where: k_{US} , k_{O_3} , and k_{US-O_3} , are the first order degradation rate constants for sonolysis, ozonolysis, and the residual kinetic effect upon combining the two systems. Degassing may be detrimental at high frequency ultrasound so that lower degradation rates are expected. The pathways of pollutant degradation and interactions of US and O₃ is illustrated in Figure 2.8.

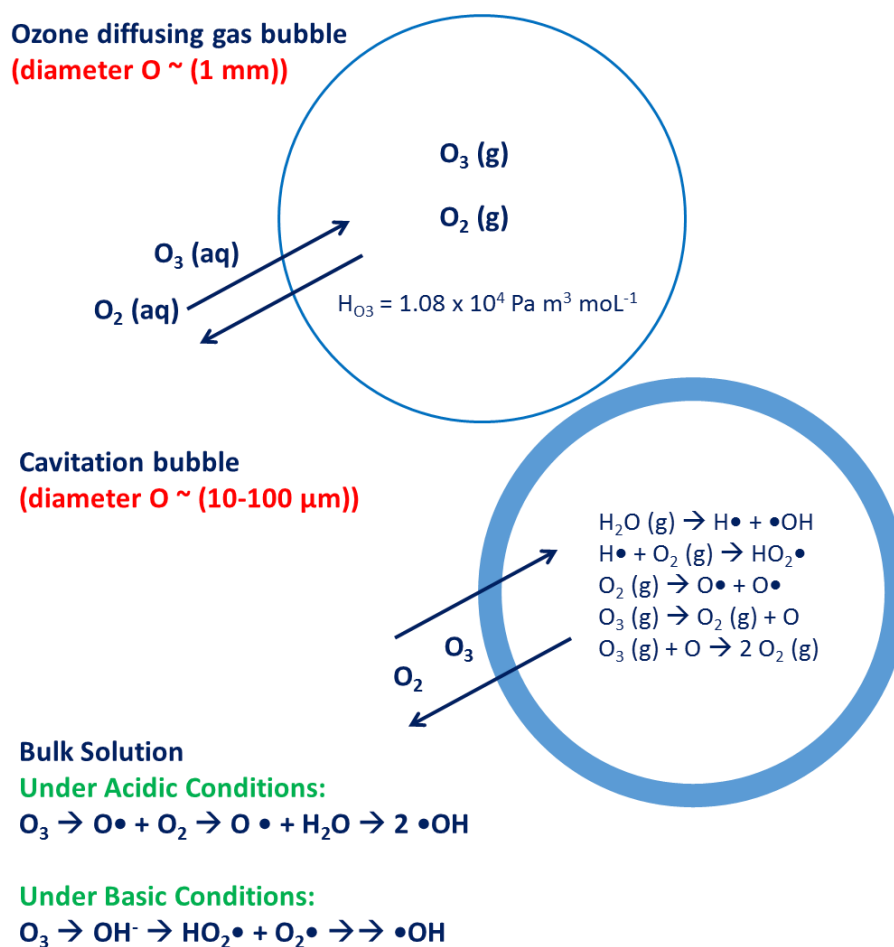
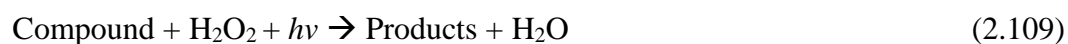


Figure 2.7. The reactions of sonolytic ozonation in an ultrasonic reactor (Weavers, 2001).

US/UV. A summary of chemical reactions taking place during US-assisted photolysis is given in the following: (Xu et al., 2013):



where: $(\cdot\text{X})$ represents all possible intermediates leading to the formation of H_2O_2 .

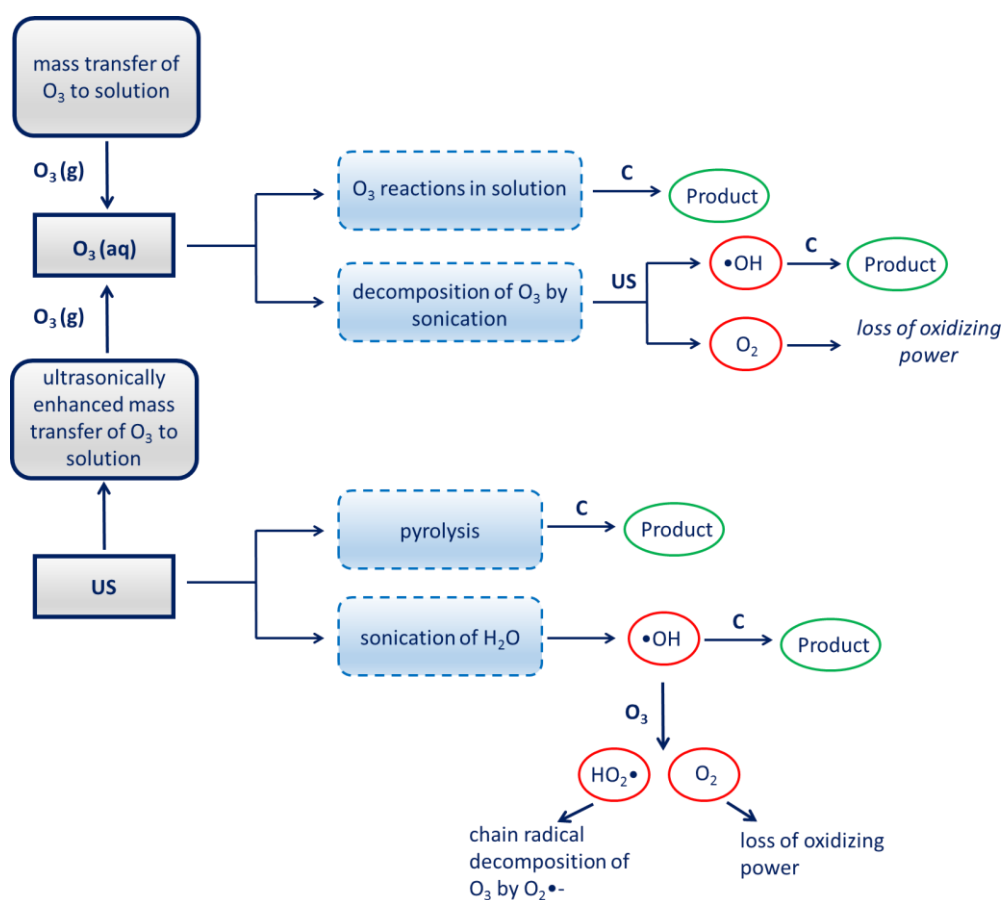


Figure 2.8. The possible pathways of contaminant degradation and the interaction between ozone and ultrasound (Weavers et al., 1998).

US/H₂O₂, US/Fenton, US/photo-Fenton. Application of US and Fenton simultaneously leads to the production of excess •OH. A majority of extremely reactive radicals do not penetrate or diffuse into the bulk medium lowering the probability of interaction between the radical and pollutant and allowing the formation of H₂O₂ through recombination process. However, the presence of soluble Fe²⁺ facilitates •OH regeneration from the dissociation of H₂O₂ through Fenton reaction (Chakma and Moholkar, 2013). Fe²⁺ is regenerated from Fe³⁺ during sonolysis by reacting with peroxy radicals but it takes a longer time because the rate of ferric iron and hydroperoxy is too small (Ricco and Naddeo, 2011).

The micro mixing effect of ultrasound provides enhanced interaction of reactive species and pollutants through micro turbulence and microstreaming resulting in better utilization of the radicals generated from either Fenton process or from the cavitation event for the destruction of compound (Chakma and Moholkar, 2013). However, excess concentration of H₂O₂ in the medium could have adverse effect on degradation as the •OH radicals generated

by either cavitation bubbles or Fenton reactions can get converted to molecular species due to scavenging action of H_2O_2 through following reactions (Chakma and Moholkar, 2013):



When sonolysis and Fenton are applied together, there are several advantages and drawbacks of the mechanism. The most obvious advantage of the reaction is the formation and utilization of $\bullet\text{OH}$ radicals through the interaction of two AOPs. However, being extremely reactive, these radicals may not penetrate or diffuse through the bulk medium. Therefore, if the concentration of pollutant in the solution is too low, the probability of interaction between the radical and pollutant molecule is also low, and under these circumstances it is very likely that the $\bullet\text{OH}$ radicals would recombine to form hydrogen peroxide.

2.2.4. Ultrasonic Production of Nanoparticles

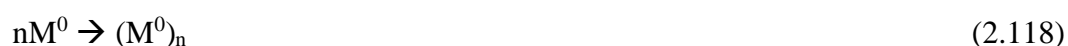
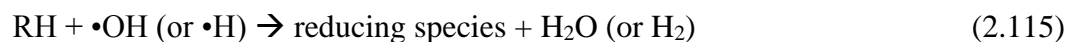
There are a great number of different methods for the production of nanomaterials, these are regarded as the chemical and engineering materials of the future (Mason, 2003). Among a variety of methods, the utilization of ultrasound for material synthesis has received special attention as one of the most powerful tools in nanostructured material synthesis via their ability to provide very small dimensions as 2-50 nm (Ashokkumar and Grieser, 2002; Bang and Suslick, 2010).

The most important parameters that makes ultrasound effective in nanoparticles synthesis are (Gedanken, 2004; Mason, 2003):

- i. no chemical reducing agent (except the stabilizer)
- ii. production of very small metal particles
- iii. production of amorphous state nanoparticles giving important properties effective in catalysis, magnetism, coatings etc.
- iv. the shorter reaction time

- v. the insertion of nanoparticles into the pores of mesoporous materials without blockage of the pores
- vi. reactions at room temperature

The method involved the reduction of the metals via a variety of primary and secondary radicals that is generated upon the formation, growth and violent collapse of acoustic cavity bubbles (Mizukoshi et al., 1999). The basis of the process is the medium which provides the conditions for the reduction of the metal by the sonolysis of water generating HO• radicals to act as reductants, and the presence of organic additives to produce a secondary radical species, which can significantly promote the reduction rate (Bang and Suslick, 2010; Mizukoshi et al., 1999):



where: M^{n+} corresponds to a metal ion and RH to an organic additive. Reactions 2.112-2.119 show the formation of those reducing agents: i) $\bullet\text{H}$ from pyrolysis of water inside the collapsing cavity bubbles, ii) H_2 from the reaction of RH with $\bullet\text{OH}$ or $\bullet\text{H}$, and iii) secondary radicals such as $\bullet\text{R}$ from pyrolysis of RH. In the presence of these species the metal salt is readily reduced to the zero-valent form (M^0), which is then converted to various forms such as M^0_{n+1} via adsorption onto a species like M^0_n .

Preparation of metallic nanoparticles by sonochemical techniques is closely related to the ambient and applied conditions, such as temperature, contact time, metal concentration, frequency, and organic additives (Caruso et al., 2002). Various forms of nanostructured

metals, oxides, sulfides and carbides can be prepared simply by changing reaction conditions as shown in Figure 2.9 (Bang and Suslick, 2010). The type and concentration of dissolved gases in solution effects the rate of reduction giving faster rates in the presence of monoatomic gas molecules owing to the higher polytrophic gas ratios (C_p/C_v) that lead to higher collapse temperatures (Okitsu, 2011). For example, the rate of sonochemical reduction of Au(III) in the present of various gases was found to alter in the order: $CH_4=CO_2 \ll N_2 < He < Ne < Ar < Kr$ (Okitsu, 2011). The organic additives (RH), which function as stabilizers are generally alcohols, surfactants and water soluble polymers (Mizukoshi et al., 1999). The particle size is inversely proportional to the concentration of the stabilizer (e.g. an alcohol) and the alkyl chain length (Caruso et al., 2002). This is related to the fact that alcohols adsorbed on the surface of metal nuclei restrict the enlargement of particle size via stabilization (Bang and Suslick, 2010). The reduction efficiency is also related to the applied frequency, which plays a critical role in controlling particle size (Okitsu et al., 2005).

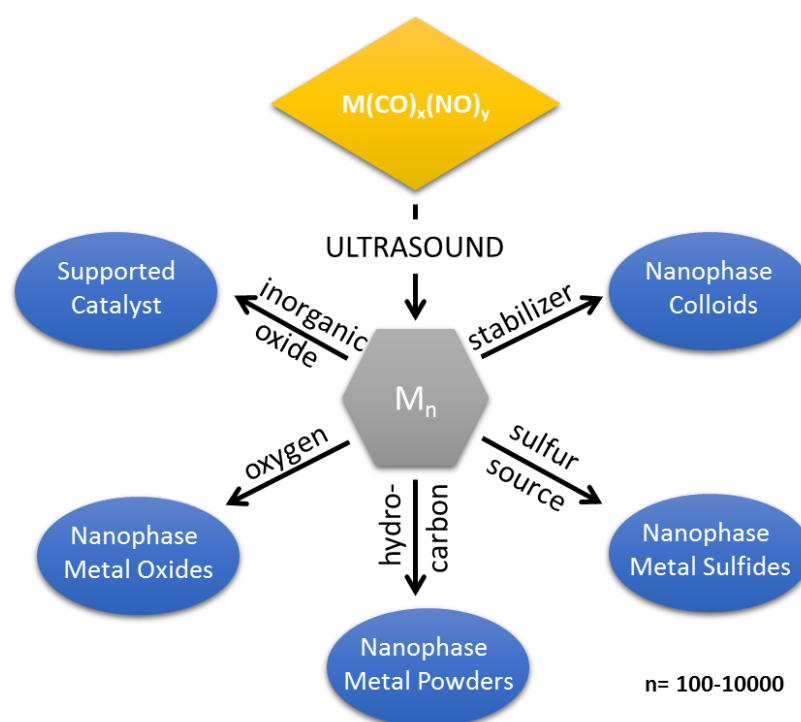


Figure 2.9. Sonochemical synthesis of various nanostructured inorganic materials (Bang and Suslick, 2010).

2.3. Catalytic Processes

2.3.1. Sonocatalysis

Heterogeneous chemistry involving solids and metals have been found successful due to mechanical impact of ultrasound illustrated in Figure 2.10. In general, there are two types of reaction involving solid/liquid interfaces: i) in which the solid is a reagent and is consumed in the process and ii) in which the solid-metal functions as a catalyst (Mason, 1999). When the solid particulates exist in cavitation, it can produce a variety of effects on the size and type of material including mechanical disaggregation and dispersion of loosely held clusters, the removal of coatings by abrasion, and improved mass transfer to the surface (Mason, 1999). The mechanical effects of ultrasound in heterogeneous systems are as follows (Mason and Peter, 2002):

- i. breaking up of hard oxide layers on soft metals by plastic deformation of the surface
- ii. removal of oxide layers on hard metals
- iii. removal of impurities on the solid surfaces
- iv. breaking up of the surface structure allowing the penetration of reactants and/or release of materials from surface
- v. reduction of particle size and increase of surface area via degradation of large solid particles due to shear forces induced by shock waves and microstreaming
- vi. production of collisions of particles smaller in size than a cavitation bubble via microstreaming
- vii. better mass transfer by accelerated motion of suspended particles
- viii. erosion of solid surfaces due to shock waves and/or jetting
- ix. intensification of mass transfer from and onto the surface microstreaming
- x. reduction of induction time
- xi. production of a large number of tiny bubbles due to asymmetrical collapse of cavitation bubble on the solid surface
- xii. decomposition of H_2O_2 on the solid surfaces

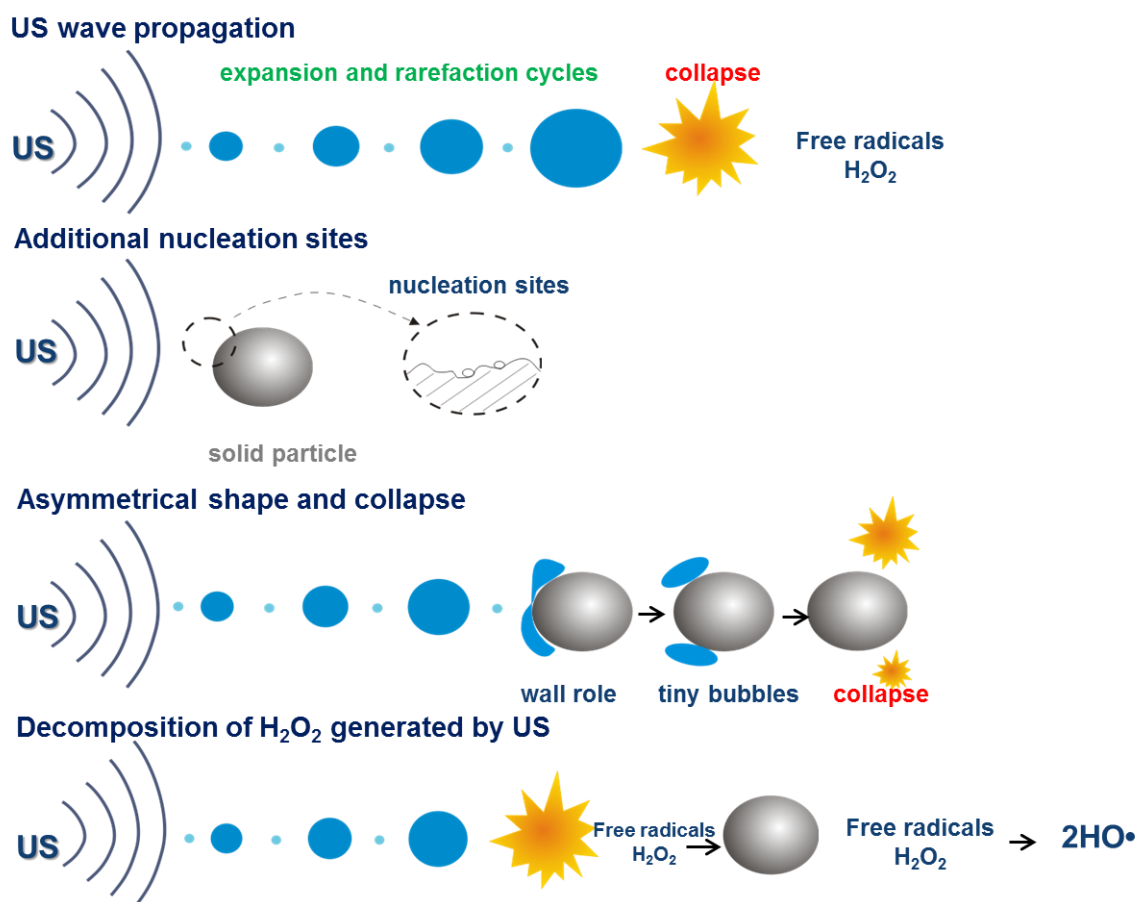


Figure 2.10. The physical and chemical effects of heterogeneous cavitation (adapted from <http://www.scs.illinois.edu/suslick/sonochemistry.html>).

2.3.2. Catalytic Ozonation

Catalysts are substances used to accelerate the rate of chemical reactions following the adsorption of reactant molecules on the surface of certain materials such as metal oxides, activated carbon, zeolites, etc. (Beltran, 2004). The active surface area of some materials which is generally supported in a porous material (i.e. alumina) with internal surface area may be used to increase the rate of ozonation (Beltran, 2004). The main function of catalysts is to i) act as adsorptive material to adsorb and then remove the organic pollutants, ii) provide active adsorptive site and combine with molecules to form active complexes with lower activation energy (Kasprzyk-Hordern, 2003). Therefore, these functions of the catalyst provides i) simply oxidation of the pollutants by gaseous and aqueous ozone or by $\text{HO}\cdot$ in solution, ii) further oxidation of the intermediates on the surface of catalysts, or desorption

from the surface to the aqueous solution to be oxidized by O_3 or $HO\cdot$ (Kasprzyk-Hordern, 2003).

In water treatment, the catalytic decomposition of ozone is based on the adsorption of ozone on the catalyst surface and the formation of active oxygen species such as ozonide, superoxide or atomic oxygen (Beltran, 2004):

For pH 2 to 6



For pH > 6



Homogenous propagation and termination reactions:



However, some heterogeneous catalytic processes with poor adsorptive ability cannot be explained by the mechanism described above and $HO\cdot$ mediated reactions dominate (Guo et al., 2012). The metal oxide catalysts can increase the solubility of ozone and initiate the ozone decomposition via surface hydroxyl groups of metal oxides to form $HO\cdot$ (Guo et al., 2012). The mechanism of catalytic ozonation with poor adsorptive ability is shown in Figure 2.11. In this system, i) ozone would oxidize metal, ii) organic acids would be adsorbed and then oxidized by an electron-transfer reaction to give again reduced catalyst, and hence iii)

reduced metal could lead to $\text{HO}\cdot$ radical (Guo et al., 2012). The organic radical species, $\text{A}\cdot$ would be then easily desorbed from catalyst and subsequently oxidized by $\text{HO}\cdot$ or O_3 either in bulk solution, or more probably, into the thickness of electric double layer (Guo et al., 2012).

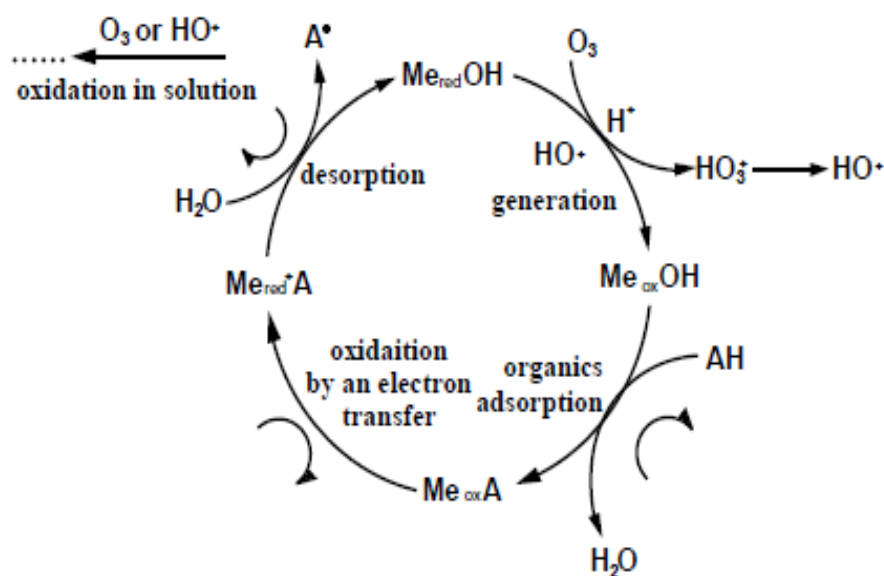


Figure 2.11. The possible mechanism for $\text{HO}\cdot$ or other radical species generation by reaction of ozone with reduced metal of catalyst (Guo et al., 2012).

Alumina and Its Modified Nanocomposites. Alumina has been successfully applied in catalytic ozonation to improve the efficiency of ozonation (Ikhlaq et al., 2012; Kasprzyk-Hordern et al., 2006; Keykavoos et al., 2013) due to promotion of $\cdot\text{OH}$ generation through the surface hydroxyl groups of γ -alumina that provides active catalytic sites for ozone decomposition (Qi et al., 2013). The interactions of aqueous ozone with the surface hydroxyl groups of alumina result in the formation of $\text{HO}_2\cdot$, $\text{O}_2^-\cdot$, $\text{O}_3^-\cdot$ and $\text{HO}_3\cdot$ (Ikhlaq et al., 2013). The formation and stability of both $\cdot\text{OH}$ and H_2O_2 is depended on pH of the solution that determines either $\text{HO}_3\cdot$ will exist in the form of its conjugate base ($\text{O}_3^-\cdot$) at basic pH or will react with H_2O to produce $\cdot\text{OH}$ (Ikhlaq et al., 2013). The mechanism of ozonation in the presence of alumina has been proposed in Figure 2.12.

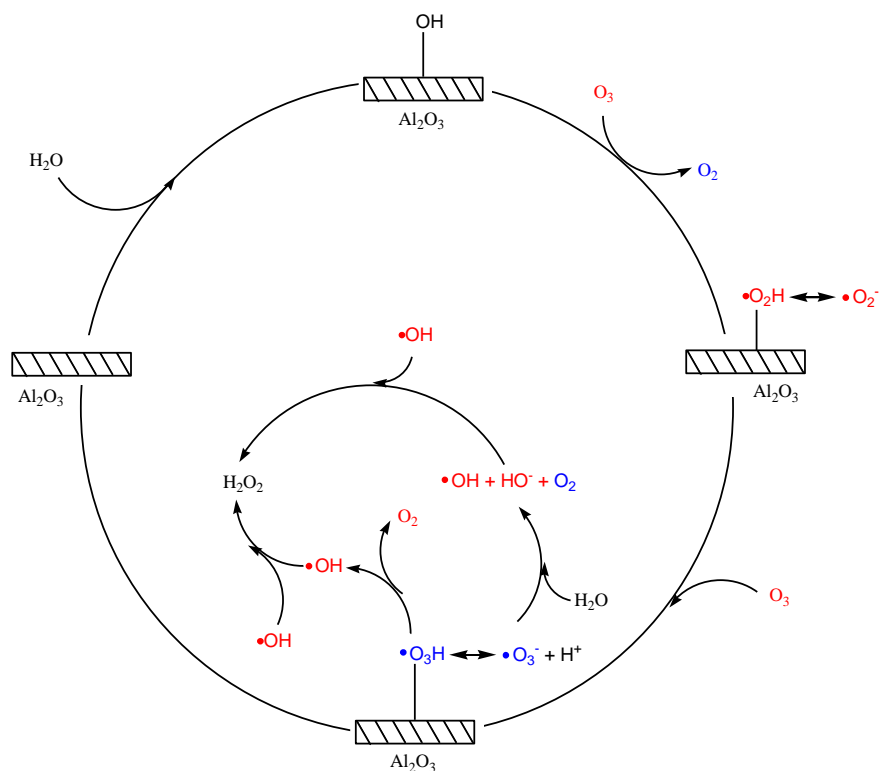


Figure 2.12. The mechanism of catalytic ozonation over alumina (Ikhlaiq et al., 2013).

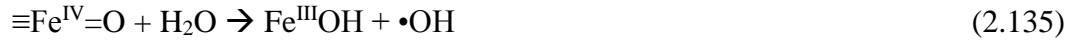
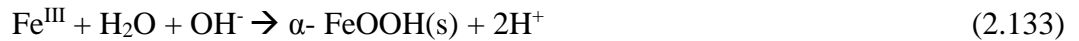
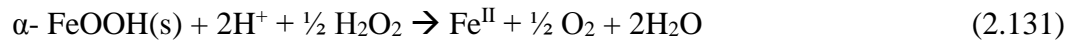
Modified Al₂O₃ Nanocomposites. It has been reported that Al₂O₃ has often been used as a catalyst's support for metals such as Pt, Ru, Rh, Pd, Cu and Ag, which are efficient redox catalysts, to enhance the catalytic activity of alumina and hence to increase the decomposition of gaseous ozone (Lin et al., 2002; Oyama, 2000). A redox catalyst is able to decompose O₂, and the bond between metal and oxygen species which is appropriately strong being favorable for the decomposition of ozone (Lin et al., 2002). It was found that the catalytic activity order of metals supported on Al₂O₃ was Pt > Pd > Ag > Ru ≈ Rh ≈ Ir > Ni > Cd > Mn > Fe > Cu > Zn ≈ Zr whereas the catalytic activity of Co, Y, Mo, Ti and Au was low or negligible (Lin et al., 2002).

2.3.3. Heterogeneous Fenton, Photo-Fenton and Fenton-like Processes

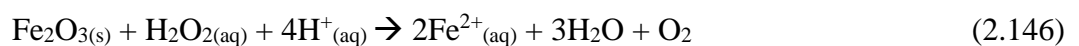
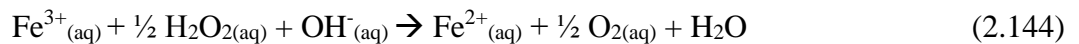
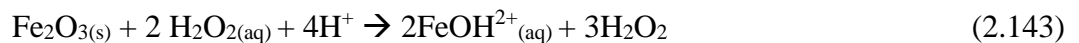
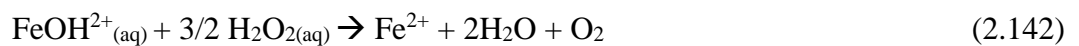
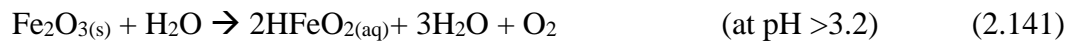
The homogenous Fenton and photo-Fenton processes are eco-friendly and economical processes, however in these processes, the removal of iron from the effluent is difficult (Ameta et al., 2013). Heterogeneous Fenton processes are of interest because most of the iron exists in the solid phase in the system, particularly in granular form such as iron oxides, sand, zeolites, etc. (Wadley and Waite, 2004).

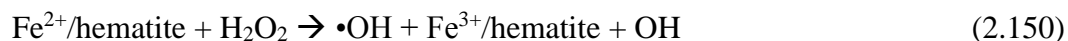
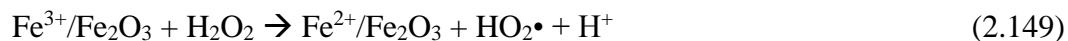
Iron oxides such as lepidocrotite (γ -FeOOH), hematite (α -Fe₂O₃), limonite (FeO(OH)·nH₂O), magnetite (Fe₃O₄), goethite (FeO(OH)), hydroxyl oxides are commonly used in heterogeneous Fenton reaction (Dantas et al., 2006; Huang, 2012; Rodríguez-Gil et al., 2010). The advantage of iron oxides is i) the loss of low amount of mass over a wide pH range, ii) the fast reaction with H₂O₂, iii) increased •OH radical formation through the interaction of H₂O₂ with surface sites, iv) increased reaction rates at higher pH conditions, v) the use over extended periods (Wadley and Waite, 2004). The mechanisms of heterogeneous Fenton reactions for iron oxides are as follows (Araujo et al., 2011; Chan et al., 2015; He et al., 2015; Kuang et al., 2013; Wadley and Waite, 2004):

Goethite

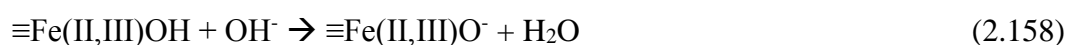
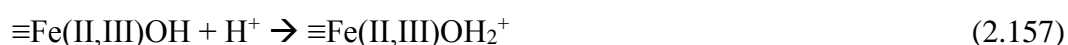
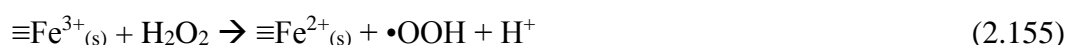


Hematite





Magnetite



2.3.4. Photocatalysis

Photo oxidation, which means oxidation processes occurring at UV/VIS radiation, may be distinguished as i) photo-induced oxidations: ejection of an e^- from the electronically excited substrate leads to the formation of a radical cation of the substrate (RX^*), ii) photo-initiated oxidations: substrate reacts with transient and reactive species that is formed from electronically excited precursor molecule such as H_2O_2 and/or O_3 , iii) photo oxygenation reactions: oxygen-containing reactive species formed by reactions of photo chemically produced radicals or ions with ground state molecular oxygen ($^3\text{O}_2$) via intermediary peroxy radicals ($\text{R-O-O}\cdot$) (Oppenlander, 2003). The most common chemical reaction pathways followed by excited state is as follows (Stefan, 2004):





Organic pollutants (RX) may undergo different reaction mechanisms in the presence and absence of dissolved oxygen resulting in the formation of peroxy ($R-O_2\cdot$) and oxyl radicals ($R-O\cdot$) due to reaction of carbon centered radical ($R\cdot$) with dissolved oxygen (Stefan, 2004). Moreover, in the presence of natural organic matter (NOM) some primary and secondary reactive species such as molecular singlet oxygen (1O_2), peroxy radicals ($R-O_2\cdot$), hydroperoxyl and superoxide anion radicals $HO_2\cdot/O_2^{\cdot-}$, hydroxyl radicals ($\cdot OH$), hydrated electrons (e^-), carbonate radicals ($CO_3^{\cdot-}$), ozone and H_2O_2 in the light-induced process may be produced (Stefan, 2004).

A photocatalyst is a species that induces photochemical reactions and photo catalysis is based on the activation of the photo catalyst in the presence of light (Ameta et al., 2013). The activation is achieved with the absorption of a photon by the photo catalyst, which is basically semiconductor particle, promoting an electron (e^-) from valance band (VB) to the conduction band (CB), creating holes (h^+) in the VB, and thus generating e^-/h^+ pair (Ameta et al., 2013). The e^- is used for the reduction of a substrate whereas h^+ can be utilized for oxidation. Photocatalysis can be categorized to: i) photo generated catalysis and ii) catalyzed photolysis as illustrated in Figure 2.13.

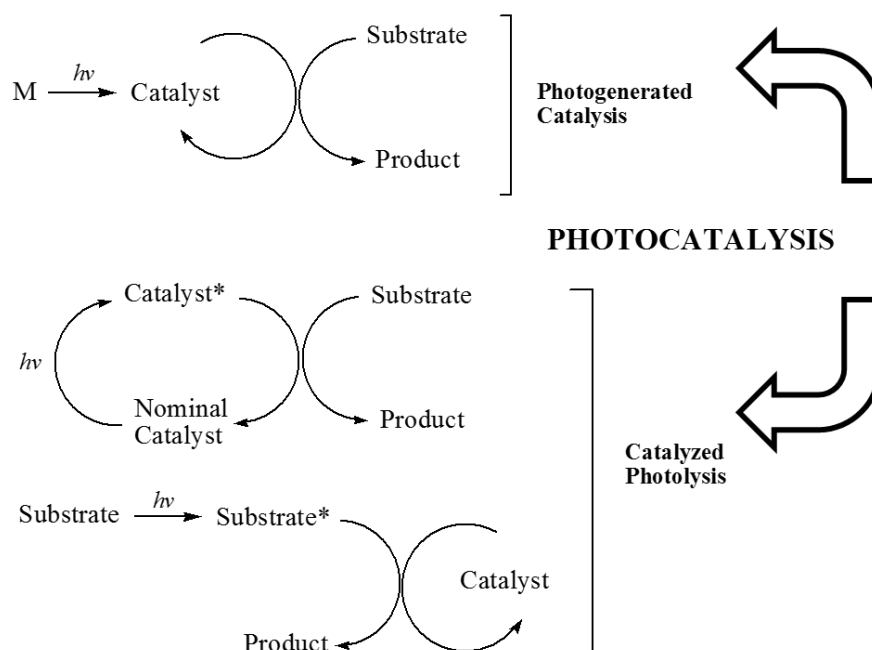


Figure 2.13. The classification of photo catalysis (Oppenlander, 2003).

In catalyzed photolysis either the catalyst molecule or the substrate molecule or both, are in an electronically excited state which produced via photon absorption by a nominal catalyst such as TiO_2 (Oppenlander, 2003). In these systems, continuous irradiation is required to maintain catalytic cycle (Oppenlander, 2003). The photocatalytic oxidation where the promotion of an electron from the valance band to the conduction band occurs at the irradiation of a semiconductor with a light greater than or equal to the band gap energy and photo excited electron leaves behind a positive hole in the valance band as shown in Figure 2.14 (Byrne and Fernandez-Ibanez, 2013).

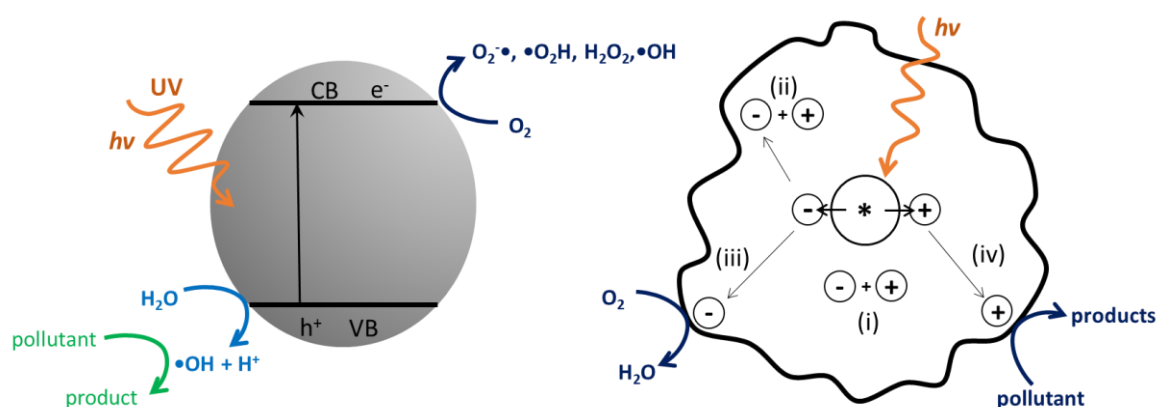


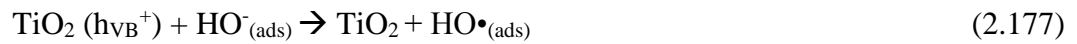
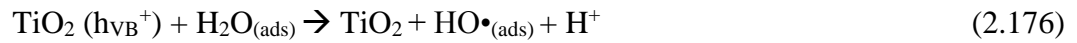
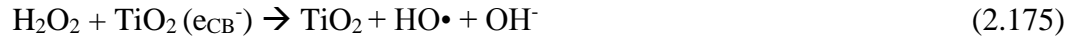
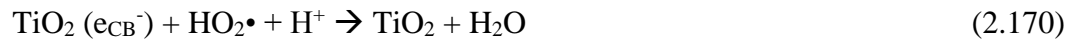
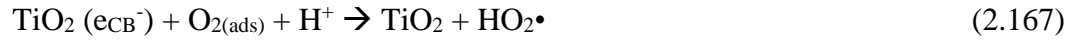
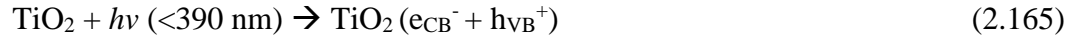
Figure 2.14. Schematic diagram of the mechanism of semiconductor photo catalysis.

The processes represents i) e^-/h^+ recombination in the bulk, ii) e^-/h^+ recombination at the surface, iii) direct/indirect reduction of O_2 or oxidizing intermediates by the photo generated e^- at the surface, iv) direct/indirect oxidation of pollutant, or an oxidized intermediate by the hole at the surface (adapted from (Byrne and Fernandez-Ibanez, 2013; Andrew Mills and Lee, 2004)).

The charge conduction occurs via the valance band hole and the conduction band electron namely electron-hole pair. The positive hole is able to oxidize water or hydroxyl groups to yield $HO\bullet$ that attack organic compounds at near the particle-solution interface (Byrne and Fernandez-Ibanez, 2013). In water treatment, the most common electron acceptor is molecular oxygen whose electron reduction yields a superoxide radical anion ($O_2^{\bullet-}$), hydroperoxy radical ($HO_2\bullet$) or hydrogen peroxide (H_2O_2) and as electron reduction progresses hydroxyl ion (OH^-) and $HO\bullet$ are formed (Byrne and Fernandez-Ibanez, 2013). Photocatalytic processes lead to complete mineralization of the substrate due to decomposition of oxidation byproducts with oxidative surface reactions via fast adsorption/desorption equilibria (Oppenlander, 2003). In water treatment, the amount of semiconductor is one of the main parameters in heterogeneous photocatalytic processes which directly effects the efficiency of mineralization proportional to the catalyst concentration (Badawy et al., 2009).

Titanium Dioxide and Its Modified Nanocomposites. Titanium dioxide (TiO_2) is one of the popular materials used as a photo catalyst in advanced photochemical oxidation processes for environmental remediation due to its ability to remove organic contaminants from various media by the light activation (Mansoori et al., 2008). TiO_2 nanoparticle has the advantage of availability, high photoconductivity, high photo stability, low cost and low toxicity as well as its semiconducting property (Mansoori et al., 2008; Watlington, 2005). When a photo catalyst is illuminated by the light with energy greater than the band gap energy of the photo catalyst results in a charge transfer process leading to the movement of an excited electron from the valence band to the conduction band. The band gap energy for TiO_2 is 3.2 eV and it is translated to the light with a wavelength shorter than 387.5 nm (Watlington, 2005). The main reaction mechanism is based on the formation of e^-/h^+ pairs upon irradiation of light energy exceeding the band gap energy ($E_{hv} \geq E_{bg} = 3.2 \text{ eV}$), formation of reactive oxygen species (ROS) via reaction of TiO_2 with electron acceptors (i.e. O_2) and

the reactions at hole with adsorbed species and the substrate (RX_{ads}) (Bekbolet, 2011; Kansal et al., 2013):



In water treatment, pH of solution significantly affects the properties of semiconductor such as the surface charge on the particles, the size of aggregates, the energies of the conductance and the valence bands (Byrne and Fernandez-Ibanez, 2013). TiO_2 in water is amphoteric like other suspended metal oxides and hydroxyl groups on the surface undergoes acid-base equilibria resulting in $pK_a = 6.25$ which implies that the adsorption of anionic species favors $pH < 6.25$ and cations at $pH > 6.25$ (Byrne and Fernandez-Ibanez, 2013).

The main problem that limits the application of photocatalytic processes in the presence of TiO_2 is the rapid recombination of photo-generated e^-/h^+ pairs and the non-selectivity of the system (Mansoori et al., 2008). The photocatalytic activity may be influenced by the

crystal structure, surface area, size distribution, porosity, bandgap and surface hydroxyl group density of the semiconductor (Sakthivel et al., 2004). One of the most appropriate alternatives to improve the efficiency of TiO₂ is the modification of TiO₂ surface with other semiconductors or noble metals to alter the charge-transfer properties and the energetic situation of surface states between TiO₂ and the surrounding environment (Ahmed et al., 2014; Mansoori et al., 2008). Modifying the surfaces of the photo catalyst with metals such as platinum, copper, silver, palladium, and gold has become an increasingly popular application to improve decontamination rates of TiO₂ inducing a sensitivity and subsequent response to visible light as well as suppressing e⁻/h⁺ recombination process and thus accelerating •OH formation (Sakthivel et al., 2004; Watlington, 2005).

The presence of noble metals on the TiO₂ surface leads to i) an increase of the surface barrier via formation of the Schottky barrier by the electron transfer from the conduction band of TiO₂ to the conduction band of the metal, ii) an increase of the efficiency of the electron-hole separation acting as electron scavenger and ultimately exhibiting the enhancement of the photo reactivity (Ahmed et al., 2014; Sakthivel et al., 2004; Xu et al., 2002). However, the presence of metal on the TiO₂ surface may also reduce the number of the surface hydroxyl groups leading to the reduction of the photo reactivity (Choi et al., 1994). The enhancement of photocatalytic activity of TiO₂ supported metal-NPs can be attributed to the different Fermi levels of noble metals which are lower than the conduction band edge of TiO₂ (Hong et al., 2007; Ismail et al., 2010; Li and Qu, 2009). Thus, photo-promoted electrons can be captured by the noble metals, while photo produced holes remain in the semiconductor valence band (Dozzi et al., 2012). Thereby the recombination process is suppressed according to the following equations (Ahmed et al., 2014; Vijayan et al., 2010):



The general mechanism of photocatalytic process of metal supported TiO₂ under O₂ is given in Figure 2.15.

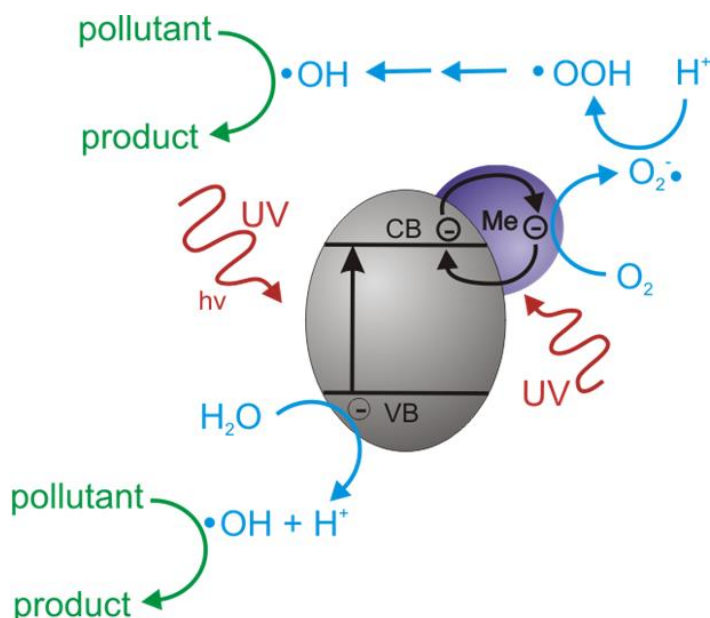


Figure 2.15. The general mechanism of photocatalytic process of metal supported TiO₂.

2.4. Occurrence, Fate and Elimination of Analgesic and Anti-inflammatory Pharmaceuticals

This section aims to present the highlights of the review article published in Journal of Hazardous Materials 187 (2011) 24-36 titled “The occurrence and fate of anti-inflammatory and analgesic pharmaceuticals in sewage and fresh water: Treatability by conventional and non-conventional processes” which is about the occurrence, fate and treatability of analgesics in water by conventional and advanced methods.

2.4.1. Emerging Pollutants in the Environment: Analgesic and Anti-inflammatories

A significant portion of pharmaceutical wastes in wastewater is composed of anti-inflammatory and analgesic drugs, which are used as pain relievers and inflammation reducers, respectively (Fent et al., 2006). Both groups of chemicals are extensively used without prescription with an estimated annual consumption of several hundred tons in

developed countries (Daughton and Ternes, 1999). Physical and chemical properties of some a-PhACs are presented in Table 2.1. and Table 2.2.

Table 2.1. Physical and chemical properties of some common analgesic and anti-inflammatory pharmaceuticals (Jones et al., 2005; Han et al., 2006; Huber et al., 2005; Kim and Tanaka, 2009; Lindqvist et al., 2005; Moldovan, 2006; Scheytt et al., 2005b; Vieno et al., 2006, 2007).

Drug	Molec. Weight (g m⁻¹)	Vapor Pressure (mm Hg)	Solubility (mg L⁻¹)	pK_a (20 °C)
Diclofenac (DCF)	296.2	6.14x10 ⁻⁸	50000	4.1-4.5
Ibuprofen (IBP)	206.3	1.86x10 ⁻⁴	21	3.5-4.9
Naproxen (NPX)	230.3	1.27x10 ⁻⁶	144	4.2-4.5
Ketoprofen (KTF)	254.3	1.46x10 ⁻⁶	51	4.5
Mefenamic (MEF)	241.3	5.83x10 ⁻⁹	20	4.2
Fenoprofen (FNF)	242.3	4.78x10 ⁻⁵	43.65	7.3
Paracetamol (PCT)	151.2	5.20x10 ⁻⁶	1400-2400	2.3
Acetylsalicylic acid (ASA)	180.0	6.56x10 ⁻⁵	4600	3.5

Table 2.2. Physical/chemical and aquatic toxicity properties of some common analgesic and anti-inflammatory pharmaceuticals (Boyd et al., 2003; Camacho-Munoz et al., 2010; Cleuvers, 2004; H. Jones et al., 2005; Henschel et al., 1997; Huber et al., 2005; Kim and Tanaka, 2009; Scheytt et al., 2005a; Tixier et al., 2003).

Drug	log K_{ow}	Henry's constant (at m³ m⁻¹)	EC₅₀ (mg L⁻¹)	
			<i>Daphnia</i>	Algae
DCF	1.9-4.5	4.7x10 ⁻¹²	22- 68	72
IBP	2.5-4.0	1.5x10 ⁻⁷	9-101	342
NPX	3.2-3.3	3.4x10 ⁻¹⁰	166.3	625
KTF	3.1	2.1x10 ⁻¹¹	164	248
MEF	5.1	1.7x10 ⁻⁸	-	4.33
FNF	3.9	1.3x10 ⁻⁸	-	32
PCT	2.0	6.4x10 ⁻¹³	50	133
ASA	1.2	1.9x10 ⁻⁹	88	107

In the following is given brief description and environmental significance of the above a-PhACs:

Diclofenac (DCF). DCF (2-[2,6-dichlorophenyl]-amino]benzeneacetic acid) is a highly consumed AI and very commonly used in ambulatory care (Buser et al., 1998). It is readily metabolized to hydroxylated (4'-hydroxy-DCF; 4'5-dihydroxy-DCF; 3'-hydroxy-DCF; 5'-hydroxy-DCF) or methoxylated derivatives (3'-hydroxy-4'-methoxy DCF) and further conjugated to glucuronides (Buser et al., 1998; Stülten et al., 2008). The presence of these metabolites in sewage treatment plant effluents signifies their potential to transfer to surface waters and threaten aquatic life forms. DCF has the highest acute aquatic toxicity within the class of ANs and AIs (Fent et al., 2006) and microorganisms that usually comprise of lotic biofilms are inhibited by concentrations around $100 \mu\text{g L}^{-1}$ (Paje et al., 2002). Moreover, ingestion of DCF by birds while scavenging on livestock results in death shortly after exposure (Stülten et al., 2008). The presence of $1 \mu\text{g L}^{-1}$ DCF has been reported to damage the liver and kidney cell functions in fish (Triebkorn et al., 2004).

Ibuprofen (IBP). IBP is commercially available as 2-(4-isobutylphenyl) propionic acid, and used widely in the treatment of rheumatic disorders, muscular pain and fever (Hutt and Caldwell, 1983; Méndez-Arriaga et al., 2008). It is a non-steroidal, antipyretic (lowering elevated body temperatures without impairing consciousness) drug that is recognized with a huge global consumption rate (Buser et al., 1999). IBP is rapidly excreted in form of various conjugates, e.g. hydroxy-IBP, carboxy-IBP, and carboxy-hydratropic acid (Buser et al., 1999; Méndez-Arriaga et al., 2008), which not only have high acute toxicity, but are also suspected of endocrine disrupting activity in human and wildlife (Buser et al., 1999).

Naproxen (NPX). NPX (6-methoxy- α -methyl-2-naphthalene acetic acid) is a non-steroidal anti-inflammatory drug widely used in mild-to-moderate pain relief and in treating *oestropause*, rheumatoid arthritis, menstruation and headaches (Boynton et al., 1988). The drug is additionally used in veterinary medicine in appreciable quantities (Boynton et al., 1988). Bioassay tests have shown that chronic toxicity of NPX is higher than its acute toxicity, and byproducts of photodegradation are more toxic than itself (Isidori et al., 2005).
Ketoprofen (KTF). KTF is a non-steroidal anti-inflammatory drug with analgesic and antipyretic effects and classified under acidic drugs because of the presence of a carboxylic

group in its chemical structure (Kim and Tanaka, 2009). The drug is metabolized mainly in conjugation with glucuronic acid (carboxylic acid), and excreted in the urine (85%) (Soulet et al., 2002).

Mefenamic Acid (MEF). MEF is another non-steroidal anti-inflammatory drug classified under “anthropogenic” pharmaceuticals and personal care products (Werner et al., 2005). It is a diphenylamine derivative, a pollutant class whose environmental relevance is of significance (Drzyzga, 2003). More than 50% of an ordinary dose of MEF is recovered in the urine mainly as conjugated metabolites (Soulet et al., 2002).

Paracetamol (PCT) or Acetaminophen (ACT). PCT (European trade) or ACT (USA trade) is a mild analgesic that is commonly used in combinatory drugs for the relief of fever, headaches and some minor pains (Holm et al., 1995; Ikehata et al., 2006). It is metabolized in the liver to the sulfate and glucuronide conjugates and excreted in the urine (Johnson and Plumb, 2005). Hence, the source of PCT pollution in surface water is majorly sewage plant effluent (Ternes, 1998), while that in soil and groundwater is caused by consumption of the drug for controlling brown tree snakes (Andreozzi et al., 2003a). The most important side effect of PCT is impairment with the liver and kidneys via the formation of hepatotoxic metabolites such as N-acetyl-p-benzoquinone imine (Fent et al., 2006; Harnagea-Theophilus et al., 1999).

Acetylsalicylic Acid or Aspirin (ASA). ASA is one of the most popular pain killers that is readily degraded to the more active salicylic acid and two other metabolites (ortho-hydroxyhipuric acid and gentisic acid), all of which are easily eliminated in conventional sewage treatment operations (Ternes, 1998). It has been reported that water bodies containing ASA derivatives exhibit high toxicity to a wide range of aquatic organisms (Cleuvers, 2004; Henschel et al., 1997).

2.4.2. Occurrence and Fate of Analgesics and Anti-inflammatory in the Aquatic Environment

World-wide investigations on contamination levels of anti-inflammatory pharmaceuticals such as DCF, IBP, KTF, FNF, MEF, NPX have shown that individual concentrations are within $\mu\text{g L}^{-1}$ range in aquatic and surface water bodies, signifying the high proportion of municipal sewage effluents (Boyd et al., 2003; Buser et al., 1999; Heberer, 2002). This is confirmed in Table 2.3, where a summary of regional variations in concentrations of analgesics and anti-inflammatory pharmaceuticals in influent and effluent of wastewater treatment plant (WWTPs) and surface water is depicted. Note that in water, concentrations lie between 0.001-4.11 $\mu\text{g L}^{-1}$ (Boyd et al., 2003; Carballa et al., 2004; Lindqvist et al., 2005; Tauxe-Wuersch et al., 2005), whereas in WWTP effluents the range is between 0.002-33.9 $\mu\text{g L}^{-1}$ (Andreozzi et al., 2003b; Miège et al., 2009; Zwiener and Frimmel, 2000). Much lower levels in surface water than WWTP effluent is not only due to dilution effect, but also to the probable removal by natural pathways such as hydrolysis, photolysis, sorption and biodegradation. However, there is also evidence that some a-PhAC residues may leach into groundwater aquifers under recharge conditions, as they have been detected in ground water samples from water works downstream of municipal sewage treatment plants (Heberer et al., 2000).

Research on the fate of a-PhACs in receiving waters have shown that many of them and their metabolites undergo transformation via combinations of abiotic and biotic processes (e.g. sorption, biodegradation, chemical degradation, gas exchange, volatilization, hydrolysis) and direct or indirect photo-transformation (Miège et al., 2009; Tixier et al., 2003). The low volatility of these chemicals implies that their distribution in compartments of the environment is governed primarily by aqueous transport mechanisms, and by dispersal of the food chain. In surface waters, some of the residues may also undergo biotransformation, but the extent of conversion by abiotic reactions is still much larger (Fent et al., 2006).

Table 2.3. Country-wise occurrence of analgesic and anti-inflammatory pharmaceuticals in surface water, and influents/ effluents of WWTPs

Drug	Surface Water ($\mu\text{g L}^{-1}$)	WWTP influent ($\mu\text{g L}^{-1}$)	WWTP effluent ($\mu\text{g L}^{-1}$)	Country
DCF	0.020-0.150	-	0.100-0.700	Switzerland
	-	-	0.25-5.45	France, Italy, Sweden
	0.001-0.370	0.470-1.9	0.310-0.930	Switzerland
	n.d-1.03	3.02	2.51	Germany
	-	0.105-4.11	0.035-1.95	France
	0.005-0.49	-	0.005-1.59	Germany
	0.272	2.33	1.561	Germany
	-	2.59	1.97	South Korea
	0.15	3.5	0.81	Germany
	0.02	3.1	1.5	Austria
	0.020-0.150	1.4	0.95	Switzerland
	0.001-0.069	-	-	Germany, Italy
	IBP	0.010-0.400	-	0.100-1.5
-		-	0.02-7.11	France, Italy, Sweden
-		-	0.061-0.115	Romania
n.d-0.201		0.17-83.5	0.002-95	Italy, France
0.05-0.28		5.533	0.05-3.35	Germany
0.002-0.146		0.03	0.07	Germany, South Korea
NPX		0.022-0.107	-	-
	0.010-0.400	-	0.100-3.5	Switzerland
	0.001-0.032	-	0.29-5.22	Germany, France, Italy, Sweden
	n.d-0.037	1.79-611	0.17-33.9	France, Italy, USA
	n.d	0.732	0.261	Germany
KTF	n.d-0.005	-	n.d-0.200	Switzerland
	n.d-0.007	0.08-5.7	0.04-1.62	Italy, France
	0.329	0.321	0.141- 1.62	Germany, France, Italy, Sweden
MFA	-	0.14-3.20	0.09-2.40	France
	-	1.6-3.2	0.8-2.3	Switzerland
PCT	n.d	5.53-292	n.d-0,001	France, USA
		0.07	0.06	South Korea
	0.005-0.066	-	0.140-1.480	Germany
ASA	-	-	0.028-0.037	Romania
	<0.05	-	0.05-1.51	Germany
FNF	0.002-0.054	-	n.d - 0.28	France, Sweden, Germany, Italy

Throughout the literature, it was found that hydrolysis is an insignificant pathway of elimination for environmentally relevant human medicine, and the majority of them is transformed by photo-and bio-degradation processes. It was also found that those human medicine that are incapable of absorbing solar radiation (non-photolabile) are relatively biodegradable, and those that are poorly or partially biodegradable are photo-reactive. IBP

was the only human medicine (within those reviewed in this study) that is characterized by a high sorption coefficient; thus it was the only pharmaceutical that accumulates in sediment layer of surface waters as an additional elimination route (Tixier et al., 2003). Table 2.4 gives a brief summary of the literature on the major metabolic forms of some common a-PhACs and their environmental fate by means of photo- and biodegradation processes.

Table 2.4. Metabolic forms and natural degradation pathways of AIs and ANs in water

Drug	Metabolic forms in water	Environmental fate
DCF	4'-hydroxy DCF, 4'-5'-dihydroxy DCF, 3'-hydroxy DCF, 5'-hydroxy DCF, 3'-hydroxy-4'-methoxy DCF	partial biodegradation photo degradation
IBP	2-[4-(2-hydroxy-2-methylpropyl)phenyl]propionic acid, 2-[4-(2-carboxypropyl)phenyl]propionic acid, carboxy-hydratropic acid (carboxy-HA)	biodegradation sedimentation
NPX	NPX, 6-O-desmethylated metabolite, DM-naproxen	biodegradation photo degradation
KTF	2-(3-benzoylphenyl)-propanoic acid, 2-[3-(3-hydroxybenzoyl)phenyl]-propanoic acid, 2-[3-(4-hydroxy benzoyl) phenyl]-propanoic acid, 2-[3(hydroxy(phenyl)methyl)phenyl]-propanoic acid	partial biodegradation photo degradation
MEF	Alkali-labile ester glucuronides	partial biodegradation
PCT	Sulfate conjugates, paracetamol cysteine, mercapturate	biodegradation
ACA	ACA, salicylic acid, ortho-hydroxy-hippuric acid, gentisic acid	biodegradation

2.4.3. Elimination of Analgesic and Anti-inflammatory Pharmaceuticals in WWTPs

The removal of PhAC residues in municipal wastewater treatment plants is a major challenge in reducing the emission of micro pollutants to the aqueous environment. As the activated sludge process (AcS) has been the most common unit operation in municipal WWTPs, the majority of research on treatability of PhACs in WWTPs is focused on this process and its relative efficiency.

The performance of AcS for analgesic and anti-inflammatory pharmaceutical removal varies from “very poor” to “complete” break-down (Kulik et al., 2008). Although the mechanism is not clear, there is consensus on processes such as sorption, adsorption,

sedimentation and biotransformation. Sorption process is ineffective for acidic drugs ($4.2 < pK_a < 4.9$) such as ASA, IBP, FNF, KTF, NPX and DCF that are highly hydrophilic and remain in the aqueous phase (Nikolaou et al., 2007). For such chemicals, biodegradation is expected to be a more potent elimination pathway in aerobic or anaerobic zones of the activated sludge. Nevertheless, common sewage treatment operations are found insufficient for complete or appreciable elimination of these pharmaceuticals from sewage water (Ternes, 1998). Some of them are reported to be released in a modified form after treatment in AcS units; such as for example IBP, which is largely (90%) transformed to its hydroxy and carboxy derivatives (Nikolaou et al., 2007). This is important because the metabolites may later be hydrolyzed and converted to the parent compound (Bendz et al., 2005).

The efficiency of a-PhACs elimination in municipal WWTPs is also related to the seasonal conditions and design/operation of the secondary treatment plant (e.g. hydraulic retention time, sludge age) (Nikolaou et al., 2007; Tauxe-Wuersch et al., 2005). Accordingly, the efficiency is lower during winter months because of heavy rainfall and low water temperature, both of which lead to slower rates of biodegradation (Buser et al., 1998; Vieno et al., 2005). In addition, elimination of some chemicals like NPX, IBP and KTF is sharply reduced at the end of October as a consequence of reduced atmospheric temperature (lower reaction rates), increased health problems (cold, flue, rheumatic pains) leading to enhanced consumption or excretion of the drugs that probably exceed the capacity of the plants (Tixier et al., 2003). Such problems can be resolved by operation of the plant at longer hydraulic retention times for a period until the concentration of the drugs in the sewage becomes stable again. Another significant operation parameter in WWTPs is pH, the value of which is particularly critical for those pharmaceuticals characterized by increasing water-sludge partition coefficients with elevated acidity (Urase and Kikuta, 2005). A more detailed information on the treatability of a-PhACs can be found in our review article (Ziylan and Ince, 2011).

2.4.4. Overview of the Treatability of Some Common a-PhACs in in WWTPs

DCF is eliminated by 0-75 %, and 21-50 % degradation is obtained in AcS plants operated at very different anoxic-oxic ratios (Joss et al., 2005; Nikolaou et al., 2007; Zhang et al., 2008). The low efficiency is due to low biodegradability of the compound arising from

the presence of -Cl and N-H functional groups that inhibit the rate of growth of sewage bacteria (Nikolaou et al., 2007).

IBP is the most efficiently eliminated a-PhAC (60-100%) in WWTPs, with 12 to 45 % removal in primary sedimentation tanks (Jones et al., 2005; Tauxe-Wuersch et al., 2005; Tixier et al., 2003). Further elimination of the compound (>90%) is possible by extending the AcS system to allow nitrification and denitrification (N/DeN) (Jones et al., 2005). In general, the mechanism of IBP elimination involves transformation of the parent drug to its hydroxyl and carboxyl derivatives followed by rapid degradation of the latter. The hydroxyl derivative is, however, much more stable and may later be hydrolyzed to yield the parent compound again (Nikolaou et al., 2007; Remberger et al., 2009).

NPX is significantly removed (50-80%) in AcS units operated with N/DeN and further eliminated by sand filtration (SF) of the effluent (Joss et al., 2005). In some cases, however, the WWTP effluent is found to contain a higher concentration of the parent drug than the influent, which is attributed to the presence of large concentrations of hydrolysable conjugates in the sewage system (Lindqvist et al., 2005). Elimination of NPX in AcS plants may be considerably improved by operating them at hydraulic retention times longer than 12-h (Jones et al., 2005).

KTF removal in WWTPs is sensitive to external perturbations as rain, and the average range reported for conventional systems is 15-98% (Lindqvist et al., 2005; Tauxe-Wuersch et al., 2005). Maximum elimination occurs during primary sedimentation of coagulation/flocculation effluent (Tauxe-Wuersch et al., 2005) and biotransformation starts only after 28 days of sludge retention time in the activated sludge reactor (Quintana et al., 2005).

PCT is relatively stable in AcS, but 99% elimination is possible if AcS treatment is applied after preliminary and final clarification and is extended to N/DeN (Onesios et al., 2009; Ternes, 1998). On the other hand, some researchers have observed almost complete removal of PCT in non-conventional lagoon treatment operations operated with hydraulic detention times of 16.5-48 d (Brun et al., 2006).

2.4.5. The Principles of Advanced Oxidation Processes on Organic Compound Elimination

Over the past 30 years, research on Advanced Oxidation Processes (AOPs) has gained a great attention and found applications as varied as water/wastewater treatment, groundwater treatment, soil remediation, sludge conditioning, and production of ultrapure water and volatile organic compounds treatment and odor control particularly based on two reasons: i) the diversity of technologies involved and ii) the areas of potential application (Klavarioti et al., 2009). Conventional treatment methods are sensitive to many environmental factors, which are often slow and generally cause unpredictable results. An AOP is defined as the aqueous phase oxidation process that generates highly reactive species such as hydroxyl radicals in sufficient quantity to degrade a number of organic and inorganic contaminants including volatile, semi-volatile, and non-volatile compounds (Adewuyi, 2005). The oxidative processes may cause complete mineralization, implying that the final products of degradation reactions are CO₂, short-chain organic acids, and inorganic ions, typically less toxic and biodegradable products (Adewuyi, 2005). Hence, AOPs are often required because conventional treatment methods are not effective for the decontamination of a wide range of contaminants existing in water or wastewater.

However, AOPs are often not cost effective and sometimes is not effective for the total elimination of some refractory organics and hence, it is generally required to apply a combination of oxidation agents, irradiation or catalysts as a mean of generating the excited hydroxyl radicals ($\bullet\text{OH}$), which are more powerful oxidants than conventional oxidizing agents such as molecular O₃ or H₂O₂ to overcome the deficiencies of traditional advanced oxidation methods. In general, AOPs include the homogeneous and heterogeneous systems based on near ultraviolet (UV) or solar visible irradiation, electrolysis, ozonation, the Fenton's reagent, ultrasound, wet air oxidation, ionizing radiation, microwaves, pulsed plasma and the ferrate reagent (Hofmann et al., 2007; Ikhlaiq et al., 2015; Jagannathan et al., 2013; Wang et al., 2009). In this dissertation, homogenous and heterogeneous systems with and without irradiation such as O₃/H₂O₂, O₃/OH⁻, Fenton's reagent H₂O₂/UV, O₃/UV, O₃/H₂O₂/UV, US/H₂O₂, US/UV, US/O₃, O₃/US/UV in the presence and absence of soluble or insoluble catalysts will be considered. The brief explanation of selected AOPs is given below:

2.4.6. Elimination of AIs and ANs in Wastewater Treatment Plants (WWTPs) Integrated with Advanced Processes

Integration of wastewater treatment plants (WWTPs) with advanced treatment processes is a promising strategy for rendering complete elimination of PhAC residues, provided that the most proper treatment units or combinations thereof are applied. Relative effectiveness of some basic or advanced processes such as sand filtration (SF), ozonation, UV irradiation and activated carbon adsorption (ACA) applied to AcS treatment effluent after sedimentation are summarized in Table 2.5.

Among all advanced processes tested, ozonation was found the most effective for complete disappearance of most ANs and AIs in secondary clarification effluent (Huber et al., 2005; Ternes et al., 2003). The reactivity of these chemicals with ozone is related to the functional groups in their structure as well as the operating conditions. Some researchers reported that lab-scale treatment of AcS effluent with $3 \text{ mg L}^{-1} \text{ O}_3$ for 27-min destroys more than 68-99 % of NPX, 54-99 % of MEF and 52-93 % of KTF residues (Huber et al., 2005; Ternes et al., 2003). The degradation of IBP and FNF under the same conditions was highly variable or poor, mainly because of low concentrations of the drugs in AcS effluent and the unfavorable structural properties that lowered their reactivity with ozone. An example to such properties is the presence of a carboxylic group attached to an aromatic ring, which due to the e-withdrawing character depresses the reactions of ozone with the ring carbons. On the other hand, the presence of e-donating functional groups such as -OH facilitates the attack of ozone to aromatic rings, which explains the high degradability of phenolic PhACs by ozonation. In addition, sulfidic groups also react very fast with ozone whereas protonated amino groups are almost non-reactive (von Gunten, 2003). This explains why DCF is efficiently degraded in neutral pH but not so in acidic solutions. Substantial elimination of NPX by ozonation is also a matter of structural character such as a naphthalene moiety, which is highly reactive with molecular ozone ($k = 3.0 \times 10^4 \text{ M s}^{-1}$). Hence, a lower but moderate degree of MEF elimination can be explained by the opposing effects of an e-withdrawing (benzoic acid) and an e-donating group in its structure (dimethylbenzene) (Nakada et al., 2007).

Table 2.5. Relative fractions of ANs and AIs removal in conventional and tertiary treatment units of WWTPs (Carballa et al., 2004; Gagnon et al., 2008; Joss et al., 2006; Nakada et al., 2007; Stumpf et al., 1999; Tauxe-Wuersch et al., 2005; Ternes, 1998; Ternes et al., 2003).

Process/Condition	% Removal						
	DCF	IBP	NPX	KTF	MEF	PCT	ASA
1° Settling*	-	12-45	-	3-12	4-16	-	-
Coag(FeCl ₃)/Floc/Settling*	-	-	-	5-36	21-36	-	-
AcS*	21-50	20-43	-	8	30-50	-	80-98
Bio-membrane (of pretreated eff)	23-87	>90	36-99	50-99	75	99	-
SF (of AcS eff)		30-96	0-48	-	0-99	-	-
Ozonation (of ACs eff)*	96	0.75-62	68-99	52-93	54-99	-	85-95
UV irradiation (250 kJ cm ⁻²)*	29	-	-	-	-	-	-

* Pilot scale

The above discussion highlights the importance of the operation pH on the efficiency of ozonation process for the elimination of AI/AN chemicals in WWTP effluents. If a compound is not reactive with ozone, such as IBP ($k = 9.1 \text{ M s}^{-1}$), it is likely to react strongly with OH radicals (OH•), which are major decomposition products of O₃ at alkaline pH. This is why ozonation at acidic or neutral pH is ineffective for compounds that react slowly with ozone, but that at highly alkaline pH is very effective as in the case of IBP, which reacts strongly with OH• ($k=7.4 \times 10^9 \text{ Ms}^{-1}$). Thus, the observed variability of IBP elimination in Table 2.5 by ozonation of sewage treatment plant effluents is the consequence of variations in the operation pH.

2.4.7. Overview of AN and AI Elimination in Drinking Water Treatment Plants (DWTPs)

The main purpose of DWTP in the past was to remove natural organic matter, hardness and microorganisms from the target source. As the presence PhACs in drinking water has lately been a significant health concern, elimination of such pollution has now become a major challenge, particularly if the source is effluent-dominated surface water. Fortunately, a conventional coagulation process (CG), which is a counterpart of most DWTPs can effectively remove pharmaceuticals with $\log K_{ow} > 5$ (Snyder, 2008). On the other hand, CG is effective for negatively charged anti-inflammatory drugs only if the coagulant is made of trivalent cations that can easily neutralize the charge on the parent drug (Suarez et al., 2009).

Positively charged ionic drugs are more easily eliminated by adsorption (ADS) on particles and by flocks that form upon electrostatic interactions (Vieno et al., 2007). However, sand filtration (SF), which is also a common unit process in DWTPs, renders no significant removal of AN and AI residues due to the low sorption properties and high persistence of most PhACs in water (Fent et al., 2006). It is reported that a rapid sand filter designed to remove excess flocks after sedimentation can eliminate an additional 10 % of DCF, IBP, NPX and KTP (Vieno et al., 2007). Oxidative degradation of PhACs in disinfection units of DWTPs such as chlorination, ozonation, and UV irradiation is limited by the functional groups and reactivity of the drugs with the oxidant. For example, DCF and NPX can be almost totally eliminated by chlorination, while IBP is only transformed to a variety of intermediate products (Boyd et al., 2005). DCF and NPX are also eliminated considerably by ozonation (>95%) owing to the amine functional groups in their structure (Benotti et al., 2009; Huber et al., 2003; Ternes et al., 2002), while IBP is not unless the reaction is run at acidic pH to promote the generation of OH radicals, which are by far more reactive than ozone. Unfortunately, the intensity of UV irradiation applied commonly in disinfection units of DWTPs is too low to render photo-transformation of even the UV-absorbing PhACs (Vieno, 2007). It was found that complete elimination of some PhAC residues (e.g. DCF) by UV treatment is possible only under extensive irradiation at pH 6-8 and at an intensity that is at least 25-fold larger than that applied in DWTPs (Gagnon et al., 2008).

Finally, advanced treatment of DWTP effluent in granular activated carbon units (GAC) has been found very effective, particularly for the elimination of non-ionic and hydrophobic pharmaceuticals with high K_{ow} (S. D. Kim et al., 2007; Snyder, 2008; Ternes et al., 2002; Westerhoff et al., 2005). The elimination of PhAC residues containing carboxyl groups (e.g., DCF, IBP and NPX) is less effective in GAC units due to deprotonation of the acidic functional group (Vieno et al., 2007; Zwiener and Frimmel, 2000). Relative fractions of PhAC elimination in some unit operations of DWTPs are summarized in Table 2.6.

2.4.8. Advanced Oxidation Processes (AOPs) as Viable Options for Destroying PhAC Residues in WWTP and DWTP Effluents

AOPs are based on the in-situ generation of very powerful oxidizing agents as the hydroxyl radical, which is highly reactive with a wide range of organic compounds

regardless of their concentration (Ince, 1999). Unlike many other oxidizing species, $\text{OH}\cdot$ is nonselective and readily attacks most organic compounds to convert them to less complex and less harmful intermediates. At sufficient contact time and proper operation conditions, AOPs may mineralize all organic carbon to CO_2 , which is the most stable end product of chemical oxidation.

Table 2.6. The fate of most common ANs/AIs in unit processes of DWTPs (1-4); further elimination in effluents or fresh water surface by photolysis (5) (Benotti et al., 2009; Canonica et al., 2008; Kim and Tanaka, 2009; Ternes et al., 2002; Vieno et al., 2006, 2007; Westerhoff et al., 2005).

Process/ Condition Compound	Fate or removal (%)			
	DCF	IBF	NPX	PCT
1. Coagulation (CG)				
$\text{Fe}_2(\text{SO}_4)_3$	66	<20		
$\text{Al}_2(\text{SO}_4)_3$		<20		
2. Sand Filtration (SF)				
(of CG effluent)	10	10	10	
3. GAC	39	16	52	72-93
4. Disinfection (DIS)				
Cl_2 (3-3.8 mg L^{-1})	80-95	0	80-95	
O_3 (1.2-1.5 mgL^{-1})	>99	92	75	
5. Photolysis (surface water)				
Solar	4			
254 nm (0.4 kJm^{-2})	97-100		29	

The most important advantage of AOPs over chemical/biological processes is that they are environmental-friendly or “green” as they neither transfer pollutants from one phase to the other as in chemical precipitation, adsorption and volatilization; nor produce massive amounts of hazardous sludge as in bio-chemical processes (Ince and Apikyan, 2000). Application of single or combined AOPs before or after bio-treatment operations may considerably reduce the concentration of PhAC residues in effluents of DWTPs and WWTPs via mineralization of organic carbon and enhancement of biodegradability, respectively. Note that AOPs are further important for the destruction of multi-resistant bacteria that may develop in wastewater bodies containing very low concentrations of PhACs (Kümmerer, 2001; Schwartz, Thomas; Kohnen, Wolfgang; Jansen, Brend; Obst, 2003).

The most common AOPs developed for water and wastewater remediation are listed in Table 2.7. Some of these processes are commercially available, e.g. UV photolysis, which has more than 3000 applications in Europe and a large number in the US (Parsons and William, 2004). Others such as Fenton's, super-critical oxidation, ionizing radiation and combinations of H₂O₂, O₃ and UV have all been used at full scale. The only AOPs that have no full scale applications so far for water remediation are photo catalysis and ultrasound.

Table 2.7. Most common AOPs for water and wastewater treatment (Parsons and William, 2004).

Advanced Oxidation Processes	
Photochemical	Other
UV oxidation	Ozonation
UV/H ₂ O ₂	Fenton
UV/O ₃	Ultrasound (US)
UV/H ₂ O ₂ /O ₃	US/H ₂ O ₂ , US/O ₃
UV/Ultrasound	Electrochemical oxidation
Photo-Fenton	Supercritical water
Photo catalysis	Ionizing radiation
Sono-photo catalysis	Electron-beam irradiation
Vacuum UV	Wet-air oxidation
Microwave	Pulsed Plasma

Klavariotti et al (2009) have recently published an extensive review on the degradability of a wide range of PhACs and some endocrine disrupting compounds in water by various AOPs (Klavarioti et al., 2009). The following sections, cover a more concise review of the literature on AOPs applied to sufficiently low concentrations of AI and AN chemicals (DCF, IBP, NPX, KTF, FNF and PCT), with emphasis on process details and relative efficiencies. A summary of the discussion is also presented in Table 2.8 (Andreozzi et al., 2003a; Beltran et al., 2004; Canonica et al., 2008; Coelho et al., 2009; Hartmann et al., 2008; Isariebel et al., 2009; Javier Benitez et al., 2009; Kim et al., 2009; Madhavan et al., 2010a; F Méndez-Arriaga et al., 2008; Naddeo et al., 2009a; Pereira et al., 2007; L. a. Pérez-Estrada et al., 2005; Ravina et al., 2002; Rosal et al., 2008; Tezcanlı-Güyer and Ince, 2011; Vogna et al., 2004; Yang et al., 2008).

Table 2.8. Efficiency of lab-scale AOPs for the degradation and mineralization of AI/AN chemicals.

PROCESS System parameters, C ₀ , t	Degradation (Mineralization) %			
	DCF	IBP	NPX	PCT
1.US				
20 kHz, 80 mg L ⁻¹ , 60 min	>55			
213 kHz, 18.5 mg L ⁻¹ , 180 min		(16)		
216 kHz, 50 mg L ⁻¹ , 60 min	87			
300 kHz, 21 mg L ⁻¹ , 60 min		98 (8)		
617kHz, 50 mg L ⁻¹ , 60 min	>90			
850 kHz, 50 mg L ⁻¹ , 60 min	24			
861 kHz, 9.5 mg L ⁻¹ , 60 min	>90 (23)			
574 kHz, 25 mg L ⁻¹ , 240 min				95
574 kHz, 25 mg L ⁻¹ , 480 min				100(39)
574 kHz, 150 mg L ⁻¹ , 240 min				56
2. O₃/US and sonocatalysis				
20 kHz, 31 g h ⁻¹ O ₃ , 80 mg L ⁻¹ , 40 min	(35)			
213 kHz, 1g TiO ₂ L ⁻¹ , 18.5 mgL ⁻¹ , 10 min		23		
213 kHz, 20 mg Fe ²⁺ L ⁻¹ , 19 mgL ⁻¹ , 15 min		45		
861 kHz, 0.09 mg L ⁻¹ NPI*, 9.5 mgL ⁻¹ , 90 min				
300 kHz, Xe-lamp, 100 mgFe ²⁺ L ⁻¹ , 10 mgTiO ₂ L ⁻¹ , 8 mg L ⁻¹ , 240 min		(92)		
3.Ozonation and catalytic ozonation				
31 g O ₃ h ⁻¹ , 80 mg L ⁻¹ , 40 min	(22)			
36 g O ₃ h ⁻¹ , 32 mg L ⁻¹ , 90 min	(32)			
220 mg O ₃ L ⁻¹ , 200 mg L ⁻¹ , 30 min	> 99			
20 mg O ₃ L ⁻¹ , 30 mg L ⁻¹ , 120 min	(40)			
5 mg O ₃ L ⁻¹ , 0.23 mg L ⁻¹			> 9	
38-40 mg O ₃ L ⁻¹ , 15 mg L ⁻¹ , 120 min			(50)	
38-40 mg O ₃ L ⁻¹ , 1g TiO ₂ L ⁻¹ , 15 mg L ⁻¹ , 120 min			(62)	
1 g O ₃ h ⁻¹ , 55 mg Fe ⁺² L ⁻¹ , 157 mg L ⁻¹ , 240 min				(83)
1.54 g O ₃ h ⁻¹ , 760 mg L ⁻¹ , 20 min				100
4. Photolysis (UV/H₂O₂)				
10 W- Lp-Hg lamp, 0.05 mg L ⁻¹ as TOC, 10 min	> 90		> 50	> 60
17 W- Lp-Hg lamp, 61.2 mg H ₂ O ₂ L ⁻¹ , 32 mgL ⁻¹ , 90 min	(39)			
1 kW- Mp lamp (200-300 nm), 10 mg H ₂ O ₂ L ⁻¹ , 1.0 mgL ⁻¹			52	
17 W- Lp-Hg lamp, 175 mg H ₂ O ₂ L ⁻¹ , 150 mg L ⁻¹ , 90 min				(39)
Lp Hg lamp (254 nm), 700 mg H ₂ O ₂ L ⁻¹ , 150 mgL ⁻¹ , 4 min				100(40)

Table 2.8. Efficiency of lab-scale AOPs for the degradation and mineralization of AI/AN chemicals (cont.).

PROCESS System parameters, C ₀ , t	Degradation (Mineralization)			
	%			
Compound	DCF	IBP	NPX	PCT
5. Dark and Light Fenton				
Fe ²⁺ / H ₂ O ₂ =1:50, 1.03 mgL ⁻¹			100	
1kW-Mp lamp (290-400 nm), 1.2 mg H ₂ O ₂ L ⁻¹ , 6.66 mg L ⁻¹ Fe ²⁺ , 179 mg L ⁻¹ , 120 min			80 (40)	
30 Wm ⁻² solar UV (320-400 nm), Fe ²⁺ /H ₂ O ₂ =1:100, 50 mg L ⁻¹ ,100 min	100 (100)			
6. Photocatalysis				
30 Wm ⁻² solar UV, 200 mg TiO ₂ L ⁻¹ , 50 mgL ⁻¹ , 200 min	(100)			
15 W- Lp Hg lamp, 800 mg TiO ₂ L ⁻¹ , 302 mg L ⁻¹ , 80 min				>95
450 W- Xe Lamp, 1 g TiO ₂ L ⁻¹ , 18.5 mg L ⁻¹ , 180 min		(88)		

*nanoparticles of super-paramagnetic iron

Ozonation. Ozonation has already been discussed in previous sections as an advanced treatment option that demonstrated high effectiveness in DWTP and WWTP effluents for destroying PhAC residues. The mechanism of destruction for phenolic PhACs (e.g. PCT, NPX) is based on ionic/radical reactions with byproducts such as hydroquinone, 1,2,4-trihydroxybenzene, 2-hydroxy-4-(N-acetyl) and aminophenol (Andreozzi et al., 2003a; Centellas et al., 2006). It is important to note that the degradability of such drugs increases with increasing pH, due to higher reactivity of phenol with hydroxyl radicals than with molecular ozone (Andreozzi et al., 2005; Javier Benitez et al., 2009). For most pharmaceuticals, the reactive species correspond to the predominant species in the pH range from 5 to 10 (Huber et al., 2005). This is why DCF reacts particularly faster with ozone than most of other amine-containing PhACs that have quite low values of pKa (<5) (Huber et al., 2005).

The most remarkable advantage of ozonation process is that it provides appreciable degrees of biodegradability enhancement when applied as a pretreatment option (Coelho et al., 2009). The process is also effective for remediation of groundwater contaminated with low concentrations of AI and AN chemicals, but less so in that of fresh water and WWTP effluent, due to the reactivity of dissolved organic matter and background constituents with OH• in the latter (Javier Benitez et al., 2009). Note also that ozonation is not effective for

toxicity reduction and mineralization, and the addition of H₂O₂ yields only slight enhancement in TOC elimination (Andreozzi et al., 2003a).

The best way of improving the efficiency of ozonation is to promote ozone mass transfer and decomposition, because the rate of oxidation is limited by the mass rate of gaseous O₃ transfer to solution. A promising method for this is catalytic ozonation, which involves adsorption of the gas on a catalytic surface to enhance its decomposition and to initiate surface reactions. Most common catalysts used in water remediation by ozone are TiO₂ and activated carbon, both of which are reported to provide more than 90% AIs and ANs removal at optimized laboratory conditions (Beltran et al., 2004; Rosal et al., 2008).

Combined Processes. Combined homogeneous AOPs such as UV/H₂O₂, O₃/UV, Fe²⁺/H₂O₂ (Fenton) and O₃/UV/H₂O₂ are also promising options for enhancing the elimination and mineralization of PhAC residues in water. In all, the enhancement is the outcome of excess OH• production by photolysis (e.g. of H₂O₂) and/or hydrolysis (e.g. of FeO⁺²) of the reagents. The following sub-sections cover some basic information and research notes on the degradation of selected AN/AI chemicals by UV/H₂O₂, Fenton and UV-Fenton (photo-Fenton) processes.

UV/H₂O₂. The process is preferable to ozonation, because it is less sensitive to the nature and concentration of background species. Kim et al. (2009) have reported 90% degradation of a large number of AIs and ANs (e.g. KPF, FNF, MEF, PCT, NPX, DCF) in lab-scale operations using 9.32 kJ m⁻² UV (medium pressure), 7.8 mg L⁻¹ H₂O₂ and drug concentration range of 3.0 x 10⁻⁶-120 x 10⁻⁶ mg L⁻¹ (Kim et al., 2009). The use of low pressure halogen light sources at the same light intensity was found to be less efficient (Pereira et al., 2007) due to lower absorption capacity of H₂O₂ at 254 nm. It was also found that the addition of excess H₂O₂ did not contribute significantly to the reactions (Ravina et al., 2002).

Fenton and UV/Fenton. Fenton oxidation is recognized as the most effective pretreatment method for pharmaceutical wastewater due to its capacity for extensive detoxification and biodegradability enhancement (Badawy et al., 2011; Badawy et al., 2009; Martinez et al., 2003). The process is based on the production of OH• from Fenton's reagent (Fe⁺²/H₂O₂) at acidic pH, Fe²⁺ acting as the homogeneous catalyst. A further advantage of Fenton process

is the formation of ferric-hydroxy complexes that promote coagulation of suspended solids after oxidation reactions (Kulik et al., 2008). A full-scale pharmaceutical wastewater treatment plant using Fenton process as primary treatment and sequencing batch-type AcS process as secondary is reported to provide 98% COD and 98% BOD₅ removal, which allowed complying with regional effluent discharge limits (Tekin et al., 2006).

Combined operation of Fenton oxidation with UV irradiation, or the so-called photo-Fenton process inherently produces more OH• and is therefore more effective than the dark method. It was found that a photo-Fenton process employed in a parabolic collector solar pilot plant (30 W m⁻²) provides partial degradation, mineralization and precipitation of DCF after a considerable decrease in pH (Javier Benitez et al., 2009; Pérez-Estrada et al., 2005). Enhanced precipitation of the drug by increased acidity is due to its weakly acidic character and insolubility in protonated form. Mineralization of DCF is also related to its solubility equilibrium, as verified by the increase in dissolved organic carbon content (DOC) of the solution shortly after reaction (via the formation of soluble intermediates) (Pérez-Estrada et al., 2005). In another study, it was also found that complete mineralization of the drug is possible using a 400-W low pressure Hg lamp (254 nm) and an activation energy of 16 K J mol⁻¹, which signifies the role of energy-requiring reactions in the overall degradation process other than radical chain reactions (Ravina et al., 2002).

Photocatalysis. Photocatalytic reactions with photo-generated holes of semiconductors (oxides of Ti, Cu, Zn, etc) have been thoroughly investigated during the last few decades for water remediation, particularly for eliminating recalcitrant compounds. The process is based on the excitation of semiconductor metal surfaces by near UV irradiation to generate active oxygen species on the crystals.

The electronic structure of most semiconductors is comprised of a highest (the valence band) and a lowest occupied band (the conductance band). Illumination of the surface of such materials by energies larger than the band-gap energy produces electron-hole pairs, h⁺/e⁻, which either recombine to release heat or hit the catalyst surface to react with surface-adsorbed species (Mills and Lee, 2004). The phenomenon is simplified in the following scheme for a surrogate semiconductor S-C:



The majority of research on photocatalytic decomposition of PhACs is carried out with TiO_2 and focused on the impact of initial solute concentration, semiconductor dose, pH and optimal solution temperature. The following discussion covers a critical review of the literature on TiO_2 -catalyzed photo-decomposition of AI/AN chemicals in water.

The efficiency of TiO_2 -based photocatalytic processes is closely related to the initial drug concentration and semiconductor dose. At small-to-moderate levels of TiO_2 (104-502 mg L^{-1}) the degradation depends only on the initial solute concentration, while at higher levels it varies proportionally with the amount of TiO_2 and the number of active sites on it (Calza et al., 2006; Zhang et al., 2008). The presence of excess TiO_2 reduces the extent of elimination; thus optimization of the catalyst dose is very important to avoid superfluous catalyst concentrations and ensure complete absorption of radiation photons (Habibi and Vosooghian, 2005).

Elimination of PCT from wastewater and drinking water samples by TiO_2 -photocatalysis is highly efficient at pH 9.0 (no toxic byproduct formation) although the drug is poorly adsorbed in the dark due to its poor chelating ability with Ti (Pérez-Estrada et al., 2005; Zhang et al., 2008). At higher pH, degradation is less effective due to electrostatic repulsions between the catalyst surface and the phenolic moiety, which exists as phenolate (Zhang et al., 2008). It was also found that the extent of degradation is further reduced by high initial concentrations of the drug, which leads to a competition for active reaction sites and photons that lower the rate of oxidant generation (Yang et al., 2008).

The process was found highly effective for detoxifying and mineralizing very small concentrations of some drugs (e.g. DCF) by using low catalyst and low radiation doses (Rizzo et al., 2009). At higher TiO_2 loadings and DCF concentrations, however, 20-min and 40-min treated samples were found to be more toxic than untreated ones, indicating

relatively long life times of the intermediate products (e.g. hydroxyl- and bi-hydroxyl derivatives) (Calza et al., 2006).

Sonolysis. The literature on sonochemical degradation of PhACs is limited to three chemicals (DCF, IBP, PAC) and some mixtures of PhACs in synthetic or real WWTP effluents to assess the impact of operation parameters such as frequency, concentration, pH, dissolved gases, ultrasonic power, radical scavengers and solid catalysts. The following discussion covers a critical review of lab-scale studies on ultrasound-assisted elimination of some AI/AN chemicals in deionized water or in effluents of WWTPs.

Hartman et al. (2008) found that irradiation of a 90 mg L⁻¹ synthetic DCF solution successively by 216, 617 and 850 kHz at 90 W for 1-h provides at least 87%, 90% and 24% degradation of the drug, respectively (Hartmann et al., 2008). Reduced efficiency at high frequency ultrasound must be due to exceeding of the threshold frequency that is specific of each experimental system (Pétrier and Francony, 1997). In accordance, sonication of DCF (C₀=30 μM) at 577, 861 and 1145 kHz showed that maximum degradation was obtained at 861 kHz and minimum at 1145 kHz (Tezcanlı-Güyer and Ince, 2011). The formation of hydroxylated derivatives, phenylacetic acid, dichloroaniline and dichlorophenol in the work of Hartman et al. (2008) during early sonolysis (30-min) was attributed to the dominance of OH•-mediated reactions in the degradation process, and that of carboxylic acid and HCl after extended sonication (60-min) to the mineralization of the intermediates.

Naddeo et al. (2009) have reported that optimum conditions for DCF elimination in urban wastewater treatment effluent (UWTP) by 20 kHz ultrasound (US) are low pH and air sparging, and the rate of OH•-mediated degradation of the compound speeds up with increases in the initial concentration. The authors reported 15% biodegradability enhancement in sonicated UWTP effluent spiked with a mixture PhACs that contained DCF, amoxicillin and carbamazepine (Naddeo et al., 2009).

Comparison of ozonation and sonication for mineralization of DCF at optimal conditions showed that sonication was more effective (30% and 36%, respectively), and combination of the two was only slightly better (39%) (Naddeo et al., 2009). The observed enhancement in combined O₃/US application is due to increased rate of ozone mass transfer

and excess OH• production by thermal decomposition of O₃ (Ince and Tezcanlı, 2001). A simplified reaction scheme is as the following (Ince and Tezcanlı, 2001):



Finally, it was shown that sonochemical degradation and mineralization of DCF ($C_0=30 \mu\text{M}$) at 861 kHz was considerably accelerated by the addition of soluble and insoluble Fe-species such as Fenton's reagent and paramagnetic Fe-oxide nanoparticles (Tezcanlı-Güyer and Ince, 2011). The positive influence of solid particles was also highlighted by Hartmann et al. (2008), who attributed the effect to the larger surface area of asymmetric cavity bubbles that accelerated the rate of reaction at the gas-liquid interface (Hartmann et al., 2008).

Degradation of IBP by 300 kHz US in synthetic solutions showed that the rate of reaction is limited by the availability of OH• and increases with increased solute concentrations ($2\text{-}21 \text{ mg L}^{-1}$), air sparging and acidity ($\text{pH} < \text{pK}_a$) (Méndez-Arriaga et al., 2008). It was also found that 30-min sonication at optimized conditions rendered complete IBP removal and 35% biodegradability enhancement. Hybrid advanced oxidation processes involving US provided more promising results in terms of full elimination and mineralization of IBP, as 92% TOC removal was obtained after combined $\text{TiO}_2/\text{Fe}^{2+}/\text{US}$ (300 kHz) application for 4-h (Méndez-Arriaga et al., 2009). Similarly, the decomposition of IBP increased synergistically by combined TiO_2/US and Fe^{3+}/US (213 kHz) applications, while the increase in mineralization was synergistic only in Fe^{3+}/US combination and additive in that of TiO_2/US (Madhavan et al., 2010a). Larger efficiency of Fe^{3+}/US process for mineralization was attributed to the formation of photo reactive complexes between Fe^{3+} and carboxylic byproducts that formed after extended contact.

The literature on sonochemical degradation of PCT is limited to a single study, which showed that maximum yield was obtained by 240-min sonolysis of the drug ($C_0=25 \text{ mg L}^{-1}$)

at 574, kHz and 32-W providing complete conversion and 39% mineralization of the drug (Isariebel et al., 2009). The authors reported that the fraction of degradation increased with reduced solute concentrations, enhanced power inputs and reduced quantities of OH• scavengers. The efficiency was further improved by the addition of an optimum dose of H₂O₂, which provided excess OH• upon decomposition in gaseous cavity bubbles.

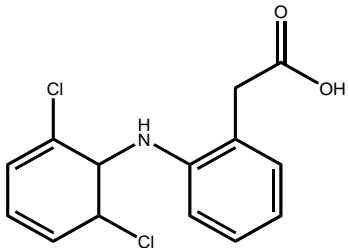
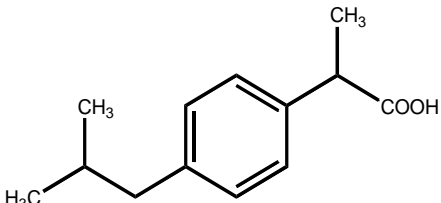
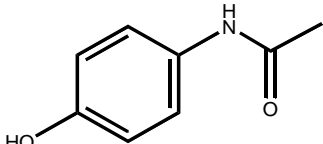
3. MATERIALS AND METHODS

3.1. Materials

3.1.1. Test Compounds

Diclofenac sodium salt, Ibuprofen and Paracetamol sulfate potassium were purchased from Sigma with >97% purity. The chemical and physical properties of the test compounds are given in Table 3.1.

Table 3.1. Molecular structures, chemical and physical properties of diclofenac, ibuprofen and paracetamol.

Compound	Parameter	Value
 DCF	Pka MW (g mol ⁻¹) Solubility (mg L ⁻¹) logKow	4.1 318.13 2400 1.9-4.5
 IBP	Pka MW (g mol ⁻¹) Solubility (mg L ⁻¹) logKow	4.8 206.28 21 2.5-4.0
 PCT	Pka MW (g mol ⁻¹) Solubility (mg L ⁻¹) logKow	9.4 151.17 14000 0.46

3.1.2. Reagents

Analytical grade acetonitrile and methanol were obtained from Merck to use as a mobile phase in HPLC analysis. The reagents potassium dihydrogen phosphate (KH_2PO_4 , Merck), sodium hydroxide (NaOH , Merck), sodium bicarbonate (NaHCO_3 , Merck), sulfuric acid (H_2SO_4 , Merck), hydrogen peroxide (H_2O_2 , Merck), potassium iodide (KI , Merck), ammonium molybdate tetra hydrate ($(\text{NH}_4)_6\text{Mo}_7\text{O}_{24}\cdot 4\text{H}_2\text{O}$, Merck), potassium hydrogen phthalate (KHP, Merck), sodium dihydrogen phosphate (NaH_2PO_4 , Merck), phosphoric acid (H_3PO_4 , Merck), dichlor-tetrahydroxy-platinic acid (H_2PtCl_2 , Merck), sodium tetrachloropalladate(II) ($\text{Na}_2\text{PdCl}_4\cdot 3\text{H}_2\text{O}$, Wako), sodium tetrachlorogold ($\text{Na}(\text{AuCl}_4)\cdot 2\text{H}_2\text{O}$, Wako), polyethylene-glycol monostearate (PEG-MS, Wako), titanium dioxide (TiO_2 , Evonik) were all reagent grade. Finisterre C18 SPE cartridges were purchased from Finisterre, Istanbul. Air, argon and oxygen gases were obtained from Ozvarislar, Istanbul with >99% purity.

3.1.3. Catalysts

The catalysts used throughout the study comprised of soluble and insoluble metallic catalysts exist in the form of powders, micro-/nano-particles and -composites. These catalysts were obtained either as purchasing commercial products or synthesizing them at the laboratory. The catalysts, their commercial or given names, particle properties and their origin are listed in Table. 3.2.

Table 3.2. The catalysts and their properties.

Catalysts	Type	Form	Size	Origin
<u>Iron Type catalysts</u>				
ZVI	Insoluble	Micro-powder	45-150 μm	Hepure
Carbide Coated- ZVI	Insoluble	Nano-particle	20-100 nm	Lab. product
Fe_2O_3 (Hematite)	Insoluble	Micro-powder	<5 μm	Sigma-Aldrich
$\text{Fe}(\text{OH})\text{O}$ (Goethite)	Insoluble	Micro-powder	0.08-1.74 μm	Sigma-Aldrich
Fe_3O_4 (Magnetite)	Insoluble	Nano-powder	10 nm	Sigma-Aldrich

Table 3.2. The catalysts and their properties (Cont.)

Catalysts	Type	Form	Size	Origin
<u>Iron Type catalysts</u>				
Ni-Fe ₂ O ₄	Insoluble	Nano-powder	< 50 nm	Sigma-Aldrich
FeSO ₄ ·7H ₂ O	Soluble			Sigma-Aldrich
FeCl ₃ ·6H ₂ O	Soluble			Sigma-Aldrich
<u>Metal Supported TiO₂ nanocomposites</u>				
TiO ₂	Insoluble	Nano-particle	30-40 nm	Evonik
Pt-TiO ₂	Insoluble	Nano-composite	< 10 nm	Lab. product
Au-TiO ₂	Insoluble	Nano-composite	13.8 nm	Lab. product
Pd-TiO ₂	Insoluble	Nano- composite	5.9 nm	Lab. product
Au/Pd-TiO ₂	Insoluble	Nano- composite	5.4 nm	Lab. product
<u>Metal Supported Al₂O₃ nanocomposites</u>				
Al ₂ O ₃	Insoluble	Powder	100 mesh	Sigma-Aldrich
Pt-Al ₂ O ₃	Composite	Nano- composite	<10 nm	Lab. product

3.2. Methods

3.2.1. Experimental Set-ups

Experiments were carried out using various reactor systems: i) the ultrasonic systems including probe, plate or ultrasonic bath reactors, ii) ozonation, iii) UV-, and iv) the hybrid reactors operated by various combinations of single reactors. The details of the reactor systems are given below:

3.2.1.1. Ultrasonic Reactor Systems: Ultrasonic systems were consisted of probe reactors, ultrasonic bath and plate type reactors emitting at low and high frequency ultrasonic irradiation.

20 kHz (R1) and 40 kHz (R1) Reactors. 20 kHz system is made of a 100 mL glass cell surrounded by a water-cooling jacket to keep the solution at a constant temperature (25±0.5 °C), a probe type transducer (Bandelin Sonoplus HD220) with a probe tip area of 1.13 cm²

emitting ultrasonic waves at 20 kHz and a 180 W generator to convert electrical power into ultrasonic energy (R1) (Fig. 3.1). The horn is submerged 3 cm from the top of the cell, which has an effective volume of 80 mL. The system is mounted in a polyurethane isolating material to prevent excessive noise. 40 kHz system consists of a probe type transducer (Weber Ultrasonics) emitting ultrasonic waves at 40 kHz and a 200 W generator to convert electrical power into ultrasonic energy (Fig. 3.1). The portable horn reactor was used either in a 250 mL glass cell for single operations or submerged either into ultrasonic bath or multi frequency reactor for combined processes. The probe was submerged 3 cm above the bottom of the cell which has an effective volume of 250 mL.

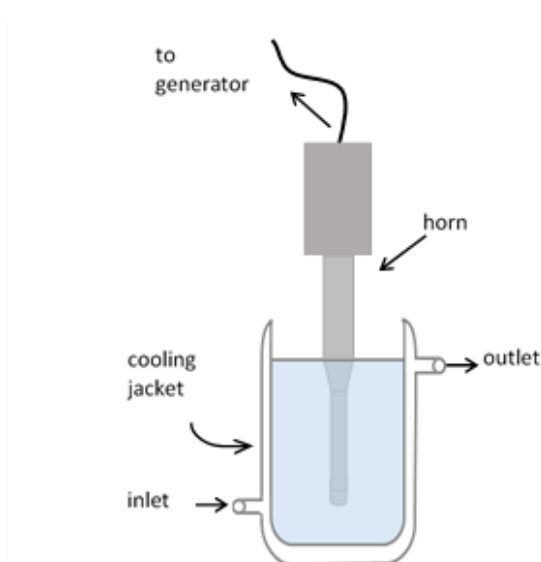


Figure 3.1. The schematic view of 20 kHz (R1) and 40 kHz (R2) type reactors.

Ultrasonic Bath (R3). The system is made of a 1 L plexy-glass outer tank, a multi-wave transducer emitting at 200 kHz and a 100 W generator (Fig. 3.2). The distance between the oscillating surface and inner vessel reaction vessel (250 mL) kept at 3 cm. A water circulation system was used to keep the solution at constant temperature (25 ± 0.5 °C).

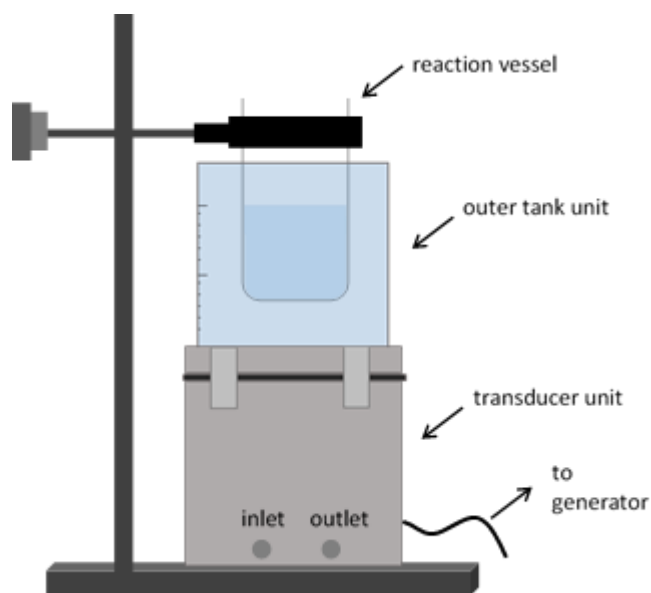


Figure 3.2. The schematic view of 200 kHz ultrasonic bath reactor (R3).

Multi-Frequency Reactor (R4). The system is made of a 500 mL glass cell surrounded by a water-cooling jacket to keep the solution at constant temperature (25 ± 0.5 °C), a multi-frequency plate type piezoelectric transducer with a vibrational area of 22 cm^2 emitting ultrasonic waves at 577 (572), 861 (856) and 1145 (1130) kHz, and a generator with an output power capacity of 120 W (Ultraschall, Germany).

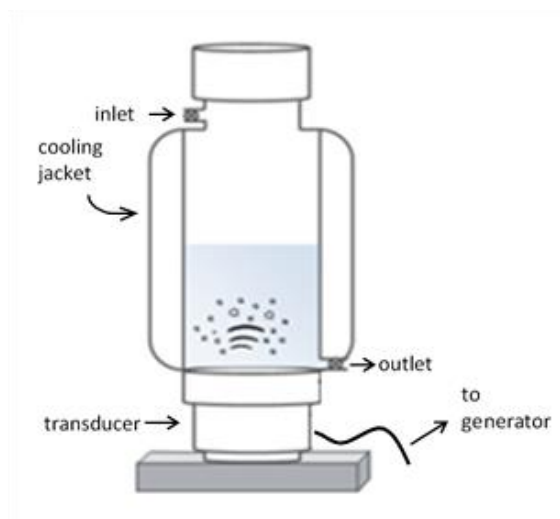


Figure 3.3. The schematic view of multi-frequency plate type reactor (R4).

3.2.1.2. Ozone and UV Systems. Ozone was generated onsite using an Ozonelab-100 Model (Ozone Services) generator and dry pure oxygen flowing at 1.5 L min^{-1} . The gas flow rate was fixed at 3, 6 and 9 mg min^{-1} , which provided aqueous ozone concentrations of 2, 4 and 8 g m^{-3} , respectively. Ozone generator was used in both ozonation (R5) and sono-ozonation (R6) experiments injecting in erlenmeyer flask (closed system) or R4 reactor.

Photolytic experiments were carried out using a low pressure Hg-UV lamp emitting at 254 nm ($I=107.4 \text{ W cm}^{-2}$). The lamp with length of 20 cm was placed in a quartz jacket to prevent the direct contact of liquid medium with the lamp and then it was submerged into R4 reactor while sono-reactor was in either silence mode or active (R7) for photolytic or sono-photolytic experiments, respectively as shown in Figure 3.4.

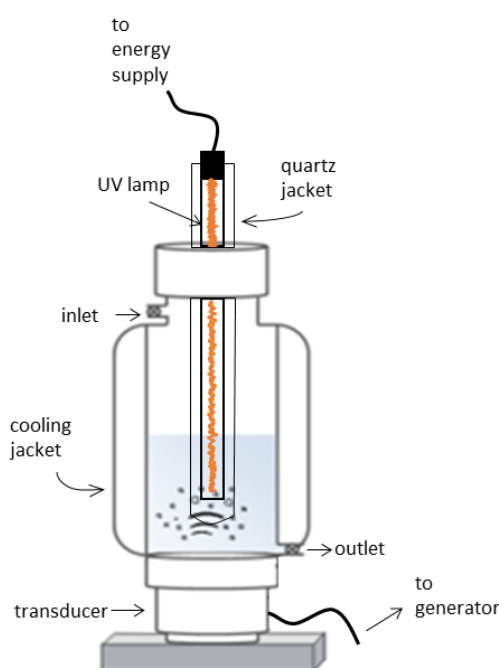


Figure 3.4. The schematic view of sono-photo reactor (R7).

3.2.1.3. Hybrid Reactors. The hybrid operations were carried out integrating two or more single reactor in one experimental set-up. The hybrid operations were run either sequential or simultaneously. As described above, R6 and R7 reactor systems were hybrid operations used in sono-ozonation and sono-photolysis experiments. These experiments were run in the sono-reactor (R4) inserting ozone or UV-lamp, respectively. Addition to this, sono-photo-ozonation (R8) were carried out in the same reactor bubbling with ozone. Simultaneous

operations of 40/572 kHz, 40/856 kHz, 40/1130 kHz were run in R9 reactor inserting R2 (40 kHz) reactor into R4 (multi frequency plate type reactor). 40/200 kHz dual frequency operation were conducted in R10 reactor system inserting R2 reactor in to ultrasonic bath (R3).

3.2.2. Experimental Procedures

The details of the experimental procedure were described within the context of each chapter that were carried out individual case studies, however, a general overview of experimental procedures was also given below:

Sonolysis. Fresh samples were saturated with air, adjusted to the desired pH using 0.1 N NaOH or H₂SO₄ before sonolytic experiments unless stated otherwise and sonicated at ambient temperature for 30-90 min to select the optimum power, frequency and bubbling gas (air, O₂, Ar) at R1, R2, R3, or R4 reactors. Each reactor system was cooled by circulating water to maintain constant temperature (25±0.5 °C). The reactors were run at optimum conditions (% power, amplitude) which were previously determined. Aliquots were collected within short intervals for the analysis of the parent compound, UV absorption maxima and TOC. The overall degradation of the chemical was also assessed by monitoring the COD, BOD₅, Cl⁻ and NO₃⁻ of the test solutions.

Ozonation. Ozone was injected to the test solutions at a flow rate of 1.5 L min⁻¹ and the aqueous concentration of the gas was maintained at 2, 4 or 8 mg L⁻¹ depending on the operating conditions. Ozonation experiments were carried out using 250 mL of test samples at R5, R6 or R7 reactors. Preliminary experiments with ozone alone were conducted in 250 mL glass chambers to estimate the ozone mass transfer coefficient at varying pH levels (3.0, 6.5 and 9.0) and ozone flow rates (3, 6 and 12 mg min⁻¹). The effluents were analyzed for the monitoring of the compound removal, carbon mineralization and UV absorption, and the residual ozone concentrations in aqueous medium were monitored.

Photolysis. The test compounds were exposed to 30-60-min photolysis under UV-C irradiation by a low-pressure mercury lamp with a maximum emission at 254 nm at R7

reactor in the presence/absence of ozone or ultrasound. The effluents were analyzed for the monitoring of the compound removal, carbon mineralization and UV absorption.

Pretreatment of Catalysts. For the catalytic experiments, all solid particles or powders were treated by mixing the particles with 20 mL water and sonicating the suspension for 3-min at 20 kHz ultrasonic probe reactor to enhance particle stability against agglomeration thus to increase the adsorption properties of the catalysts.

Sono-catalytic Experiments. Sono-catalytic experiments were run in the presence of various catalysts under previously optimized sonolysis conditions. The varying masses of the micro- or nano-particles were added to select the most effective catalyst concentration or the optimum dose. The experiments were repeated at varying pH conditions to observe the effect of pH on the performance of the catalysts. The impact of the catalysts was assessed by the apparent rate of compound disappearance, carbon mineralization, and the formation of Cl^- and NO_3^- ions as indicators of mineralization during 30-60-min sonication. The soluble metal concentrations leaching into solution during sonication were monitored to assess whether the heterogeneous reaction dominates or the homogeneous reactions may have a considerable contribution. The catalytic activity of nanocomposites of metal supported- TiO_2 and $-\text{Al}_2\text{O}_3$ were evaluated comparing the efficiency obtained during control experiments which were carried out in the presence of pristine TiO_2 and Al_2O_3 .

Photo-catalytic Experiments. Photo-catalytic experiments were carried out by 60-min irradiation of the sample solution by low pressure Hg-UV lamp in R7 (silence mode of ultrasound) described 4.1.3.2 section in the presence of varying doses of the catalysts and at various pH conditions. Sono-photocatalytic experiments were also run in the sono-reactor (R7) illuminating by UV and ultrasonic irradiation at 856 kHz or 572 kHz simultaneously.

Catalytic Ozonation. Catalytic ozonation of the compounds were run in the presence of optimum catalyst concentrations during 60-min at varying ozone flows ($3\text{-}12\text{ mg min}^{-1}$) and pH conditions. Ultrasound-assisted ozonation was carried out in R4, plate-type reactor emitting at 856 kHz or 572 kHz. (Ultraschall/ Meinhardt, Germany). The reactor was operated at optimum conditions.

3.2.3. Analytical Methods

High Pressure Liquid Chromatography (HPLC) analysis. The removal of model compounds was monitored by HPLC analysis using a Shimadzu LC-20AT HPLC with a 20A UV-vis photo diode array detector equipped with Inertsil ODS-3V (C18) (Hypersil BDS), 250 × 4.6 mm, 5 μm particle size column. The measurement conditions were summarized in Table 3.3.

Table 3.3. The operation conditions of HPLC for analysis of DCF, PCT and IBP.

Compound	Wavelength (nm)	Mobile Phase	Injection Volume (μL)	Retention Time (min)
DCF	254	80:20 ACN: KH ₂ PO ₄ (0.01 M) flow= 1 mL min ⁻¹	50	3.70
PCT	220	25:75 MTN:Water flow=1 mL min ⁻¹	10	3.45
IBP	220	75:25 ACN: H ₃ PO ₄ (0.1%) Flow= 0.8 mL min ⁻¹	10	4.70

By-product Analysis (by GC/MS) The analysis of byproducts was carried out using gas chromatography- mass spectrometry (GC/MS) which were run following a solid phase extraction (SPE) procedure. The GC equipment was a Shimadzu-2010 analyzer with a TRB-5MS (30 m×0.25 mm×0.25 μm) column and a detector operating in EI mode (scanning between m/z 40 and m/z 400). The flow rate of the carrier gas (helium) was 1 mL min⁻¹. The temperature and volume of the injector were 250 °C and 1 μL, respectively. The formation of by-product was also evaluated by spectrophotometrically monitoring of the change in UV-absorption spectra.

Solid Phase Extraction. Prior to the GC/MS analysis, all samples have been extracted to organic phase by solid phase extraction. The extraction were run following the procedure: i) 5 mL methanol was used to conditioning the C18 cartridges, ii) the cartridges were washed up by 5 mL distilled water, iii) 250 mL of treated samples were run through the cartridges and the elution was carried out by 5 mL methanol.

Total Organic Carbon Analysis. Total organic carbon (TOC) was monitored using a Shimadzu TOC-V CSH analyzer operating in the non-purgeable organic carbon (NPOC) mode. The instrument was calibrated by standard solutions of potassium hydrogen phthalate (1-10 mg L⁻¹). Samples were acidified with HCl to pH 2.0 and purged for 1.5 min prior to injection to ensure that all carbonate, bicarbonate and carbonic acid are removed as carbon dioxide in gas form from the solution. All samples were measured in triplicate.

Spectrophotometric Analysis. The visible and UV absorbance of effluent samples were analyzed using a Unicam Helios Alpha/Beta double beam spectrophotometer with a 1 cm quartz cell.

Microtox Toxicity Analysis. The acute toxicity of reactor aliquots was determined using a Microtox-500 Toxicity Analyzer and the manufacturer's standard protocols (Azur, Environmental, USA). The method is based on the spectrophotometric determination of the light emission of the test organisms (*Vibrio fischeri*) at 15-min exposure to various dilutions of the toxic solution to compare the results with that of the control. The data were evaluated using the MicrotoxOmni© Software and reported as 15-min EC₅₀, which is equivalent to the percentage of initial solution (dilution is % v/v unless indicated otherwise) that renders 50% light inhibition in time. All reagents (reconstitution solution, diluents, osmotic adjustment solution) and the freeze-dried bacterial strain were delivered by the manufacturer.

Respirometric Oxygen Uptake Analysis. Biodegradability of the reactor aliquots was determined by respirometric analysis using a PF-8000-Model Respirometer (USA). The method is based on measurement of the dissolved oxygen accumulated in solution via the pressure gradient that forms upon injection of gaseous O₂ into the reaction vessels. The test system consisted of a biological reaction vessel, a stirring base, a water bath, an oxygen control module, and a computer. Oxygen was injected in small, calibrated increments and transferred from headspace to the liquid phase by high-rate magnetic stirring units. The microbial seed was an activated sludge sample obtained from a domestic wastewater treatment plant that was fed daily in the laboratory. The initial concentration of active bacterial strain in each vessel was 2 000 mg L⁻¹ as volatile suspended solids and the biomass was fed from a synthetic feed solution containing 5 mL ethanol (5 %); 6 g peptone; 6 g glucose and 20 000 mg L⁻¹ COD. The volume of the feed solution in each vessel was

adjusted to provide 400 mg L⁻¹ COD per vessel. The ratio of food to mass (F/M) was 0.2. The oxygen uptake or accumulation was recorded automatically at 10-min intervals during 24, 48, 72, and 96 h.

Hydrogen Peroxide Analysis. The concentration of hydrogen peroxide (H₂O₂) was analyzed by the potassium iodide method described by Klassen et al. (1994). The method is based on the reaction of iodide (I⁻) with H₂O₂ to form triiodide ion (I₃⁻), which has a strong absorbance at 351 nm. The analysis of H₂O₂ at concentrations as low as 1 mM is conveniently made by determining the yield of I₃⁻ formed when H₂O₂ reacts with KI in a buffered solution containing ammonium molybdate tetrahydrate as a catalyst. Two solutions (A and B) were prepared as described below and 2.5 mL from each solution was mixed with 1 mL of sample and diluted to 10 mL to record the absorbance at 351 nm.

Solution A: 33 g of KI, 1g of NaOH and 0.1 g of ammonium molybdate tetrahydrate were diluted to 500 mL with milli-Q water. The solution was stirred for 1 h to dissolve the molybdate and kept in the dark to prevent the oxidation of I⁻. Solution B: 10 g of potassium hydrogen phthalate was dissolved in 500 mL to serve as the buffer solution.

Dissolved Ozone Analysis. The aqueous ozone concentration was analyzed by the indigo colorimetric method (APHA/AWWA/WPCP, 1998). The method is based on the decolorization of indigo by ozone in solution. The decrease in absorbance is linear with increasing ozone concentration. Two solutions (indigo stock and indigo reagent) were prepared: i) 77 mg potassium indigo trisulfonate (C₁₆H₇N₂O₁₁S₃K₃) and 0.1 mL concentrated phosphoric acid were diluted to 100 mL with milli-Q water to prepare Indigo stock solution, ii) 25 mL indigo stock solution, 2.5 g sodium dihydrogen phosphate (NaH₂PO₄), and 1.75 mL concentrated phosphoric acid were diluted to 250 mL with milli-Q water. 10 mL indigo reagent and 10 mL sample were mixed and diluted to 100 mL with milli-Q water to prepare Indigo reagent solution. The absorbance of both solutions were measured at 600 nm and the aqueous ozone concentration was calculated by the following equation:

$$mgO_3 / L = \frac{100 \times \Delta A}{f \times b \times V} \quad (\text{Eq 3.1})$$

where: ΔA is the difference in absorbance (600 nm) between blank and sample, b is the path length of cell (cm), V is the volume of the sample (mL), and f is the proportionality constant which is $0.42 \pm 0.01 \text{ cm mg}^{-1} \text{ L}^{-1}$ ($\Delta \epsilon = 20\,000 \text{ M}^{-1} \text{ cm}^{-1}$) at 600 nm compared to the ultraviolet absorption of pure ozone of $\epsilon = 2950 \text{ M}^{-1} \text{ cm}^{-1}$ at 258 nm.

Dissolved Iron Analysis. The aqueous iron concentrations was analyzed by AAnalyst 300 Atomic Absorption Spectrophotometer (Perkin Elmer) to monitor dissolution of total iron from solid catalyst. Samples were filtered by 0.45 μm syringe filter before analysis.

Common Anion Analysis. Ion concentrations of Cl^- , NO_2^- , NO_3^- and SO_4^- were analyzed using ICS-3000 Ion Chromatograph (Dionex) following filtration with 0.20 μm syringe filter of the test solution.

Elemental Analysis. The carbon content of nanoparticles was measured using an ECS 4010 elemental combustion system (Costech Instruments).

Metal Analysis. The solubilized concentrations of palladium, platinum, gold and aluminum in sample solution were measured using Perkin Elmer-ICP-OES Optima 2100 DV.

Image Analysis of Nanoparticles. The structure, morphology and size of commercial and synthesized particles were analyzed by environmental scanning electron microscope (ESEM)-Philips XL30 ESEM-FEG/EDAX equipped with a SE detector. Multi-elemental mapping (EDX MEM/Line Scanning/Particle) and phase analyses (SUTW-Sapphire detector- EDAXZAF Quantification) were carried out to detect, characterize and classify the indefinite features under low/high vacuum conditions without limitation (kV:15, resolution:139.70, Lsec:47–49,take-off:35.21–35.23). Nanocomposites were further analyzed by scanning-transmission electron microscopy (STEM, FEI Titan80–300 operated at 300 kV) equipped with a large-angle annular dark field (HAADF) detector to obtain more precise information on particle sizes less than 10 nm. The beam convergence and inner angles of HAADF detector were 10 mrad and >60 mrad, respectively.

Hydrodynamic Size Analysis. Hydrodynamic diameter and size distribution analyzes were made in dilute solutions of the particles using a Brookhaven 90-Plusnanoparticle size analyzer operated with the method of dynamic light scattering (DLS).

Analysis of Band Gap Energy. The band gap energies of TiO₂ and the nanocomposites were determined by recording the UV-diffuse reflectance spectra of the solids (200–600 nm) using a UV–vis spectrophotometer (UV-2450, Shimadzu) equipped with an integrating sphere reflectance accessory. The data were evaluated by reference to Kubelka–Munk (KM) transformations and linear extrapolation of the diffuse reflectance spectra as described in the literature (Ökte et al., 2014).

Calorimetry. The ultrasonic power density in solution was determined by using the calorimetric method based on the assumption that all of the energy delivered to the system is dissipated as heat (Mason and Peter, 2002). The power dissipated (P) in a reaction mixture is expressed by:

$$P = \left(\frac{dT}{dt} \right)_{t=0} M \cdot C_p \quad (\text{Eq. 3.2})$$

where: C_p (4.182 J g⁻¹ K⁻¹) is heat capacity of water. M is mass of water, and dT/dt is the initial slope of the temperature rise of the reaction mixture versus time (Mason and Peter, 2002).

UV-Actinometry. The intensity of the light source was determined by a chemical actinometer (Mark et al., 1990). The actinometer consisted of a well-oxygenated aqueous solution containing potassium peroxodisulphate (0.01 mol L⁻¹) and tert-butanol (0.1 mol L⁻¹). Upon irradiation with 254 nm light, the mixture produced sulphuric acid and the generation of hydrogen ions (H⁺) was monitored by a pH meter recording the drop in pH as a function of irradiation time (Mark et al., 1990). The quantum yield of H⁺ formation was defined as the ratio of the number of H⁺ ions formed per the number of photons absorbed. The linear relationship between pH data (pH = -log [H⁺]) and irradiation time was used to calculate the quantum yield. The quantum yield of H⁺ formation (Φ (H⁺)) is expressed by Equation 3.3:

$$\Phi(H^+) = \frac{[H^+] \cdot N_L \cdot V_{tot} \cdot 10}{t \cdot I_{abs} \cdot M} \quad (\text{Eq. 3.3})$$

where: V_{tot} denotes the total volume (cm^3) of the solution in the reactor, M is the surface area of the solution (cm^2), t is the irradiation time and I_{abs} is the absorbed fluence rate in terms of Einstein's $\text{m}^{-2} \text{s}^{-1}$ and N_L is Avogadro number. $[H^+]/t$ value was obtained from the slope of $[H^+]$ vs. t plot. Absorbed fluence rate was calculated by using the constant values of $\Phi(H^+)$ (1.8). Incident fluence rate was calculated by Equation 3.4.

$$I_{abs} = I_0(1 - 10^{\epsilon cl}) \quad (\text{Eq. 3.4})$$

where: I_{abs} is the absorbed photon fluence rate, I_0 is the incident photon fluence rate, l is the path length, ϵ and C are the molar extinction coefficient ($20 \text{ dm}^3 \text{ mol}^{-1} \text{ cm}^{-1}$) and concentration of potassium peroxodisulphate (0.01 M), respectively (Mark et al., 1990).

3.2.4. Adsorption

Prior to catalytic experiments, silent batch tests were carried out with the test compounds at varying pH (3.0-10.0) and concentrations of the catalysts in a Julabo SW22 shaker to determine the ability of the compound to be adsorbed on the metal surface and the equilibrium conditions, and to assess the contribution of adsorption on the elimination of the test compounds. The rate of mixing were fixed at 250 rpm for 30-min to 24-h reaction time.

3.3. Synthesis of Nanoparticles

Nanocomposites of Pd-TiO₂, Au-TiO₂ and Pd/Au-TiO₂ were synthesized sonolytically using Na₂PdCl₄·3H₂O, Na(AuCl₄)·2H₂O and powdered TiO₂ (Degusa P-25) in a multi-wave ultrasonic bath with a frequency of 200 kHz and a power intensity of 6 W cm^{-2} (Kaijo, 4021, Japan). The procedure comprised of the following steps: i) mixing of 1 mM of each metal salt with 0.4 mM PEG-MS (polyethylene-glycol monostearate) in 60 mL of ultrapure water followed by purging of the solutions with Ar for 10 min (in bi-metallic solutions, the ratio of Au:Pd was kept at 50%:50% by molar); ii) sonication of noble

metal/PEG-MS solutions for 60 min under Ar atmosphere; iii) addition of 8 mmol, 15 mmol and 22.5 mmol TiO_2 to each solution followed by sonication again for 30 min during air bubbling; iv) separation of the nanocomposites via filtration through 0.2 μm membrane-Milipore (OmniPore) followed by washing with pure water and drying at constant temperature (60 °C) for 12 h (Ziylan-Yavas et al., 2015).

Pt- TiO_2 nanocomposites were synthesized sonolytically using H_2PtCl_2 and powdered TiO_2 (Evonik, P-25) in a multi-wave ultrasonic bath emitting at 200 kHz (Kaijo, Quava Mini, Japan). Pt- TiO_2 nanocomposites were in three different Pt concentrations to test the effect of Pt-loading on the activity of the catalyst. The procedure was the same as described above. The particles were labeled as P1, P2 and P4, respectively referring to 1 mM, 2 mM and 4 mM Pt-loading using 232.5, 456.1 and 912.2 mg L^{-1} H_2PtCl_2 (Ziylan-Yavas and Ince, 2016).

Platinum-supported nanocomposites of alumina (Pt- Al_2O_3) were prepared sonolytically by mixing 11.7 mg H_2PtCl_2 and 1.17 g $\gamma\text{-Al}_2\text{O}_3$ in a glass vessel inserted in a multi-wave ultrasonic bath emitting at 200 kHz. The procedure is illustrated in Figure 3.5 following steps described above.

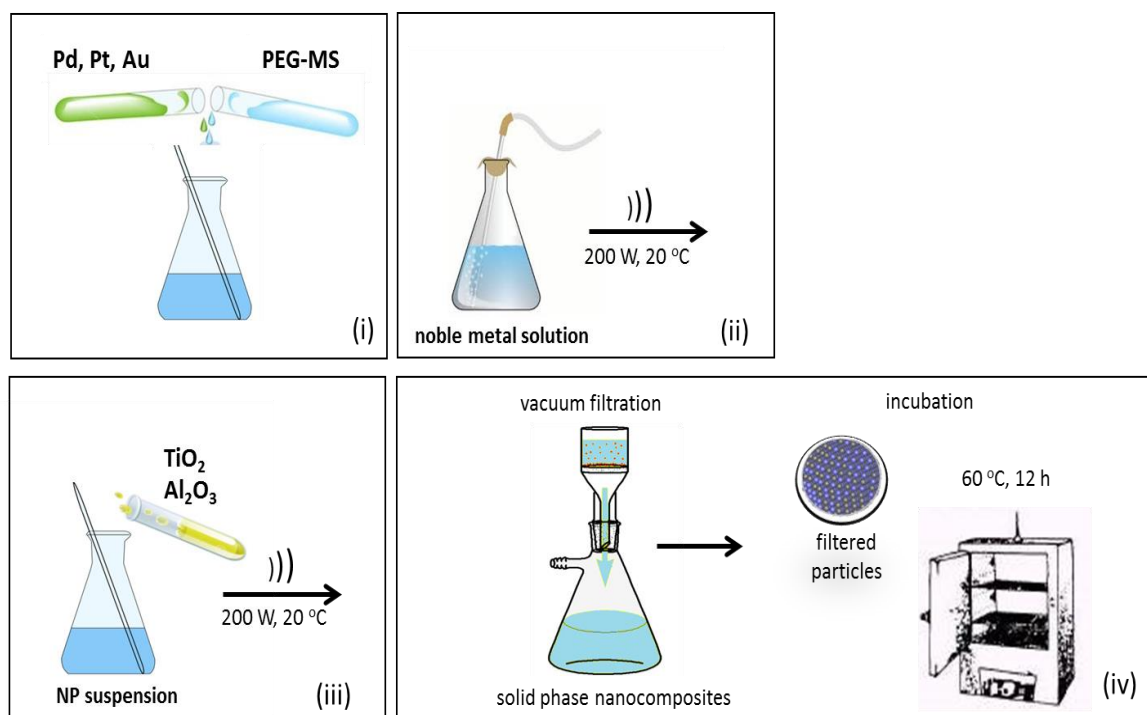


Figure 3.5. The procedure of nanocomposite preparation by sonochemical method.

3.4. System Parameters of Ultrasonic Systems

Deposited Power in the Reactors. Power density is a crucial parameter to assess the efficiency of ultrasonic systems because the observed degradation rates cannot be directly correlated for all systems however, the general trend is an increase in the yield with an increase in power density (Sivakumar et al., 2002). Power density directly gives an idea about the amount of energy dissipated in a given volume of the solution.

The applied electrical power was manually adjusted to dissipate the optimum percentage of its total capacity (P_{app} , %) and the heat dissipation was estimated calorimetrically as described in 3.2.3 section. The power density (P_d) were calculated by the following equation:

$$P_d = \frac{\text{Power}_{diss.} (W)}{\text{Volume} (mL)} \quad (\text{Eq. 3.5})$$

The operation parameters of ultrasonic reactors were summarized in Table 3.4.

Table 3.4. The operation parameters of ultrasonic reactors.

Reactor, frequency	Power_{out.}, W	P_{app.}, %	Power_{diss.}, W	P_d, W mL⁻¹	Volume, mL
20 kHz	180	30	37.28	0.47	80
40 kHz	200	90	44.75	0.18	250
200 kHz	100	70	16.75	0.07	250
572 kHz	120	83	48.83	0.19	250
577 kHz	120	83	57.75	0.23	250
856 kHz	120	83	46.86	0.19	250
861 kHz	120	83	57.50	0.23	250
1130 kHz	120	83	46.23	0.18	250
1145 kHz	120	83	46.81	0.19	250
40/200 kHz	120	83	83.99	0.34	250
40/577 kHz	120	83	115.37	0.46	250
40/1130 kHz	120	83	116.11	0.46	250

The Effect of Air Bubbling on Dissipated Power. The presence of dissolved gases in ultrasonic systems is another important parameter to enhance the sonochemical activity due to its role to act as nucleation sites for cavitation. Figure 3.6 clearly demonstrates that the temperature increase under continuous air sparging indicating the higher power dissipation into the solution (deionized water) was greater than without air. Hence, the ultrasonic experiments were all carried out under air sparging throughout the study unless stated otherwise. The effect of gas type on the performance of sonochemical reactions was also tested within the context of different case studies that will be discussed in the next sections.

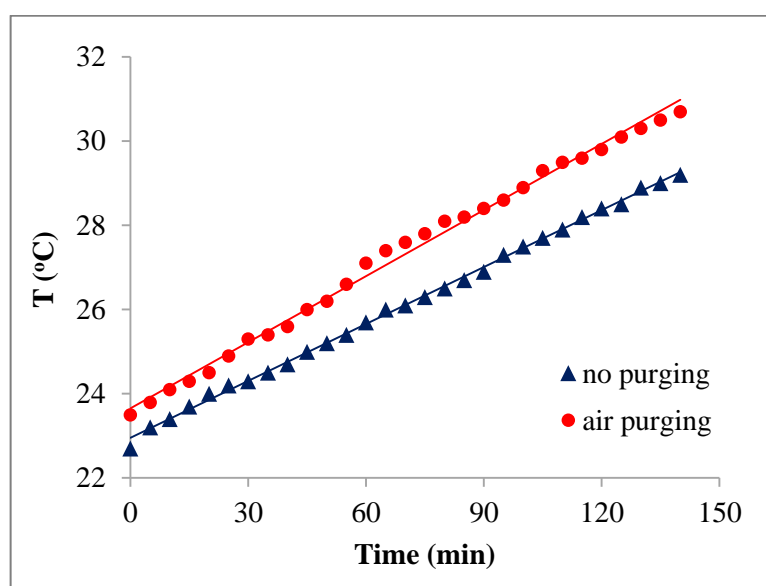


Figure 3.6. The temperature increase in R4 reactor (frequency (f)=861 kHz) in the presence and absence of air bubbling.

The Effect of Water Impurity on Dissipated Power. The constituent of the test solution is another important parameter in sonolytic experiments. The temperature profile during the sonolysis of three type of water i) deionized-, ii) distilled- and iii) tap-water was recorded as shown in Figure 3.7(a) and it was found that the highest power dissipation was obtained in deionized water. The highest power dissipation and accumulation of ultrasound generated H_2O_2 (Fig.3.7 (b)) in deionized water may be attributed to the presence of $\bullet OH$ scavengers such as SO_4^- , Cl^- etc. existing in either tap- or distilled-water. Therefore, the ultrasonic experiments were all carried out in ultrapure water (Millipore, MilliQ).

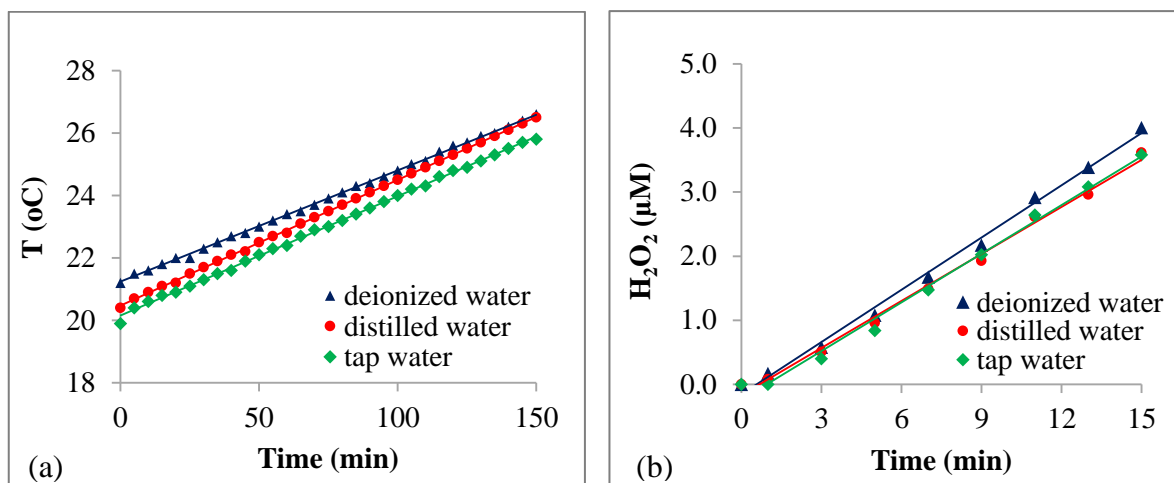


Figure 3.7. The effect of water impurities on temperature increase (a) and formation of H₂O₂ during sonolysis of water at (R4), $f=861$ kHz.

Sonoluminescence. During the ultrasonic irradiation of liquids, either particulates or stable gas bubbles may produce light, termed as "sonoluminescence" on every acoustic cycle which derives from acoustic cavitation (Suslick, 2001). The flushes of sonoluminescence involve intense ultraviolet light with a comparatively wide wavelength range and hence, sonoluminescence caused by bubble implosion may induce the excitation of semiconductors in the ultrasonic system (Shimizu et al., 2007). Moreover, it is known that asymmetric bubble collapses with a vortex ring may produce sonoluminescence in heterogeneous sonochemistry, which result in free radical production in the near vicinity of the solid surface, a rich region for sonochemical reactions (Her et al., 2011).

The test procedure for the measurement of sonochemiluminescence (SCL) in sono-reactor consisted of i) air saturation of aqueous luminol (0.1 mM luminol in 0.1 M NaOH) solution and ii) sonolysis of the solution (Fernandez Rivas et al., 2012). During the sonolysis, the image of sonoluminescing bubbles generated in R4 reactor (at 861 kHz) was recorded by EOS 600D, 35-50 mm lens, 4.5 lens aperture, exposure time 30". Figure 3.8 shows the sonochemical active regions at R4 (at 861 kHz).



Figure 3.8. The image of sonochemiluminescence in luminol solution (250 mL) at R4 reactor ($f=861$ kHz).

4. SONOLYTIC AND SONOCATALYTIC DECOMPOSITION OF DICLOFENAC USING ZERO-VALENT IRON

The present chapter is a summary of the work published in *Ultrasonic Sonochemistry* 20 (2013) 580-586 as “More on sonolytic and sonocatalytic decomposition of Diclofenac using zero-valent iron”. It highlights the significance of operation parameters and the effect of novel magnetic nanoparticles of ZVI on the elimination of diclofenac by sonolysis and sonocatalysis.

4.1. Introduction

Current research on the degradability of DCF by ultrasound has shown that complete conversion of the drug to more readily biodegradable forms is possible, but its ultimate mineralization is not (Naddeo et al., 2010). Accordingly, hybrid processes such as sonozonolysis and sonocatalysis are effective, as they provide complete degradation and appreciable mineralization of the compound (Hartmann et al., 2008; Naddeo et al., 2009a; Tezcanlı-Güyer and Ince, 2011). The increase in efficiency by such combinations is related to factors such as enhanced mass transfer rates of gases and solutes, enlarged surface areas of solids, excess bubble nuclei and excess $\text{OH}\cdot$ formation. Furthermore, the use of zero-valent iron (ZVI) separately or in combination with AOPs has also received much attention during the last decade, particularly for the destruction of non-biodegradable micro-pollutants. The potential of the method is based on the reactivity of iron to initiate surface chemistry and Fenton-like or “advanced Fenton” reactions. In the presence of ultrasonic cavitation, ZVI is further effective via the synergy of ultrasound and surface chemistry leading to enhanced mass transport of pollutants to the metal surface with increased surface defects and active sites, and continuous cleaning of the surfaces (Chand et al., 2009; Eren and Ince, 2010; S. D. Kim et al., 2007; Tezcanlı-Güyer and Ince, 2011; Zhou et al., 2008). In addition, the chemical reactions occurring at the metal surface produce ferrous/ferric ions and H_2O_2 to promote oxidation, reduction and mineralization of the reactants. A list of aqueous and surface reactions occurring in sonicated water containing ZVI can be found in the literature (Molina et al., 2006; Tezcanlı-Güyer and Ince, 2011).

The aim of this study was to investigate the operation parameters of sonochemical elimination of DCF in water (e.g. frequency, pH, sample preparation, sparging gas, ultrasound dose) and to assess the effect of a cost-effective catalyst made in the laboratory as magnetic nanoparticles of zero valent iron (ZVI). The efficiency of the process was evaluated not only by the rate of DCF elimination at optimized conditions, but also by the change in chemical and biochemical oxygen demands; and the extent of carbon, chlorine and nitrogen mineralization. The study also encompasses the assessment of $\bullet\text{OH}$ radical production in the presence of the catalyst and comparison of the catalyst efficacy with that of commercial micro-particles of ZVI.

4.2. Materials and Methods

Diclofenac sodium salt (with properties as given in 3.1.1 Section) was used as received. The zero-valent iron was made in the laboratory as nano-scale magnetic particles coated with disordered carbon, iron carbide and graphite (ZVI-I). The chemical/physical composition and average particle size of the catalyst is as listed in Table 4.1.

The particles were synthesized using edible oils to produce an identical product to that obtained previously by sonication of $\text{Fe}(\text{CO})_5$ in diphenylmethane in a two-stage process at the laboratory of Prof. Gedanken at Bar-Ilan University, Israel (Koltypin et al., 2004; Nikitenko et al., 2001).

Table 4.1. Characteristics of the catalyst.

Characteristics	ZVI-NP
Fe (%)	29
Carbon (%)	5.6
Hydrogen (%)	0.008
Sulfur	-
Oxygen	-
Silicon	-
Diameter (nm)	20-100

4.2.1. Analytical

DCF was analyzed using HPLC analyzer as described in Section 3.2.3. Alternatively, DCF was analyzed spectrophotometrically at 276 nm using a Unicam Helios α -Double Beam Spectrophotometer with a 1 cm quartz cell. Total organic carbon, H₂O₂, COD, BOD₅, Cl⁻ and NO₃⁻ were analyzed in accordance with the procedures described in Section 3.2.3. The concentration of total iron and carbon content of nanoparticles was measured by Atomic Absorption Spectrophotometer and Elemental Combustion System, respectively.

4.2.2. Experimental

The reactor was either: i) a high-frequency plate-type (500 mL) (R4) that emitted optionally at 577, 861 or 1145 kHz or ii) a low-frequency horn-type (150 mL) emitting at 20 kHz (R1). Both were surrounded by water-cooling jackets to maintain constant temperature (22±0.5 °C). The power inputs were adjusted such that the reactors had closely similar specific powers of 0.23 W mL⁻¹ and 0.19 W mL⁻¹, respectively.

4.2.3. Procedure

Preparation of the Magnetite Nano-particles (ZVI-I). Commercially refined and rapeseed corn oils and Fe(CO)₅ (99.5% STREM) were used as received without additional purification. A 100 mL solution of 1 M Fe(CO)₅ in oil was sonicated for 3 h under argon atmosphere by means of a Sonics and Materials VCX600 ultrasonic device with a direct-immersion titanium horn (surface area=1 cm²) and an electric generator operating at 20 kHz and 600 W, respectively. The absorbed acoustic power was measured by the thermal probe method as 0.45 W mL⁻¹. The temperature of the solution was kept at 0 - 10°C by a Julabo FT-901 cooler during the reaction. The black solid product after sonication was removed by centrifugation, washed three times with dry pentane inside a N₂-filled glove box, and dried under vacuum at room temperature. Annealing of the solids was performed at 750 °C for 3.5 h under an argon flow (99.996%). The coating material was made of air stable Fe₂C+C with a Fe to Fe₂C ratio of 4:1. As such, the product was found highly effective in eliminating TCE and PCE from contaminated water despite the air-stability of the carbon shell wrapping (Tiehm et al., 2009).

Sonolysis and Sonocatalysis. A stock DCF solution of 3000 μM was made by dissolving 0.954 g of DCF in 1 L of ultrapure Milli-Q water during magnetic stirring. Samples were saturated with air, adjusted to the desired pH using 0.1 N NaOH or H_2SO_4 and sonicated at ambient temperature for 30-90 min to select the optimum power, frequency and sparging gas (air, O_2 , Ar). Aliquots were collected from the reactors within short intervals for the analysis of DCF and UV absorption of the treated solutions. The overall degradation of the drug was assessed by monitoring the TOC, COD, BOD_5 , Cl^- and NO_3^- of the test solutions during 30-, 45-, 60- or 90-min sonication at pH 3.0 and $5.5 < \text{pH} < 6.0$ (the range of pH right after air saturation). All samples were initially 30 μM , except those aimed to evaluate the change in biodegradability, in which concentrated samples of 420 μM were made to minimize the standard problems associated with the analysis of very low BOD_5 .

Catalytic experiments were run at varying solids mass of the nanoparticles under optimized sonolysis conditions to select the most effective catalyst concentration or the best dose of Fe^0 as g Fe: g DCF. The impact of the catalyst was assessed by the apparent rate of DCF disappearance at the optimum solids mass concentration, the effective ratio of Fe^0 to DCF at the optimum, and the formation of Cl^- and NO_3^- ions as the indicators of mineralization. Silent experiments were run at pH 3.0 and the natural pH of the samples (following air saturation) in 50 mL test solutions shaken at 150 rpm at 35°C to determine the effect of adsorption and silent surface reactions of DCF with the catalyst. Finally, TOC control experiments were run during 90-min sonication of Milli-Q water spiked with the effective catalyst concentration to determine the quantity of organic carbon released from the coating material.

Separation of ZVI from Solution. Nanoparticles of ZVI were separated from sonicated solutions using a N-35 grade neodymium magnet ($d=2.0$ cm, $h=1.5$ cm, flux density= 11000 G) placed under a soft iron sheet mounted at the lower end of a 0.5 L cylindrical glass tube. Samples were transferred to the tube right after sonication to allow complete attachment of the particles on the metal sheet within 5-minutes followed by withdrawal and filtration of the supernatant. The system was cleaned by removing the magnet and washing the metal sheet thoroughly with pressurized water. A schematic diagram of nanoparticles separation system is demonstrated in Figure 4.1.

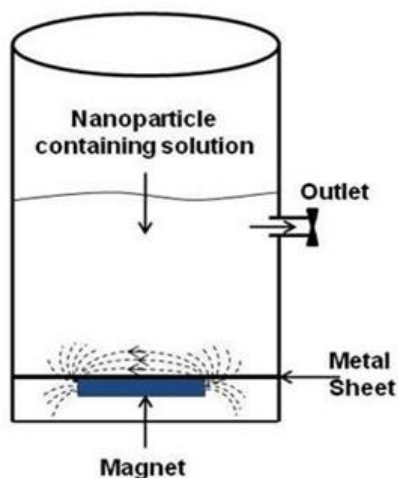


Figure 4.1. Nanoparticle separation system.

4.3. Results and Discussion

4.3.1. Optimization of the Reaction Parameters

Normalized plots of DCF against sonication time are presented in Figure 4.2 (Upper right corner shows the rate of H_2O_2 formation in pure water during 60 min sonication at 20 and 861 kHz). The data show that regardless of the applied frequency, the rate of reaction followed an exponential pattern, but with a considerably smaller rate constant at 20 kHz than at high frequencies. Pseudo-first order reaction rate constants were estimated as 0.011 min^{-1} , 0.041 min^{-1} , 0.071 min^{-1} and 0.032 min^{-1} at 20 kHz, 577 kHz, 861 kHz and 1145 kHz, respectively. Slow reactions of hydrophilic solutes at short-frequency ultrasound are due to long bubble life times and low incidence of efficient bubble collapse that hinder the ejection of $\text{OH}\cdot$ to the bulk solution (Eren and Ince, 2010). This is confirmed by the inset at the top right corner of the figure, showing the zero-order rate of H_2O_2 formation during 60-min sonication of Milli-Q water by 20 and 861 kHz ($k_0=0.55$ and $1.58 \mu\text{M min}^{-1}$, respectively).

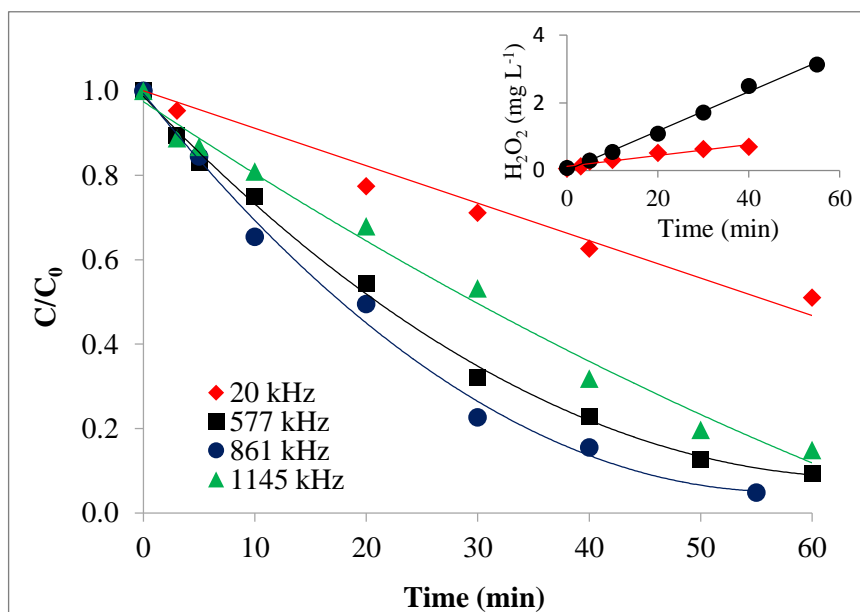


Figure 4.2. Sonochemical rate of DCF degradation at low and high frequency ultrasound ($C_0 = 30 \mu\text{M}$, $\text{pH} = 2.8\text{-}3.0$, $P = 0.20 \pm 0.04 \text{ W mL}^{-1}$).

Lower reactivity of low-pKa (4.35 for DCF) hydrophilic compounds at acidic pH (than at near-neutral pH) is not common; so we repeated the experiments at pH 3.0 in an acetate-buffered solution. We found that the rate of degradation was considerably faster than that at non-buffered condition and the acceleration was attributed to the formation of acetic acid, which exists in molecular form at acidic conditions and is converted to the acetate radical via a moderate reaction with $\bullet\text{OH}$ ($k = 1.6 \times 10^7 \text{ M s}^{-1}$ (De Laat et al., 2004)). It is also possible that some of the acetate radicals reacted with $\bullet\text{SO}_4^{2-}$ thus reducing the concentration of $\bullet\text{OH}$ scavenging species in solution, while others were oxidized to form reactive acetyl peroxy radicals.

We also found that pH was a crucial parameter in the solubilization of DCF, as depicted in Figure 5.3 by the UV spectrum of the compound at acidic and natural pH. The absorption maximum was around 276 nm with peak values of 0.139 and 0.294 at pH 3.0 and 5.6, respectively. Low solubility of the compound at acidic pH was improved by re-preparation of the test samples from a heated stock solution (40°C), as shown by the data at the top right corner of Figure 4.3 presenting the relative fractions of DCF transferred to solution at pH 3.0 and 5.6 using heat-treated and untreated stock solutions.

Further operation parameters of significance were the bubbling gas and the applied ultrasound dose, the impacts of which are presented in Figure 4.4 and Figure 4.5, respectively for 861 kHz ultrasound. It was found that the rate of DCF degradation was most rapid under air bubbling ($k=0.071 \text{ min}^{-1}$), but slowed down under argon (0.056 min^{-1}) and oxygen atmospheres ($k=0.038 \text{ min}^{-1}$) as shown by the data in Figure 4.4. Factors affecting the performance of sparging gases and air have been described in the section 2.2.2 and the results obtained in this work are consistent with the majority of the literature reporting gas effects (Gültekin and Ince, 2008; Méndez-Arriaga et al., 2008; Sivasankar and Moholkar, 2010).

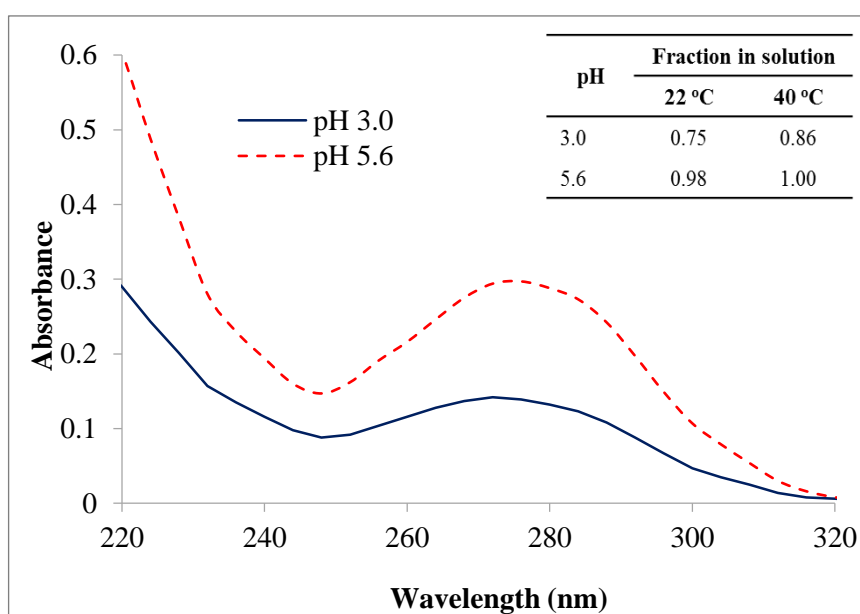


Figure 4.3. The effect of pH and temperature on the UV spectrum of DCF.

Regarding the impact of specific power or ultrasound dose, we found that fractions of DCF elimination after 50-min sonication (861 kHz) of $30 \mu\text{M}$ test samples at 9 W, 14.5 W and 57.5 W were 60%, 75% and 95%, respectively. Hence, we used an input power of 57.5 W in all experiments that corresponded to a specific power of 0.23 W mL^{-1} in the high-frequency reactor.

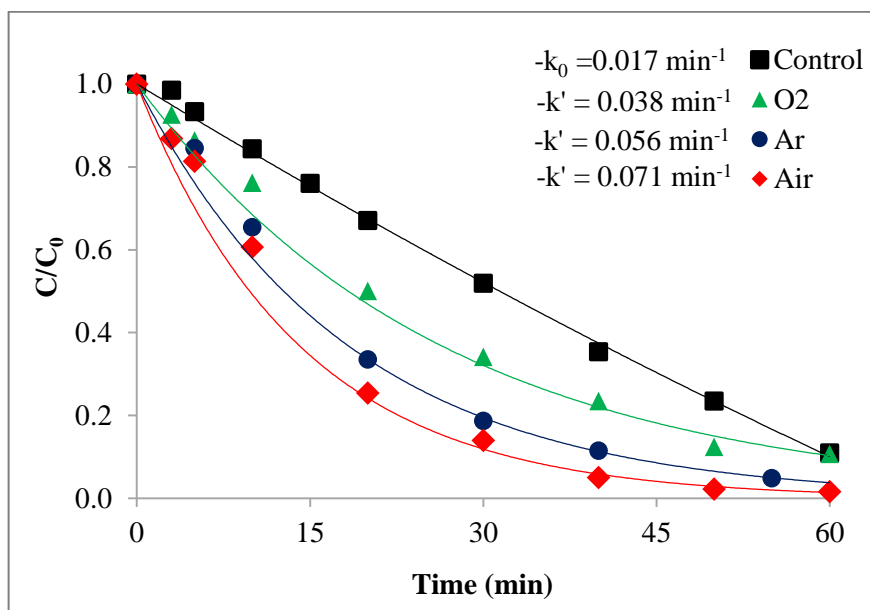


Figure 4.4. Relative degradation of DCF under air, argon and oxygen atmospheres ($C_0=30 \mu\text{M}$, $\text{pH}_i=3.0$, gas flow rate= 0.5 L min^{-1}). “Control” refers to sonication with no gas addition.

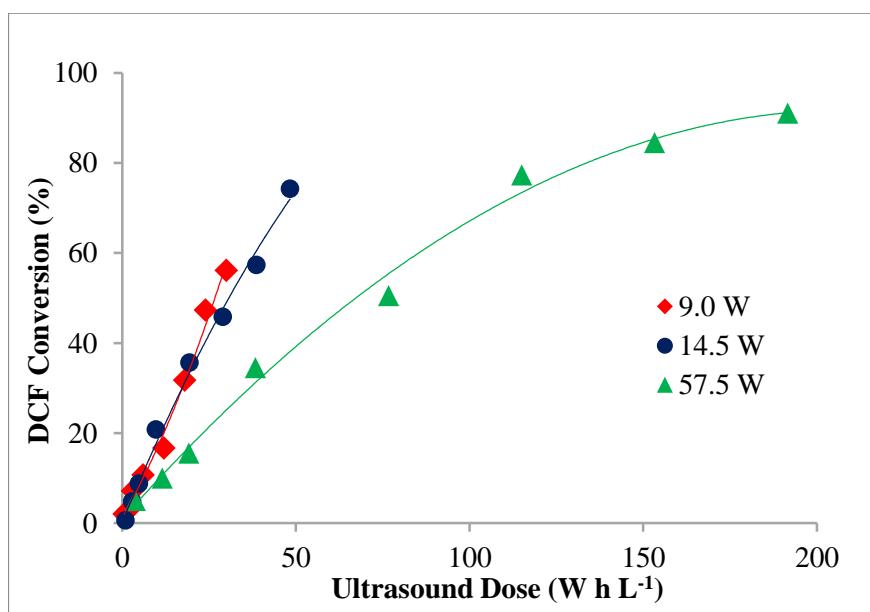


Figure 4.5. The effect of ultrasonic power or dose on the fraction of DCF elimination ($C_0=30 \mu\text{M}$, $\text{pH}_i=3.0$, at 861 kHz).

4.3.2. Conversion and Degradation of DCF by Sonolysis

Oxidation of complex organic compounds by sonication leads to the formation of less complex and more biodegradable byproducts, which however still exert chemical oxygen demand and total organic carbon. Hence, monitoring of the overall degradation process (vs. conversion of the parent compound) provides more significant information on the environmental safety of the water following oxidative treatment. The overall degradation of DCF at optimized conditions was assessed by changes in BOD₅, COD, TOC, Cl⁻ and NO₃⁻ during 60- or 90-min sonication at 861 kHz. Accordingly, the data show that a slow rate of DCF reaction during the first 30-min resulted in slightly biodegradable oxidation byproducts. After longer contact the rate of conversion sharply increased with a mild increase in the overall degradation of the compound, as observed by the raise in BOD₅ and the drop in COD and TOC of the solution. This was further confirmed by the release of Cl⁻ and NO₃⁻ ions after 45-min reaction and the formation of a dark red color that signals the presence of a quinone moiety (De Laat et al., 2004). Note that the interference of chlorine in COD tests was accounted for by adding mercuric sulfate to the COD reactor.

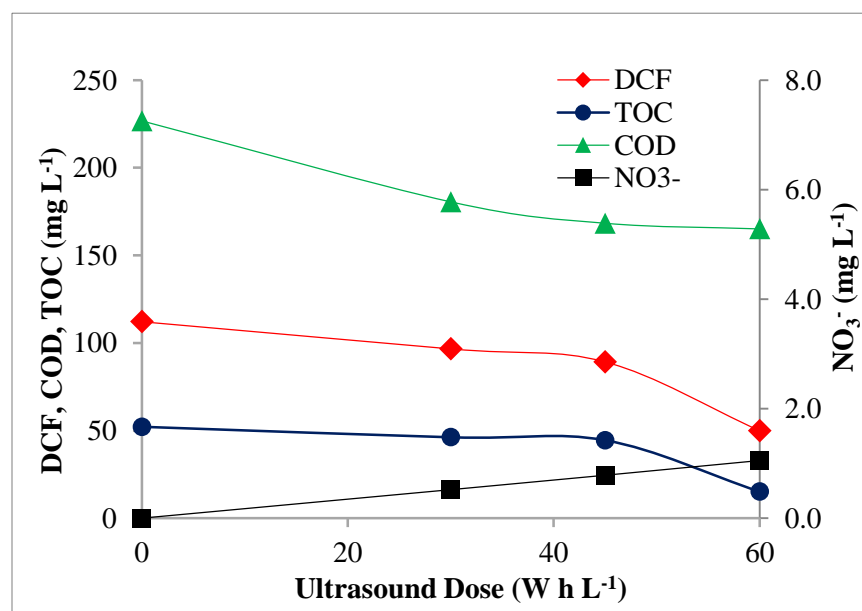


Figure 4.6. Relative conversion, degradation and mineralization of DCF at 861 kHz ($C_0=420 \mu\text{M}$, $\text{pH}=3.0$, air flow rate= 0.5 L min^{-1}).

4.3.3. Sonocatalysis

DCF test samples were contacted silently with ZVI for 0.5, 1, 1.5 and 24-h during mild mixing to depict the effect of sorption and silent reactions. The results of the tests showed that after 30-min contact with 0.2 g L^{-1} of the catalyst at pH 3.0, the aqueous concentration of DCF decreased by 41%, while that of total Fe increased to 8.55 mg L^{-1} . Further alterations in DCF at longer contact were insignificant, as total DCF disappearance after-24 h was 45% in the presence of the same quantity of ZVI, and that of iron was 9.21 mg L^{-1} . Another set of control experiments run with the nanoparticles and ultrasound alone (without DCF) showed that sonication (861 kHz) rendered solubilization of organic carbon from the coating material of the catalyst and dissolution of ionic Fe species, highlighting the unique effect of ultrasound for wearing out surface coatings to allow solubilization and discharge of the contents. The data are presented in Table 4.2.

Table 4.2. The release of TOC and Fe from 0.2 g L^{-1} ZVI during sonication at pH 3.0.

Time (min)	ZVI	
	TOC (mg L^{-1})	Fe (mg L^{-1})
30	1.21	1.90
60	1.38	7.00
90	1.41	9.20

Selection of the Optimum pH, Frequency and Catalyst Concentrations. The optimum operation parameters of sonocatalysis were selected based on the rate of DCF degradation during 30-min sonication at 20 and 861 kHz, three distinct pH levels and increasing mass ratios of Fe^0 to DCF. It was found the reactions were most rapid at non-buffered pH 3.0, the catalyst was more effective at high frequency irradiation, and the rate of degradation was negligible at pH 10.0. Moreover, the rate was found to approach a maximum with increasing concentrations of solids between $0.05 - 0.2 \text{ g L}^{-1}$, and declined sharply with a further increase. Consequently, the reaction kinetics revealed pseudo-first order character only at low solids concentrations or early contact, but saturation-type kinetics at higher solids and longer reaction times. Deviation from pseudo-first order kinetics is a consequence of heterogeneous chemistry and the adsorptive behavior of DCF when in contact with the catalyst silently. As

such, we considered the first 20-min of sonication and to estimate the apparent reaction rate constants.

It was found that the most effective solids concentration was 0.2 g L^{-1} , corresponding to a Fe: DCF mass ratio of 6.09, at which the apparent reaction rate constant was 1.86 s^{-1} . Slowing down of the reactions at the next higher dose must be due to the presence of excess solids, excess bubble nuclei and excess Fe species in solution, the interaction of which caused destabilization and coalescence of the particles and the bubbles thus leading to smaller particle surfaces and less energetic bubble collapse. The initial reaction rate constants at each test condition and Fe: DCF mass ratios are listed in Table 4.3 together with those observed in the presence of commercial ZVI micro-particles used in a similar study carried out at the same conditions (Tezcanlı-Güyer and Ince, 2011). The data show that the rate constants were comparable at low catalyst concentrations, but the sharp decline in the presence of nanoparticles with an increase in concentration from 0.2 g L^{-1} to 0.3 g L^{-1} was not valid for the micro-particles.

Table 4.3. Initial reaction rate constants at the applied catalyst concentrations and Fe doses ($C_0=30 \text{ }\mu\text{M}$, $\text{pH}=3.0$, $t=20\text{-min}$).

Catalyst	Total solids (g L^{-1})	Total Fe (mM)	Fe dose ($\text{gFe}^0/\text{g DCF}$)	-k (sec^{-1})
ZVI nanoparticles	0.05	0.25	4.463	1.16
	0.10	0.51	2.985	1.30
	0.20	1.04	6.087	1.86
	0.30	1.56	9.131	0.98
ZVI microparticles	0.05	0.89	5.206	1.23
	0.10	1.71	26.047	1.48
	0.20	3.42	57.947	1.56
	0.30	5.13	104.187	1.30

To check the role of $\bullet\text{OH}$ and/or Fenton-like reactions on the observed catalytic effects, we monitored the concentration of H_2O_2 during sonolysis in the absence and presence of three test concentrations of ZVI. The data as presented in Fig. 5.7 show that the rate of H_2O_2 formation was slow and zero-order in “Control” (pure water) and “DCF” (pure water with DCF), but faster and non-zero-order with DCF and the catalyst. That the rate is slightly slower in “DCF” than in “Control” is an indication of $\bullet\text{OH}$ consumption by the drug during oxidation. The most striking feature of Figure 5.7 is the accumulation of large excesses of

H₂O₂ in “ZVI2”, i.e. the sample with the most effective catalyst test concentration (0.2 g L⁻¹), which provided maximum DCF elimination (Table 5.3). This can be explained by the following hypotheses: i) there are definitely other major routes of •OH generation than water pyrolysis (e.g. chemical reactions at the iron surface that produce ferrous/ferric ions, H₂O₂ and gaseous hydrogen; ii) the reactions of DCF occur at solid surfaces or the interfacial regions such that all or most of the •OH ejected to the bulk liquid are available for recombination.

Increased rates of •OH and H₂O₂ formation has also been reported by others for sonolysis in the presence of metal oxides such as CuO·ZnO/Al₂O₃ and attributed to the interaction between ultrasound waves and metal catalysts (Papadaki et al., 2004). The benefits of using nanoparticles of metal catalysts as in this study lie on the synergy of ultrasound and massive solid surfaces, the outcome of which are extensive nucleation/reaction sites, large excesses of •OH radicals/H₂O₂ and continuous cleaning of the surfaces. It is also interesting that rates of H₂O₂ formation in “ZVI1” and “ZVI3”, i.e. samples with the less effective catalyst concentrations (0.1 g L⁻¹ and 0.3 g L⁻¹, respectively) were much lower, but still in excess of the control. Hence, addition of the right solid mass is of utmost significance, for otherwise the increase in the rate of •OH formation is compromised by their waste through recombination reactions.

4.3.4. Mineralization

Carbon mineralization was hard to assess due to the irregular pattern of TOC release from the catalyst during sonication and the difficulty of generating reproducible TOC data. Hence, the overall degradation of DCF was evaluated in terms of Cl⁻ and inorganic nitrogen formation, the latter indicating late transformation of the compound by oxidation processes (Calza et al., 2006; Coelho et al., 2009; Hartmann et al., 2008). Figure 5.8 shows relative rates of chloride and nitrate build-up during elimination of DCF at pH 3.0 by sonolysis (Control) and sonocatalysis using ZVI. It was found that there was almost no mineralization before 45-min sonication, and the rate of chloride formation thereafter exceeded that of nitrate, with a final Cl⁻ that was close to the stoichiometric quantity. Slower rate of N-mineralization is reasonable, because the cleavage of a C-N bond first releases NH₂-N, which is slowly and subsequently oxidized to NO₂⁻ and NO₃⁻. This is why the final NO₃⁻

concentration was no more than half the stoichiometric level. However, the result is far better than that obtained by Advanced Oxidation Processes, which mainly transform the amino moiety to ammonium ions with very little NO_3^- formation (Calza et al., 2006; Coelho et al., 2009). Larger efficiency of N-mineralization here is due the decomposition of $\text{NH}_2\text{-N}$ inside the gaseous cavity bubbles via the extreme conditions generated by cavitation collapse. Note that the slight background Cl^- level in “Control” (most likely arising from the impurities in DCF) was neglected because the same quantity was also present in “ZVI”, but the Cl^- released from the particles was accounted for by running another control experiment with the particles without DCF. Similarly, nitrate data for ZVI in Figure 4.8 are free from nitrate released from the particles.

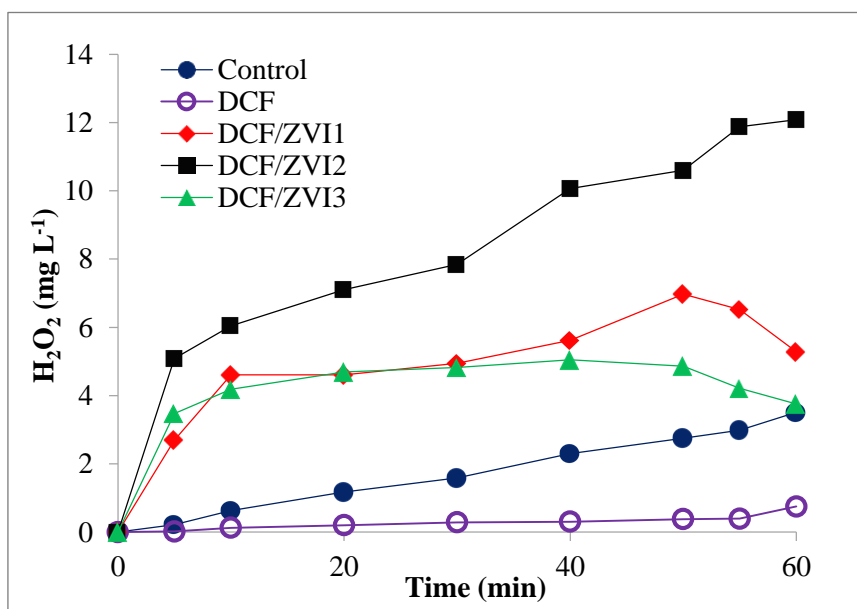


Figure 4.7. Accumulation of H_2O_2 during sonolysis of DCF in the presence of 0.1 g L^{-1} (“ZVI1”), 0.2 g L^{-1} (“ZVI2”) and 0.3 g L^{-1} (“ZVI3”) ZVI at 861 kHz. “Control” and “DCF” refer to ultrasound alone and US-DCF with no catalyst, respectively.

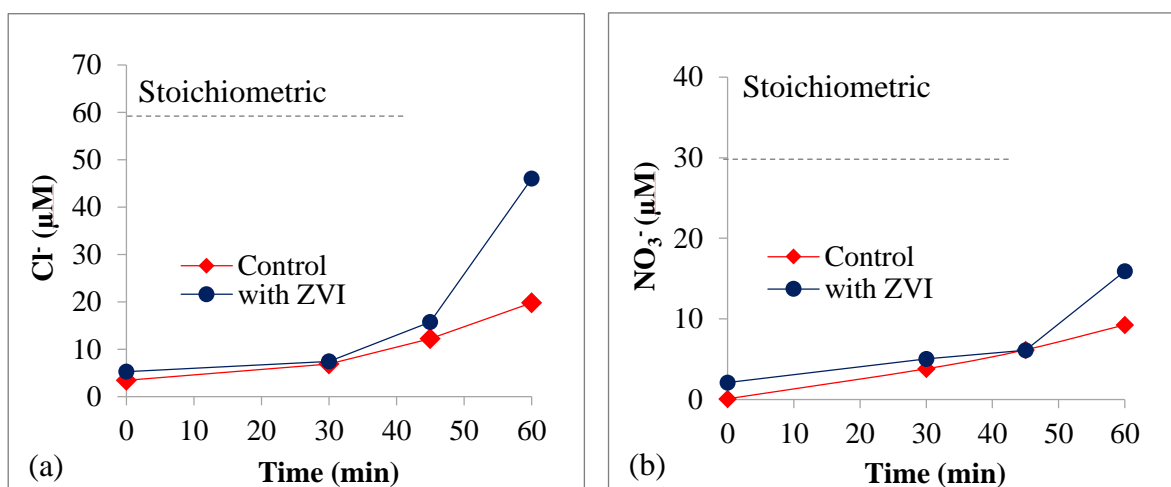


Figure 4.8. Relative rates of chlorine (a) and nitrogen (b) mineralization by sonocatalysis ($C_0=30 \mu\text{M}$, $\text{pH}=3.0$, $\text{ZVI}=0.2 \text{ g L}^{-1}$). “Control” refers to sonolysis without ZVI.

4.3.5. Comparison of Nano-and Micro-ZVI for the Efficiency of DCF Elimination

The relation between the initial rate of DCF elimination and the applied Fe dose is presented in Figure 4.9 to assess the relative efficacies of nano- and micro-particles of ZVI. In each case the data were fitted to a polynomial, the linear slope of which was considered an estimate of the amount of DCF eliminated in time per unit mass of metallic iron added. Defining the efficiency (E), we found that catalytic effect of the nanoparticles was one order of magnitude larger than that of micro-particles despite the 3-fold lower Fe content of the former at identical mass concentrations. Hence, the effect of nanoparticles was by far related to the surface properties and massive surface areas rather than to the incidence of Fenton or advanced Fenton reactions. This is also confirmed by the accumulation of excess H₂O₂ when sonication was carried out in the presence of nano-ZVI.

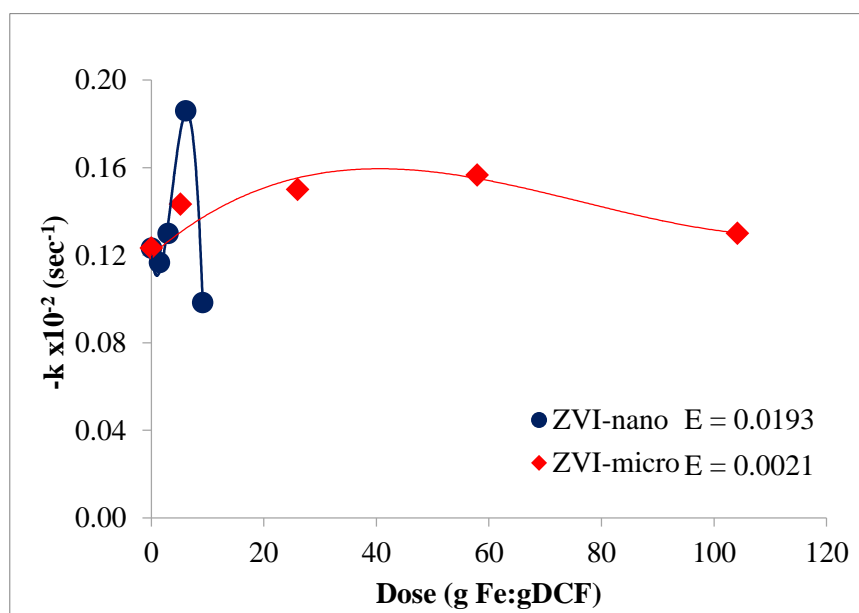


Figure 4.9. Relative efficacies of ZVI-nano and ZVI-micro as a function of the Fe dose.

4.4. Conclusions

The study has shown that the undesired presence of DCF in surface and sewage water can be managed by pretreating the contaminated water/wastewater by high frequency ultrasound to produce less complex byproducts, which are not only more biodegradable but also have less chemical oxygen demand and less organic carbon. The technique involves pre-heating of the water sample to 40°C to enhance solubility of the drug, followed by air saturation and sonolysis at acetate-buffered pH 3.0 during continuous aeration. As such, it is possible to obtain complete elimination of DCF with 22% and 9% reduction in COD and TOC, respectively and a three-order of magnitude increase in the ratio of BOD₅:COD (0.0003 to 0.35). Integration of sonolysis with lab-made nanoparticles of zero valent iron is an excellent means of improving the efficiency of the overall degradation of the drug via the synergy of ultrasound and nanoparticle surfaces that lead to accelerated rates of mass transfer from the bulk solution to the gas-liquid and solid-liquid interfaces, as well as excess sites for adsorptive reactions and bubble nucleation.

Finally, the study has highlighted the promise of low-cost metallic nanoparticles as powerful alternatives to commercially available and costly micro-particles for catalyzing ultrasonic remediation of contaminated water containing recalcitrant micro-pollutants.

5. SONOCHEMICAL DEGRADATION OF DICLOFENAC: BY-PRODUCT ASSESSMENT, REACTION MECHANISMS AND ENVIRONMENTAL CONSIDERATIONS

The present chapter is a summary of the work published in *Environmental Science and Pollution Research* (2014) 21:5929–5939 as “Sonochemical degradation of Diclofenac: byproduct assessment, reaction mechanisms and environmental considerations”. This study covers a thorough assessment of the overall degradation of diclofenac-Na (DCF) by high frequency ultrasound focusing particularly on identification, interpretation, and characterization of the oxidation byproducts and their reaction mechanisms.

5.1. Introduction

A thorough literature survey on AOP-treatment of DCF has shown that there is plenty of information on the intermediate products that form during ozonation, UV/H₂O₂, γ -irradiation, photo-Fenton reaction and TiO₂-based photocatalysis (Homlok et al., 2011; Martínez et al., 2011; Pérez-Estrada et al., 2005; Vogna et al., 2004), while only two specific studies report the oxidation byproducts of US-mediated AOPs (Hartmann et al., 2008; Madhavan et al., 2010b). Owing to the fact some of these products, particularly the chlorinated ones may be more harmful than DCF itself (as reported for 2,6-dichloroaniline (Calza et al., 2006), it is necessary to determine the environmental safety of the process or of the reaction byproducts. This is possible either by monitoring the acute toxicity or the oxygen uptake rate of the reactor aliquots at well-selected time intervals to compare the results with that of the untreated solution. As such, it is possible to control the operation of the process to allow sufficient energy or time for appreciable degrees of Cl-mineralization.

The present study aims to present a novel approach to the overall degradation of DCF under high frequency sonication to highlight: i) the formation, identification, and characterization of the oxidation byproducts and the corresponding reaction mechanism; ii) the assessment of the overall degradation of the target compound and the environmental friendliness of the applied process using the acute toxicity and biodegradability of the reactor

aliquots. The novelty of the work lies on the fact that previous studies on sonochemical destruction of DCF cover either the analysis of oxidation byproducts (Hartmann et al., 2008; Madhavan et al., 2010b), or determination of carbon mineralization and the acute toxicity of the test solutions (Naddeo et al., 2010, 2009a). None of these works encompass an overall assessment of the oxidation process to highlight the relationship between byproduct formation and variations in the UV spectrum, toxicity and biodegradability of the solution.

5.2. Materials and Methods

Diclofenac, all analytical grade reagents and Finisterre C18 SPE cartridges were obtained from Sigma, Merck and Finisterre, Istanbul, respectively. A stock solution of 100 mg L⁻¹ (314 μM) was prepared by dissolving 0.099 g DCF in 1 L of ultrapure water during magnetic stirring. Fresh test samples of 5 mg L⁻¹ (15.72 μM) were made via heating the stock solution to 40°C as described earlier (Ziylan and Ince, 2013). Additionally, a standard solution was prepared by dissolving DCF in a mixture of 50 % (v/v) acetonitrile-water to use in LC/MS/MS analysis.

5.2.1. Experimental

Sonication was run in a multi-frequency plate-type (250 mL) reactor (R4) emitting at 861 kHz as presented in Figure 3.3. The reactor was cooled by circulating water to maintain constant temperature (20±0.5°C), and the specific power during operation was 0.012 W mL⁻¹ as estimated by calorimetric analysis (Mason and Peter, 2002). Selection of a low operation power was due to uncontrollable voltage fluctuations, which despite their rare occurrence could easily damage the generator if it were operated at a higher capacity. Nevertheless, low power input allowed the detection of very short-lived intermediate products, which at more rapid reactions would be difficult to identify. Air-saturated test samples were sonicated at ambient temperature and natural pH of the solutions (6.0±0.5) for 90-min (unless stated otherwise), and aliquots were collected within short intervals for the analysis of DCF, TOC, Cl⁻, NO₃⁻, toxicity and oxygen uptake rate, as well as for the identification of oxidation byproducts.

5.2.2. Analytical

LC/MS/MS analyses were performed using a Shimadzu LC-20AD liquid chromatography with 3200 Q-TRAP MS/MS detector and CTO-10A(C)vp oven equipped with Inertsil ODS-3 (C18), 150x4.6mm, 5 μm particle size column. Concentration of DCF was determined periodically using a mobile phase that consisted of two components: A (pure acetonitrile) and B (0.04% acetic acid in water). The separation based on A was performed as follows: 40% in 1-min: 60% in 3-min, 95% in 4-min (with a hold time of 8 min), 90% in 13-min, 80% in 14-min, 65% in 15-min, 40% in 17-min, 30% in 18-min, 5 % in 19-min (with a hold time of 50 s). The mobile phase was delivered at a flow rate of 1.0 mL min⁻¹. Sample injection volume was 10 μL and the retention time was 3.80 min.

GC/MS analyses were run following a solid phase extraction (SPE) procedure as described in 3.2.3 Section. The overall degradation process was assessed by monitoring the total organic carbon (TOC) of the reactor aliquots and the concentrations of Cl⁻ and NO₃⁻. Toxicity and biodegradability of the aliquots were measured by Microtox Toxicity and Respirometric analysis as described in 3.2.3 Section.

5.3. Results and Discussion

5.3.1. A Synopsis of the Overall Degradation Process

A normalized plot of DCF concentration against time and the corresponding ion intensities obtained by LC/MS/MS and GC/MS analyses, respectively are presented in Figure 5.1. It was found that the decay of concentration (C) and intensity (I) with time were both exponential, but described with an expression that was slightly different from the pseudo-first order law:

$$\left(\frac{I}{I_0}\right) \text{ or } \left(\frac{C}{C_0}\right) = Ae^{-kt} + P \quad (\text{Eq. 5.1})$$

where: A and P are empirical constants related to the decay regime and k is the apparent reaction rate constant. Estimated values of A , $-k$ and P for each data set are as given in the figure caption.

Spectrophotometric analysis of the test solution at time zero showed that DCF had a maximum absorption at 276 nm, which varied marginally throughout the reaction time (fluctuating and shifting within a close region) despite the exponential decay in its concentration. As such, we believed that the intermediate products contained moieties that also absorbed at around the same wavelength. (A list of such compounds, chromophores, functional groups and aromatic substituents and their corresponding absorption maxima can be found in Table 5.1).

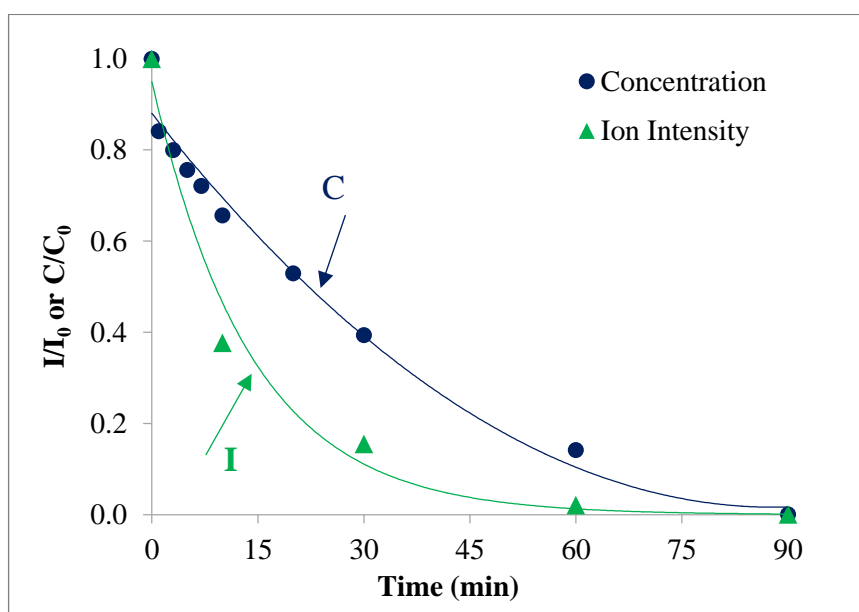


Figure 5.1. Time rates of concentration and intensity decay during 90-min sonication of DCF (15.7 μM) at pH 6.5. The solid lines represent fits of normalized concentration (line C) and ion intensity (line I) to Eq.6.1 with $R^2=(\text{C,I})=0.99, 0.92$; $A(\text{C,I})=1.03;1.51$;

$$P(\text{C,I})=0.17, 0.0; -k=(\text{C,I})=0.02 \text{ min}^{-1}, 0.09 \text{ min}^{-1}.$$

Table 5.1. The absorption maxima of some selected chromophores, functional groups and substituents that are potential components of the oxidation byproducts.

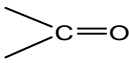
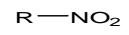
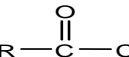
Compound/chromophore	λ_{\max} (nm)	Reference
Phenol	270-273	(Anderson et al., 2004)
Benzoic acid	275	(Anderson et al., 2004)
Aniline derivatives	235-295	(Kenzo, 1967)
Quinone derivatives	241-398	(Kenzo, 1967)
Aminophenols	233-286	(Kenzo, 1967)
Benzene	268	(Kenzo, 1967)
Isolated functional groups		
	270-295	(Schirmer, 1991)
	270-280	(Schirmer, 1991)
	280	(Schirmer, 1991)
e^- donating/abstracting substituents		
-OH	270	(Pavia et al., 2001)
-NH ₂	280	(Pavia et al., 2001)
-CN	271	(Pavia et al., 2001)
-OCH ₃	268	(Pavia et al., 2001)
-COOH	273	(Pavia et al., 2001)

Figure 5.2 shows the UV-absorption of a sample solution at 264-284 nm bands during 90-min sonication as a surface response chart, which by reference to Table 5.1 provides valuable information about the structure of the oxidation byproducts. In accordance, the sharp increase in 280 nm band at 50-60-min interval when the concentration of DCF was less than 1/10 of its initial value, and the increased absorption at 264-268 and 280-282 nm bands after 60-min may indicate the formation of amino/amine groups and phenolic, anilinic, benzene, quinone derivatives, respectively. The hypothesis was supported by the chemical structures of the detected oxidation byproducts, the details of which are discussed in the next section.

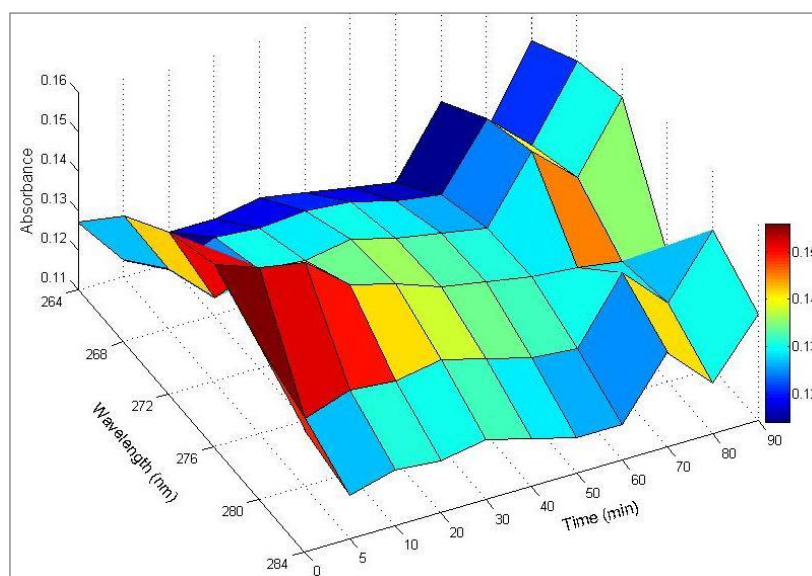


Figure 5.2. Relative impacts of sonication time and absorption wavelength on the optical density of DCF test solution ($C_0=5 \text{ mg L}^{-1}$).

The overall degradation of DCF is plotted in Figure 5.3 in terms of variations in TOC and UV-absorption (a); and accumulation of Cl^- and NO_3^- ions (b), respectively. The data show that C-mineralization during the first 30-min was much faster than that during the rest of the reaction time to be attributed to the formation of more stable intermediates with time, as also supported by the increase in UV-254 nm band after 30-min reaction. The efficiency of carbon, chlorine and nitrogen mineralization in 90-min was 45%, 30% and 25%, respectively with respect to their stoichiometric limits. A lower rate of N-mineralization (than Cl^-) is due to a longer oxidation pathway of organic nitrogen from $\text{NH}_2\text{-N}$ to NO_2 and $\text{NO}_3\text{-N}$. Note that the solution pH shifted from 6.50 to 5.23 during the first 30-min as a sign of the formation of acidic intermediates of organic origin. Some further pH decline was observed towards the end of reaction to signal the formation of hydrochloric and nitric acids, as amenable with the build-up of chlorine and nitrate ions during this period.

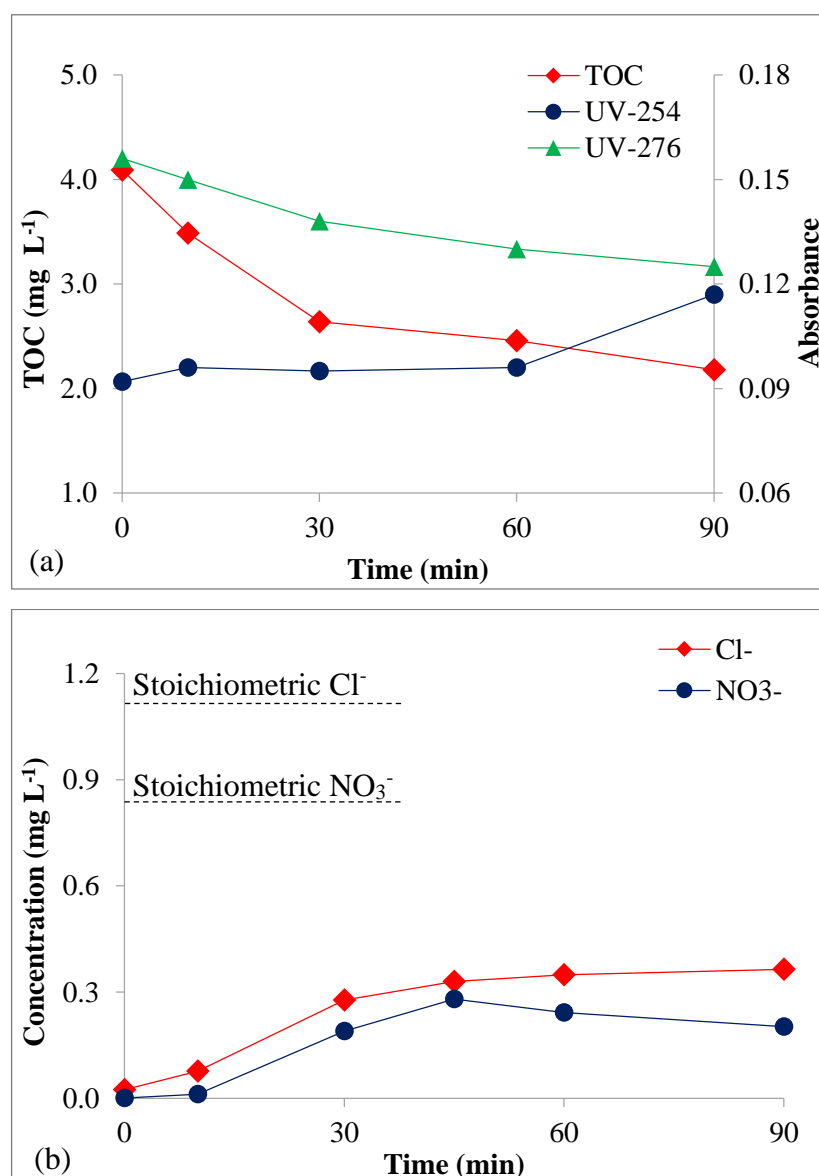


Figure 5.3. Relative rates of carbon, chlorine and nitrogen mineralization and the accompanied alterations in UV absorption of a test solution during 90-min sonication ($C_0=5 \text{ mg L}^{-1}$, $\text{pH}_0=6.5$) at 861 kHz.

5.3.2. Byproduct Analysis

The oxidation byproducts and their relative distribution/retention times are listed in Table 5.2 and Table 5.3, respectively. The octanol-water partition coefficients ($\log K_{ow}$) are also added (Table 5.2-last column) to provide information on the relative reactivity and/or environmental safety of the compounds. It was found that the most abundant byproduct was 2,6-dichloroaniline (D1), which formed at early reaction; accumulated rapidly during the

first hour; and decayed thereafter to a value equivalent to two thirds of its maximum concentration. Consequently, the last five compounds (D6-D10) that were detectable only in the 90-min aliquot and at relatively low quantities are most likely produced via subsequent oxidation of D1.

Table 5.2. The oxidation byproducts and their octanol-water partition coefficients.

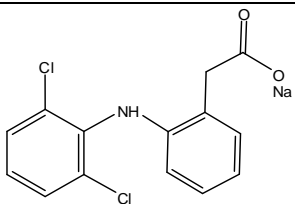
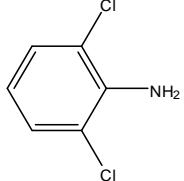
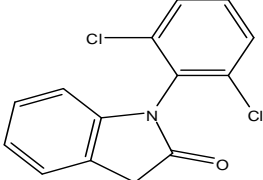
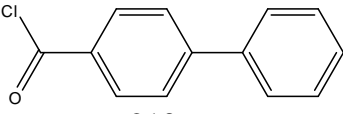
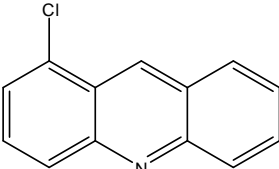
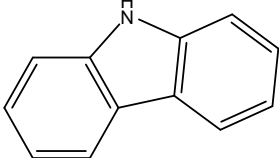
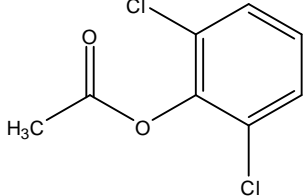
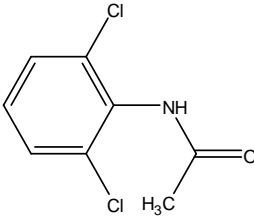
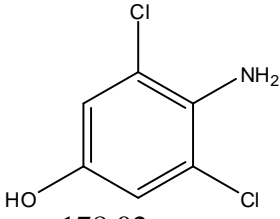
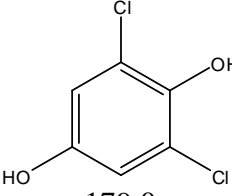
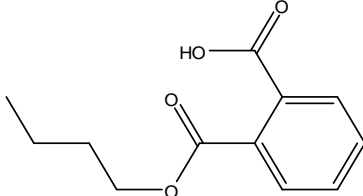
DCF and its oxidation byproducts	Structure Molecular Weight (g mol ⁻¹)	log K _{ow}
D0 Diclofenac-Na salt 2-[(2,6-Dichlorophenyl) aminobenzene-acetic acid sodium salt (C ₁₄ H ₁₀ Cl ₂ NNaO ₂)	 318.13	1.90-4.50 ^a
D1 2,6-Dichloroaniline (C ₆ H ₅ Cl ₂ N)	 162.02	2.36 ^b
D2 1-(2,6-dichlorophenyl)-2-indoline- one (C ₁₄ H ₉ Cl ₂ NO)	 278.13	3.11 ^b
D3 4-Phenylbenzoyl chloride (C ₁₃ H ₈ ClN)	 213.66	3.20 ^b
D4 1-Chloroacridine (C ₁₃ H ₈ ClN)	 213.66	3.96 ^b
D5 9H-Carbazole (C ₁₂ H ₉ N)	 167.20	3.23 ^b

Table 5.2. The oxidation byproducts and their octanol-water partition coefficients (cont.)

D6 2,6-Dichlorophenyl acetate (C ₈ H ₆ Cl ₂ O ₂)	 205.04	2.88 ^b
D7 2,6-Dichloroacetanilide (C ₈ H ₇ Cl ₂ NO)	 204.05	1.32 ^b
D8 3,5-Dichloro-4-aminophenol (C ₆ H ₅ Cl ₂ NO)	 178.02	1.53 ^b
D9 2,6-Dichlorohydroquinone (C ₆ H ₄ Cl ₂ O ₂)	 179.0	2.32 ^b
D10 1,2-Benzenedicarboxylic acid, mono-butyl ester (C ₁₂ H ₁₄ O ₄)	 222.24	2.84 ^b

^a (Scheytt et al., 2005a; Tixier et al., 2003).

^b Calculated using EPI Suit 4.0- The Estimation Programs Interface

It is noteworthy that earlier oxidation reactions produced compounds with increasing hydrophobicity (**D0 to D4**) to imply toxification of the reactor; succeeding reactions led to reduced hydrophobicity (**D4 to D8**); and a further hydrophobic enrichment was observed towards the end of reaction (**D9 to D10**). However, despite the fact that the reactivity of organic compounds declines with increasing hydrophobicity, the products **D2-D4** (with highest log K_{ow}) were found to decay more rapidly than those with lower K_{ow} . This is due to cavitation phenomenon that the larger the hydrophobicity the easier is to diffuse to the bubble-liquid interface, where the quantity of hydroxyl radicals is significantly larger than

that in the bulk liquid (Gutierrez et al., 1991). This also explains why the rate of C-mineralization during the first 30-min (at which more hydrophobic byproducts were formed) was considerably faster than that at prolonged reaction.

Table 5.3. Relative occurrence of DCF and its oxidation byproducts. The synonyms “D0-D10” are as denoted in Table 5.2.

DCF and byproducts	Retention Time (min)	Intensity (cps×10 ⁴)			
		10-min	30-min	60-min	90-min
D0	5.75	62.397	25.692	3.547	0.000
D1	4.35	7.203	23.076	76.742	50.704
D2	5.80	7.128	13.413	-	-
D3	11.50	9.519	10.189	16.427	-
D4	14.29	9.079	10.749	11.959	3.029
D5	14.42	-	10.613	15.735	6.428
D6	4.40	-	-	-	5.257
D7	7.75	-	-	-	5.150
D8	6.02	-	-	-	3.590
D9	7.30	-	-	-	6.950
D10	11.51	-	-	-	6.539

Relative ion intensities and the distribution of oxidation byproducts with sonication time are plotted in Figure 5.4 to provide an insight into the potential reaction pathway. The solid lines confirm that 2,6-dichloroaniline (**D1**) is the main intermediate product, which despite its relatively short retention time has rapidly accumulated during the first three quarters of the reaction time and declined in the last quarter. Sein et al (2008) have reported that the mechanism of its formation is based on OH• addition to the ipso-position of the amino group (Sein et al., 2008). The same compound was also found as the main intermediate product of sonocatalysis and the formation was attributed to the cleavage of C-N bond in 2,6-dichloro-N-o-tolyaniline, 2,6-dichloro-N-phenylaniline and 2-(2-(2,6-dichlorophenyl amino) phenyl) acetic acid, which were detected as the earliest transformation products (Hartmann et al., 2008; Ryu et al., 2007).

The second product 1-(2,6-dichlorophenyl)-2-indoline-one (**D2**) was also detected in the earliest reaction aliquot and in the same intensity as **D1**, but it was totally depleted within 30 minutes. The formation of D2 as explained by Hartmann et al. (2008) is based on a rapid ring closure under decreasing pH (Hartmann et al., 2008). **D3** (4-Phenylbenzoyl chloride) **D4** (1-chloroacridine) were also produced at early reaction; but they did not reach

appreciable yields. The final compound in this group is 9H-Carbazole (**D5**) that was detected in the 30-min aliquot and distinguished with its longest retention time.

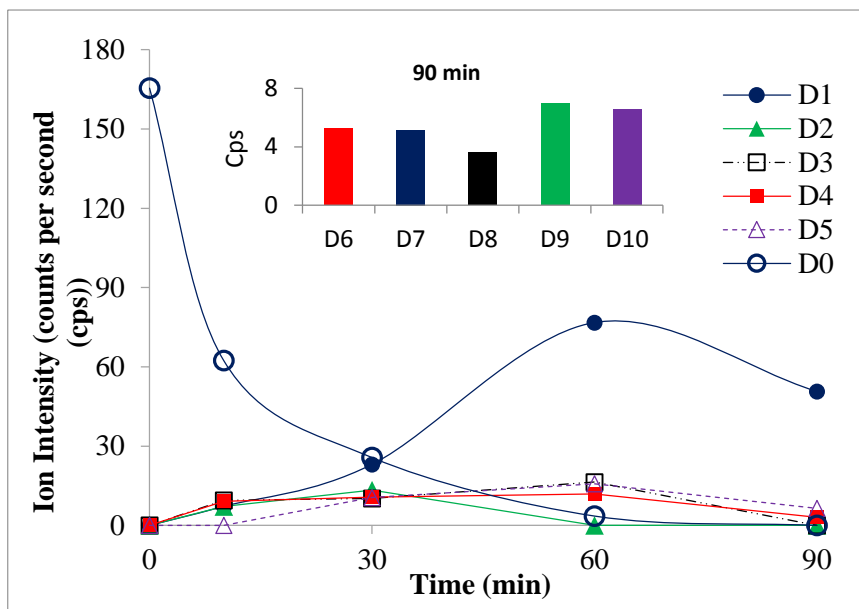


Figure 5.4. Relative distribution of DCF and its oxidation byproducts during 90-min sonication ($C_0=5 \text{ mg L}^{-1}$) at 861 kHz.

The mechanism of its formation is complex involving routes such as cyclization and dechlorination followed by hydroxylation, dehalogenation of the ring and oxidation with O_2 (Agüera et al., 2005; Barrera-Salgado et al., 2016; Martínez et al., 2011). The last five compounds (**D6-D10**) that were detected only in the latest aliquot at moderate intensities and varying retention times must have formed via delayed degradation of **D1** ($t > 60$ -min), as predicted from the spectrophotometric data in the previous section. Some of these compounds were hydroxylated derivatives (**D8-D10**) that formed via the cleavage of C-N bond in the less reactive dichloroaniline moiety as a consequence of the preference of $OH\cdot$ attack at the 1'-position to form 4-amino-3,5-dichlorophenol (**D8**) and 2,6-dichloro-p-hydroquinone (**D9**) (Vogna et al., 2004).

Note that hydroxylated byproducts in this study were formed only after prolonged sonication (due to the low power input of the sonicator), while some researchers have reported 5-hydroxydiclofenac as the primary byproduct of DCF and explained its formation by the preference of $\cdot OH$ to attack activated sites of aromatic rings to generate hydroxylated derivatives via transition through an unstable carbon-centered radical (Sein et al., 2008).

Nevertheless, dissimilarities in the sequence and time of byproduct formation must be anticipated between different laboratories, different AOPs and vastly different experimental conditions.

5.3.3. Environmental Considerations

5.3.3.1. Toxicity. Microtox toxicity of the reactor aliquots was determined using the “whole effluent” protocol described in the test manual. The tests were employed not only in aliquots of 90-min sonication, but also in those of 300-min to envision the progress of toxicity at a sufficiently long time. The data showed that toxicity had a fluctuating pattern during the degradation process increasing from a “non-toxic” to a “toxic” level throughout the first 30-min; remaining “toxic” for the next hour with positive and negative fluctuations; and declining thereafter to reach a “non-toxic” level at t=300-min. The data are presented in Table 5.4 as 15-min EC_{50} , and a unitless toxicity index TU defined as $100/\%EC_{50}$. Additionally, each aliquot is classified in the last column for its toxicity level using the reference % EC_{50} scale provided in the literature for the Microtox bioassay (Chang et al., 2013).

If the Microtox toxicity of each byproduct were available in the literature, it would be easy to assess the correlation between byproduct formation and the observed toxicity profile of the reactor. However, no such data existed so that we had to use an estimation method (“EPA, EPI Suit 4.0,” 2008) which only the algal toxicities of the byproducts. Estimated values of EC_{50} 's and the corresponding toxicity classifications as based on the related EU Directive are listed in Table 5.4, from which we selected three “highly toxic” (D2, D8, D9) and three “toxic” (D3, D4, D5) byproducts. Relative intensities of these compounds at time and the corresponding Microtox toxicity of the reactor aliquots are plotted in Fig. 5.5.

It was found that D2- the byproduct with highest algal toxicity (as depicted in Table 5.3) reached a maximum intensity at t₂ or in the 30-min aliquot, in which the Microtox toxicity was also a maximum. Although D3, D4 and D5 were also detected in the same aliquot, their contributions to toxicity were insignificant as confirmed by the decline in the next aliquot (t₃), in which no D2 was detected. A further increase in toxicity was observed in the 90-min aliquot that contained the byproducts D8 and D9, the latter being the

hydroquinone. Extended sonication for 300-min showed that the solution was rapidly detoxified after 90-min and moved closely to the “non-toxic” level as that of the initial solution.

Table 5.4. Microtox toxicity of the reactor during 300-min sonication

Time (min)	15-min EC ₅₀ (%)	TU	Classification
0	354.0	0.28	Non-toxic
30	51.9	1.92	Toxic
60	72.3	1.38	Toxic
90	65.0	1.53	Toxic
180	99.0	1.01	Slightly Toxic
300	218.3	0.45	Non-toxic

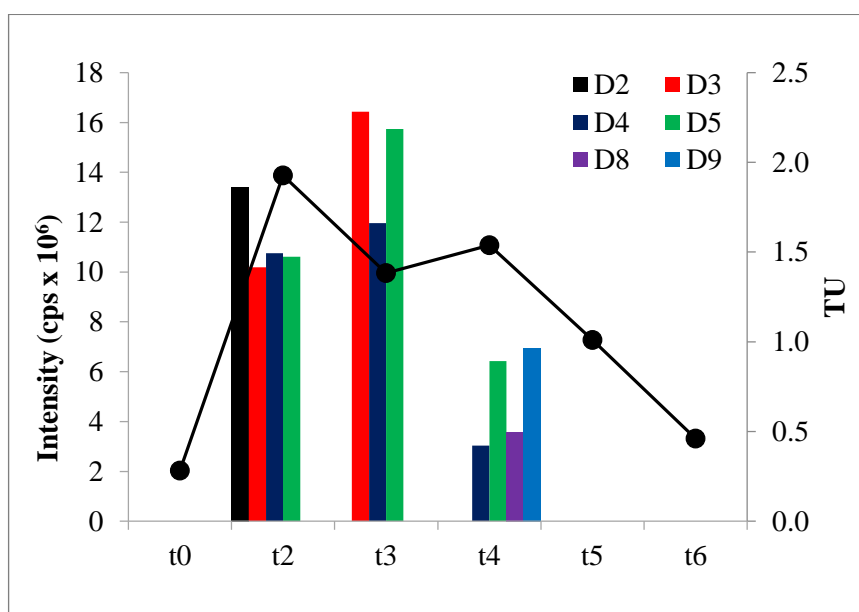


Figure 5.5. Interaction of byproducts formation and Microtox toxicity during 300-min sonication of DCF ($C_0=5 \text{ mg L}^{-1}$). The symbols “t0–t6” refer to the reactor aliquots collected at t=0, 30, 60, 90, 180, and 300-min, respectively. $TU=100/\% \text{ EC}_{50}$.

Note that Table 5.4, Table 5.5 and Fig. 5.5 all reflect acute toxicities of DCF and its oxidation byproducts, i.e. they give no information about long-term effects or the potential of the compound to bio-accumulate in cell tissues. Hence, the fact that DCF is found as “non-toxic” or estimated as “slightly toxic” in this study does not mean that its presence in the water environment is acceptable, because based on its long-term effects on aquatic organisms and the observed bird deaths shortly after ingestion it has been classified as an

“emerging” contaminant (Stülten et al., 2008). Moreover, phyto-toxicity of water bodies containing DCF was found to significantly increase upon solar degradation of the compound to signal potential harmfulness of the oxidation byproducts, as well (Schmitt-Jansen et al., 2007).

Table 5.5. Calculated algal toxicities and classification of the oxidation byproducts

Compound	EC ₅₀ ^a (mg L ⁻¹)	Classification ^b
D0 (DCF)	33.26	Slightly Toxic (10-100 mg L ⁻¹)
D1	7.04	Toxic (1-10 mg L ⁻¹)
D2	0.30	Highly Toxic (0.1-1 mg L ⁻¹)
D3	5.83	Toxic (1-10 mg L ⁻¹)
D4	1.31	Toxic (1-10 mg L ⁻¹)
D5	5.83	Toxic (1-10 mg L ⁻¹)
D6	6.24	Toxic (1-10 mg L ⁻¹)
D7	139.08	Non-toxic (>100 mg L ⁻¹)
D8	0.72	Highly Toxic (0.1-1 mg L ⁻¹)
D9	0.45	Highly Toxic (0.1-1 mg L ⁻¹)
D10	12.74	Slightly Toxic (10-100 mg L ⁻¹)

^a Estimated by EPI Suite Model (“EPA, EPI Suit 4.0,” 2008)

^b EU Directive 93/67/EEC (EUDirective, 1993)

5.3.3.2. Biodegradability. The aim of respirometric analysis was to determine the inhibitory effects of oxidation byproducts on the growth of heterotrophic bacteria in the activated sludge sample; in other words to envision the variations in biodegradability of the solution with the progress of oxidation. It was found that the raw sample solution (Control) with 50 mg L⁻¹ DCF was originally biodegradable, because its oxygen uptake rate at 24, 48, 72 and 96 hours was always higher than that of the seed. On the other hand, 10 and 30-min sonicated solutions were non-biodegradable as they resulted in significant degrees of growth inhibition.

With further reaction, biodegradability rapidly improved and finally at 90-min it exceeded that of the control. The data are presented in Figure 5.6 as percentage of growth inhibition.

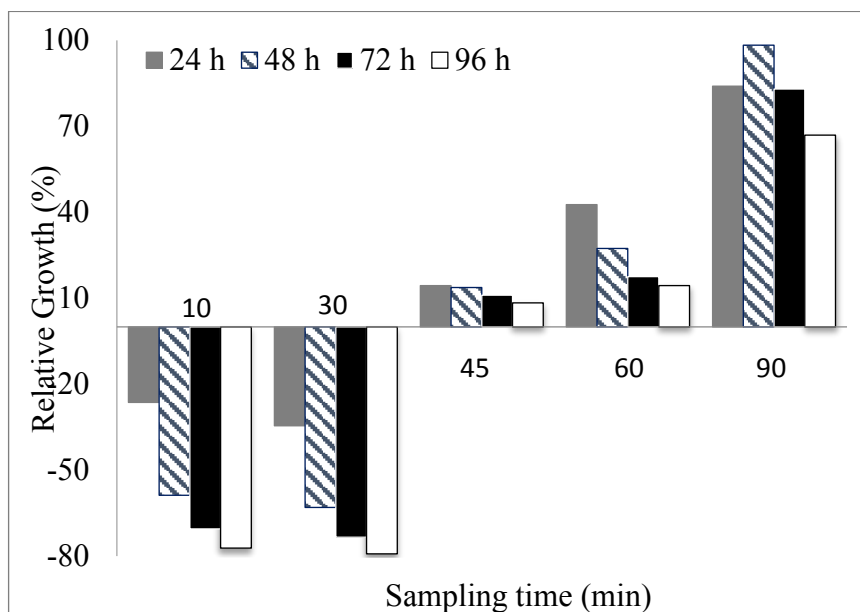


Figure 5.6. Inhibition of biomass growth during 24-96-h incubation in the presence of 10-90-min sonicated solutions of DCF.

Note the early similarity and subsequent dissimilarity of respirometric and toxicity data: both signify environmentally unsafe conditions at early reaction (0-30-min); however, respirometric data show a significant enhancement in biodegradability after 30-min sonication, while toxicity fluctuates for a long time before reaching a declining phase at $t=90$ -min. Such different patterns of improvement in the selected environmental quality parameters are obviously due to the nature of the bioassays, i.e. properties of heterogeneous and homogeneous bacteria, respectively and the ease of the former to adapt to the ambient conditions.

5.4. Conclusions

The study has shown that Diclofenac-Na (DCF) is completely eliminated by 90-min sonication of 5 mg L^{-1} DCF at near-neutral pH. The formation and depletion of most of the degradation byproducts were explained by $\bullet\text{OH}$ addition, substitution, cyclization and bond-cleavage mechanisms in the bulk solution, while more complex cases were attributed to physical/chemical reactions in the hot bubble-liquid interface. The predominant oxidation

byproduct was 2,6-dichloroaniline, which rapidly accumulated during the first hour and decayed thereafter to yield 3,5-dichloro-4-aminophenol and 2,6-dichloro-hydroquinone.

The research has further underlined the principles and evolution of $\bullet\text{OH}$ -mediated oxidation of DCF in water and its conversion to biodegradable and non-toxic byproducts with time. Last but not least, the toxicities reported here do not reflect long-term effects so that classification of DCF as “non-toxic” by the applied analytical method does not necessarily mean that it is an environmentally safe compound. It is also important that DCF undergoes biochemical oxidation in digestive tracts and the sewage system, thus ending up in the water environment not only in its original form, but also in a variety of metabolic derivatives. Hence, transformation of the compound (and its metabolites) to environmentally friendly end products is a challenging and emerging issue of advanced water treatment.

6. OZONATION-BASED ADVANCED OXIDATION FOR PRE-TREATMENT OF WATER WITH RESIDUALS OF ANTI-INFLAMMATORY MEDICATION

The present chapter is a summary of the work published in *Chemical Engineering Journal* 220 (2013) 151–160 as “Ozonation-based advanced oxidation for pre-treatment of water with residuals of anti-inflammatory medication”. This study is about the pre-treatment of water by O₃-based AOPs such as O₃/UV, O₃/US, O₃/H₂O₂, O₃/UV/US and O₃/US/FeSO₄ to remove residuals of diclofenac and to propose a simple modification to a conventional drinking water treatment plant (WTP) containing a pre-ozonation unit.

6.1. Introduction

Most of the literature on ozonation of PhAC-containing water with or without AOPs is focused on lab-scale investigations using distilled, natural or sewage water samples yielding case specific information (Benitez et al., 2011; Centellas et al., 2006; Ternes et al., 2002; Zwiener and Frimmel, 2000). On the other hand, it was later found using O₃-based AOPs that the water matrix had little or no impact on the second order reaction rate constants of PhACs with OH•, as the constants predicted in different natural waters were closely similar to those found in pure water (Huber et al., 2003). However, in no study so far were O₃/AOPs tested as pretreatment steps to show treatability in real or simulated coagulation/flocculation basins. The aim of this study was to assess the effect of the following processes as pre-treatment options for partial or complete destruction of anti-inflammatory medication in water: **1) Ozonation:** i) single (O₃); ii) with H₂O₂ (O₃/H₂O₂); iii) with UV-irradiation (O₃/UV); iv) with ultrasound (O₃/US); iv) with UV/ultrasound (O₃/UV/US); v) with ultrasound/FeSO₄; **2) Sonication** i) (US) with UV-irradiation (US/UV); ii) with ozone (US/O₃); iii) with H₂O₂ (US/H₂O₂); iv) with both (US/O₃/UV). The study further aimed to test the treatability of AOP-pre-treated samples by coagulation/flocculation using Al₂(SO₄)₃ or no coagulant to evaluate the potential of a full-scale water treatment plant for eliminating residuals of anti-inflammatory medication.

6.2. Materials and Methods

Diclofenac-Na salt was obtained from Sigma and used as received. The chemical structure and physical/environmental properties of the compound are as presented in 3.1.1 section. A stock DCF solution of 3000 μM was made by dissolving 0.954 g of DCF in 1 L of ultrapure water (Mili-Q) during magnetic stirring. Fresh test samples of 30 μM were prepared from the stock using either Milli-Q water or untreated water collected from the aeration tank of a WTP. The fresh water samples were collected from the aeration tank of a water treatment plant were readily shipped to the laboratory to preserve in the dark at 4 °C. The quality of the influent water is presented in Table 6.1.

6.2.1. Experimental

All AOP experiments were carried out in the high-frequency plate-type ultrasonic reactor (R4) (250 mL) emitting optionally at 577, 861 or 1145 kHz. The reactor was operated at 861 kHz and a specific power of 0.23 W mL⁻¹; and cooled by circulating water to maintain constant temperature (22±0.5°C). Ozone was generated on site and it was injected at a flow rate of 1.5 L min⁻¹ and the aqueous concentration of the gas was maintained at 2, 4 or 8 mg L⁻¹ depending on the operating conditions. The UV-lamp was immersed vertically along the center of the reactor (R7) and turned on only in UV-combined applications. Hydrogen peroxide was added from a stock solution of 35% (w/w) at different initial doses varying between 0.025-0.500 as g H₂O₂ per g O₃ (0.05-1.00 mg L⁻¹ H₂O₂). Note that the ultrasonic generator was shut down in US-free test processes. The experiments were carried out at R4, R5, R6 and R7 reactor systems.

6.2.2. Analytical

DCF and dissolved organic carbon (DOC) was analyzed by HPLC and TOC analyzer after filtration of the treated solutions through a 0.45 μm membrane filter as described in 3.2.3 Section. The aromatic and phenolic content of the samples were screened before and during treatment by their absorption at 254 nm and 276 nm, respectively using a Unicam Helios α Double Beam Spectrophotometer with a 1 cm quartz cell. Concentrations of Cl⁻, NO₂⁻, NO₃⁻, Br⁻ and F⁻ were determined by ion chromatography in accordance with the

procedure described in Section 3.2.3. Conductivity and turbidity were measured using a LF 320/SET conductivity meter and a WTW A 2100P HACH turbidimeter, respectively.

Table 6.1. Properties of the influent water in WTP after aeration.

Parameter	Value
pH	7.16
Alkalinity (mg L ⁻¹ CaCO ₃)	99
Hardness (mg L ⁻¹ CaCO ₃)	91
Turbidity (NTU)	3.71
Conductivity (μS cm ⁻¹)	235.8
TDS (mg L ⁻¹)	457
TOC (mg L ⁻¹)	5.22
DOC (mg L ⁻¹)	4.64
UV ₂₅₄ (cm ⁻¹)	0.10
UV ₄₃₆ (cm ⁻¹)	0.003
SUVA* (L mg ⁻¹ m ⁻¹)	2.16
Fluoride (μg L ⁻¹)	66.70
Bromide (μg L ⁻¹)	410
Chloride (mg L ⁻¹)	23.23
NH ₃ -N (mg L ⁻¹)	0.055
NO ₃ ⁻ (mg L ⁻¹)	1.46
SO ₄ ⁻ (mg L ⁻¹)	31.99
Total Fe (mg L ⁻¹)	0.037

$$\text{*SUVA is "specific ultraviolet absorption"} = \frac{UV_{254} (m^{-1})}{DOC (mgL^{-1})}.$$

6.2.3. Procedure

Two types of test samples were used throughout the experiments: i) S1: samples of Milli-Q water (MQW) spiked with 30 μM DCF; ii) S2: samples of raw water (RW) collected from the aeration tank of the WTP and spiked with 30 μM DCF. Additionally, a control sample of raw water with no DCF (S3) was run simultaneously to assess the effects of water matrix on mineralization of the oxidation by-products. All experiments were run in duplicate at the natural pH (6.0±0.5) of the samples unless stated otherwise. Quality parameters of S1, S2 and S3 before pre-treatment by the test AOPs are listed in Table 6.2.

Table 6.2. Chemical/physical properties of the test samples.

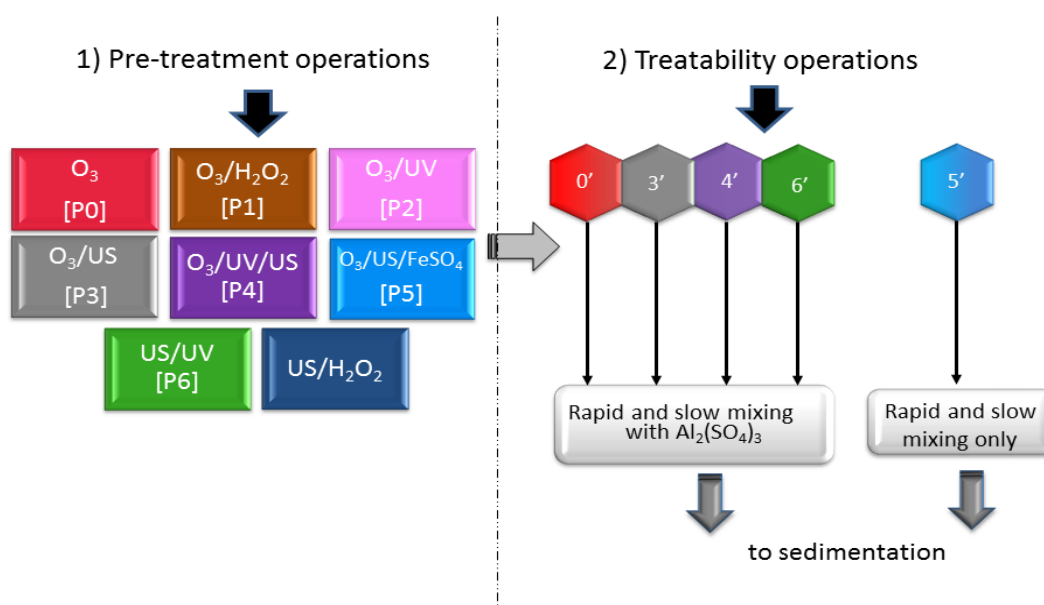
Parameters	S1	S2	S3
TDS (mg L ⁻¹)	4.00	465	457
Conductivity (μS cm ⁻¹)	3.50	410	236
Turbidity (NTU)	0.24	1.01	3.71
DOC (mg L ⁻¹)	4.67	9.32	4.64
SUVA (L mg ⁻¹ m ⁻¹)	3.77	3.14	2.16
Alkalinity (mg L ⁻¹ CaCO ₃)	n.d	110	99

S1=DCF+MQW; S2=DCF+RW; S3=Control (RW only).

The experimental method consisted of the following phases:

- i) Ozonation of S1 and S2 at varying ozone test concentrations and time periods to select and optimize the aqueous ozone concentration and contact time. Process symbol is P0.
- ii) Ozonation of S1, S2 and S3 at the selected conditions with: H₂O₂, UV light, ultrasound, ultrasound/UV and ultrasound/FeSO₄. Process symbols are P1, P2, P3, P4, P5, respectively.
- iii) Sonication of S1, S2 and S3 in the presence of H₂O₂, O₃ (P3), UV light (P6), and O₃/FeSO₄ (P5).
- iv) Coagulation/flocculation of P0-, P3-, P4-, P5- and P6-pretreated samples of S2 followed by gravity settling at pH 6.5. Additionally, P5-pretreated samples (of S2) were exposed to coagulation/flocculation at pH 9.0.

In single ozonation experiments ozone contact times and concentrations were selected as 3, 5, 10 min and 2, 4, 8 mg L⁻¹, respectively (3 min/2 mg L⁻¹ is the condition in the pre-ozonation unit of the WTP under investigation). In combined applications, contact times and ozone concentrations were 5 and 10 min, and 2 and 8 mg L⁻¹, respectively. Relative effectiveness of each process was evaluated by analyzing the reactor contents periodically for DCF, DOC, UV-254, UV-276, UV-436 and SUVA. Treatability experiments were run in 250 mL AOP-pretreated samples (of S2) spiked with 60 mg L⁻¹ alum (Al₂(SO₄)₃), except for the sample pretreated by US/O₃/ferrous sulfate to which no coagulants were added. Samples were stirred at 150 rpm for 2 min and 30 rpm for 30 min, followed by 1-h settling at quiescence (to simulate the conditions in the WTP). The experimental scheme consisting of pretreatment operations and coagulation/flocculation of selected pre-treated streams are presented in Figure 6.1. The corresponding operating conditions are listed in Table 6.3.



0', 3', 4', 5', 6' are pre-treated streams from operations [0], [3], [4], [5], [6], respectively.

Figure 6.1. The experimental scheme.

Table 6.3. Experimental Conditions.

Test Process	Sample*	Conditions**
(1) O ₃	S1, S2	O ₃ (mg L ⁻¹) = 2, 4, 8; t(min) = 3,5,10
(2) O ₃ /H ₂ O ₂	S1, S2	O ₃ /H ₂ O ₂ (g/mg)=2/0.05, 2/0.1, 2/1; t(min) = 2,3,5,10
(3) O ₃ /US	S1, S2, S3	O ₃ (mg L ⁻¹) = 2, 4, 8; US dose (W h L ⁻¹) = 7.66, 11.50, 19.16, 30.66
(4) O ₃ /US/UV	S1, S2, S3	O ₃ (mg L ⁻¹)= 2; US dose (W h L ⁻¹) = 7.66, 11.5, 19.16, 30.66; UV dose (m W cm ⁻² sec) = 56.4, 84.6, 141, 282
(5) O ₃ /UV	S1, S2, S3	O ₃ (mg L ⁻¹) = 2; UV dose (m Wcm ⁻² sec ⁻¹) = 56.4, 84.6, 141, 282
(6) US/H ₂ O ₂	S1, S2, S3	US dose (W h L ⁻¹)=7.66, 11.50, 19.16; H ₂ O ₂ (mg L ⁻¹)=0.05, 0.1, 1.0
(7) US/UV	S1, S2, S3	US dose (W h L ⁻¹)=7.66, 11.5, 19.16, 30.66 UV dose (m Wcm ⁻² sec ⁻¹)=56.4, 84.6, 141, 282
(8) O ₃ /US//Fe ⁺²	S1, S2	O ₃ (mg L ⁻¹) = 2,8; US dose (W h L ⁻¹) =11.50, 19.16, 30.66; FeSO ₄ (mg L ⁻¹) = 60
(9) Coagulation with Al ₂ (SO ₄) ₃	S2 from (1), (3), (4), (7)	Al ₂ (SO ₄) ₃ (mg L ⁻¹) = 60; mixing = 2-min (150 rpm), 30-min (30 rpm) followed by 60-min settling at pH 6.5
(10) Coagulation at pH 9.0.	S2 from (8)	Mixing/settling (same as above)

*S1=DCF+MQW; S2=DCF+RW; S3=Control (RW only).

** pH=6.0±0.5 in [1]-[9], 9.0 in [10] and 6.5 in the settling units.

6.3. Results and Discussion

6.3.1. Are Hydrolysis and Adsorption Potential Pathways in the Observed Decay of DCF in Raw Water?

DCF is a highly soluble acidic pharmaceutical (50 g L^{-1} at 25°C ; $\text{pK}_a=4.35$) with a potential to undergo hydrolysis at acidic-neutral or alkaline pH. In addition, it is possible that hydrophobic interactions and hydrogen bonding between molecules of NOM and DCF may confine the compound, thus reducing its apparent concentration in solution (Bui and Choi, 2010; Hajibabania et al., 2011). To check the role of hydrolysis and confinement in the observed decay of the compound by AOPs, a RW test solution (S2) was moderately stirred (150 rpm) for 24-h at pH 6.5 (natural pH of the sample) and $T=35^\circ\text{C}$. It was found that fractions of DCF elimination and carbon- mineralization at the end of the test period were 2.3% and 1.7%, respectively. Thus, hydrolysis and/or adsorption were neglected as possible routes of DCF disappearance during exposure of the samples to AOPs.

6.3.2. Selection of the Effective Operation Parameters and Comparison of Process Efficiencies

Ozonation and Combinations. The critical operation parameters affecting the efficiency of O_3 -based test processes were chemical concentrations (O_3 , H_2O_2) and the contact time. Relative impacts of these parameters were evaluated by ozonation of synthetic (S1) and real (S2) samples for 3, 5 and 10-min at three and two test concentrations of ozone and H_2O_2 , respectively while monitoring the degree of DCF and DOC elimination. The results are presented in Figure 6.2 without the 5-min data, which were closely the same as those of 3-min.

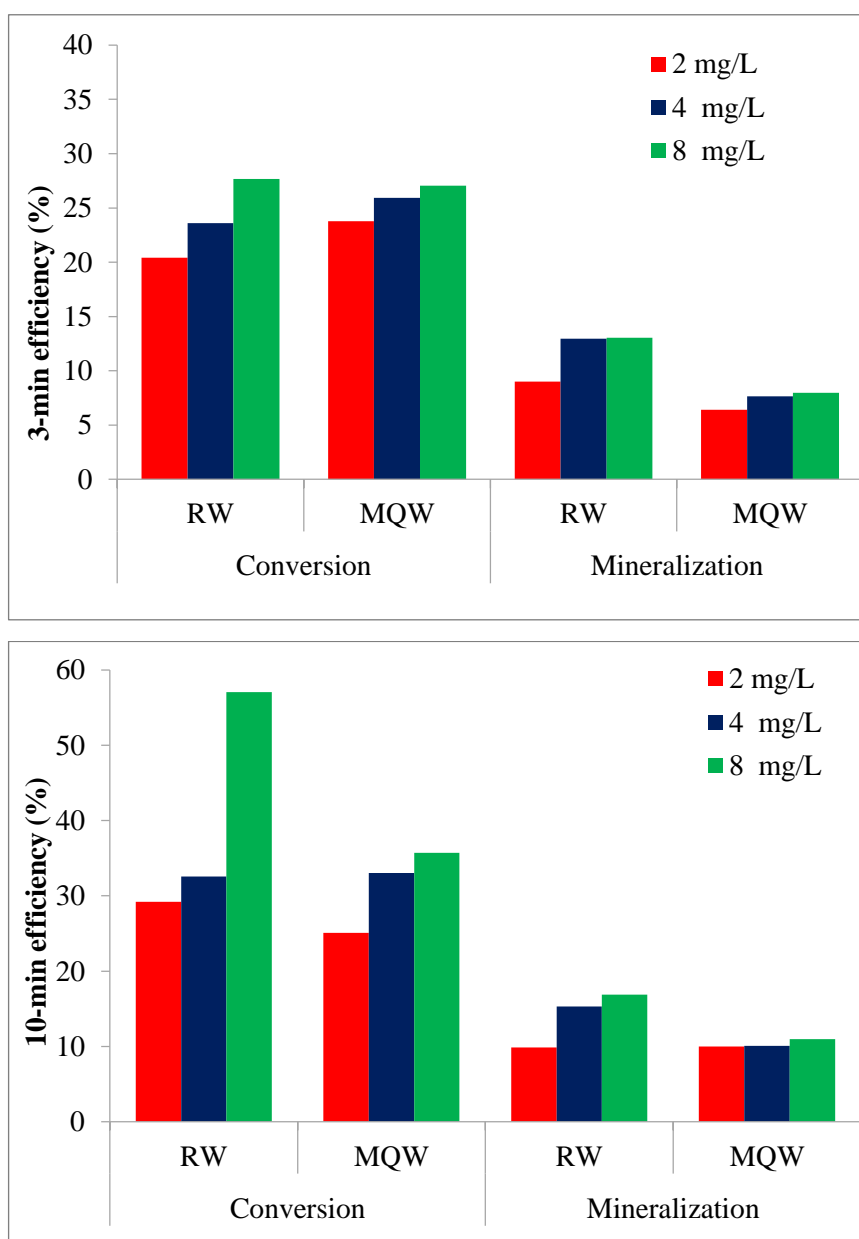


Figure 6.2. Relative impacts of the applied ozone test concentration and contact time on fractions of DCF conversion and mineralization in Milli-Q (S1) and raw (S2).

We found that the efficiency of oxidation in 3-min was not strongly affected by the water matrix as it was nearly the same in both samples, varying between 20%-28% in proportion to the applied ozone concentration. Mineralization during the same period was around 6.4%-11.0% and slightly higher in S2, due to a larger initial DOC and the likely production of some reactive species via oxidation of NOM by molecular ozone, as reported in the literature (Kasprzyk-Hordern, 2003). The efficiency of DCF conversion was appreciably increased in S2 (to 47 %) and that of mineralization to 17 % by extending the

contact time to 10 min and the O₃ concentration to 8 mg L⁻¹, while no remarkable enhancements were observed in S1 under the same conditions. The results signify the positive impact of NOM and other impurities in natural water (by provision of additional reactive species), and the negative impact of excess byproduct formation (2,6-Dichloroaniline, DCF-2,5-iminoquinone; 5-hydroxy-DCF) in S1 that leads to a competition for ozone.

The data in Figure 6.2 also show that there was little difference between the performance of the process at 2 and 4 mg L⁻¹ ozone; therefore all O₃-combined processes were tested at aqueous ozone concentrations of 2 and 8 mg L⁻¹ and for contact times of 5 and 10-min. Accordingly, relative effectiveness of single and combined O₃ operations for the conversion and mineralization of DCF in ultrapure and raw water are presented in Figure 6.3 (a) and (b), respectively. Note that a four-fold increase in the dissolved O₃ concentration brings little or no additional cost to the operation of the WTP, because the O₃ generator consumes constant energy at half or the maximum capacity (Sein et al., 2008).

The first chart (conversion) shows that the efficiencies of P0, P1 and P3 at 8 mg L⁻¹ O₃ were larger in RW (S2) than MQW (S1) as a result of the contribution of water constituents (e.g. NOM, alkalinity, Cl⁻, SO₄⁻) via the production of reactive radical species (e.g. CO₃²⁻•, Cl•) upon oxidation by ozone or H₂O₂/HO₂⁻ pair. The most effective process was P2 (O₃/UV), because the yield of OH• per mass of ozone is a maximum here (Gottschalk et al., 2000). Note also that the efficiency of this process for conversion was closely the same in both samples, despite the absence of additional reactive species (in S1), which was compensated by the ease of photolytic cleavage of the parent compound, as confirmed by a high UV-absorption potential of DCF in pure water (Encinas et al., 1998; Packer et al., 2003). Moreover, photolytic cleavage of NOM in natural waters was reported to have no significant impact on DOC removal, because NOM components were only transformed to stable intermediate byproducts (Katsumata et al., 2008).

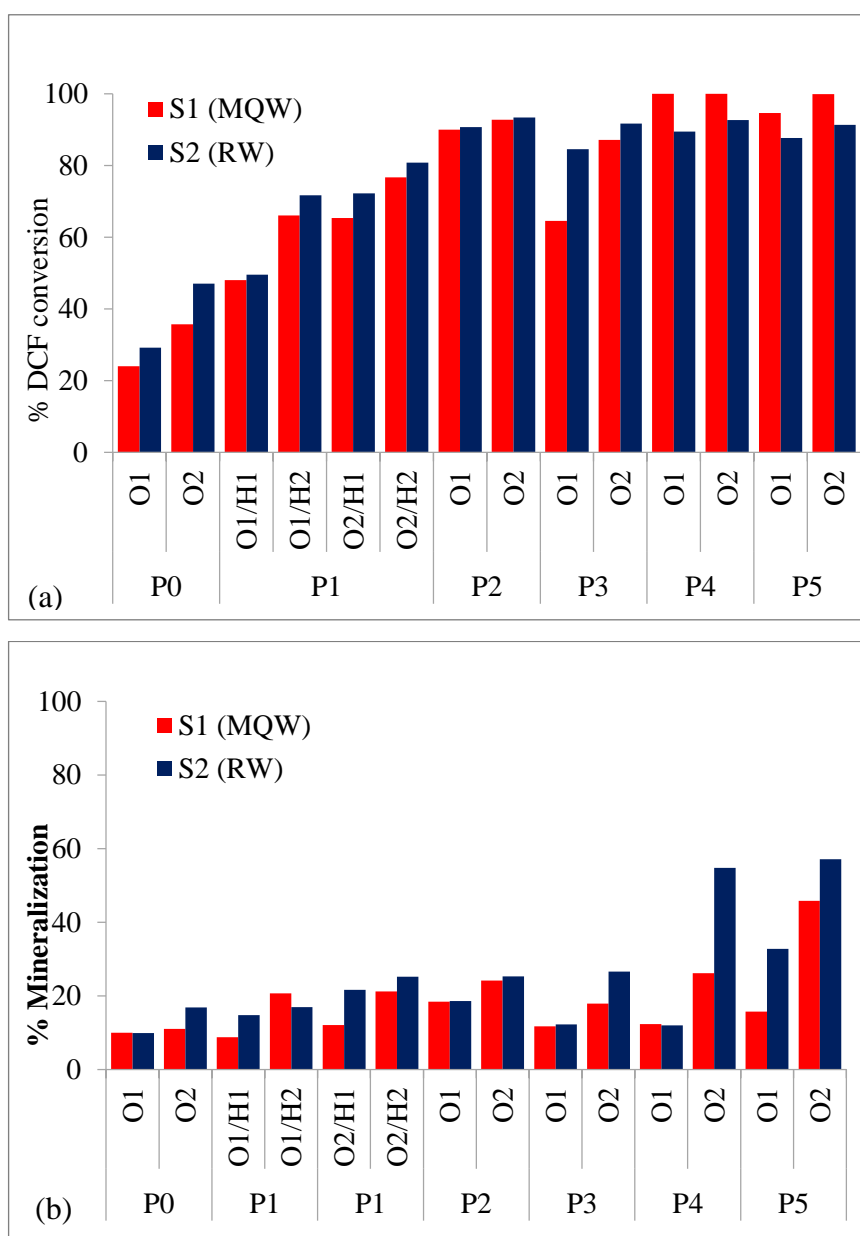


Figure 6.3. Relative effectiveness of single and combined ozonation processes (AOPs) for converting and mineralizing DCF (30 μM) in pure (MQW) and raw water samples (RW). PO = O_3 ; P1 = $\text{O}_3/\text{H}_2\text{O}_2$; P2 = O_3/UV ; P3 = O_3/US ; P4 = $\text{O}_3/\text{UV}/\text{US}$; P5 = $\text{O}_3/\text{US}/\text{Fe}^{2+}$. O1, O2 are the ozone test concentrations (2, 8 mg L^{-1} , respectively); H1, H2 are peroxide test concentrations (0.05, 1.0 mg L^{-1} , respectively).

The last two processes (P4, P5), in which oxidation is mediated by reactions with $\text{OH}\cdot$, were highly effective for the conversion of DCF, but with lower conversion rates in S2 (than S1), to be attributed to the competition for $\text{OH}\cdot$ (between DCF and NOM) that predominated over the production of additional reactive species (e.g. organic peroxy and hydroxyl-

cyclohexadienyl radicals (Lamsal et al., 2011; Matilainen and Sillanpää, 2010). Nevertheless, the high performance of these processes for converting DCF is the outcome of the synergy, i.e. enhanced ozone diffusion and radical production rates (via the turbulence of acoustic cavity bubbles and the local hot spots formed by their implosion to promote thermal fragmentation of hydrophobic solutes), as well as the contribution of Fenton and sono-Fenton reactions promoted by US-generated H_2O_2 (R198). Note also that the impact of ozone test concentration was insignificant in P2, P4 and P5 ($\text{OH}\cdot$ -controlled reaction rates), slightly significant in P0 and P1 (O_3 -controlled reaction rates) and considerably significant in P3, showing that the rate of conversion was limited by the diffusion of O_3 into or near the gaseous cavitation bubbles.

Analysis of the reaction kinetics showed that the rates obeyed pseudo-first order law during early contact, at which the reactions were considerably faster in MQW (S1) particularly under P2, P3, P4 and P5, as depicted by the fitted curves in Fig. 6.4. However at prolonged reaction time, the fraction of DCF eliminated in RW (S2) exceeded that in MQW to be explained by the oxidation of organic impurities that produced additional reaction routes and/or reactive species. A list of 5-min rate constants and 5/10-min oxidation efficiencies in MQW and RW matrices are summarized in Table 6.4.

Table 6.4. The role of solution matrix on 5-min reaction rate constants and 5/10-min oxidation efficiencies of the test processes at $8 \text{ mg L}^{-1} \text{ O}_3$ ($C_0=30 \text{ }\mu\text{M}$).

S1 (MQW)				S2 (RW)			
Process*	5-min k' (min^{-1})	Efficiency (%)		Process*	5-min k' (min^{-1})	Efficiency (%)	
		5-min	10-min			5-min	10-min
P0	0.100	39.81	43.95	P0	0.078	32.56	44.37
P1	0.098	39.42	44.38	P1	0.108	41.08	48.17
P2	0.859	98.48	99.67	P2	0.526	92.65	97.78
P3	0.198	62.82	74.88	P3	0.184	61.61	91.82
P4	1.098	99.57	100.0	P4	0.737	97.22	99.23
P5	0.483	92.20	99.11	P5	0.171	58.25	90.11

*P0= O_3 ; P1= $\text{O}_3/\text{H}_2\text{O}_2$; P2= O_3/UV ; P3= O_3/US ; P4= $\text{O}_3/\text{UV}/\text{US}$; P5= $\text{O}_3/\text{US}/\text{Fe}^{+2}$

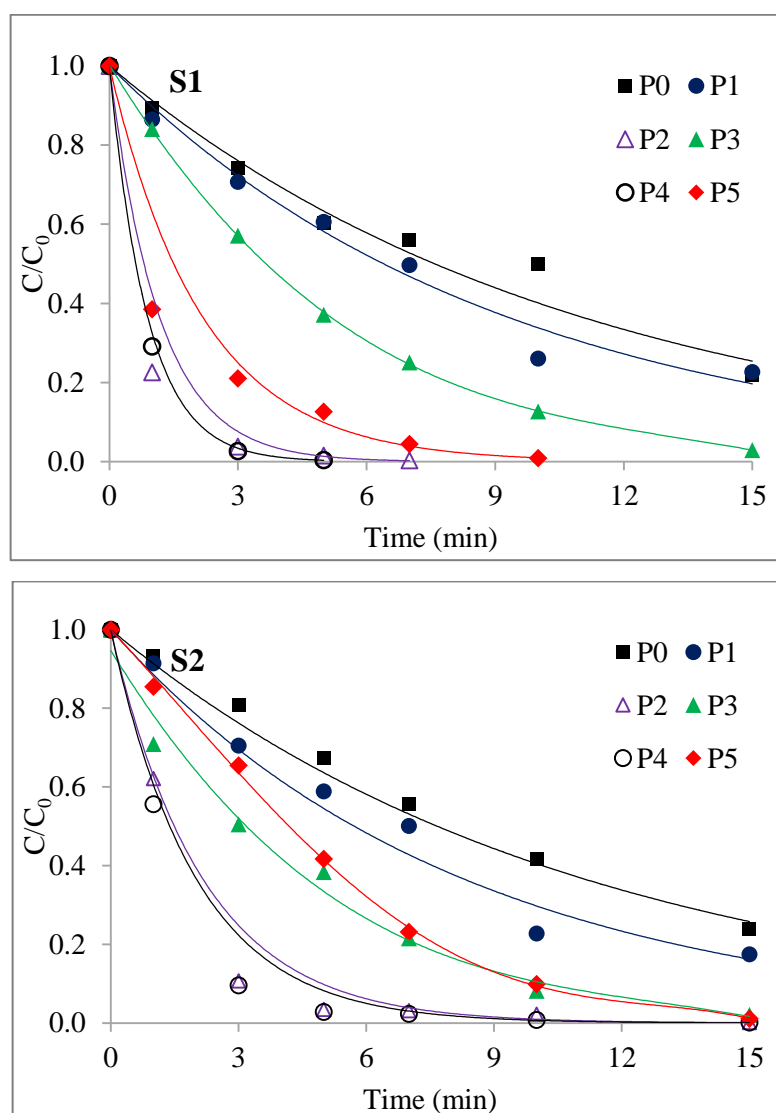


Figure 6.4. Relative rates of DCF transformation during 5-min exposure of S1 and S2 ($C_0 = 30 \mu\text{M}$) to ozone-combined AOPs (process symbols same as in Figure 6.3).

The second chart (b) in Figure 6.3 shows that at $8 \text{ mg L}^{-1} \text{ O}_3$ mineralization in RW was always larger than that in MQW and the most effective processes were P4 and P5, as was also true for the oxidation process. Note also that the role of ozone test concentration was remarkably significant in mineralization by these two combinations, while it was insignificant for the conversion of DCF. To assess the impact of the water matrix, the efficiency of 10-min mineralization in S2 was compared with that in the control (S3) using the data presented in Figure 6.5, which shows that mineralization in raw water (S2) was at all conditions higher than that in the control. This is clearly the evidence of a positive interaction of DCF and its oxidation byproducts with NOM (and other impurities). Note also that the relation between the abatement in DOC and UV-254 absorption of the control

sample as presented on top of Figure 6.5 shows an excellent consistency of the two parameters upon pretreatment with P4 and P5.

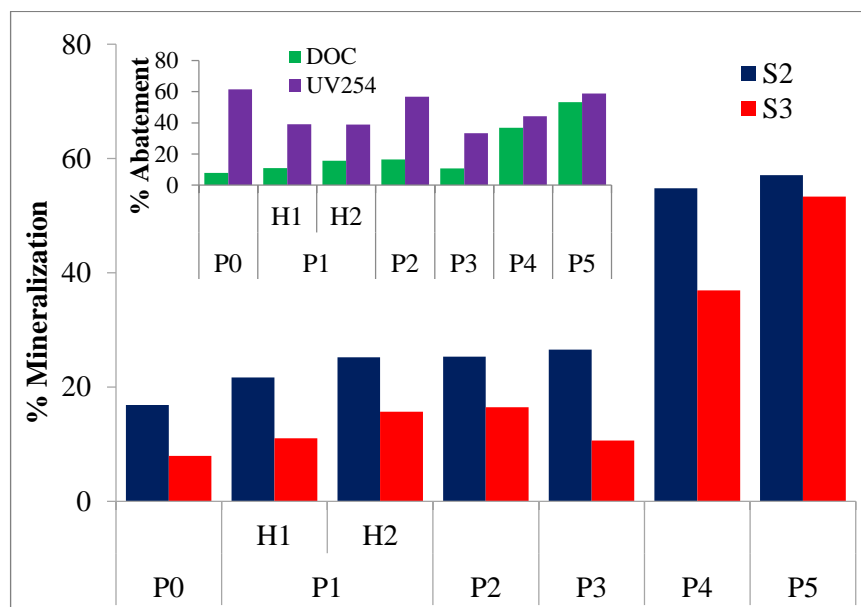
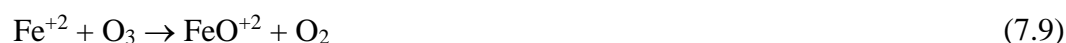


Figure 6.5. Relative mineralization in sample (S2) and control (S3) after 10-min contact with the test AOPs at $8 \text{ mg L}^{-1} \text{ O}_3$. The inset shows relative abatements in UV absorption (254 nm) and DOC in control upon 10-min pretreatment by the test processes.

The outstanding performance of P5 is based on the synergy of ultrasound and catalytic ozonation that lead to enhanced rate of ozone diffusion and decomposition to yield radicals such as O_2^\bullet and HO^\bullet (Cooper and Burch, 1999). Hence, in addition to the reactions outlined in reactions R195-198, the following were also effective during $\text{O}_3/\text{US}/\text{Fe}^{2+}$ catalytic system (Kasprzyk-Hordern, 2003):



Ultrasound-assisted Processes. The second experimental phase involved sonication in the presence of H_2O_2 , UV-irradiation, O_3 and/or FeSO_4 . The results showed that the addition of H_2O_2 was relatively ineffective for the conversion of DCF (34 and 32 % in S1 and S2, respectively), while additions of O_3 or UV provided more than 82 % conversion in both

matrices. The efficiency was remarkably enhanced when the samples were sonicated simultaneously with O₃ and UV or with O₃ and FeSO₄. Relative conversion and mineralization of DCF upon 10-min pretreatment by the test processes is summarized in Table 6.5. Note that the last two process defined as “P4” and “P5”, respectively in the previous section provided complete and more than 90% transformation in S1 and S2, respectively via the synergy discussed earlier. Note that higher efficiency of P5 for mineralization in S1 is inconsistent with previous observations on higher mineralization efficiencies in S2. The difference might be the result of a series of complex reactions involving rapid oxidation of DCF by US/Fe catalytic system to form metal-organic complexes that are readily oxidized by OH•.

Table 6.5. Relative conversion and mineralization efficiencies of 10-min sonication with H₂O₂, O₃, UV and combinations in pure (S1) and raw water (S2) samples spiked with 30 μM DCF (O₃=8 mg L⁻¹, H₂O₂=1.0 mg L⁻¹, I_{UV}=4.7 W m⁻², P_{US}=0.23 W mL⁻¹).

Process	% Conversion		% Mineralization	
	S1	S2	S1	S2
US/H ₂ O ₂	34.22	32.23	12.34	9.38
US/O ₃	87.17	91.74	17.86	26.55
US/UV	99.94	81.85	31.93	9.26
US/O ₃ /UV	100.00	92.68	26.12	54.76
US/O ₃ /Fe ²⁺	99.95	91.37	45.78	57.11

Note also that low mineralization in S2 by US/UV indicates the production of non-reactive hydrophilic compounds upon photolytic cleavage of NOM as was also reported by others (Ratpukdi et al., 2010). Hence, the power running of US/O₃/UV simultaneously is based on the synergy of photolytic decomposition and excess OH• radicals that facilitate the destruction of NOM and its hydrophilic components in the bulk solution.

Changes in the UV-vis spectra of the samples during reaction showed that under US/UV application the absorption at 254 nm increased sharply in both solutions at early reaction and stabilized after longer contact, signifying the rapid formation of aromatic and/or olefinic intermediates. A similar but moderate increase in UV-254 absorption was also observed during the first 5-min of US/O₃/Fe²⁺ process, which was then followed by a soft decline showing initiation of the mineralization process. Maximum degree of mineralization in pure water was also observed under these two processes as depicted in Table 6.5. Relative UV-

vis spectra of S1 and S2 during 10-min pretreatment are presented in Figure 6.6, where the absorptions at 276 and 436 nm are signs of phenolic moieties and colored compounds, respectively.

6.3.3. Treatability of AOP- pretreated Samples by Coagulation

A very good indicator of raw water treatability by coagulation/flocculation is the value of SUVA, which provides information about the distribution of organic matter (NOM) as hydrophobic/hydrophilic, low/high molecular weight and low/high charge density properties (Bose and Reckhow, 2007). For example, a low value such as $2.16 \text{ L mg}^{-1} \text{ m}^{-1}$ as reported in Table 6.1 for the raw water shows NOM is composed of a mixture of aquatic humics and other components that are mostly of hydrophilic and low molecular weight character, 25 % or a little greater of which is expected to be eliminated as DOC by coagulation with alum and ferric, respectively (Edzwald and Tobiason, 1999).

It was found that the selected pre-treatment operations led to significant enhancements in the expected removal of DOC by coagulation as depicted in Figure 6.7. Maximum efficiency obtained at the coagulation process at the same conditions but with no pre-treatment was 34 % with alum and 41 % with FeSO_4 (slightly higher than predicted); whereas values as high as 63-65 % were obtained by pre-treatment of the influent by $\text{O}_3/\text{UV}/\text{US}$ or $\text{O}_3/\text{US}/\text{Fe}^{2+}$ prior to coagulation. Note that a higher efficiency of coagulation in samples pretreated with $\text{O}_3/\text{US}/\text{Fe}^{2+}$ (than those coagulated with alum) is due to better adsorptive capacity of $\text{Fe}(\text{OH})_3$ (than $\text{Al}(\text{OH})_3$) as was also reported by others (Julien et al., 1994). Note also that coagulation without pretreatment (regardless of the coagulant type and dosage) was unable to remove DCF (less than 0.5%), but it rendered complete removal when followed by advanced pretreatment processes such as P4, P5 and P6.

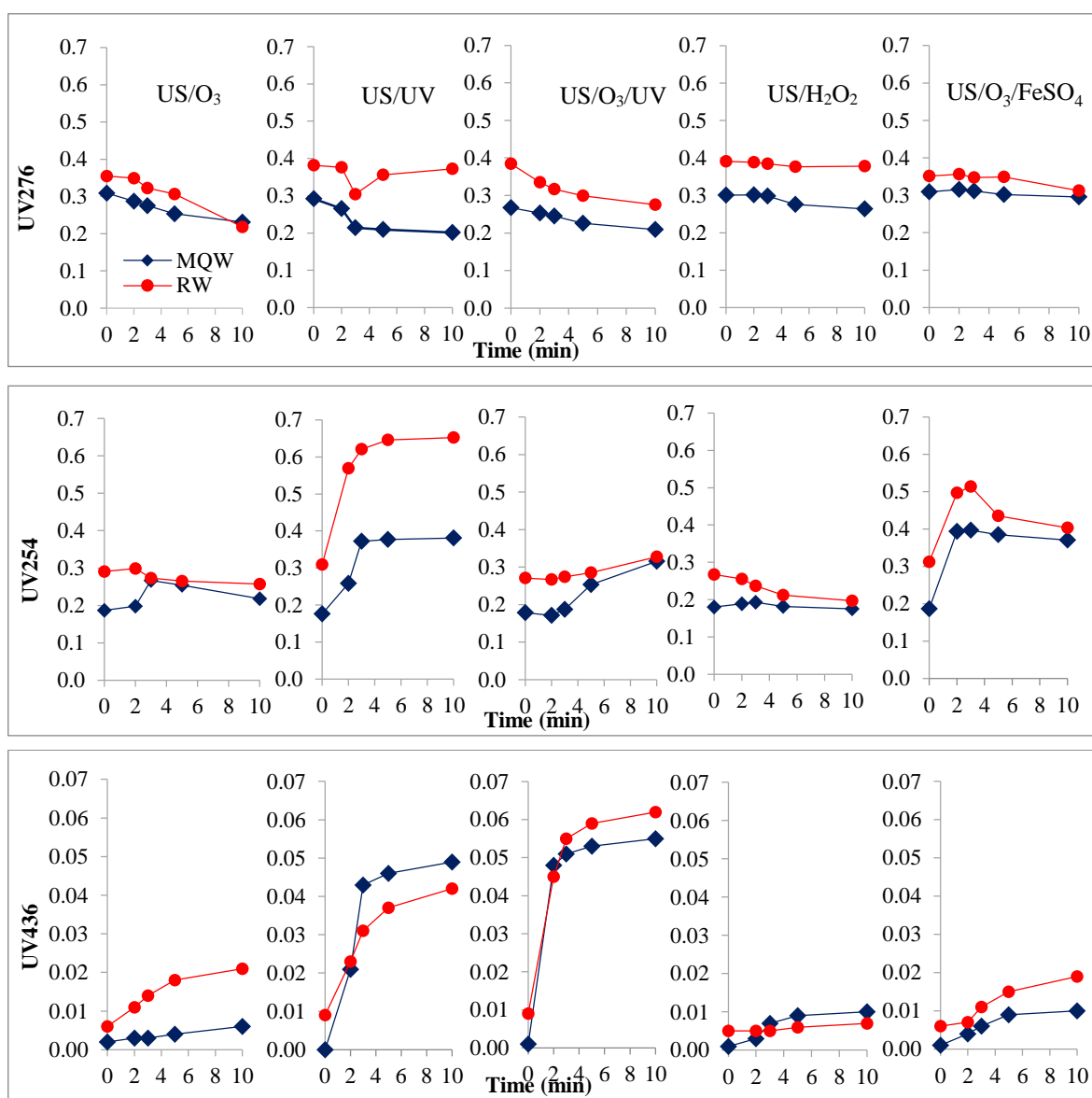


Figure 6.6. Variations in the UV-vis spectra of S1 and S2 during 10-min exposure to US-combined processes.

In accordance, we propose that the pre-ozonation unit is operated simultaneously with either of the following: i) US/UV; ii) US/Fe²⁺. As such, the water will not only be free of DCF (or similar anti-inflammatory pharmaceutical residues), but will also contain significantly less NOM, which otherwise will promote the production of THM during or after chlorination practices. A flow chart of a conventional and proposed WTP operation is presented in Figure 6.8.

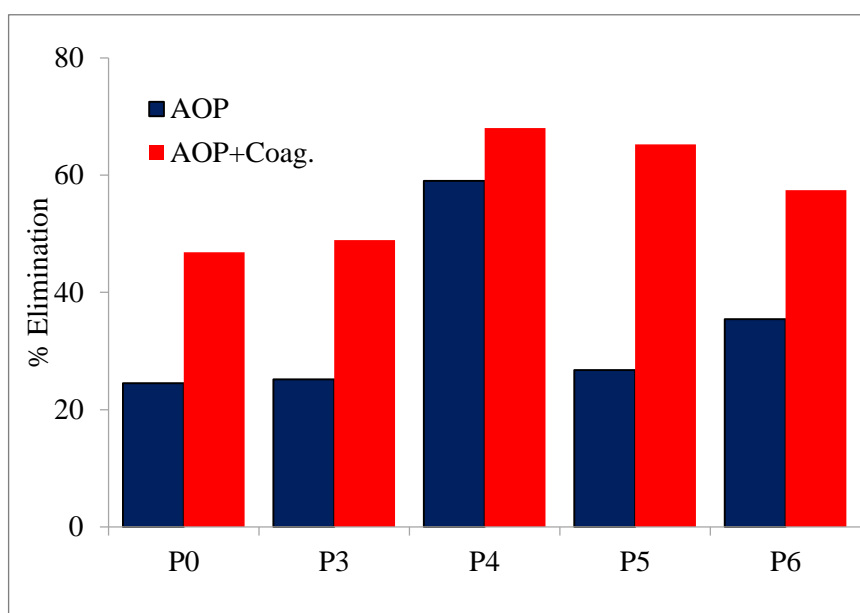


Figure 6.7. The impact of AOP-pretreatment on the efficiency of DOC elimination by coagulation. P0=O₃; P3 =O₃/US; P4 = O₃/UV/US; P5 = O₃/US/FeSO₄; P6 = US/UV.

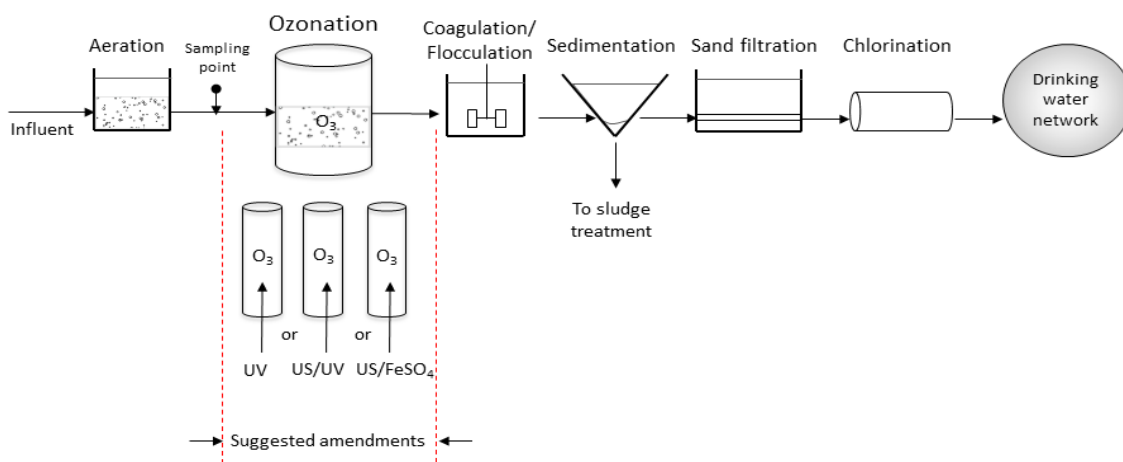


Figure 6.8. The modified WTP flow chart.

6.4. Conclusions

The study has shown that the presence of pharmaceutical residues such as DCF in natural or surface water can be managed by integrating the conventional WTPs with O₃ and US-based Advanced Oxidation Processes. More specifically, it was found that DCF can be completely eliminated in water by simple modifications in the pre-ozonation unit of the WTP under investigation, e.g. by running the process in the presence of US/UV-irradiation or US/Fe²⁺. As such, coagulation/flocculation of the pretreated effluent is an excellent unit

operation not only for rendering DCF-free water, but also for providing significant degrees of mineralization so as to lower the probability of THM formation in the chlorination unit.

An economic assessment of the proposed modification scheme is essential before scaling it up for large-scale applications.

7. CATALYTIC OZONATION OF IBUPROFEN WITH ULTRASOUND AND Fe-BASED CATALYSTS

The present chapter is a summary of the work published in *Catalysis Today* 240 (2015) 2–8 as “Catalytic ozonation of ibuprofen with ultrasound and Fe-based catalysts”. This study is about a method of decomposing and mineralizing the emerging contaminant ibuprofen (IBP) by catalytic ozonation using catalysts such as high-frequency ultrasound (US) and soluble/insoluble Fe-bearing species.

7.1. Introduction

Catalytic ozonation is a modified AOP technology, whereby the rate of ozonation is accelerated by the addition of active metallic catalysts, which also lead to a reduction in the operation cost despite the additional cost of catalyst separation. The process can be operated heterogeneously via complex formation between the organic compound and catalyst; or homogeneously with the decomposition of ozone by active metal species (Kasprzyk-Hordern, 2003). The governing mechanism of the heterogeneous process is “chemisorption” of ozone, organics or both on the catalyst surface leading to the formation of active oxidizing species and redox reactions, the efficiency being dictated by the type and surface properties of the catalyst and the operation pH (Kasprzyk-Hordern, 2003). Among a wide variety of heterogeneous catalysts to enhance the rate of ozonation of organic compounds, Fe-bearing minerals have been found highly effective (Ahmad et al., 2010; Matta et al., 2007; Xue et al., 2009a, 2009b). Furthermore, the O₃/US application has received considerable attention due to the advantages obtained by enhanced rate of ozone mass transfer and the thermal decomposition of the gas inside the collapsing cavity bubbles to generate additional reactive species (Ince and Tezcanlı, 2001; Weavers and Hoffmann, 1998).

There are only few studies in the literature related to the catalytic ozonation of IBP, but they all involve heterogeneous catalysis with MnO₂, goethite or bio-solids obtained from activated sludge (Yang et al., 2010; Yang et al., 2009). The current study, therefore, has aimed to investigate the effects of some catalysts such as ultrasonic irradiation and a variety of homogeneous/heterogeneous Fe-bearing species on ozonation of IBP. The processes were

compared at their optimized conditions for their relative efficiencies in accelerating the oxidation and mineralization of IBP during 1-h ozonation.

7.2. Materials and Methods

All reagents and ibuprofen were purchased from Sigma-Aldrich, Istanbul. Fresh test samples of IBP were prepared by dissolving the compound in proper volumes of ultrapure water (Mili-Q) at 45°C during magnetic stirring. The catalysts, their commercial or given names and particle properties of the solid forms are listed in Table 7.1. Note that we used two different zero-valent iron species: the first one (ZVI) was purchased from Hepure (USA) in micro-size and the second one (ZVI-Graphite) was synthesized in Kanbar Laboratory for Nano-materials at Bar-Ilan University, Israel (Koltypin et al., 2004; Nikitenko et al., 2001).

Table 7.1. The catalysts.

Catalyst	Type	Label	Relative size range
Fe(OH)O (35%)	Insoluble	Goethite	Micro-
Fe ₂ O ₃ (>99%)	Insoluble	Hematite	Micro- (<5 μm)
Fe ₃ O ₄ (98%)	Insoluble	Magnetite	Nano- (10 nm)
Ni-Fe ₂ O ₄ (98%)	Insoluble	Ni-supp. Ox.	Nano- (<50 nm)
Zero valent iron (I)	Insoluble	ZVI	Micro- (45-150 μm)
Zero valent Iron (II)	Insoluble	ZVI-Graphite	Nano- (20-100 nm)
FeCl ₃ .6H ₂ O	Soluble	Chloride	-
FeSO ₄ .7H ₂ O	Soluble	Sulfate	-

7.2.1. Experimental

Preliminary experiments with ozone alone were carried out in 250 mL glass vessels (R5) to estimate the ozone mass transfer coefficient at varying pH levels (3.0, 6.5 and 9.0) and ozone flow rates (3, 6 and 12 mg min⁻¹, corresponding to inlet concentrations of 2, 4 and 8 g m⁻³, respectively). Single experiments with solid catalysts alone were carried out at pH 3.0 and 6.5 to assess the degree of IBP adsorption and the extent of solids leaching into the sample solutions. The concentration of IBP, the mixing rate and the contact time were 50

μM , 250 rpm and 24 h, respectively. The catalyst dose in each test was adjusted so as to maintain 5 mg L^{-1} Fe in all samples.

Catalytic experiments with Fe-bearing species were run with $50 \mu\text{M}$ IBP (10 mg L^{-1}) and 5 mg L^{-1} Fe-equivalent of each catalyst during a gas flow rate of 12 mg min^{-1} for 1-h at pH 6.5 unless stated otherwise. The experiments with ultrasound were carried out in a high-frequency plate-type ultrasonic reactor (R4). The reactor was operated at a specific power of 0.23 W mL^{-1} , cooled by circulating water to maintain constant temperature ($20 \pm 0.5^\circ\text{C}$), and occupied by a sample volume of 250 mL. The flow rate of O_3 into the reactor was 12 mg min^{-1} throughout the reaction time.

7.2.2. Analytical

IBP was analyzed by HPLC as described in Section 3.2.3. The aqueous iron concentration, residual dissolved ozone concentration, total organic carbon was monitored by a Shimadzu TOC-V CSH analyzer after filtration of the treated samples through a $0.45 \mu\text{m}$ membrane filter.

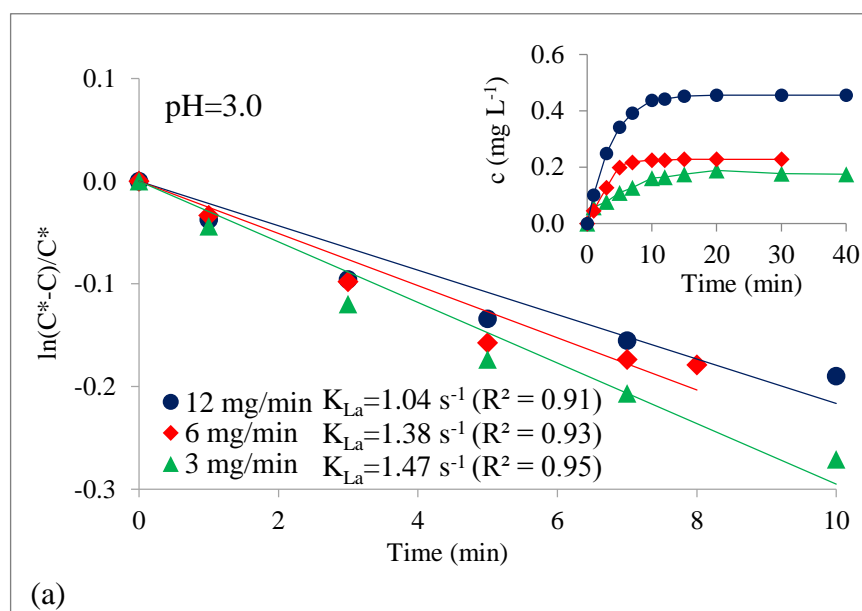
7.3. Results and Discussion

7.3.1. Prediction of the Ozone Mass Transfer Rate Coefficient

The aim of preliminary experiments without catalysts was to select the optimum ozone flow rate and pH based on rates of ozone mass transfer and IBP degradation. Mass transfer rate coefficients were estimated using the non-steady state aqueous concentration of O_3 in ultrapure water during 40-min ozonation at 20°C . Accordingly, the early unsteady-state concentrations were plotted as $[(C_t - C^*)/C^*]$ against time, based on the law of diffusional mass transfer of gases into pure water:

$$dC/dt = K_{La}(C^* - C) \quad (\text{Eq. 7.1})$$

where: C^* and C are maximum and observed concentrations of aqueous ozone, respectively (mg L^{-1}) and K_{La} is the gas-liquid mass transfer rate coefficient (s^{-1}). The value of C^* was calculated using the applied flow rate and a constant solubility coefficient of 0.34 mg L^{-1} as reported in the literature for ozone in pure water at 20°C (Roth and Sullivan, 1981). Analysis of the data by linear regression provided a fairly good estimate of K_{La} at each condition, as presented in Figure 7.1 for gas flow rates of 3, 6 and 12 mg min^{-1} (a) and for pH levels of 3.0, 6.5 and 9.0 at a gas flow rate of 12 mg min^{-1} (b). The insets at the top show the initial build-up and subsequent stabilization of the aqueous ozone concentration with time. It was found that the value of K_{La} decreased with increasing gas flow rate and alkalinity, being largest at a flow rate of 3 mg min^{-1} and pH of 3.0.



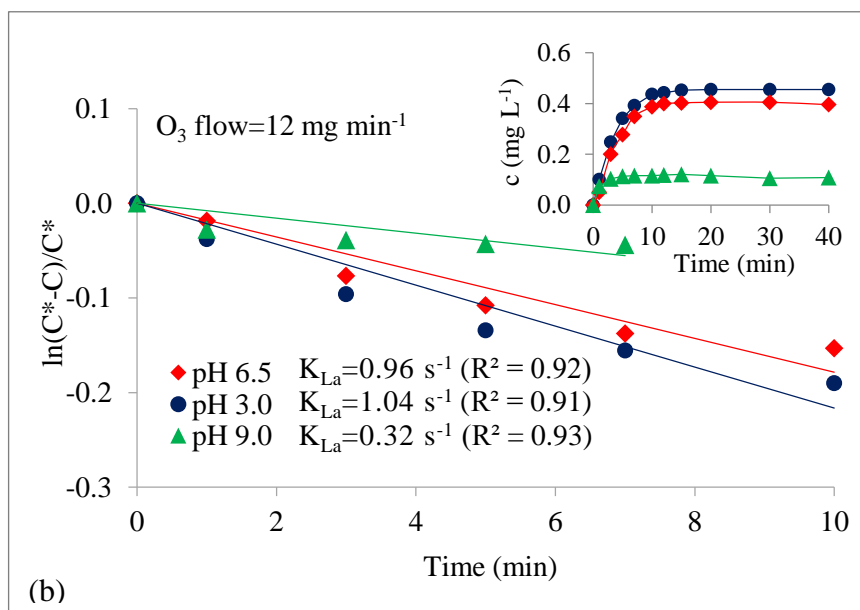


Figure 7.1. Estimation of O_3 mass transfer rate coefficient using the unsteady-state concentration data at varying O_3 flow rates ($O_3=2, 4, 8 \text{ mg L}^{-1}$) (a) and pH levels (b). The insets at the top right corners show the source data, i.e. the initial unsteady-state and the subsequent stabilization of the aqueous O_3 concentration with time.

7.3.2. Selection of the Ozone Dose, pH and IBP Concentration

Despite the increasing trend of ozone mass transfer rate with decreasing gas flow (Figure 7.1), the degradation and mineralization of IBP was found to accelerate with increasing O_3 flow rates, so that all experiments were carried out at $12 \text{ mg min}^{-1} O_3$ unless stated otherwise. Figure 7.2 shows the apparent pseudo-first order degradation of IBP as a function of the initial solute concentration (a), and pH (b). The data reflect low reactivity of the compound at higher solute concentrations and lower pH, as signs of competition for oxidizing species, and low reactivity with molecular ozone, respectively. The latter is a consequence of increased stability of O_3 with decreased alkalinity. However, the noticeable rate enhancement by increasing the pH from 3.0 to 6.5 (despite the relative stability of O_3 at this pH) is due to anionic enhancement of IBP at $\text{pH} > \text{pK}_a$ (4.9), at which the reactivity with molecular ozone is larger (Zwiener and Frimmel, 2000). Note also that the aqueous concentration of O_3 was found to sharply decline upon increasing the pH from 3.0 to 6.5, justifying a high rate of ozone consumption or decomposition i.e. higher reactivity of the solutes with ozone. Hence, a low rate of reaction at $\text{pH} < \text{pK}_a$ is not only due to the stability

of O₃ alone, but also to the fact that a relatively large fraction of the compound exists in a suspension at this condition and therefore is less reactive.

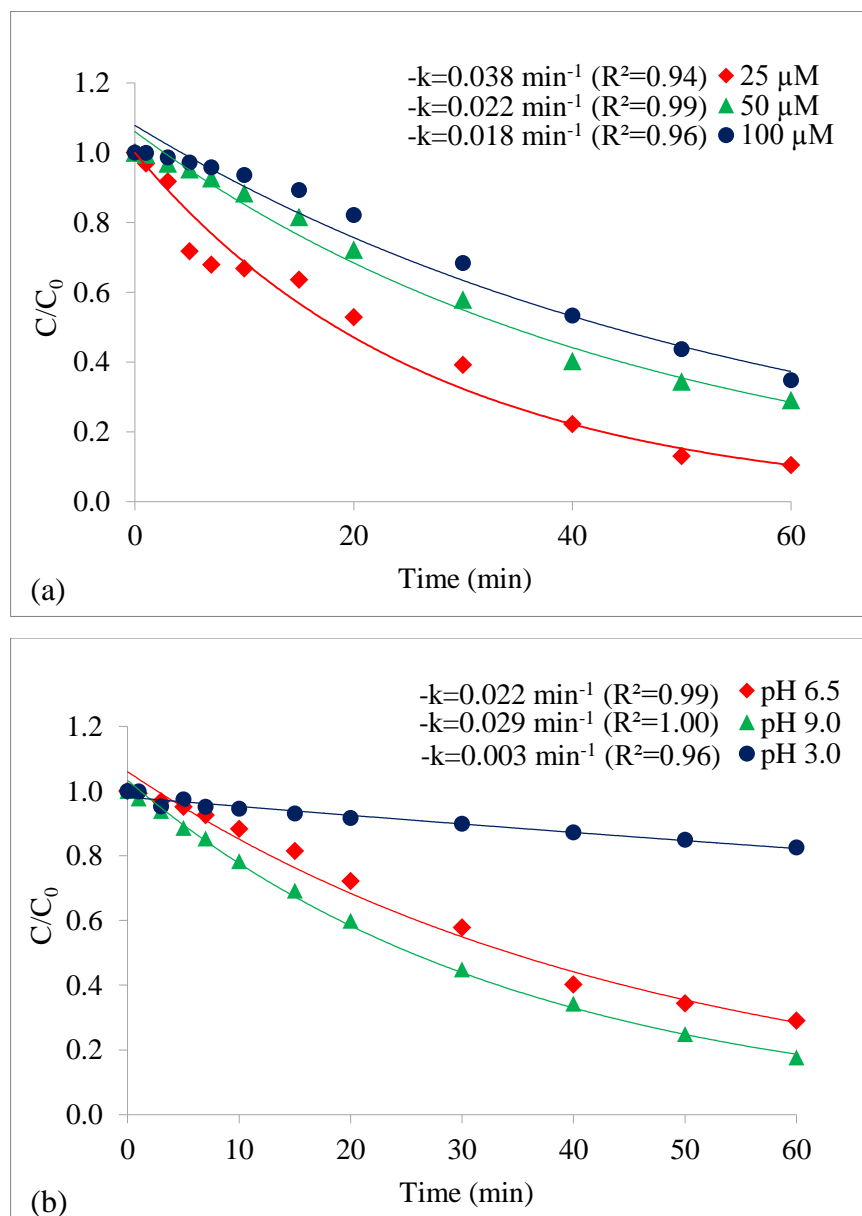


Figure 7.2. Variations in the rate of IBP degradation with the initial solute concentration (a) and the applied pH (b). The operating pH in (a) is 6.5, the solute concentration in (b) is 50 μM . Ozone flow rate is 12 mg min^{-1} (8 mg L^{-1}) in both cases.

Ozonation alone was found inadequate for mineralization regardless of the applied conditions, as depicted in Figure 7.3 imply: i) low reactivity of the oxidation byproducts with O₃ (as that of the parent compound), ii) rate limiting effect of HO• in mineralization;

and iii) rate-inhibiting effect of HO• scavenging, which becomes more pronounced as the input concentration of IBP increases.

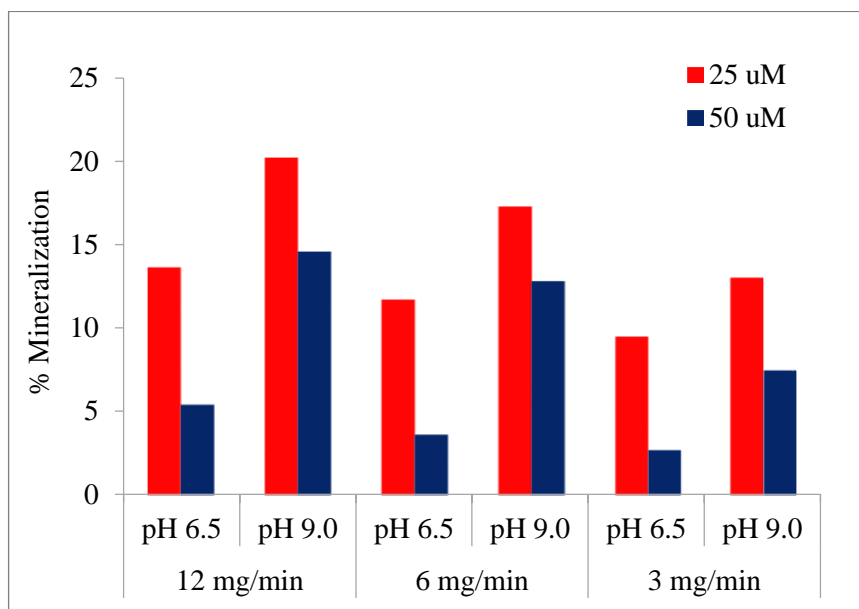


Figure 7.3. Interactive effects of concentration, pH and gas flow rate on mineralization of IBP by 1-h ozonation ($O_3 = 2, 4, 8 \text{ mg L}^{-1}$).

7.3.3. Catalytic Ozonation with Ultrasound

Preliminary sonication of IBP without ozone showed that ultrasound was much more effective, justifying our argument in previous section about low reactivity of the compound with molecular ozone and the rate determining effect of HO•. However, unlike O_3 the reactivity of IBP under ultrasound was significantly higher at acidic pH to be attributed to hydrophobic enrichment of the compound, which enhances its diffusion to the bubble-liquid interface, where the concentration of HO• is much larger than that at the bulk solution (Ince et al., 2009). Relative degradation and mineralization of IBP with ozone, ultrasound and ozone/ultrasound combination at three pH test levels are presented in Figure 8.4 (a) and (b), respectively. The observed synergy for mineralization at pH 6.5 (increasing from 5.41% by O_3 to 32.10% by O_3/US) is due to enhanced rate of O_3 diffusion to the bulk solution and into the cavity bubbles, which upon collapse lead to thermal decomposition of the contents for an additional and major route of HO• production (Song et al., 2007; Ziyilan and Ince, 2013; Zwiener and Frimmel, 2000).

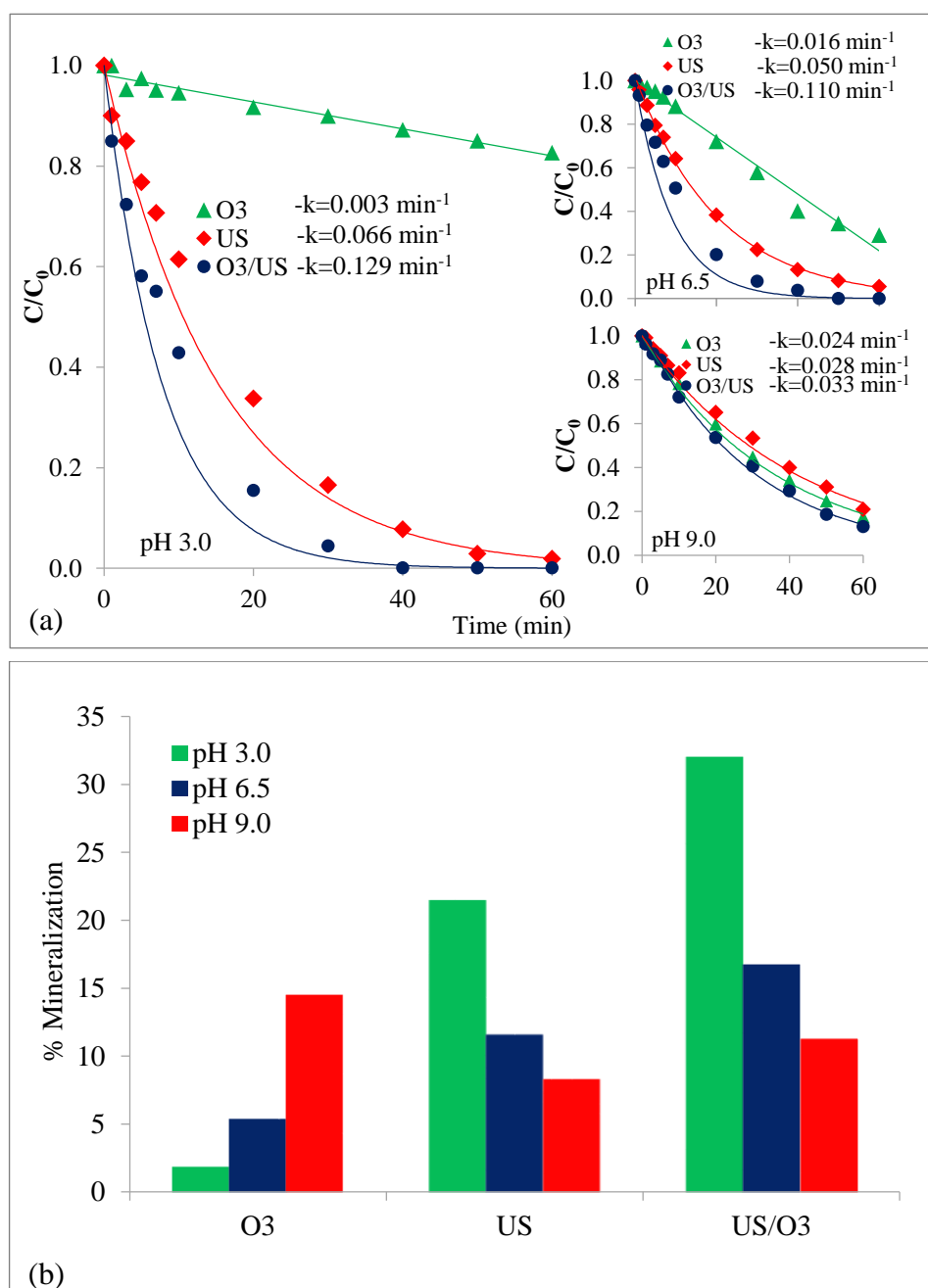


Figure 7.4. pH-related degradation and mineralization of IBP by singly and simultaneously applied ozonation and sonication ($C_0 = 50 \mu\text{M}$, $f = 861 \text{ kHz}$, $\text{O}_3 \text{ flow} = 12 \text{ mg min}^{-1}$ ($\text{O}_3 = 8 \text{ mg L}^{-1}$)).

7.3.4. Catalytic Ozonation with Fe-bearing Species

Preliminary experiments with the solid catalysts and IBP carried out at pH 3.0 and 6.5 showed that adsorption can safely be ignored as a potential elimination pathway during 1-h ozonation, because the disappearance of the compound from solution was none or negligible

at short contact times with the catalysts, reaching a maximum after 20-h only in the presence of ZVI and ZVI-graphite at pH 6.5 (22 % and 18 %, respectively). On the other hand, no leaching of Fe-species was observed at pH 6.5 and various degrees of leaching at pH 3.0, signifying a low probability of homogenous Fenton or Fenton-like reactions at pH 6.5 in the bulk solution. Fractions of IBP adsorbed on and $\text{Fe}^{\text{n+}}$ leached out from the solid catalysts are listed in Table 7.2.

Table 7.2. Adsorption of IBP on surfaces of solid catalysts after 24 h contact of 50 μM IBP with 5 mg L^{-1} Fe-equivalent of the catalysts at pH 6.5, and leaching of $\text{Fe}^{\text{n+}}$ from the catalysts in pure water (without IBP) at the same conditions.

Catalyst	% IBP adsorbed	$\text{Fe}^{\text{n+}}$ in solution
Goethite	8.44	0.003
Hematite	9.21	0.006
Magnetite	12.66	0.002
Ni-supported Oxide	9.06	0.100
ZVI-Graphite	17.95	0.153
ZVI	21.95	0.167
Goethite	8.44	0.003
Hematite	9.21	0.006

Catalytic ozonation with Fe-species were run at $C_0=50 \mu\text{M}$, $\text{pH}=6.5$ and an initial $\text{Fe}:\text{O}_3$ molar ratio of 11:1 (based on the steady state ozone concentration in the sample). Relative fractions of IBP and TOC elimination after 1-h ozonation in the presence of 5 mg L^{-1} (as Fe) of each catalyst are presented in Figure 7.5 (a) and (b), respectively. The performance of ozonation alone is added as “control” for comparison.

The data show that all catalysts except ZVI provided a positive enhancement to the degradation of IBP, while only the solid forms were effective in enhancing the mineralization of the compound. Good performance of the solids in general signifies their reactivity with O_3 to allow adsorption and decomposition (by reaction with $\text{Fe}^{\text{n+}}$) on the surfaces. As such, very low efficiency of ZVI (commercial) can be attributed to its inert properties with respect to ozone. The most effective catalyst was ZVI-Graphite, which increased the degradation and

mineralization of IBP from 71% (by control) to 79% and from 5% (by control) to 41%, respectively. Note also that while FeSO_4 was the most effective catalyst in the degradation process, it was the least effective in mineralization. The former is a consequence of enhanced decomposition of O_3 in solution by reaction with Fe^{n+} to yield additional $\text{HO}\cdot$ and the $\text{H}_2\text{O}_2/\text{HO}_2\cdot$ pair, which is much more reactive than ozone (R8.1-8.9), while the inefficacy (mineralization) implies an unexpected termination of the cycle and/or the scarcity of Fe^{3+} and the generated radicals to fulfill the excess demand of the oxidation byproducts.

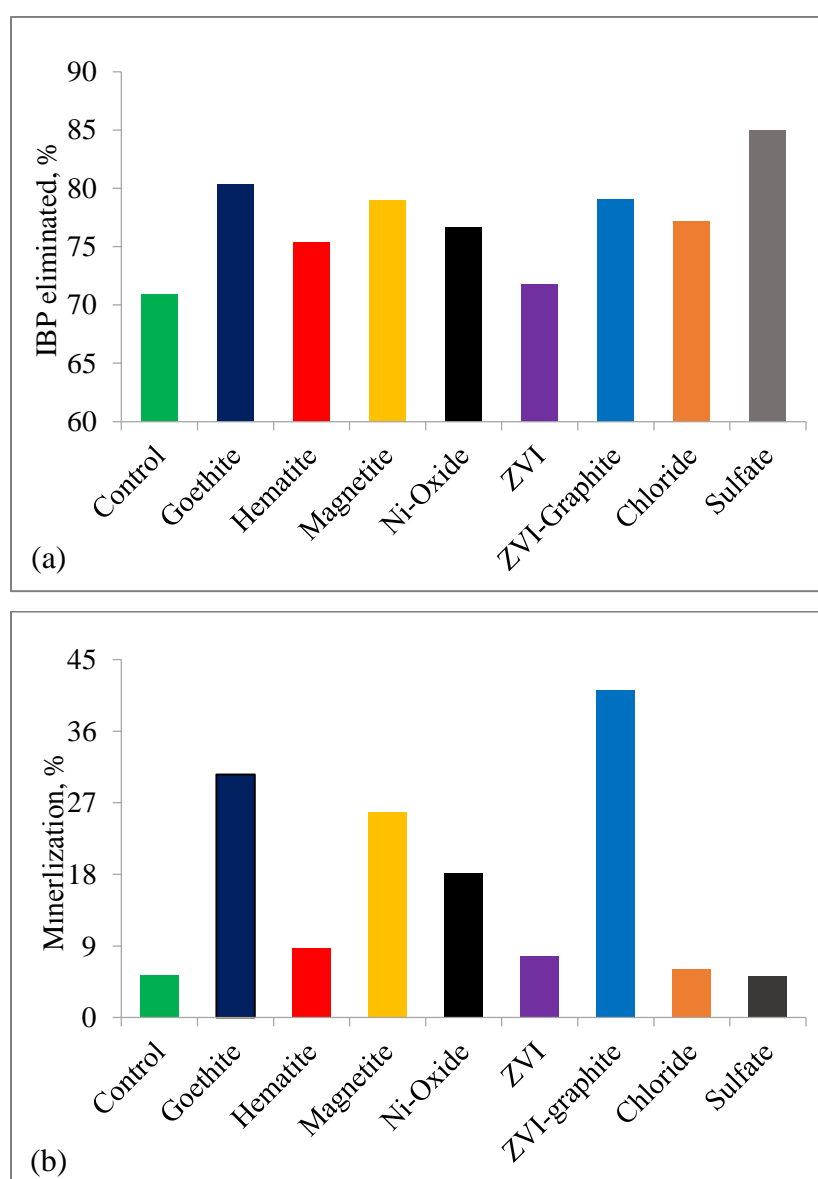


Figure 7.5. Relative degradation and mineralization of IBP ($C_0=50 \mu\text{M}$) by 1-h ozonation at pH 6.5 and a gas flow rate of 12 mg min^{-1} ($\text{O}_3=8 \text{ mg L}^{-1}$) in the presence of 5 mg L^{-1} of the catalysts (as Fe). “Control” refers to O_3 alone.

7.3.5. Catalytic Ozonation with US and Fe-bearing Solids

Final experiments with O₃/US/Fe-species were run only with those catalysts that provided maximum enhancement in mineralization of IBP by Fe-catalyzed ozonation; namely Goethite, Magnetite and ZVI-Graphite. The contact time was 40-min, at which 100% IBP elimination was obtained with ZVI-Graphite. The apparent rate of IBP decay by ozonation with US and the selected catalysts, and estimated pseudo-first order reaction rate constants are presented in Figure 7.6. The data for single processes (Control-1, Control-2) and ozonation with US (no Fe-species) are added for comparison. It was found that the rate of reaction under O₃/US/Goethite was almost the same as that with O₃/US, implying that O₃ decomposition occurs principally inside the collapsing bubbles and reactions with Fe-active surfaces of the solid are not much significant. Accelerated reaction rates with Magnetite and ZVI-graphite signify additional reaction pathways such as adsorption and decomposition on Fe-active surfaces. Higher efficacy of ZVI-graphite than Magnetite despite the larger particle size of the former (Table 7.1) must be due to higher activity of the ZVI surfaces, most likely due to the presence of carbon, which promotes the decomposition O₃, thus accelerating the rate of oxidation reactions (Kasprzyk-Hordern, 2003).

The three solid catalysts were also assessed for their relative performance in the mineralization of IBP, as presented in Figure 7.7. The outstanding performance of O₃/US/ZVI-Graphite (increased efficiency from 2 %-by O₃ to 58 %) at pH 3.0 is due to tearing of the coating material by hydrodynamic shear forces of US to furnish out the reactive Fe species to the massive surfaces with extensive nucleation and reaction sites. Note that two different pH are depicted in the bars, namely pH 6.5 for Goethite and Magnetite, and pH 3.0 for ZVI-graphite. This is because only the ideal pH is considered, i.e. the condition at which the catalysts exhibited best performance.

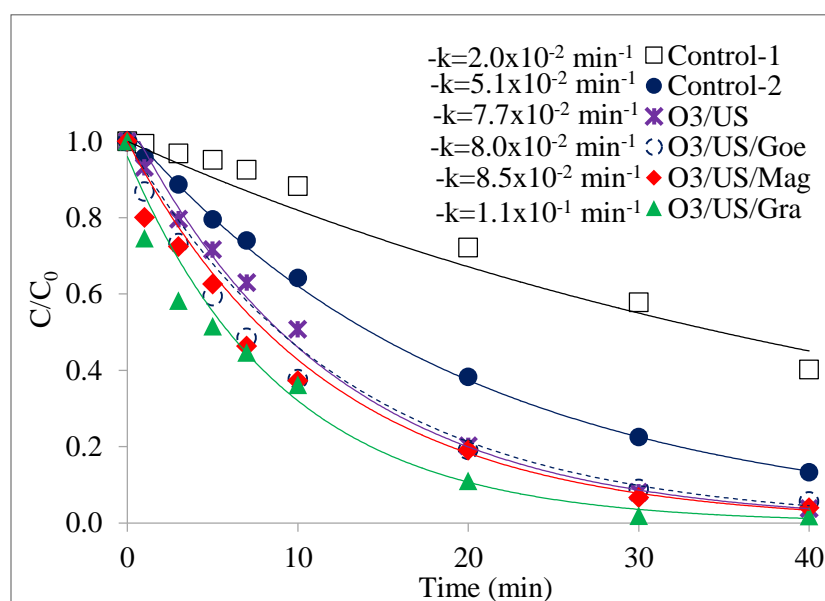


Figure 7.6. Degradation IBP by 40-min sono-catalytic ozonation with Fe-based solids at optimized conditions ($C_0 = 50 \mu\text{M}$, O_3 flow = 12 mg min^{-1} ($\text{O}_3 = 8 \text{ mg L}^{-1}$), specific $\text{US}_{\text{power}} = 0.23 \text{ W L}^{-1}$, $\text{pH} = 6.5$). “Control-1” and “Control-2” refer to singly applied ozonation and sonication, respectively.

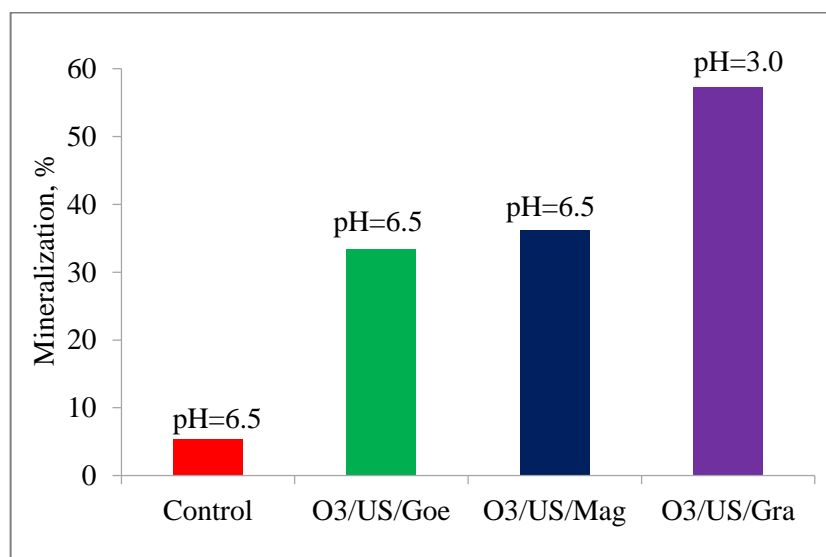


Figure 7.7. Mineralization of IBP by 40-min sono-catalytic ozonation in the presence of 5 mg L^{-1} Fe-equivalent of Goethite, Magnetite and ZVI-graphite at optimized conditions ($C_0 = 50 \mu\text{M}$, O_3 flow = 12 mg min^{-1} ($\text{O}_3 = 8 \text{ mg L}^{-1}$), specific $\text{US power} = 0.23 \text{ W mL}^{-1}$, $\text{pH} = 6.5$ or 3.0). “Control” is ozonation alone.

7.4. Conclusions

The study has shown that ozonation at pH 9.0 provides sufficient decomposition of the anti-inflammatory pharmaceutical IBP, but is ineffective for its mineralization (15%), while sonocatalytic ozonation with Fe-bearing species at pH 6.5 provides not only decomposition but also appreciable degrees of mineralization of the compound. As such, pH is the most critical operation parameter for it controls the formation and distribution of reactive oxygen species, the mass transfer and diffusion of ozone and organic solutes within the bulk solution and the gas-liquid/liquid-solid interfaces, and the reactivity of all species on Fe-active surfaces of the solid particles. The study has also shown that both IBP and its oxidation byproducts react very slowly with molecular ozone and the rate of degradation is controlled by the availability of HO• and Fe-bearing species.

The most effective catalysts in the absence of ultrasonic irradiation were FeSO₄ (84% IBP decay) and ZVI-graphite (41% TOC decay) at pH 6.5. The high performance of FeSO₄ was attributed to the reactions of O₃ with Fe²⁺ followed by the formation of Fe³⁺ and H₂O₂/HO₂• pair, which is considerably more reactive with IBP than molecular O₃. The larger efficacy of ZVI-nanoparticles than all other catalysts in enhancing the mineralization process must be due to the high reactivity of the oxidation byproducts on the massive surfaces of the catalyst with a high affinity for them.

Finally, the study has shown that ultrasound is not only a good catalyzer of ozonation reactions, but also a wonderful means of building up synergies between different processes. As such, maximum IBP elimination and TOC decay were observed after 40-min ozonation of IBP with US and ZVI-graphite (100%, 58%) at pH 3.0, which facilitates the diffusion of solutes from the bulk solution to the bubble-liquid and solid-liquid interfaces. Regarding the additional cost of operation due to reducing the pH from the natural level (6.5) to 3.0, it is possible to consider operating the same process without any pH change, with however a lower degree of mineralization (45%) and thus a higher environmental cost.

8. SINGLE, SIMULTANEOUS AND SEQUENTIAL APPLICATIONS OF ULTRASONIC FREQUENCIES FOR THE ELIMINATION OF IBUPROFEN IN WATER

The present chapter is a summary of the work published in *Ultrasonics Sonochemistry* (<http://dx.doi.org/10.1016/j.ultsonch.2017.01.032>) as “Single, Simultaneous and Sequential Applications of Ultrasonic Frequencies for the Elimination of Ibuprofen in Water”. The research is about the assessment of the performances of single and multi-frequency operations in the overall degradation of a widely consumed analgesic pharmaceutical-ibuprofen (IBP). The work also covers evaluation of the effect of ZVI on the efficiency of the degradation process and the performance of the reaction systems.

8.1. Introduction

The critical issue of sonochemistry is the selection and optimization of the operating parameters such as frequency, power, bubbling gas and the reactor geometry, among which frequency has always been the most crucial parameter (Asakura et al., 2008; Eren and Ince, 2010; Sivakumar et al., 2002). The frequency that is most appropriate for specific application depends on the desired physical and/or chemical effects, and the properties of reactants dissolved in solution. Simultaneous irradiation of water by two or more frequencies has been demonstrated to enhance the overall activity of ultrasonic systems via increased temperature and population of the active bubbles, provided that the operating conditions are well-selected (Brotchie et al., 2007; Gogate et al., 2011; Sivakumar et al., 2002). Such applications involve low-to-low, high-to-high and low-to-high frequencies, all ending up with an excellent synergy (Brotchie et al., 2007; Dezhkunov, 2003).

The use of zero-valent iron (ZVI) in combination with ultrasound has lately received much attention in research with water decontamination processes. The potential of the method is based on the reactivity of iron to initiate surface chemistry and advanced Fenton reactions, and the synergy of ultrasound for enhanced mass transport to the metal surface (with additional surface defects and active sites), increased rate of $\bullet\text{OH}$ generation and

continuous cleaning of the metal (Chand et al., 2009; Kim et al., 2007; Tezcanlı-Güyer and Ince, 2011). Moreover, ultrasound resolves the shortcomings of Fenton's reaction such as limitations to the availability of $\text{Fe}^{+2}/\text{Fe}^{+3}$ pair in the medium, which is controlled by rapid dissolution of the metal and the production of excess $\bullet\text{OOH}$ and $\bullet\text{OH}$ radicals (Ghauch et al., 2012). The most critical issue of the process is the selection of the right frequency keeping in mind that low frequencies are excellent for keeping metallic surfaces clean and free of oxide scales, while high frequencies are preferred for the high incidence of bubble collapse and $\bullet\text{OH}$ radical ejection to the bulk medium.

The objective of the present study was to assess relative efficacy of single and dual frequencies (the latter applied in simultaneous and sequential modes) for the decomposition and mineralization of ibuprofen (IBP) in the presence of ZVI. The ultrasonic devices used were: i) two horns (20 kHz, 40 kHz) (R1, R2), ii) a bath (200 kHz) (R3) and iii) a plate-type reactor with three transducers emitting optimally at 577 kHz, 856 kHz, and 1130 kHz (R4). The operating conditions in each system was optimized for power and reactor position and the performances were compared in terms of the "sonochemical yield", the rate of IBP elimination and percentage of TOC decay. The impact of latent cavitation was also investigated by determining the change in TOC of the treated samples after a 12-h inactive period in dark and silent conditions. The choice of the probe chemical is based on the fact that it is a widely used non-steroidal anti-inflammatory medication obtained world-wide without prescription. Moreover, IBP is classified as an emerging water pollutant due to the fact that both the parent compound and its metabolites are frequently detected in surface water with moderate toxicity (Ziylan and Ince, 2014).

8.2. Materials and Methods

Ibuprofen was obtained from Sigma with >98% purity and fresh samples of the compound were prepared by dissolving it in ultrapure water at 45°C. All reagents were obtained from Merck, Istanbul. ZVI was purchased from Hepure (USA) in micro-size.

8.2.1. Experimental

Devices, Experimental Setup and Modes of Application. The ultrasonic equipment consisted of: i) a high-frequency plate-type reactor (R4) (250 mL) equipped with a 120 W generator (used at 90% capacity) and a piezo-electric transducer (22 cm²) that emitted optionally at 572, 856 or 1130 kHz (Ultraschall/Meinhardt), ii) a low-frequency horn (R1) with a 150 mL glass cell and connected to a 180W generator (used at 30% capacity) and a piezo-electric transducer emitting at 20 kHz (Bandelin Sonoplus HD2200), iii) a multi-wave ultrasonic bath emitting at 200 kHz (R3) (Kaijo, Quava Mini), and iv) a low-frequency horn (R2) emitting at 40 kHz and connected to a 200 W generator and a 250 mL cell (Weber Ultrasonics). The power densities in all reactors were determined by calorimetry (Mason and Peter, 2002).

Singly operated frequencies were 40 kHz, 200 kHz, 577 kHz, 856 kHz and 1130 kHz all in solutions spiked with 50 μ M IBP and adjusted to pH 3.0. Simultaneous and sequential operations were run in variations of 40 kHz, 200 kHz, 577 kHz and 1130 kHz. Total reaction time in all operations was 30-min. A schematic diagram of the experimental set-up is presented in Figure 8.1. The time sequence in sequential operations were as the following: Seq1, Seq2, Seq3: 10-min+20-min; Seq4: 7.5-min+7.5-min+15-min.

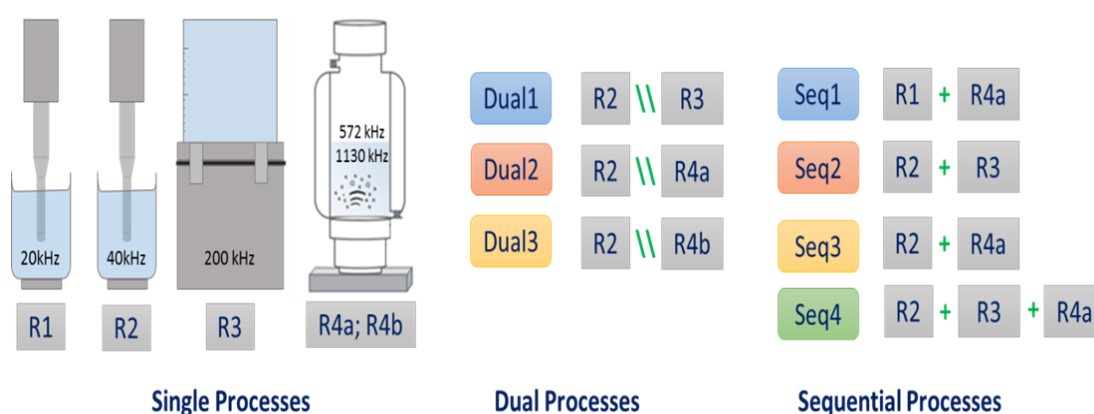


Figure 8.1. The experimental Scheme (R1, R2, R3 and R4a, R4b refer to Reactor1, Reactor2, Reactor3 and Reactor 4 (a, b) described in Table 8.2).

8.2.2. Procedure

Silent batch tests (4-h) were carried out with 50 μM IBP and varying concentrations of ZVI (10, 50, 75 and 100 mg L^{-1}) in a Julabo SW22 shaker at pH 3.0 to determine the ability of the compound to adsorb on the metal surface. In accordance with the results of these preliminary experiments, a 50 μM solution of IBP adjusted to pH 3.0 was sonicated for 30-min in single, dual and sequential modes in the presence of various concentrations of ZVI. Control experiments without ZVI were carried out in parallel to isolate the impact of Fenton reactions. Samples were collected periodically from each reactor system for the analysis of IBP, aqueous Fe species, H_2O_2 and total organic carbon (TOC). The reactor contents at the end of each reaction were kept silently in the dark for 12-h to determine if C-mineralization continued via sustained cavitation effects.

8.2.3. Analytical

IBP was analyzed by HPLC in accordance with the procedure described in Section 3.2.3. The aqueous concentration of Fe was analyzed to determine the fraction of leaching out from the metal surface. Total dissolved organic carbon, hydrogen peroxide concentration was monitored following filtration of the samples through a 0.45 μm filter.

8.3. Results and Discussion

8.3.1. Power Efficiencies of the Reactor Systems

The results of calorimetric analysis listed in Table 8.1 show that the lowest power was deposited in Reactor 3 and the highest in Reactor 4. We also found that the total power estimated for multiple frequency operations by calorimetry was lower than the algebraic sum of individual powers, as the evidence of increased cavitation activity by combination of different frequencies.

Table 8.1. Results of Calorimetric Analyses.

Reactors/operation modes	Input Power (W)	Specific Power (W L⁻¹)
<u>Singles</u>		
Reactor1 (20 kHz)	17.28	466
Reactor2 (40 kHz)	44.75	179
Reactor3 (200 kHz)	16.75	67
Reactor4a (572 kHz)	57.75	231
Reactor4b (1130 kHz)	46.23	185
<u>Duals</u>		
Dual1 (40 kHz/200 kHz)	83.99	336
Dual2 (40 kHz/572 kHz)	115.37	461
Dual3 (40 kHz/1130 kHz)	116.11	464
<u>Sequentials</u>		
Seq1 (20 kHz+572 kHz)	118.79	480
Seq2 (40 kHz+200 kHz)	76.87	310
Seq3 (40 kHz+572 kHz)	128.12	510
Seq4 (40 kHz+200 kHz+572 kHz)	149.10	600

8.3.2. Silent Absorption of IBP on ZVI

Batch adsorption tests without ultrasound showed that adsorption of IBP on the surface of ZVI increased substantially with increasing doses of the metal, as depicted in Figure 8.2. Equilibrium was reached at around 120-min in the presence of 75 and 50 mg L⁻¹ ZVI, but no equilibrium was observed within the contact time in that of the low doses. Nevertheless, we selected 10 mg L⁻¹ as the application dose based on environmental and economic considerations, as well as the expected advantages of ultrasound for enhancing the dissolution of the metal and the rate of solute transfer to its surface.

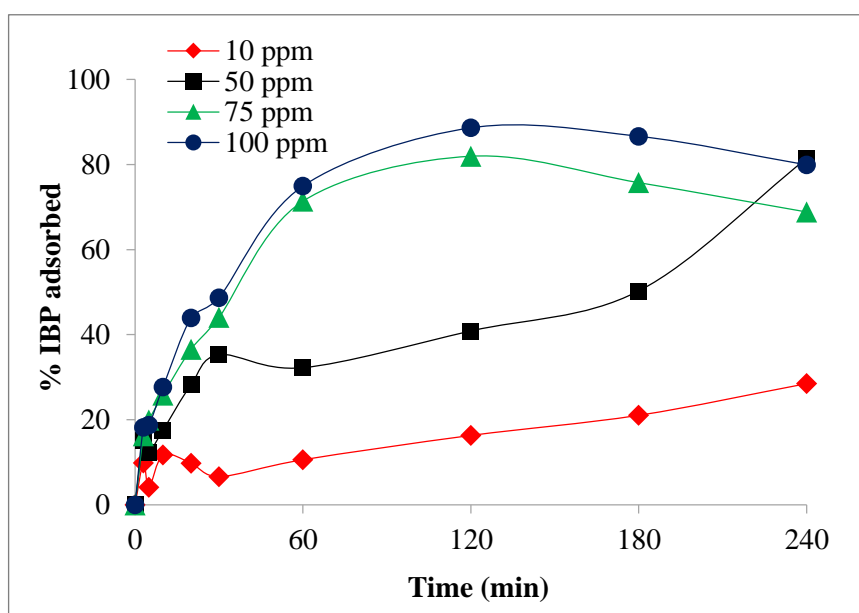


Figure 8.2. The effect of ZVI dose on the adsorption of IBP ($C_0 = 50 \mu\text{M}$) at pH 3.0.

8.3.3. Control Experiments: Sonolysis without ZVI

Relative effectiveness of single frequencies applied at the conditions specified in Table 8.1 under “Singles” is presented in Figure 8.3 for the rate of IBP decomposition and mineralization. It was found that the reactions were appreciably fast at high frequency irradiation (Reactor4-a, b) and relatively slow at short frequencies. The result is obviously the outcome of high solubility of IBP (that prevents its diffusion to the gas bubbles and/or the bubble-liquid interface), and the nature of bubble dynamics that dictates the bubble life times and the incidence of $\bullet\text{OH}$ ejection to the bulk solution. As such, elimination of IBP was much faster at high frequency irradiation due to reduced resonant bubble size, which leads to a larger number of active bubbles and oscillations and ultimately a larger efficiency of $\text{OH}\bullet$ ejection to the bulk solution (Eren and Ince, 2010). Higher efficiency of 572 kHz than 1130 kHz is due to surpassing of the “threshold” frequency, above which the size of resonant bubbles get too small and the frequency of collapse events are insufficient for sonochemical effects (Tezcanlı-Güyer and Ince, 2011). Note also that carbon mineralization was in general low, with a maximum at 577 kHz (10.4%).

In combined frequency applications, we found that neither dual nor sequential applications provided any improvement in the efficiency of IBP degradation, except in Dual2, at which the percentage of TOC decay was slightly larger (13.6 %) than that observed under

572 kHz irradiation alone. Moreover, we found that the reaction rate coefficients in dual and sequential operations with 572 kHz were lower than those observed under single operation of the same frequency. The result must be due to inhibition of the bubble activity or destruction of 572 kHz standing waves in the reactor, as also reported in the literature (Brotchie et al., 2008).

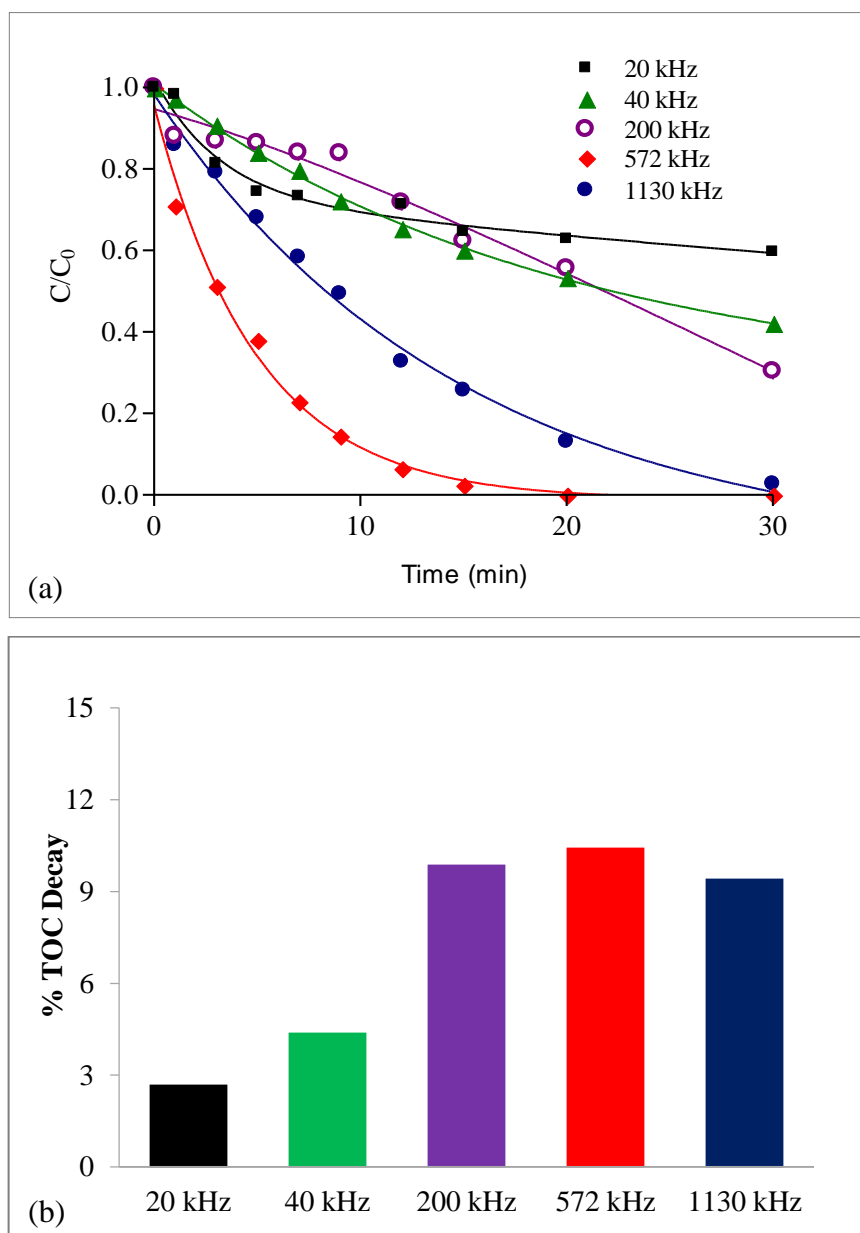
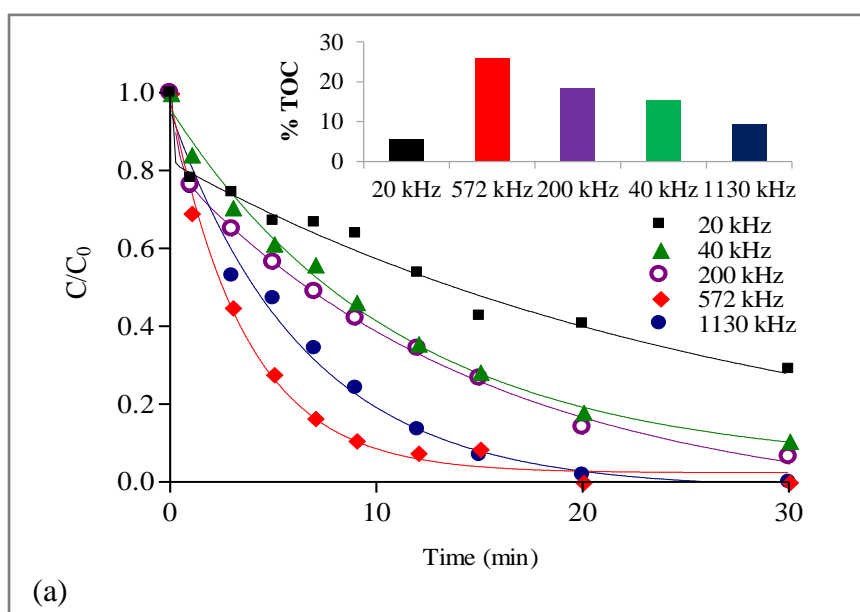


Figure 8.3. Time-rate of elimination (a) and mineralization of IBP (b) by single frequency irradiation at pH 3.0 ($C_0=50 \mu\text{M}$). The apparent reaction rate constants in (a) were: 0.033, 0.035, 0.038, 0.234 and 0.090 for 20 kHz, 40 kHz, 200 kHz, 572 kHz and 1130 kHz, respectively.

8.3.4. Sonolysis with ZVI

Single-Frequency Operations. The addition of ZVI increased substantially the rate of IBP decomposition under all low frequency operations, as the rate constants at 20, 40 and 200 kHz irradiation were almost triplicated in the presence of the metal. On the other hand, the concentration of H_2O_2 (as the indicator of $\bullet\text{OH}$ radicals in solution) during the reactions showed that the reagent was considerably more abundant at high frequencies, under which, however ZVI was found relatively less effective. The data are presented in Figure 8.4. Accordingly, the observed enhancement in the rate of IBP degradation by low-frequency irradiation must be the output of either or both of: i) rapid dissolution of the metal and/or ii) enhanced movement of the contaminant to the heterogeneous surface that is enriched with reactive species (forming upon the collapse of surface-bound cavitation bubbles), which enabled effective decomposition of the contaminant.



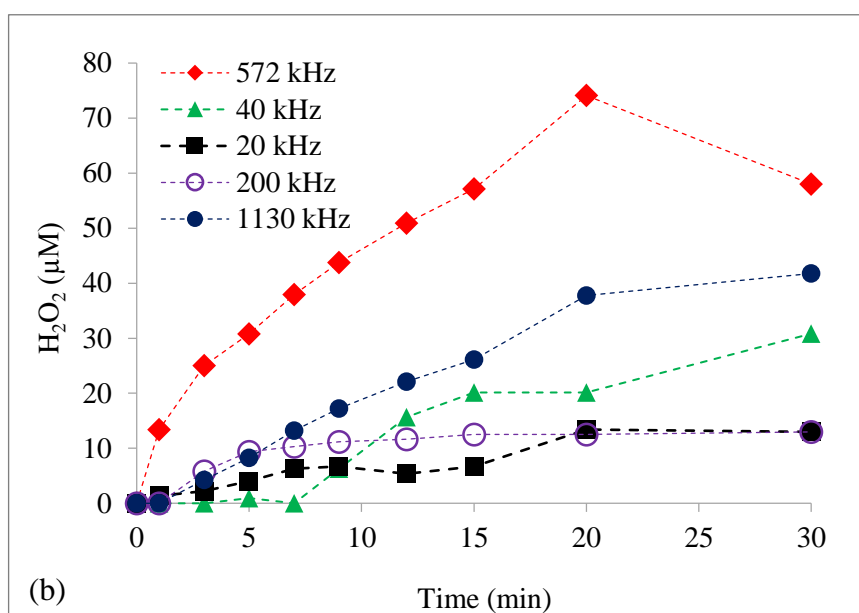


Figure 8.4. Time-rate of IBP elimination (a) and H₂O₂ formation (b) during single-frequency operations with ZVI. The inset in (a) shows relative fractions of TOC decay after 30-min reaction. Initial conditions were pH= 3.0, C₀=50 μM, ZVI=10 mg L⁻¹. The apparent reaction rate constants in (a) were 0.067, 0.090, 0.095, 0.250 and 0.154 min⁻¹ or 20 kHz, 40 kHz, 200 kHz, 572 kHz and 1130 kHz, respectively.

Multiple-Frequency Operations. In dual and sequential operations of multiple frequencies, the reaction rate constants and fractions of TOC decay improved significantly relative to those observed in the absence of the metal. The results are listed in Table 8.2 together with those of single-frequency operations. Most importantly, the data show that the addition of ZVI was most effective in sequential operations, in which the rate of mineralization was enhanced by factors of 3-10. Note also that sequential operations were considerably more effective in the decomposition of IBP, regardless of the presence or absence of ZVI.

On the other hand, the values listed in Table 8.2 do not reflect the real efficiency of the applied systems and/or reactors for the fact that they do not consider energy efficiencies. In fact, comparison of different reactors operated with different configurations and different frequencies requires consideration of the “sonochemical yield”, which can be estimated by the following equation (Mason and Peter, 2002):

$$Y = \frac{\Delta C}{P_s} \quad (\text{Eq. 8.2})$$

where: Y is the sonochemical yield (MW^{-1}), ΔC is the change in molar concentration of the compound after reaction (mol L V^{-1}) and P_s is the specific power in solution (W V^{-1}).

Table 8.2. Comparison of system performances in terms of the apparent reaction rate constants and percentages of IBP and TOC decay. Experimental conditions were: $t=30\text{-min}$, $C_0=50 \mu\text{M}$ (10 mg L^{-1}), $\text{pH}=3.0$, $\text{ZVI}=10 \text{ mg L}^{-1}$.

Reactors/ Operation modes	$-k, \text{min}^{-1}$		% IBP Reduction		% TOC Reduction	
	Control	ZVI	Control	ZVI	Control	ZVI
Singles						
Reactor 1	0.033	0.067	40.36	70.99	2.68	5.72
Reactor 2	0.035	0.090	57.75	89.27	4.38	15.51
Reactor 3	0.038	0.095	69.61	93.49	9.86	18.35
Reactor 4a	0.234	0.280	100.00	100.00	10.40	25.93
Reactor 4b	0.090	0.135	97.30	91.83	9.39	11.78
Duals						
Dual1	0.074	0.087	55.73	87.49	5.42	28.44
Dual2	0.094	0.106	80.63	94.43	13.58	30.25
Dual3	0.069	0.105	59.18	91.83	4.59	24.64
Sequentials						
Seq1	0.162	0.223	100.00	96.48	2.29	23.55
Seq2	0.083	0.107	86.62	96.15	8.44	26.45
Seq3	0.197	0.226	98.48	99.61	3.19	26.97
Seq4	0.138	0.119	98.56	100.00	11.09	26.68

Hence, for a more accurate assessment of the system performances, we calculated the reaction yields to compare the reactors/operations in terms of yields, reaction rate constants, and total TOC decay (estimated by summing up the 30-min and 12-h silent percentages of mineralization). The results are given in Table 8.3. The data show that in terms of sonochemical yields, the most efficient system was singly operated 200 kHz bath (Reactor3), which consumed a considerably lower power than all other systems, but provided no more than 20% mineralization. Combined operations using 200 kHz, i.e. Dual1, Seq2 and Seq4 were not energy-efficient, but provided nearly 30% mineralization. The Table 8.3 also shows that among multiple-frequencies maximum TOC decay was obtained in Dual2 (40/572 kHz), which however was energy inefficient. As such, sequential operation of Seq2 (40+200 kHz) with highest energy efficiency of all combined systems, providing a total of 30% TOC decay

seems to be a suitable operation for the removal of IBP and its oxidation byproducts from water. Figure 8.5 demonstrates the interaction of power, yield coefficient and percentage of TOC decay in all reaction systems. The most important feature in the figure is that it shows in most cases an inverse relationship between the fraction of TOC decay and the sonochemical yield, which is an indicator of the power efficiency of the system. Hence, selection of the most suitable operation based on these relations is very difficult; nevertheless R3, R4a and Seq2 seem to be the most viable options.

8.3.5. The Effect of H₂O₂

The role of H₂O₂ in Fenton reactions is very important, as it facilitates the cyclic oxidation/reduction of Fe²⁺/Fe³⁺ species thus sustaining the stability of the system. The advantage of ultrasound in such systems is that it maintains the availability of peroxide in solution via generation and recombination of •OH radicals as depicted in R8.3 and R8.4. As such, no H₂O₂ was added to the reactors, except in several cases for elucidating the role of excess peroxide (50 mg L⁻¹). The results of these tests showed that the addition of H₂O₂ did not provide appreciable improvements in the efficiency of the reactions, except in one case (Dual2), where the rate of IBP decomposition was enhanced from a rate constant of 10.6x10⁻² min⁻¹ (without H₂O₂) to 14.7 x10⁻² min⁻¹.

In the same case, however, mineralization of the compound was slightly reduced most likely due to reduced number of active adsorption sites on the surface of ZVI (by the adsorption of H₂O₂) and scavenging of some of the •OH by H₂O₂. As a result, it was concluded that the amount of H₂O₂ in the reactors provided by ultrasound was sufficient to sustain the continuity of redox reactions.

Table 8.3. Comparison of ZVI-added operations for sonochemical yields, reaction rate constants and mineralization efficiencies. Initial conditions were: $C_0=10 \text{ mg L}^{-1}$, $\text{pH}=3.0$ and $\text{ZVI}=10 \text{ mg L}^{-1}$. The time span for “k”, “Y” and “apparent mineralization” is 10-min and that for “latent mineralization” is 12-h.

Reactors	Y ($\mu\text{MW}^{-1} \text{L}^{-1}$)	k x10 ⁻² (min ⁻¹)	TOC Decay (%)		
			Apparent	Latent	Total
<u>Singles</u>					
Reactor1	0.07	6.72	5.72	3.68	9.41
Reactor2	0.24	8.90	15.51	0.59	16.10
Reactor3	0.72	9.51	18.35	2.29	20.64
Reactor4a	0.22	28.51	25.93	6.82	32.75
Reactor4b	0.26	11.53	11.78	0.37	12.15
<u>Duals</u>					
Dual1	0.12	8.72	28.44	1.48	29.93
Dual2	0.10	10.61	30.25	6.61	36.49
Dual3	0.09	10.49	24.64	8.85	33.49
<u>Sequentials</u>					
Seq1	0.10	22.31	23.55	3.73	27.28
Seq2	0.14	10.70	26.45	2.34	29.79
Seq3	0.10	22.63	26.97	1.67	28.64
Seq4	0.08	11.89	26.68	1.17	27.85

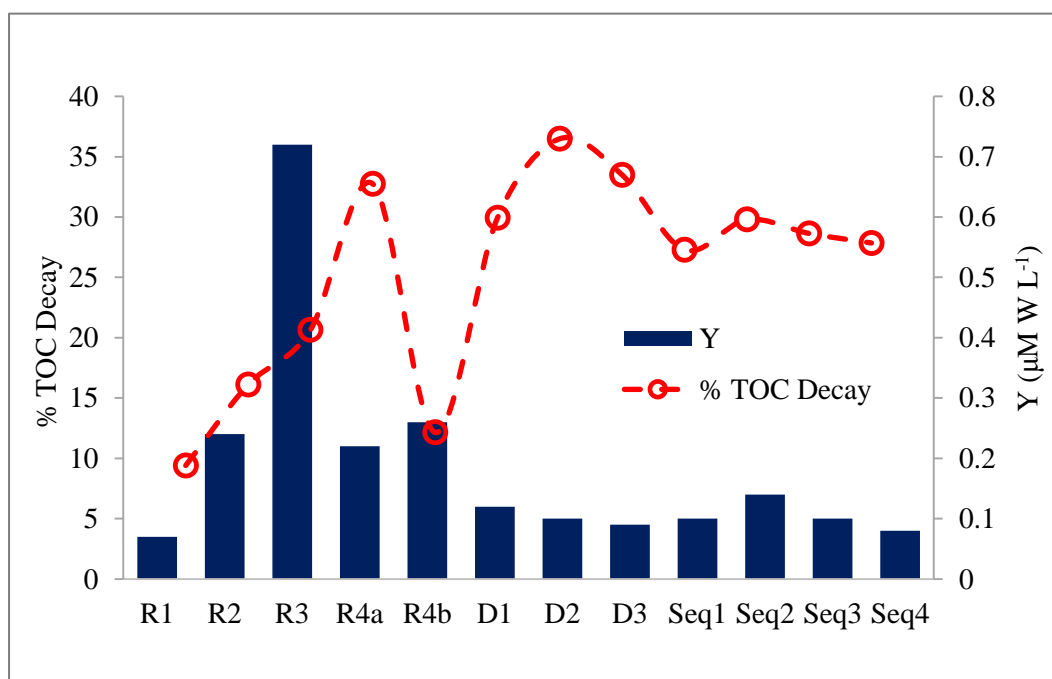


Figure 8.5. Interactive relations between the reactor systems, the yield coefficient and total TOC decay. “R1-R4b” and “D1-D3” refer respectively to Reactor1-Reacto4b and Dual1-Dual3.

8.4. Conclusions

The efficiency of ibuprofen degradation by sonolysis in the presence of ZVI is closely related to the applied frequency and the power efficiency of the reactor. It was found that among low frequencies, the most effective one was the bath operated at 200-kHz ($Y=0.72 \mu\text{M W}^{-1} \text{L}^{-1}$), which provided 93% IBP removal and 21% TOC reduction in the presence of ZVI. High frequency operations in that sense were more effective, particularly the plate-type reactor at 577 kHz, which provided 100% IBP and 33% TOC removal within the same time. Combined applications of multiple frequencies improved the degradation of the compound and were particularly effective in sequential operations. Low frequency operation at 20 kHz was the least effective of all test systems, not only for the low efficiency of chemical reactions, but also for its low power efficiency. Combined operations were inherently more energy intensive than their single counterparts, as they required higher power inputs and provided lower sonochemical yields with, however, substantial increases in the mineralization of the compound. It was also found that the mechanism of degradation was more highly related to heterogeneous reactions on the surface of ZVI that contained extensive nucleation, adsorption and reactive sites than to the availability of $\text{OH}\cdot$ and Fe species in the bulk solution.

9. SUPPORTING OF PRISTINE TiO₂ WITH NOBLE METALS TO ENHANCE THE OXIDATION AND MINERALIZATION OF PARACETAMOL BY SONOLYSIS AND SONOPHOTOLYSIS

The present chapter is a summary of the work published in *Applied Catalysis B: Environmental* 172 (2015) 7–17 “Supporting of pristine TiO₂ with noble metals to enhance the oxidation and mineralization of paracetamol by sonolysis and sonophotolysis”. This study is about the elimination and overall degradation of a common anti-inflammatory pharmaceutical-paracetamol (PCT) in water by catalytic oxidation using high-frequency ultrasound, UV-irradiation (254 nm) and both in the presence of modified nanocomposites of TiO₂.

9.1. Introduction

The majority of research on photocatalytic degradation of PCT with TiO₂ reports the downside of the process for long irradiation times (at around 365 nm), high catalyst concentrations (500-2000 mgL⁻¹) and poor mineralization efficiency (Moctezuma et al., 2012; L. Yang et al., 2009; Zhang et al., 2008). There are almost no studies on the use of TiO₂ nanocomposites for PCT degradation except a single one that reports complete mineralization after 1-h electrolysis of the solution (with a carbon electrode) in the presence of a TiO₂ nanocomposite containing CuO and Al₂O₃ (Valdez et al., 2012). The use of precious metals such as Pt, Pd, Ag and Au has lately emerged as a promising option to enhance photocatalytic activity of TiO₂ in the UV-visible band via inhibition of e⁻/h⁺ recombination and evasion of photo-corrosion of the metal surface owing to the high Schottky barriers of these metals that inhibit recombination of e⁻/h⁺ pairs by acting as e⁻ traps or by promoting interfacial charge transfer processes (Sclafani and Herrmann, 1998; Wold, 1993). An additional benefit of gold is its activity in the UV-visible region, which is expected to extend the active spectrum range of the nanocomposite (Kalathil et al., 2012; Kamat, 2007; Primo et al., 2011).

The literature on sonocatalytic degradation of PCT is also limited, and the most interesting studies are those related to the use of hybrid processes such as US/UV/TiO₂, US/AC/bio-char and US/CNT (Im et al., 2014; Jagannathan et al., 2013), where AC and CNT refer to activated carbon and carbon nanotubes, respectively. Nevertheless, there are no studies so far that report the degradability of PCT in the presence of a mono or bi-metallic nanocomposite of TiO₂ supported by precious metals and activated by US or a combination of US and UV irradiation. However, photocatalytic activity of TiO₂ can also be enhanced by irradiating a solution of the metal salt with ultrasound (Shimizu et al., 2007).

The present study aims to investigate the degradation of PCT by sonolysis (861 kHz), photolysis (254 nm), sonocatalysis and sono-photocatalysis using metal-supported nanocomposites of TiO₂ (Pd-, Au- and Pd/Au-). The impact of the metals was assessed by monitoring the activity of the nanocomposites and pristine TiO₂ in the decomposition and mineralization of the target compound under each test process. The study also highlights the effect of persulfate addition, the reusability performance of the composites and the synergy of the hybrid process (ultrasound/photolysis) with emphasis on the properties of the solids and the supporting metals.

9.2. Materials and Methods

Paracetamol sulfate potassium salt was purchased from Sigma and used for preparing a standard solution of the compound. PCT test samples were prepared using 500 mg of commercially available tablet pills. The chemical structure and some of the physical/environmental properties of the product may be found in Section 3.1.1.

A stock solution of PCT was made by grinding and dissolving a pill tablet in pure water at 50°C during magnetic stirring. The solution was filtered and adjusted to pH 9.5 with NaOH to keep it stable. The concentration of PCT in the stock was determined via calibration with a standardized solution. All analytical grade reagents were obtained from Merck, noble metals, TiO₂ (Degussa P-25) and polyethylene-glycol monostearate (PEG-MS) from Wako (Japan).

Preparation of the Catalysts. Nanocomposites (Pd-TiO₂, Au-TiO₂ and Pd/Au-TiO₂) were synthesized sonolytically in accordance with the procedure described in Section 2.3. Before experiments and silent adsorption tests, the nanocomposite was further treated by mixing a small sample with 20 mL water and sonicating the suspension for 3-min in a water bath (35 kHz) to enhance particle stability against agglomeration thus to increase the adsorption properties of the catalysts.

Adsorption Tests. Batch adsorption tests were carried out at varying concentrations of the catalysts (1 mg L⁻¹, 2.5 mg L⁻¹, 5 mg L⁻¹, 10 mg L⁻¹, 25 mg L⁻¹ and 50 mg L⁻¹) in a Julabo SW22 shaker at pH 3.0, 5.3 (natural pH of test solutions), 6.5 and 10.0 for 24-h to assess the effect of catalyst dose and pH on the degree of PCT adsorption and to optimize the equilibrium conditions. The concentration of PCT and the rate of mixing were fixed at 35 μM and 250 rpm, respectively.

9.2.1. Experimental

Sonolysis/Sonocatalysis. Sonication of the test solution was carried out in a 500 mL glass cell (R4) equipped with a multi-frequency piezo-electric transducer (22 cm²) and a 120 W generator (Ultraschall/ Meinhardt, Germany). The volume of the solution was 250 mL and the power intensity (at 861 kHz) was determined by calorimetry as 1.14 W cm⁻² (Mason and Peter, 2002). The optimum values of PCT concentration, frequency and pH were determined based on the rate of PCT degradation at various test levels of each parameter. The effective catalyst concentration was selected by adding 1, 2.5, 5, 10 and 50 mg L⁻¹ of each to the selected optimum concentration of PCT while monitoring the concentration of the compound during 60-min sonication. The experiments were repeated in the presence of commercial TiO₂-Degusa to assess the effect of immobilization. The impact of persulfate addition was tested by monitoring the concentration of PCT in the presence of 5 mg L⁻¹ of the catalysts and various concentrations of the reagent (0.5-5.0 mM). Control experiments were run with persulfate/ultrasound in the absence of the catalysts.

Photolysis/Photocatalysis/Sonophotocatalysis. Photolytic and photocatalytic experiments were carried out by 1-h irradiation of a PCT sample solution in the absence and presence of 5 mg L⁻¹ of each catalyst using a low press Hg-UV lamp emitting at 254 nm. The light

fluence in solution was determined by using the peroxy-disulfate actinometer as 107.4 W cm^{-2} (Mark et al., 1990). The optimum Ph was selected by monitoring the concentration of PCT during sonocatalysis at Ph 3.0, 5.3 and 6.5 and estimating the reaction rate constant. Sonophotocatalytic experiments were also run in the sonoreactor described above and the same UV source under the optimized conditions.

Stability Tests of the Catalysts. Following 40-min sonolysis of PCT with each synthesized catalyst (not exposed to post-treatment), the remaining solution was adjusted to Ph 12 and kept inert for 1-h to allow desorption of organic material from the surface of the catalyst. The spent catalyst was then separated under vacuum by membrane filtration, washed with hot water, dried at $60 \text{ }^\circ\text{C}$ for 24-h and reused in another sonocatalytic run. The procedure was repeated three times to allow four consecutive uses of the catalyst in order evaluate its reusability. The initial concentration of PCT in each use was adjusted so as to maintain an equivalent mass ratio of PCT to catalyst at all times.

Separation of post-treated catalysts (3-min post-sonication in a bath) by the same technique was not possible due to the strong resistance of the particles to destabilization and collection on the filter surface. Other techniques such as desorption followed by evaporation and centrifugation were also tested, but the overall recovery was always lower than that obtained with non-treated catalysts.

9.2.2. Analytical

PCT, TOC and the concentration of H_2O_2 was analyzed by HPLC, TOC analyzer and potassium iodide method (Kiassen et al., 1994) after filtration of the samples through a $0.45 \text{ }\mu\text{m}$ membrane filter. The decomposition of $\text{S}_2\text{O}_8^{2-}$ via activation with ultrasound was determined spectrophotometrically (UNICAM, Helios α -Double Beam) in samples collected from the reactor at given time intervals during 30-min sonication. The method was based on the reaction of $\text{S}_2\text{O}_8^{2-}$ with Fe^{2+} to form $\text{SO}_4^{\cdot-}$ and Fe^{3+} and subsequent formation of ferric cyanate $[\text{FeSCN}]^{2+}$ upon the addition of ammonium thiocyanate (Huang et al., 2002). The formation of sulfate radicals was verified by adding 2.5 Mm t-butanol to a test solution spiked with 2.5 Mm persulfate and monitoring the evolution of H^+ during 40-min sonication. The method is based on the stoichiometry of t-butanol reaction with $\text{SO}_4^{\cdot-}$ to generate H^+

(Mark et al., 1990). The interference of US-generated $\bullet\text{OH}$ with the target reaction was taken into account by monitoring the Ph of a control solution during sonolysis of t-butanol in the absence of $\text{S}_2\text{O}_8^{2-}$.

The structure, morphology and size of commercial and synthesized particles were analyzed by environmental scanning electron microscope (ESEM) and scanning-transmission electron microscopy (STEM) as described in Section 3.2.3. Multi-element mapping and phase analyses were carried out to detect, characterize and classify the indefinite features under low/high vacuum conditions without limitation. Hydrodynamic diameter and size distribution analyses were made in dilute solutions of the particles using a Brookhaven 90-Plus nanoparticle size analyzer operated with the method of dynamic light scattering (DLS).

The band gap energies of TiO_2 and the nanocomposites were determined using a UV-vis spectrophotometer as described in Section 3.2.3. The data were evaluated by reference to Kubelka–Munk (KM) transformations and linear extrapolation of the diffuse reflectance spectra as described in the literature (Ökte et al., 2014).

9.3. Results and Discussion

9.3.1. Characterization of Nanocomposites

SEM analysis of catalyst surfaces for chemical layer characterization and homogeneity showed that neither the noble metals nor TiO_2 were concentrated in any specific area of the composite surface signifying a uniform dispersion, i.e. the metals were homogeneously distributed throughout the TiO_2 surface with no particle aggregation (the images obtained by multi-element mapping are provided in (Appendix A, Figure A9.1). Particle size analysis by SEM showed that the size of P-25 or TiO_2 -Degussa was between 30-40 nm, which is consistent with the data reported by the current manufacturer (Evonik), that of Au- TiO_2 was around 14-20 nm, and those of Pd- TiO_2 and Pd/Au- TiO_2 were less than 10 nm. As such, STEM analysis was used to acquire higher resolution images that allow determination of the exact size, composition and localization of the metals on the nanocomposites. The images obtained are depicted in Figure 9.1 (a), (b), and (c), for Pd- TiO_2 , Au- TiO_2 and Pd/Au- TiO_2 ,

respectively. The brighter spots in the first two represent Pd and Au immobilized on TiO₂; the brighter core and the darker shell in the last one signify locations of the heavier Au and the lighter Pd, respectively in accordance with the interpretation of STEM images of bimetallic nanocomposites, as reported previously (Mizukoshi et al., 2010). The average particle size in Au-TiO₂, Pd-TiO₂ and Pd/Au-TiO₂ was 13.8 nm, 5.9 nm and 5.4 nm, respectively.

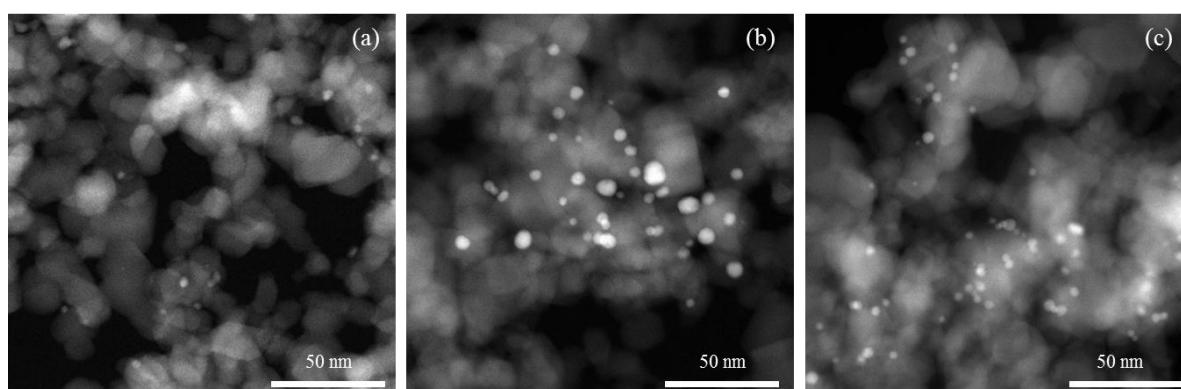


Figure 9.1. HAADF-STEM images of (a) Pd-TiO₂, (b) Au-TiO₂, (c) and Pd/Au-TiO₂.

The band gap energies of all particles were found to be the same at around 3.25 ± 0.01 eV, and the result was attributed to the absence of doping agents that would generate new energy levels between the valence band and the conduction band.

9.3.2. Silent Adsorption of PCT on TiO₂ and/or Its Nanocomposites

Silent adsorption tests revealed that equilibrium was reached at around 6-h with all of the catalysts and the highest fraction of PCT accumulation after 24-h was on Au-TiO₂ as 17% at pH 6.5, implying that adsorptive elimination of the compound under applied conditions (1-h) was insignificant. The data are presented in Figure 9.2(a) for commercial and post-treated nanocomposites, the adsorptive properties of which were slightly better than that of the original untreated portion (via improved particle stability that inhibited agglomeration).

It was found that the value of pH that provided maximum adsorption on the surface of the catalysts was 6.5, most likely because the surface of TiO₂ is slightly positive at pH < zero point charge (6.8), at which PCT is neutral (nonionic state) and poorly soluble (pK_a=9.4) so that there is practically no repulsion between the solute and the solid surface. In accordance,

acidic pH was less favorable due to increased electrostatic repulsion between protonated molecules of the compound and the positively charged adsorbent surface. Note also that no adsorption was observed at pH 10 due to the negative charge on the surface of the solids and the anionic form of the compound at $\text{pH} > \text{pK}_a$.

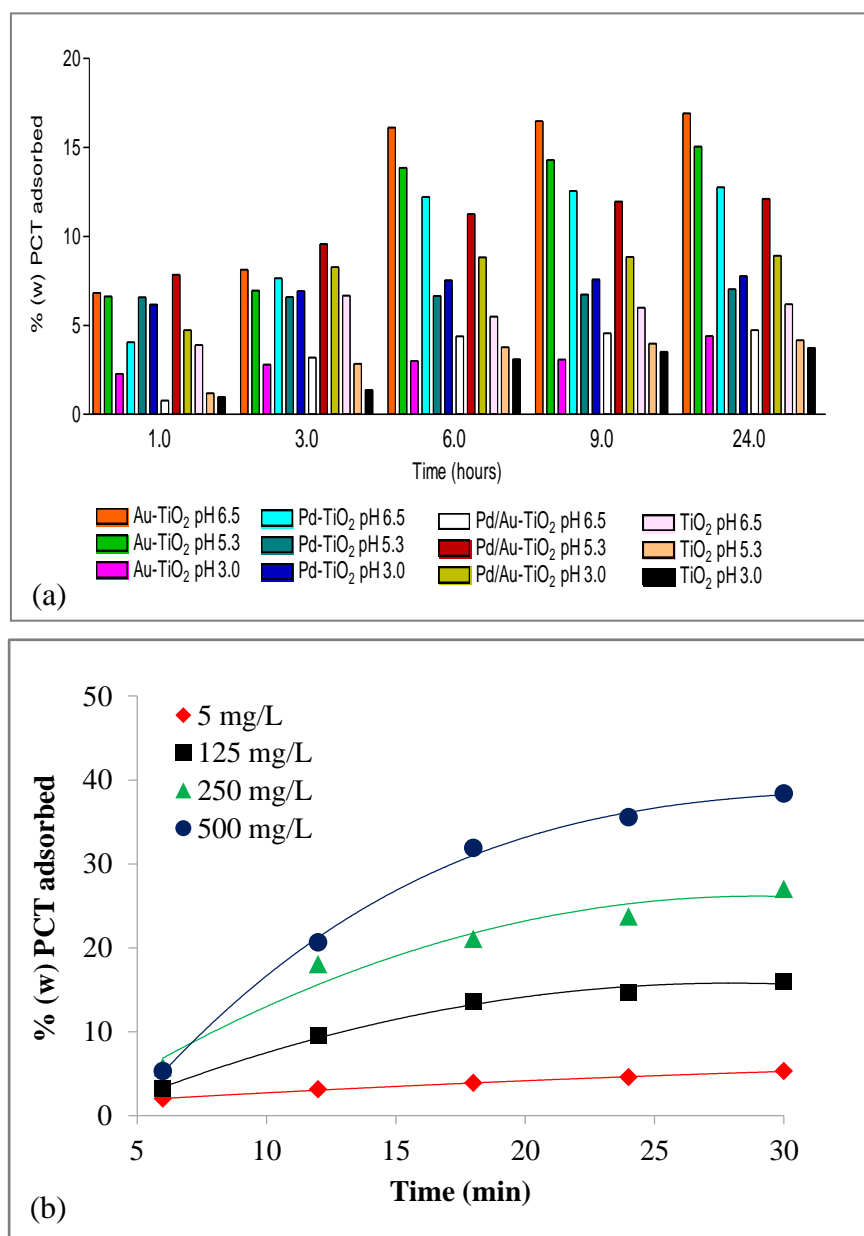


Figure 9.2. Relative adsorption of PCT (C₀ = 35 M) on 5 mg L⁻¹ of commercial and immobilized TiO₂ during silent shaking: (a) the effect of pH; (b) the effect of increasing the adsorbent concentration (data are representative of sono-treated Pd-TiO₂).

It was also observed that the fraction of PCT adsorbed was remarkably increased when the adsorbent concentration was 50- and 100-fold increased as depicted in Figure 9.2(b) for post-treated Pd-TiO₂. The adsorption equilibrium and the corresponding Langmuir isotherm parameters for the same catalyst are provided in Appendix A, Figure A9.2.

9.3.3. Sonolysis and Sonocatalysis

The optimum conditions of frequency, PCT concentration and pH by sonication alone were selected (based on maximum rate of degradation and carbon-mineralization) as 861 kHz, 35 μM and 3.0, respectively as shown in Figure 9.3 (a, b, c, d). Higher reactivity under acidic conditions, lower solute concentrations and the selected frequency had been discussed thoroughly in the previous sections with emphasis on the ability of solutes to diffuse to the bubble-liquid interface, reduced competition for radical species, and higher incidence of •OH ejection to the bulk solution, respectively (Eren and Ince, 2010; Ince et al., 2009; Ince and Tezcanli-Güyer, 2004). Hence, the degradation of PCT by sonolysis was realized by •OH-mediated oxidation reactions mostly in the bulk liquid and partly at the bubble-liquid interface, where the concentration of •OH is very high. It was also found that the rate of degradation in most cases deviated from the pseudo-first order law and fitted perfectly to the following expression:

$$\frac{C}{C_0} = e^{-kt} + \delta \quad (\text{Eq. 9.1})$$

where: C and C₀ are concentrations of PCT at time t and zero, respectively, k is the apparent reaction rate constant (time⁻¹) and δ is the deviation factor that is equal to a non-zero plateau representing the ultimate value of C/C₀. In fact, a plot of ln(C/C₀) against time for a sonochemical reaction usually ends up with two straight lines: the steeper one represents the rapid decay of the solute at early reaction while the other is responsible for the rest of the time, as typical of heterogeneous reaction systems (e.g. gas-liquid heterogeneity in sonicated water) with exhausting sites of adsorption.

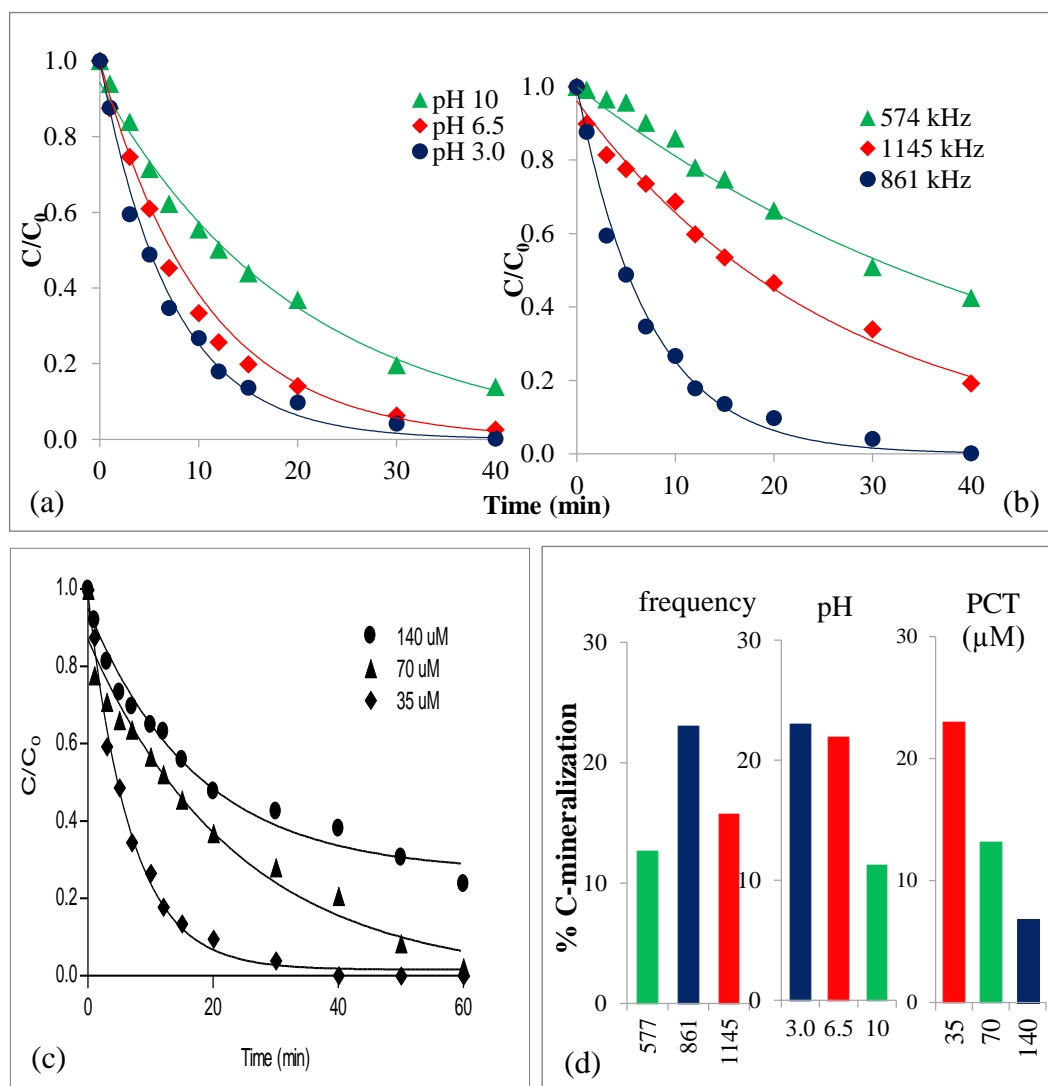


Figure 9.3. The impact of pH, frequency, and concentration on the rate of PCT degradation (a, b, c) and C-mineralization (d) by ultrasound. The solid lines represent exponential fits of Eq. 9.1 to the observed data.

Sonication of PCT in the presence of the catalysts showed that previously optimized values of solute concentration and frequency could be kept at the optimized levels, but the value of pH needed re-optimization due to faster degradation of the compound at near neutral pH than at acidic. The effect of pH on the degradation ($t=40$ -min) and mineralization ($t=60$ -min) of PCT by sonolysis in the presence of Pd-TiO₂ are presented in Figure 9.4 (a, b, c). Note that at acidic pH the rate of PCT decay is slower than that obtained by sonication without catalysts to be attributed to ineffective transport of PCT molecules to the catalyst surface, which contains reactive oxygenated species as well as e^-/h^+ pairs. Higher reactivity at pH 6.5 is the consequence of better adsorptive properties, as also observed in silent

adsorption experiments and probably well activation of catalysts at pH near zero point charge. Note also that the reaction rate in this process also deviated from the pseudo-first order law and the relation between the initial rate and PCT concentration confirmed Langmuir-Hinshelwood type of kinetics. The data are presented in Appendix A, Figure A9.3. This is due to the fact that there existed multiple interfaces in the system (gas-liquid, gas-solid, solid-liquid) we were justified in expressing the fraction of concentration decay with time by Eq. 9.1.

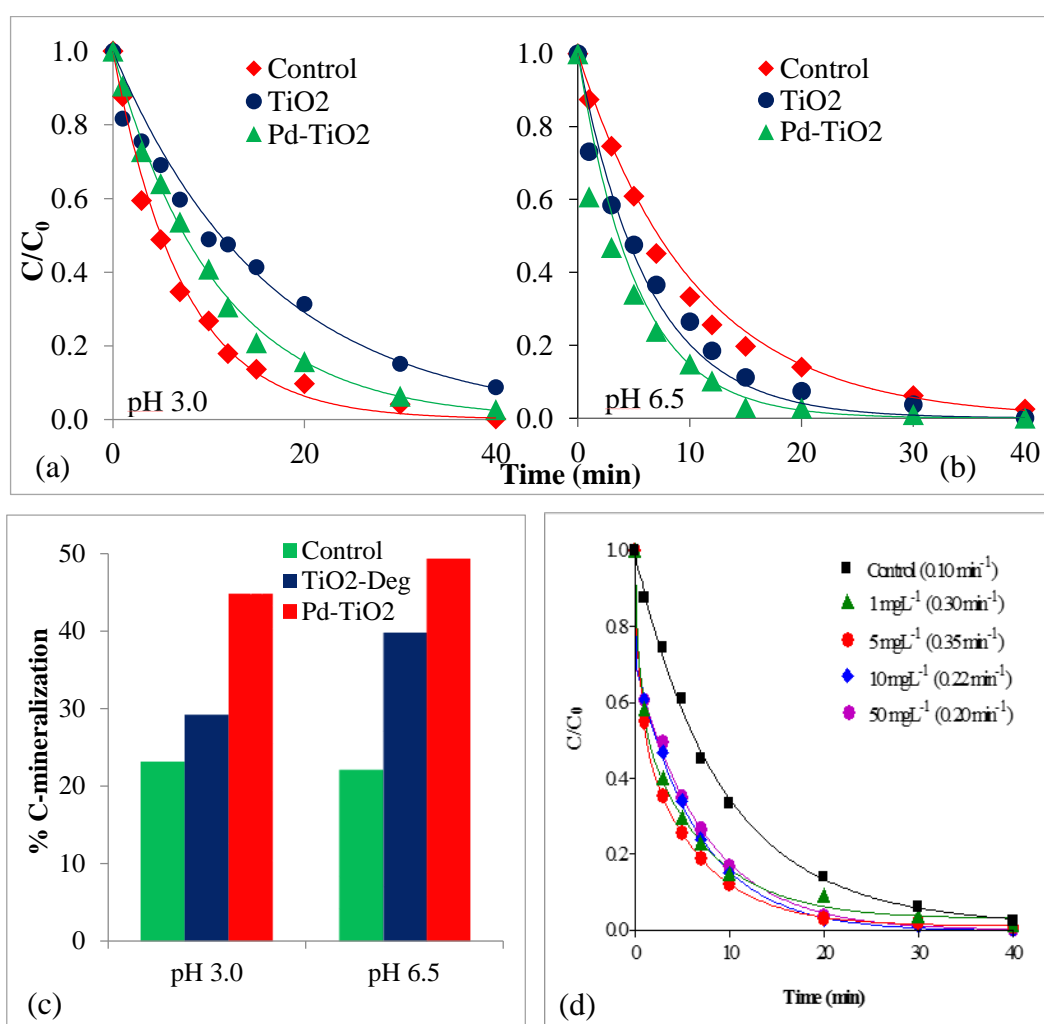


Figure 9.4. The impact of pH on sonocatalytic degradation and mineralization of (35 μM , 861 kHz) in the presence of 5 mg L^{-1} of commercial and Pd-supported TiO_2 (a, b, c); the effect of catalyst (Pd- TiO_2) concentration at pH 6.5 (d). “Control” and “ TiO_2 -Deg” refer to ultrasound alone and commercial TiO_2 -P25 (Degussa), respectively.

It was also found that the rate of PCT decay was very sensitive to the mass of catalyst in the reactor, increasing within a low concentration range (1-10 mg L⁻¹) and declining at higher loadings, as depicted in Figure 10.4(d). Such a rate pattern is the sign of adsorption-mediated reactions and implies the presence of too many particles and noble metals at high loadings that partially block the surface of TiO₂ (or hinder the adsorption of •OH on the surface). Another factor that may be responsible for the slower reactions is agglomeration of particles at high concentrations (despite the effect of ultrasound to disaggregate) that leads to reduced efficiency of energy transmission and attenuation of the ultrasonic field. The tendency for agglomeration was confirmed by the zeta potentials of the composites, as depicted in Appendix A, Figure A9.4.

Relative efficacy of all catalysts for the decomposition and mineralization of PCT by sonocatalysis is presented in Figure 9.5. The data show that catalytic activity increased with decreasing particle size and the most effective catalysts during the oxidation and mineralization processes were Pd-TiO₂ and Pd/Au-TiO₂, respectively. The superiority of Pd is believed to arise from its high surface energy, which enables a more efficient contact between the metal and the oxygen vacancies on the surface of TiO₂ (Fu et al., 2005). Moreover, noble metals such as Pt and Pd are reported to increase the acidic strength of catalyst surfaces, thus improving the adsorption efficiency of solutes (Jin et al., 2011).

The biphasic character of PCT decay in the presence of Pd-TiO₂ (very fast only during the first 10-min and slower thereafter) justifies why it was more effective in the oxidation of PCT and less in mineralization (41 % and 54 % reduction in TOC with Pd-TiO₂ and Pd/Au-TiO₂, respectively). Such bi-phasic character also implies different selectivity of the catalyst for the parent and the oxidation compounds. Note also that both of Pd-supported particles (Pd-TiO₂, Pd/Au-TiO₂) were remarkably more effective than Au-supported counterparts as a consequence of their much smaller particle size that promoted the formation of excess cavitation nuclei and thus the production and adsorption of excess •OH and ROS on their surface. Analysis of hydrodynamic diameters in dilute suspensions showed that smaller particles had also smaller hydrated diameters and vice versa, indicating that the activity of the catalysts in solution was reduced by increased coverage of their surface with molecules of water. The data and distribution of particle size in water are represented in Appendix A, Figure A9.5.

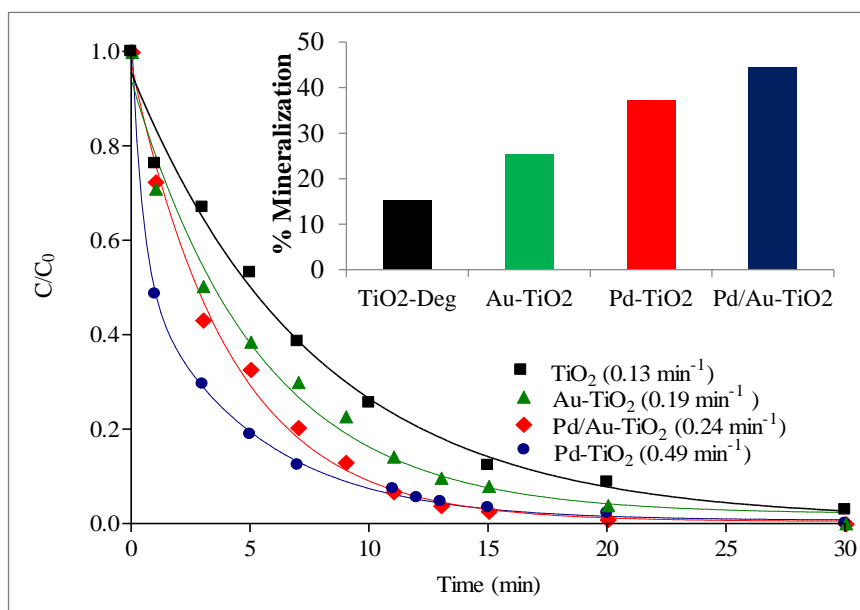
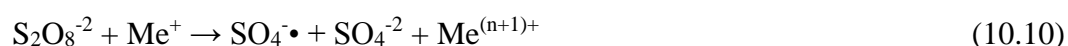


Figure 9.5. Relative rate of PCT degradation during 30 min sonocatalysis at pH 6.5. The insert shows the decay of TOC in 1-h reaction under the same conditions: $C_0 = 35 \mu\text{M}$ PCT, $f = 861 \text{ kHz}$, $\text{cat} = 5 \text{ mg L}^{-1}$. Figures in brackets are the reaction rate constants estimated by (Eq. 9.1).

9.3.4. The effect of Persulfate Addition

It has been previously demonstrated that persulfate ($\text{S}_2\text{O}_8^{2-}$) is an excellent reagent in AOPs via its activation to generate $\text{SO}_4^{\cdot-}$ with an oxidation potential of 2.16 Ev (Hao et al., 2014) that is lower but comparable with that of the $\cdot\text{OH}$ radical (2.83 Ev). The process requires the use of heat, UV-irradiation, ultrasound or transition metal additives as demonstrated respectively in the following reactions (Hao et al., 2014; Tsitonaki et al., 2010):



When ultrasound is the method of activating persulfate (PS), additional benefits are obtained such as production of $\bullet\text{OH}$ and H_2O_2 via water pyrolysis, and acceleration of mass transfer and chemical reaction rates via mechanical effects of ultrasound. As such, PS was found a highly effective additive in sonochemical elimination of some refractory/toxic compounds in water (Gayathri et al., 2010; Hori et al., 2012; S. Su et al., 2012; Wang et al., 2014; Zhou et al., 2013). Moreover, at neutral and alkaline conditions sulfate radical readily reacts with H_2O and/or OH^- , respectively to yield additional hydroxyl radicals as (Lee et al., 2012):



Silent reaction of PCT with persulfate showed that the most effective concentration of the reagent was 2.5 Mm, below and above which the reaction was slowed down due to the scarcity and abundance of $\text{SO}_4^{\bullet-}$, respectively (the latter leading to $\bullet\text{OH}$ scavenging). More significantly, the reaction was very sensitive to variations in pH as depicted in Figure 9.6. The data show that at pH 10, PCT was completely decomposed within 20-min via a zero-order reaction rate and formation of a pale yellow color. This is consistent with the literature, where direct reaction of PCT with persulfate at alkaline pH was reported to produce p-nitrophenol ($\text{C}_6\text{H}_5\text{NO}_2$) and acetic acid (CH_3COOH), the former recognized with its yellowish color (Lee et al., 2012). However, alkaline pH was ineffective for the mineralization of PCT by persulfate, because only 4% of TOC was decomposed at the end of 1-h contact.

Considering that decomposition of the oxidation byproducts is at least as important as that of the parent compound, we conducted sonolytic experiments with persulfate at pH 6.5, which was selected as the optimum operating pH for all reactions. Before we started the experiments, we monitored the decay in the concentration of persulfate and the activity of sulfate radical by the methods described in Section 9.2.5. The results of these preliminary analyses (Appendix A, Figure A9.6) showed that $\text{S}_2\text{O}_8^{2-}$ was effectively activated by ultrasound to produce sulfate radicals.

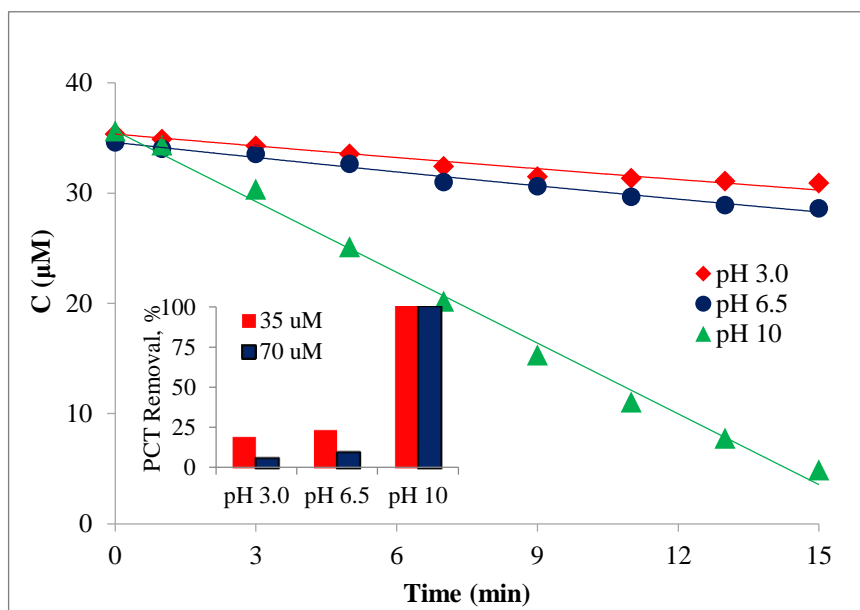


Figure 9.6. Oxidation decay of PCT ($C_0= 35 \mu\text{M}$) by 15 min reaction with persulfate (2.5 Mm) under silent conditions at pH 3.0, 6.5 and 10. The inset shows the impact of PCT initial concentration on the fraction of decay after 1-h contact with PS.

The rate of PCT elimination and % TOC decay by sonocatalysis in the presence of 2.5 Mm PS are presented in Figure 9.7 (a, b), respectively. It was found that Pd-Au/TiO₂ and Pd-TiO₂ were the most effective catalysts in the oxidation and mineralization processes, respectively. Different performance of the catalysts in this and the previous process (without S₂O₈²⁻) must be due to differences in the reaction byproducts and selectivity of the particles for them or additional routes for the reaction of persulfate or reactive species with the surface of semiconductors to produce additional/excess radical species. Note also the remarkable improvement obtained in the performance of TiO₂-Degussa for mineralization (from 15 % to 38 %) implying the enhancement in the quantity of adsorbed radical species and a higher selectivity of the catalyst for the oxidation products.

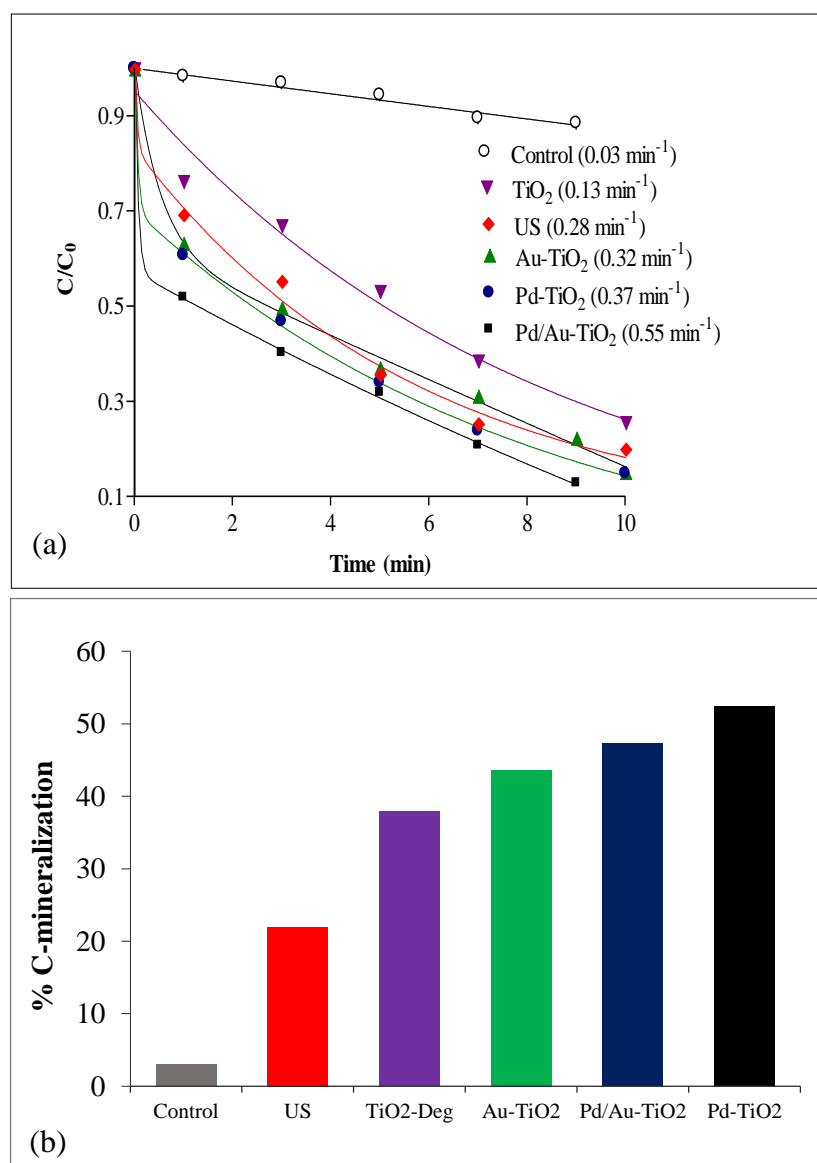


Figure 9.7. The impact of PS addition (2.5 Mm) on the initial rate of degradation (a) and 1-h mineralization of PCT (b) in the presence of ultrasound and 5 mg L^{-1} of commercial and immobilized TiO_2 at pH 6.5. “Control” refers to PS alone; figures in brackets are 10-min reaction rate constants as estimated by Eq. 9.1.

9.3.5. Stability of the Catalysts

One of the most important features of solid catalysts is their stability, i.e. the ease of recovery and the loss of efficiency upon multiple-use. In general, the higher the recovery of a spent catalyst and the lower is the loss of efficiency in the next use, the more stable and economical it is. In that sense, Pd- TiO_2 was found as the most stable catalyst with 84 %, 72 %

and 69 % recovery, respectively at the end of 1st, 2nd and 3rd consecutive uses in sonocatalytic degradation of PCT. It was also found that although the activity of the spent catalyst was initially less than that in the previous run, it rapidly improved within the first 7-min and closely equalized with the original activity. Relative efficacy of the fresh and spent Pd-TiO₂ during 10-min reaction of PCT under ultrasonic irradiation is presented in Figure 9.8.

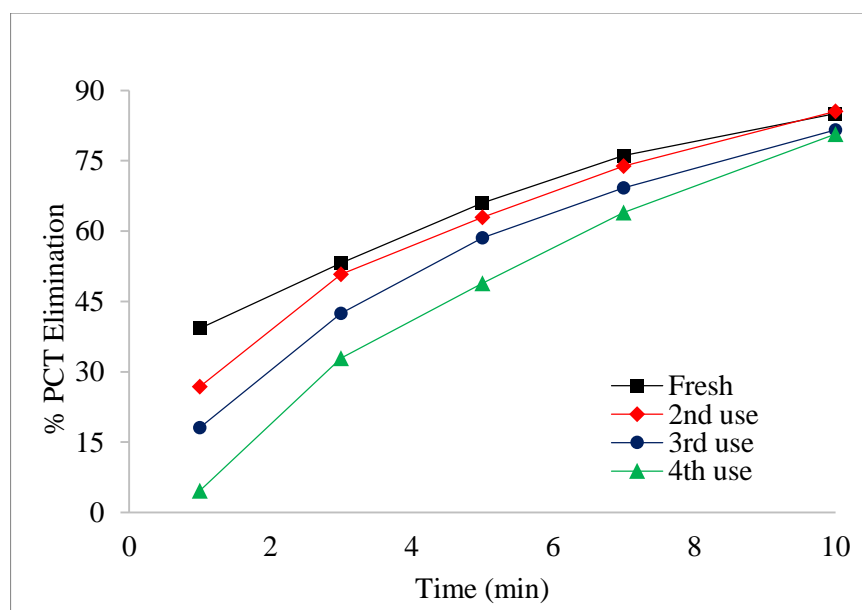


Figure 9.8. The loss in the efficiency of Pd-TiO₂ upon recovery and reuse of the spent catalyst successively in sonocatalytic degradation of PCT.

The very good performance of the nanocomposite in recovery and reuse does not only highlight the role of ultrasound in continuous cleaning of surfaces and disaggregation of particles to allow efficient trapping of sono-generated electrons, but also implies the insignificance of dynamic changes in particle size (via leaching of the immobilized metals) with successive uses. A similar and even higher efficiency of reusability has been reported for a high-temperature annealed Au/TiO₂ sample, with data showing that particle densities and size distributions were indistinguishable from the fresh counterparts (Su et al., 2012).

9.3.6. Photo- and Sono-photocatalysis

The use of UVC irradiation ($\lambda_{\max}=254$ nm) in photocatalytic experiments with the synthesized particles was found to be remarkably effective that was attributed to the dual function of the UV-254 nm for excitation of the catalyst surface and decomposition of the target compound. Direct reaction of PCT with UV-254 nm irradiation has also been reported in the literature and explained by the migration of the acetyl group onto the aromatic ring in *o*-position to the amino moiety (Pozdnyakov et al., 2014). Hence, all light-bearing experiments were carried out using the low-pressure Hg-UV lamp described in section 9.2.3.

It was found that the rate of PCT decay by photolysis alone and photocatalysis with P-25 was the same, implying that the surface of the catalyst in commercial form was not activated by the test light source. However, the reaction was considerably faster when catalyzed by metal-supported counterparts as depicted in Figure 9.9 together with the absorption properties of the catalysts. The reason for presenting these two data sets together is because the band gap energies of all particles were the same and particle size alone was insufficient to explain the observed differences in catalytic activities. The absorption properties in the table show that the effect of single metal support was to extend the active spectrum range of the semiconductor, while that of bi-metallic support was to enhance the intensity of absorption. Hence, much faster degradation of PCT in the presence of Pd/Au-TiO₂ than the other composites must be the output of very small size and largest intensity of surface absorption. Nevertheless, Au-TiO₂ despite its largest size was the second most active catalyst. The paradox can be explained by the “shadowing” effect, i.e. when the size of the nanocomposite is too small as in Pd-TiO₂, the surface may be shadowed by the presence of too many metals on it leading to a low efficiency of light absorption (Mizukoshi et al., 2007). Although a similar or even larger “shadowing” should be present on the surface of Pd/Au-TiO₂, the effect is believed to be offset by the activity of Au in the UV-visible region as reflected by the absorption intensity of the composite. Some researchers have reported that the unique role of Au in photocatalysis may also arise from its ability for surface plasmon band absorption, which enables the absorption of the nanocomposite in the same wavelength thus leading to more effective utilization of the excited electrons (Tian and Tatsuma, 2005). Finally, the work function of Au (promotion effect) is high enough to enhance the efficiency

of trapping the photo-excited electrons on the semiconductor to restrict recombination of electron-hole pairs (Mizukoshi et al., 2007).

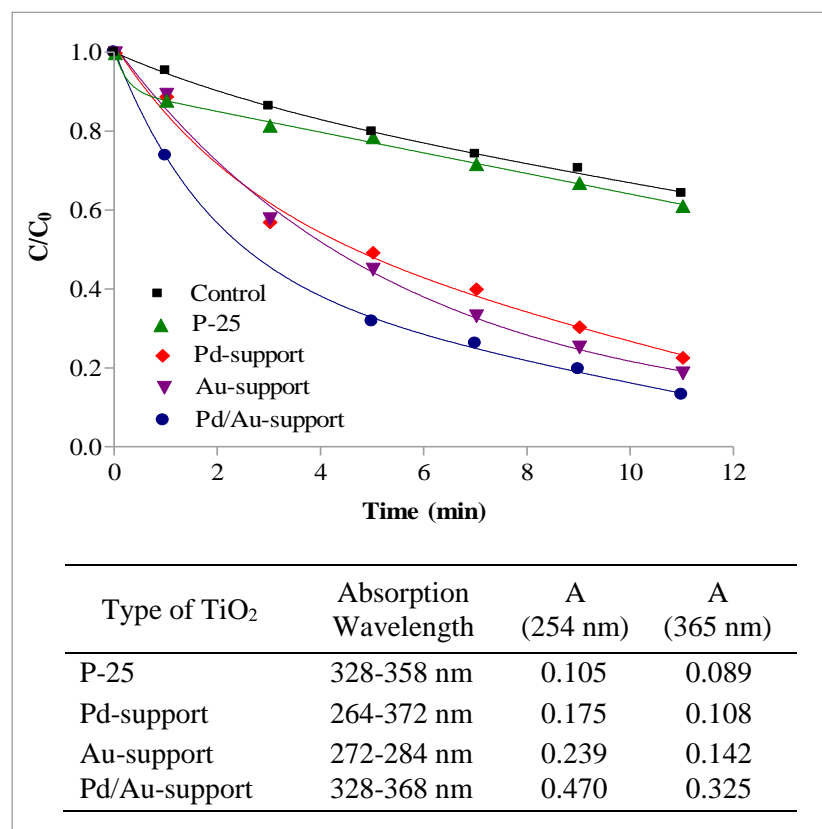


Figure 9.9. Initial rate of PCT decay by photolysis (254 nm) in the presence of 5 mg L⁻¹ of commercial and metal-supported TiO₂ (“Control” refers to UV alone). The apparent rate constants are 0.09, 0.11, 0.19, 0.21 and 0.30 min⁻¹ for Control, P-25, Pd-TiO₂, TiO₂ and Pd/Au-TiO₂, respectively.

The final test process was sono-photocatalysis, which was expected to provide a synergy via enhanced rate of surface excitation, reduced surface corrosion and increased rate of mass transfer to the solid surfaces. The synergy was estimated by Eq. 9.2 where S is the synergy index, k_{SP} , k_S , k_P and P_{sp} , P_s , P_p are the apparent reaction rate constants (min⁻¹) and the deposited energy (W cm⁻²) in sono-photolysis, sonolysis and photolysis, respectively. Owing to variations in the activity of the catalysts in the mineralization process, we also estimated the synergy in mineralization by replacing the rate constants in Eq. 9.2 with % TOC decay in 1-h.

$$S = \frac{k_{sp}P_{sp}}{k_sP_s+k_pP_p} \quad (\text{Eq. 9.2})$$

A list of 10-min reaction rate constants and 60-min mineralization efficiencies of each test process and catalyst and the corresponding synergy indices are given in Table 9.1. The results show that the highest synergy in the oxidation of PCT was obtained with Pd-TiO₂, and no synergy was present with the commercial particles, as expected. The former is the outcome of combinative effects of high work function (under UV) to reduce recombination of e⁻/h⁺ pairs (Zhou et al., 2013), and higher surface energy of the metal to enhance the adsorption of solutes.

Table 9.1. The apparent reaction rate constants of PCT decay (min⁻¹) by sonolysis, photolysis and sono-photolysis and the corresponding synergy indices. The last two columns show relative mineralization efficiency of the hybrid process for each catalyst and the corresponding synergy, respectively. Initial conditions were TiO₂ = 5 mg L⁻¹, PCT = 35 μM, pH 6.5.

Catalyst	k_s	k_p	k_{sp}	S_{ox}	(%)-Miner	S_{Miner}
P-25	0.13±0.03	0.11±0.07	0.13±0.02	1.00	26.41	1.71
Au-	0.19±0.04	0.21±0.02	0.25±0.04	1.31	56.80	2.23
Pd-	0.49±0.04	0.18±0.05	0.65±0.05	3.42	58.74	1.37
Pd/Au-	0.24±0.09	0.30±0.08	0.67±0.06	2.80	61.02	1.58

Surprisingly, the hybrid process was found synergistic with all particles for carbon mineralization and the most remarkable enhancement was that obtained with P-25. The implication is that the addition of acoustic cavitation to a suspension of pristine TiO₂ under UV-irradiation minimizes the inefficiencies of the semiconductor, such as for example rapid corrosion of the surface. Note also the high synergy obtained with Au-TiO₂ in the mineralization process that could have arisen from a variety of factors such as i) the special function of Au on TiO₂ for accelerating the decomposition of water and the production of hydrogen gas to provide additional oxidation and reduction pathways for the degradation of the byproducts (Wang et al., 2008): ii) the high work function and ability of the metal for surface plasmon band absorption, as pointed out in relation to its high performance in photolysis.

Relative performance of all test catalysts and processes (including sono-persulfate) for the ultimate degradation of PCT (mineralization) is presented in Figure 9.10 together with the observed pH changes. The lower efficiency of photolysis (than sonolysis) has been discussed in relation to incomplete decomposition of PCT (sustained competition for photons) and the effect of shadowing induced by too many metals on the surface of the catalyst. Still another factor that may be effective is the unsuitability of the stereo-chemical configuration of PCT for chelating with titanium (Pozdnyakov et al., 2014). However, it should be kept in mind that the energy deposited in solution during sonolysis was more than two orders of magnitude larger (than that in photolysis), which explains why the hybrid process was highly synergistic in the mineralization of the compound. It is also true that in sono-photolysis PCT was completely eliminated within the first 7-min, so that the two unfavorable conditions of photolysis (photon competition and stereo chemical unsuitability) disappeared during the mineralization process. The implication is that the oxidation byproducts were inactive under UVC irradiation, as supported by the literature reporting non-reactivity of the primary photolysis byproducts of PCT with UV-254 nm (Pozdnyakov et al., 2014).

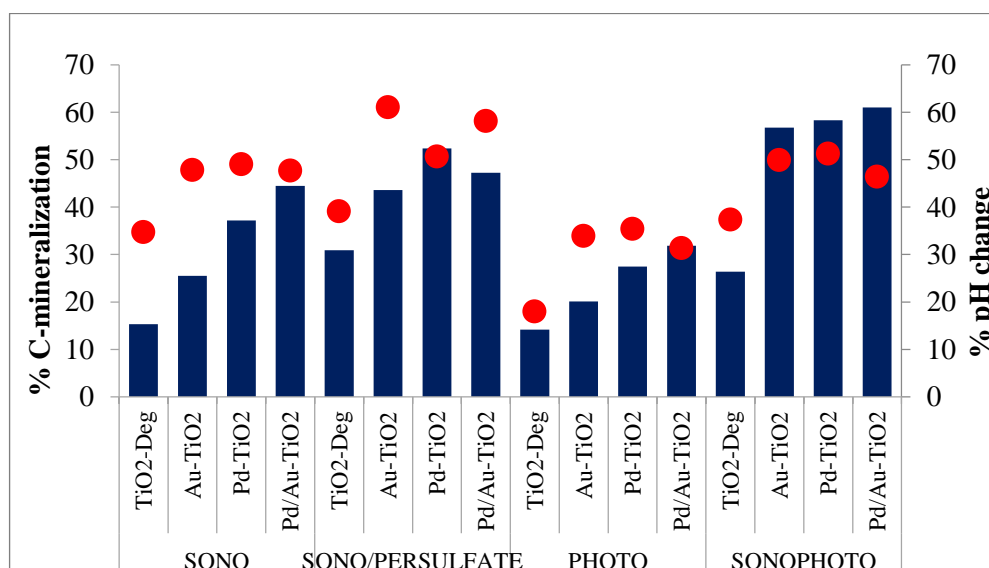


Figure 9.10. Relative mineralization of PCT ($C_0=35 \mu\text{M}$) after 60-min exposure to the test processes in the presence of commercial and immobilized TiO_2 (5 mgL^{-1}) at pH 6.5.

9.4. Conclusions

Decoration of noble metals on the surface of pristine TiO₂ is a promising method of enhancing the sonolytic and photolytic activity of the semiconductor, as demonstrated in this study via enhanced rate of PCT decomposition and mineralization in the presence of Pd-, Au- and Pd/Au-supported TiO₂ nanocomposites. The enhancement was related to the size of the particles and the enlargement in surface area that allowed more efficient adsorption of solutes and larger formation/availability of cavitation bubbles, e⁻/h⁺ pairs and oxygenated species. Different performance of the catalysts under ultrasound and UV irradiation was attributed to different absorption properties and work functions of the metals. Simultaneous application of ultrasound and UV-irradiation induced a remarkable synergy in the oxidation of PCT and degradation of the byproducts, signifying the role of cavitation in increasing the rate of mass transfer to heterogeneous interfaces, cleaning of solid surfaces, disaggregating of particles and minimizing undesired corrosion of the catalyst surface upon excitation by a light source. The study has also highlighted the role of persulfate in enhancing the efficiency of the processes and the superiority of Pd-supported particles in relation to their activity under ultrasonic irradiation and good performance in recovery and reuse.

10. ENHANCED PHOTO-DEGRADATION OF PARACETAMOL ON n-PLATINUM-MODIFIED TiO₂: THE EFFECT OF ULTRASOUND AND •OH/HOLE SCAVENGERS

The present chapter is a summary of the work published in *Chemosphere* 162 (2016) 324-332 as “Enhanced photo-degradation of paracetamol on n-platinum-modified TiO₂: the effect of ultrasound and •OH/hole scavengers”. Elimination/mineralization of paracetamol (PCT) was investigated by catalytic oxidation under ultrasound, UV and both. The catalyst was synthesized by immobilization of nPt on TiO₂ to benefit from the ability of Pt to facilitate charge transfer processes and to separate e⁻/h⁺ pairs.

10.1. Introduction

Studies on the degradation of PCT by AOPs have focused on ozonation (Andreozzi et al., 2003a; Centellas et al., 2006; Hamdi El Najjar et al., 2014), radiolysis (Szabo et al., 2012), Fenton and Fenton-like oxidation (Pupo et al., 2012; Su et al., 2013; Velichkova et al., 2013), sonolysis (Isariebel et al., 2009; Naddeo et al., 2009b; Villaroel et al., 2014) and photocatalysis with TiO₂ (Desale et al., 2013; Yang et al., 2008). The latter has been particularly popular owing to the stability and low cost of the semiconductor, which however has significant disadvantages such as a narrow UV absorption band, inability to absorb visible light, rapid corrosion of the surface and recombination of photo-generated e⁻/h⁺ pairs (Jagannathan et al., 2013; Ziylan-Yavas et al., 2015). Platinum is one of the most effective noble metals for making TiO₂ nanocomposites, because it has the highest Schottky barrier, resulting in longest e⁻/h⁺ lifetime and easier transmission of holes and electrons to the oxygen adsorbed on the catalyst surface (Li and Li, 2002; Mogyorósi et al., 2009; Rosseler et al., 2010; Salas, 2013).

There are very few studies on the decomposition of PCT by combined photolysis and sonolysis using TiO₂ or its metal-modified nanocomposites despite the well-known benefits of ultrasound such as decomposing water molecules to OH radicals, cleaning of solid surfaces, enhancing mass transfer and gas diffusion rates, and disaggregating flocs of

particles. In the presence of ultrasound, TiO₂ acts as an excellent nucleation center for the formation of excess cavity bubbles, the collapse of which releases sufficient energy to yield free radicals from entrapped gases and vapors, and to excite the semiconductor surface for excess e⁻/h⁺ pairs (Shimizu et al., 2007; Tuziuti et al., 2005).

The addition of potassium iodide during photocatalysis provides information about the reactivity of organic compounds with surface-adsorbed species, based on the fact that iodide is a strong scavenger of h_{vb}⁺ (k=1.2x10¹⁰ M⁻¹ s⁻¹) and •OH (k=1.1x10¹⁰ M⁻¹ s⁻¹) over the surface of TiO₂ (Wei and Yi-zhong, 2004; Yang et al., 2009). Another common scavenger in the bulk media is 2-propanol (k_{OH}=1.9x10⁹ M⁻¹ s⁻¹), the presence of which gives information about relative contributions of h_{vb}⁺ and •OH to the oxidation process. Moreover, the compound is highly hydrophobic so that it easily diffuses to the gas-liquid interface during sonolysis and scavenges US-generated •OH, as well.

The objective of this study was to investigate the effect of decorating the surface of commercial TiO₂ powders (P25-Evonik) with nanoparticles of platinum to enhance the decomposition of the emerging pollutant-paracetamol by sonocatalysis, photocatalysis and sono-photocatalysis. The study further aimed to assess the mineralization of the compound, the major reaction sites and the relative significance of •OH radicals and photo-generated holes on the overall degradation process.

10.2. Materials and Methods

Paracetamol sulfate potassium was used to make a standard solution. Test samples were prepared using commercially available pills (500 mg), as described in Chapter 9. All analytical grade reagents were obtained from Merck (Istanbul), powder TiO₂ (Aeroxide P25) and polyethylene-glycol-400 (PEG) were obtained from Evonik, Istanbul and Eksoy Kimya, Istanbul, respectively.

Preparation of the Catalysts. Pt-TiO₂ nanocomposites were synthesized sonolytically using three different Pt concentrations to test the effect of Pt-loading on the activity of the catalyst as described in Section 3.3. The particles were labeled as P1, P2 and P4, respectively referring to the use of 1 mM, 2 mM and 4 mM H₂PtCl₂. Based on their tendency to

agglomerate, the nanocomposites were exposed to 5-min sonication (20 kHz) prior to catalytic experiments with them.

10.2.1. Procedure

Adsorption of PCT on the Nanocomposites. Batch adsorption tests were carried out with 5 mg L⁻¹ of P1, P2 and P4 for 3-hours at pH 6.5 to determine the tendency of the compound to adsorb on the composites and the impact of Pt-loading on the degree of adsorption.

Sonolysis and Photolysis. The sono-reactor (R4) was spiked with air-saturated PCT (to promote cavitation) and adjusted to the desired pH. The reactor contents were sonicated for 1-h and samples were collected meanwhile for the analysis of PCT, TOC, H₂O₂, nitrogen species and UV absorption. The operating conditions (frequency, power) were selected on the basis of maximum rate of PCT degradation, TOC decay, nitrogen mineralization and H₂O₂ formation. PCT was exposed to 1-h photolysis under UVC-irradiation by a low-pressure mercury lamp with a maximum emission at 254 nm ($I=107.4 \text{ W cm}^{-2}$).

Sonocatalysis and Photocatalysis. Four equal concentrations of PCT were mixed successively with powder TiO₂ (Aeroxide, Evonik), P1, P2 and P4 and sonicated for 1-h at previously optimized conditions to select the most effective catalyst. The tests were repeated in the photo-reactor using the light source specified above.

Sono-photocatalysis. Experiments were repeated with UV- and ultrasonic irradiation (572 kHz-optimum frequency) together. In another run, raw samples of PCT were spiked separately with potassium iodide (1.4 mM, 8.75 mM) and 2-propanol (8.75 mM) to shed light on the primary reaction sites (e.g. the bulk liquid, gas-liquid/solid-liquid interfaces, or the solid surface) and the primary oxidizing species (e.g. OH radicals, $h_{\nu b}^+$).

10.2.2. Analytical

Samples were collected at short intervals during 1-h reaction time to analyze the concentration of PCT, TOC, NO₃⁻/NO₂, H₂O₂ and Pt that may have leached out from the surface of the catalysts. PCT was analyzed by HPLC and spectrophotometrically to shed

light on the formation of hydroquinone and benzoquinone as the major oxidation byproducts of the compound (Moctezuma et al., 2012). Hydroquinone (HQ) and 1,4- benzoquinone (BQ) was monitored spectrophotometrically which were readjusted for emission at 225 nm and 247 nm, respectively. The structure, morphology and size of Pt-decorated TiO₂ were analyzed by environmental scanning electron microscope (ESEM).

10.3. Results and Discussion

10.3.1. Characterization of the Catalysts

SEM analysis of catalyst surfaces for chemical layer characterization and homogeneity showed that nanoparticles of Pt were uniformly distributed over the surface of TiO₂ when they remained discrete; but the uniformity was spoiled when they agglomerated whereas the unmodified TiO₂ particle agglomerated severely (Appendix B, Figure B10.1). This is why nanocomposites were pretreated with an ultrasonic probe prior to catalytic experiments to minimize the effect of particle growth. The images obtained for P1, P2 and P4 are presented in Figure 10.1 (a-c). It was observed that there were not significant change in shape or morphology of catalysts with Pt-loading and they were irregular in shape. The last image at the bottom (d) shows the structure of a spent P4 sample, i.e. the surface of P4-TiO₂ after 60-min use in sono-photocatalysis of PCT. The image signifies the stability of the catalyst, because there are no obvious damages on the surface and some of the flocs observed in the raw catalyst (c) have disappeared with a distinct improvement in the uniformity of particle distribution. Analysis of Pt in solution during sono-photocatalysis also confirmed the stability, as only a trace concentration was detected, indicating that metal leaching from the catalyst surface was insignificant. Note also that the effective particle size in the fresh and spent catalysts was less than 10 nm.

10.3.2. Control Experiments

Adsorption. Batch adsorption tests with PCT and the nanocomposites showed that the time to reach equilibrium changed with the quantity of platinum loaded, as 60-min with P4, 90-min with P2 and 120-min with P1. The data as presented in Figure 10.2 show that the

equilibrium maximum was $4.11 \mu\text{M}$, corresponding to 9.44% PCT adsorption on P4 after 60-min contact.

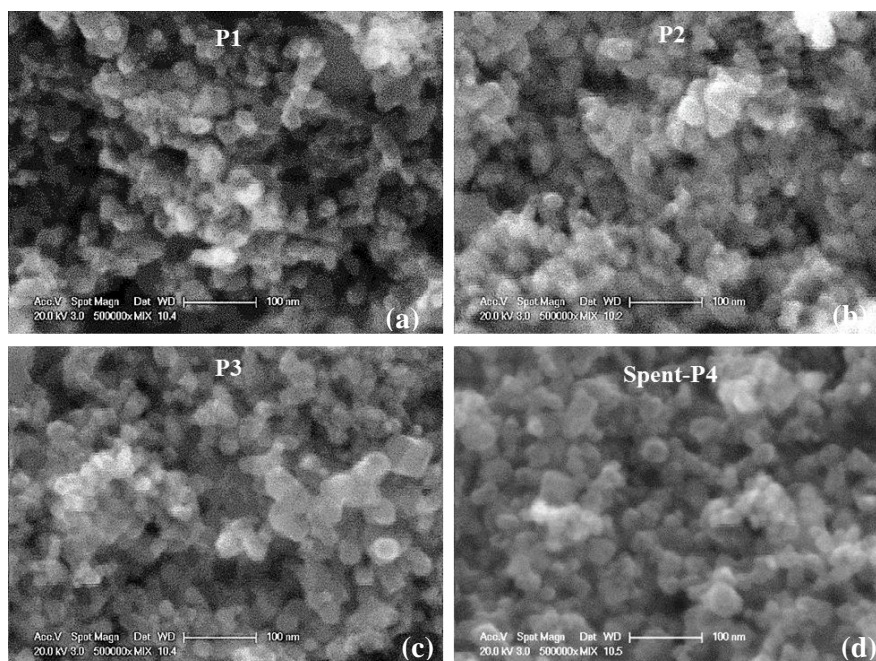


Figure 10.1. ESEM images (500000x) of P1-TiO₂, P2-TiO₂, P4-TiO₂ and spent P4-TiO₂.

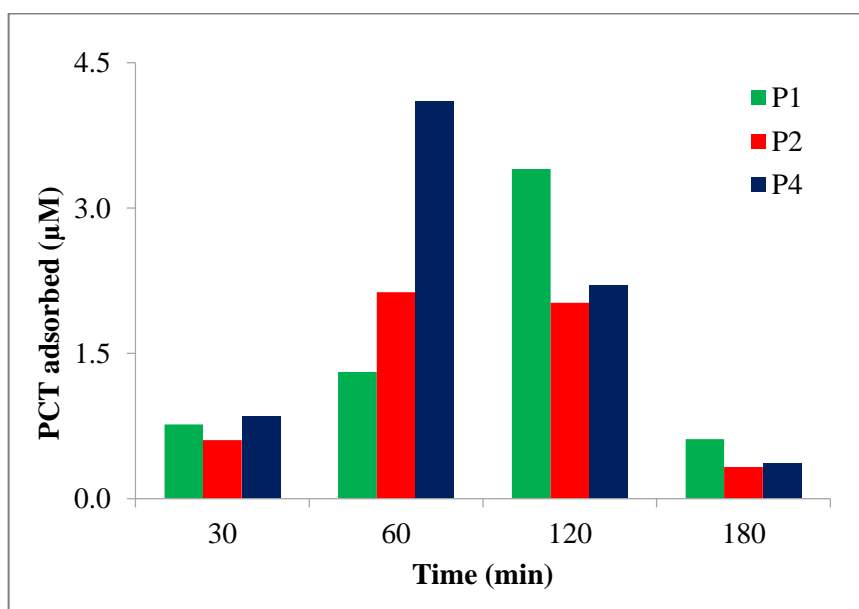


Figure 10.2. Sorption of PCT ($40 \mu\text{M}$) on 5 mg L^{-1} P1, P2 and P4 at pH 6.5 during 3-h shaking.

Sonolysis. PCT was sonicated at three different frequencies to select the most effective one. The power deposited in the reactor in each run was estimated by calorimetric analysis as 0.184 W L^{-1} , 0.188 W L^{-1} and 0.146 W L^{-1} , respectively for 572, 856 kHz and 1130 kHz. Lower power deposition at 1130 kHz implies that more of the applied energy is lost as heat, to be explained by the threshold concept, i.e. the existence of a critical frequency above which a negative pressure is produced by the rarefaction cycle of the sound wave (less cavity initiation, lower collapse intensity) and the frequency of compression cycles is thus larger than that required for effective bubble collapse (Thompson and Doraiswamy, 1999).

An additional tool for selecting the best frequency was monitoring of the H_2O_2 concentration during sonolysis of ultrapure water, based on the fact that under high frequency ultrasound the hydroxyl radicals generated by water pyrolysis upon bubble collapse readily combine to form H_2O_2 (Ciawi et al., 2006; Hua and Hoffmann, 1997; Sochard et al., 1997).

The rate of peroxide formation during 15-min sonication of pure water is presented in Figure 10.3. The data show H_2O_2 accumulated most rapidly at 572 kHz and least rapidly at 1130 kHz irradiation. Hence, as a result of higher energy input and faster $\bullet\text{OH}$ generation, we selected 572 kHz as the operating frequency for the rest of the experiments.

Sonication of PCT for 1-h at the selected optimum frequency showed that 90% of the compound decomposed via a pseudo-first order rate ($k'=2.34 \text{ s}^{-1}$) and the reaction was accompanied with 15% TOC decay. Relative fractions of C-mineralization at all test frequencies and the rate of H_2O_2 formation at the optimum are presented in Figure 10.4. The fact that the concentration of H_2O_2 in the bulk solution is the same as in pure water implies that PCT was decomposed in the proximities of the bubbles or at the bubble-liquid interface, where the concentration of uncombined $\bullet\text{OH}$ is very large (Ince et al., 2009).

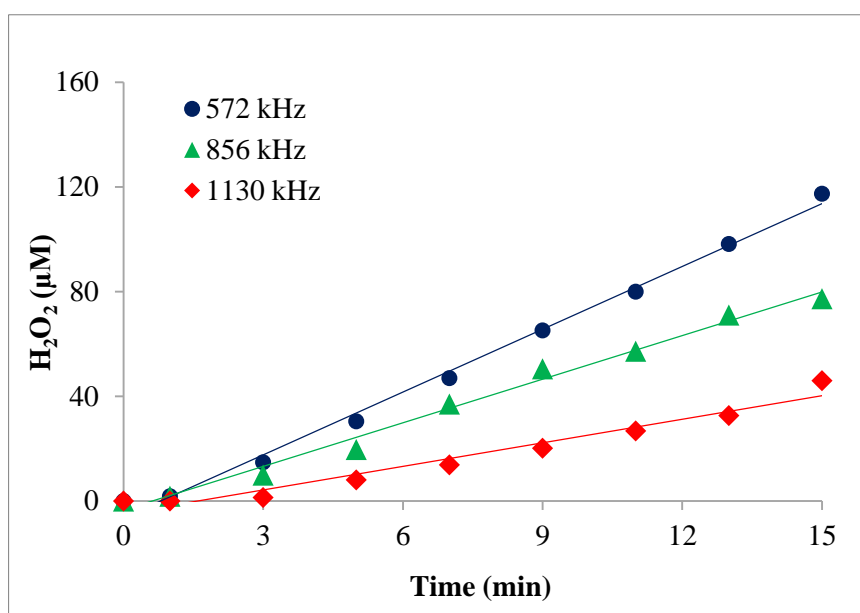


Figure 10.3. Relative rate of H₂O₂ formation during 15-min sonication of ultrapure water with 572 kHz, 856 kHz and 1130 kHz at non-buffered natural pH 6.5.

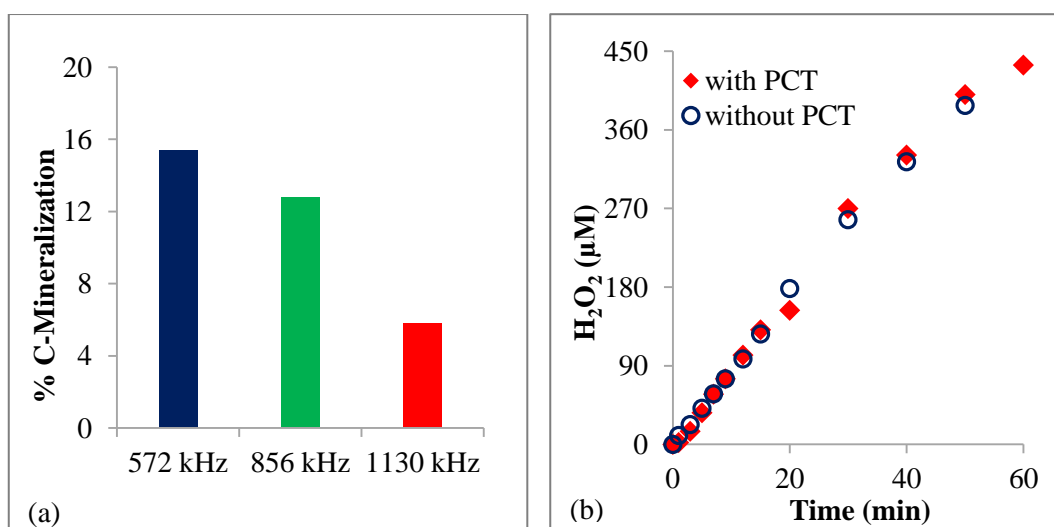


Figure 10.4. The impact of frequency on C-mineralization (a) and the relative rate of H₂O₂ formation by sonolysis of pure water and the sample solution at 572 kHz (b). Initial conditions were C₀=40 μM, pH=6.5.

Photolysis. In our previous work reporting the elimination of PCT with Pd- and Au-supported TiO₂, we stated that UVC irradiation ($\lambda_{\max} = 254$ nm) was effective due to the double action enabling direct photolysis of the compound and surface excitation of the catalysts. We found that PCT was appreciably decomposed by photolysis, but with no carbon mineralization; while UV and ultrasound (US) together provided nearly 35 % mineralization

of the compound. A summary of the performances of control experiments for the decomposition and mineralization of PCT is presented in Figure 10.5.

10.3.3. Catalytic Experiments with US, UV and TiO₂

Sonocatalysis. During the last decade a number of researchers have shown that the sonoluminescence produced during cavitation collapse is capable of exciting surfaces of metallic semiconductors through their band gap energies, leading to the generation of e⁻/h⁺ pairs and oxidative destruction of organic compounds (Sathishkumar et al., 2016). In the present study however, we observed no difference between the rate of PCT decomposition by sonication alone (Control) and sonication with TiO₂, P1 and P2 ($k' = 0.039, 0.040, 0.041$ and 0.044 min^{-1} , respectively), implying inability of ultrasound for exciting the catalyst surfaces. The data are presented in Figure 10.6.

The result can be explained by the ineffective collapse conditions of transient cavitation, and thus insufficient sonoluminescence energy. On the other hand, the process was considerably more effective in the presence of P4 ($k' = 0.061 \text{ min}^{-1}$), obviously due to its much higher Pt content. Hence, at sufficiently high Pt-loading there were too many nanoparticles (with massive areas) at the semiconductor surface and they served as excess nucleation sites for cavitation bubbles, leading to the enhancement of the energy of sonoluminescence. Moreover, the large Schottky barriers at the metal-TiO₂ junction of P4 can facilitate the separation of US-generated carriers and the transfer of electrons to the surface. Note also that the rate of reaction in the presence of P4 was pseudo-first order during the first 10-min, and became zero-order thereafter, typical of adsorption-mediated oxidation reactions (Ince et al., 2009).

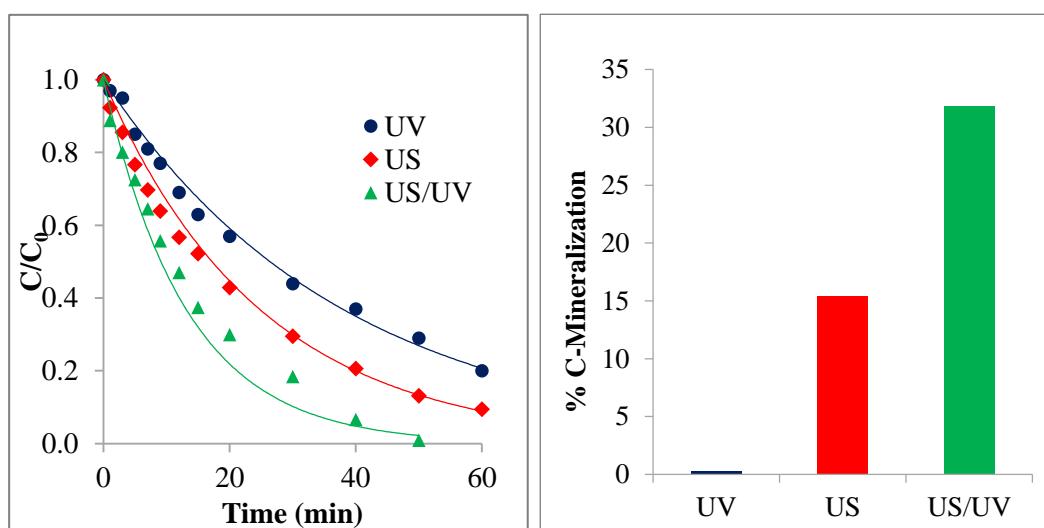


Figure 10.5. Relative effectiveness of “control” processes (US, UV, US/UV) for the decomposition and mineralization of PCT. Initial conditions were $C_0 = 40 \mu\text{M}$, $f = 572 \text{ kHz}$, $P_{\text{US}} = 0.19 \text{ W L}^{-1}$, $\text{pH} = 6.5$, $I_{\text{UV}} = 0.104 \text{ W cm}^{-2}$. The pseudo-first order reaction rate constants were 0.063, 0.039 and 0.030 min^{-1} for US/UV, US and UV, respectively.

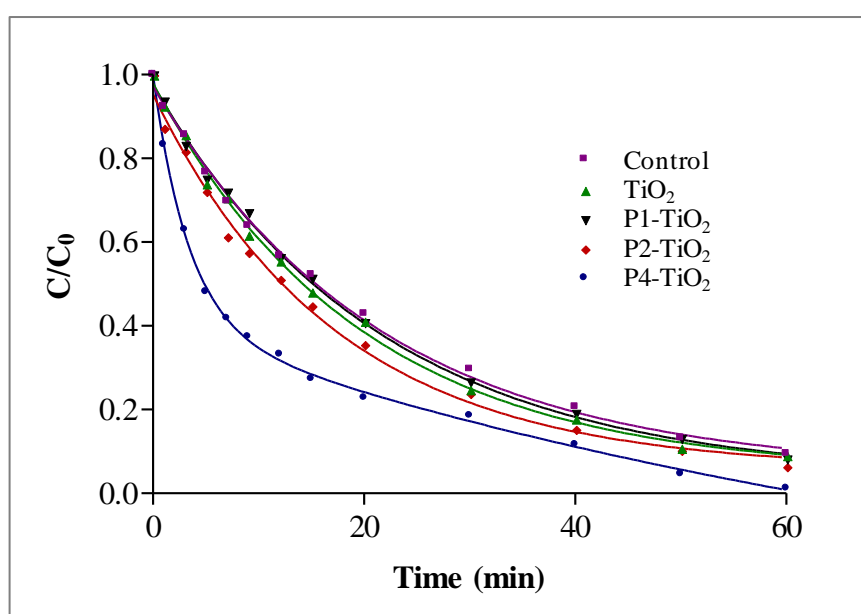


Figure 10.6. Sonocatalytic decay of PCT in the presence of TiO_2 , P1, P2 and P4. Initial conditions were: $C_0 = 40 \mu\text{M}$, $P = 0.19 \text{ W L}^{-1}$, $f = 572 \text{ kHz}$, catalyst dose = 5 mg L^{-1} , $\text{pH} = 6.5$.

“Control” refers to ultrasound alone.

Photocatalysis. Photocatalytic decomposition of PCT with P2 and P4 was found to proceed faster than that with P1 and TiO_2 during the first 5-7 min, but slowed down thereafter. The initial apparent and pseudo-first order rate constants estimated for $t = 7$ and 60 min,

respectively are listed in Table 11.1. The data show that at initial contact, the reactions were fast and the rate increased with the amount of Pt-loading on the surface of the semiconductor, while at prolonged contact the effect was reversed. The implication is that the reactive sites on P2 and P4 were rapidly obstructed most likely due to the growth and agglomeration of the nanoparticles, as also reported by others in the literature (Yi et al., 2008). Hence, the basic functions of the co-catalyst (as an e-trapper) were weakened by its absorption and scattering of UV irradiation (Rothenberger et al., 1985). Moreover, the presence of larger particles leads to a “shadow” on the surface of the semiconductor to further reduce its UV absorption and catalytic activity.

Nevertheless, the nanocomposites were slightly better than TiO_2 for carbon mineralization, the degree of which decreased again with increasing Pt-loading on the surface. Profiles of decomposition and mineralization of PCT during and after 60-min photocatalysis are presented in Figure 10.7. Higher efficiency of the nanocomposites for mineralization is due to reduced photon competition upon decomposition of the parent compound, higher stability than TiO_2 against corrosion and the reactivity of Pt with some of the oxidation byproducts, as it is very effective in ring reduction, along with hydrogenation of phenolic compounds (William. et al. 1956).

Table 10.1. Estimated reaction rate constants and the efficiency of photocatalysis for decomposing PCT ($C_0=40 \mu\text{M}$) and its oxidation byproducts (k_{ap} and k are the initial and pseudo-first order rate constants for $t=7$ min and 60 min, respectively; “% decay” refers to 60-min reaction).

Catalyst	k_{ap} (min^{-1})	k (min^{-1})	PCT decay (%)	TOC decay (%)
TiO_2	-0.019	-0.028	84	34
P1- TiO_2	-0.016	-0.024	81	38
P2- TiO_2	-0.027	-0.014	69	38
P4- TiO_2	-0.036	-0.017	62	37

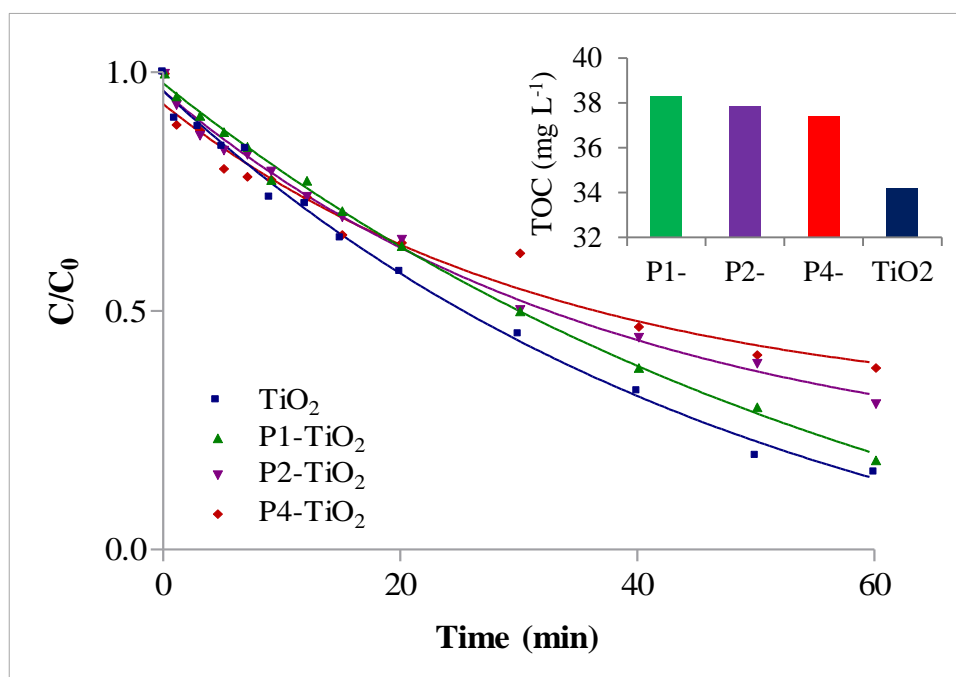
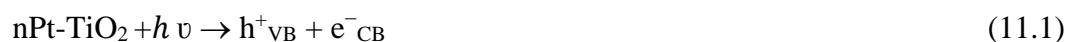


Figure 10.7. Photocatalytic elimination and mineralization of PCT ($C_0=40 \mu\text{M}$) in the presence of 5 mg L^{-1} TiO_2 and Pt/ TiO_2 containing 1 mM, 2 mM and 4 mM Pt (P1, P2, P4), respectively.

Sono-photocatalysis. As discussed in the previous sections, the presence of platinum nanoparticles on TiO_2 increases the surface barrier in proportion to the amount of Pt loaded, and this in turn reduces the space charge for more efficient separation of e^-/h^+ pairs (Ahmed et al., 2014). As such, electrons from the conduction band of TiO_2 are easily transferred to the conduction band of Pt, where they are trapped and prevented from recombining with the holes. A simplified reaction scheme to represent this phenomenon is given in the following (Hussein and Rudham, 1984; Vijayan et al., 2010):



Application of photolysis together with acoustic cavitation was expected to provide a synergy via the unique properties of ultrasound for cleaning and polishing of solid surfaces, for separating agglomerated particles, for accelerating the diffusion and mass transfer of solutes (to solid surfaces and their interfaces), and for generating excess reactive species that

enhance the rate of redox reactions over the catalyst surface (Ziylan-Yavas et al., 2015). We found that PCT decomposition without catalysts was slower ($k=0.063 \text{ min}^{-1}$) than that with catalysts; there was no difference between the activities of TiO_2 , P1 and P2 ($k=0.074 \text{ min}^{-1}$), and the rate was a maximum in the presence of P4 ($k=0.108 \text{ min}^{-1}$). Mineralization of organic carbon also followed the same pattern with 32%, 40%, 42% and 48% TOC decay in control (US/UV), TiO_2 , P1, P2 and P4, respectively. In addition to the above factors, the synergy may also be due to homogenization of the primary light effect leading to improved reaction rates and yields (Xu et al., 2009). The analysis of peroxide throughout the reactions showed that the net rate of production was slightly smaller than that observed in sonocatalysis (due to photolysis), but it was practically the same in all samples. As such, we concluded that the main reaction sites were the heterogeneous surfaces and/or interfaces of gas-liquid, gas-solid and solid-liquid biphasic systems. The data are presented in Figure 10.8.

10.3.4. The Effect of $\bullet\text{OH}/h^+_{\text{vb}}$ Scavengers

In sono-photocatalytic experiments, while e_{cb}^- was consumed by oxygen due to continuous air purging during experiments as well as Pt- nanoparticles over TiO_2 , its reaction product, superoxide radical anions ($\text{O}_2^{\bullet-}$), could directly contribute to paracetamol degradation through reaction of oxygen with O_2 to produce $\text{O}_2^{\bullet-}$ (Yang et al., 2009). In addition, $\text{O}_2^{\bullet-}$ can undergo reactions to generate H_2O_2 and HO_2^{\bullet} , which then could oxidize paracetamol (Yang et al., 2009). Thus, in the literature, it was reported that oxygen in air played multiple roles in oxidation of paracetamol in UV photocatalysis by acting as an e_{cb}^- scavenger to enhance reactants directly ($\text{O}_2^{\bullet-}$) and indirectly (HO_2^{\bullet} , H_2O_2 , h^+_{vb} , and $\bullet\text{OH}$) (Yang et al., 2009). It was assumed that suppressing e_{cb}^- via O_2 addition and using modified nanocomposite the concentrations of the five reactants, h^+_{vb} , $\text{O}_2^{\bullet-}$, HO_2^{\bullet} , H_2O_2 , and $\bullet\text{OH}$ were elevated.

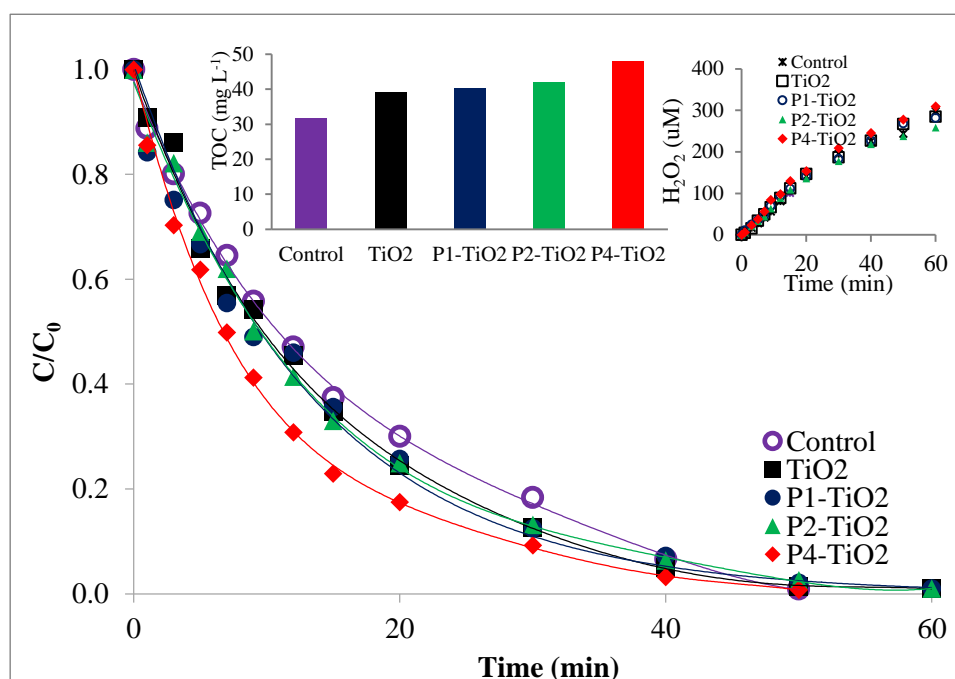


Figure 10.8. Sono-photocatalytic elimination and mineralization of PCT in the presence of pristine and Pt-loaded TiO₂. The insets at the top show relative TOC decay after 1-h and the rate of H₂O₂ production during reactions.

The experiments were repeated in the presence of 2-propanol (PR) and potassium iodide (KI) to shed light on the reaction site and the reactive species. It was found that the presence of PR led to a significant inhibition in the rate of decomposition and mineralization of PCT via the competition for •OH in the bulk medium. On the other hand, the addition of the same quantity of KI, which is two times more reactive with •OH led to an unexpected enhancement in the rate of PCT decay. To find out if the improvement was dependent on the concentration of the reagent, we repeated the experiments with lower and higher concentrations and found that the reaction was further promoted at a properly selected lower concentration. The data as presented in Figure 10.9 depicts that PCT was completely eliminated after 15-min reaction in the presence of 1.4 mM KI (KI:PCT molar ratio=35), 30-min in that of 8.75 mM KI and 60-min in the absence of KI (Control). The rate constants given on the top right corner of the figure show that the reaction was 173 % and 151 % faster (than control) in the presence of low and high doses of KI, respectively and 87 % slower in that of 2-propanol.

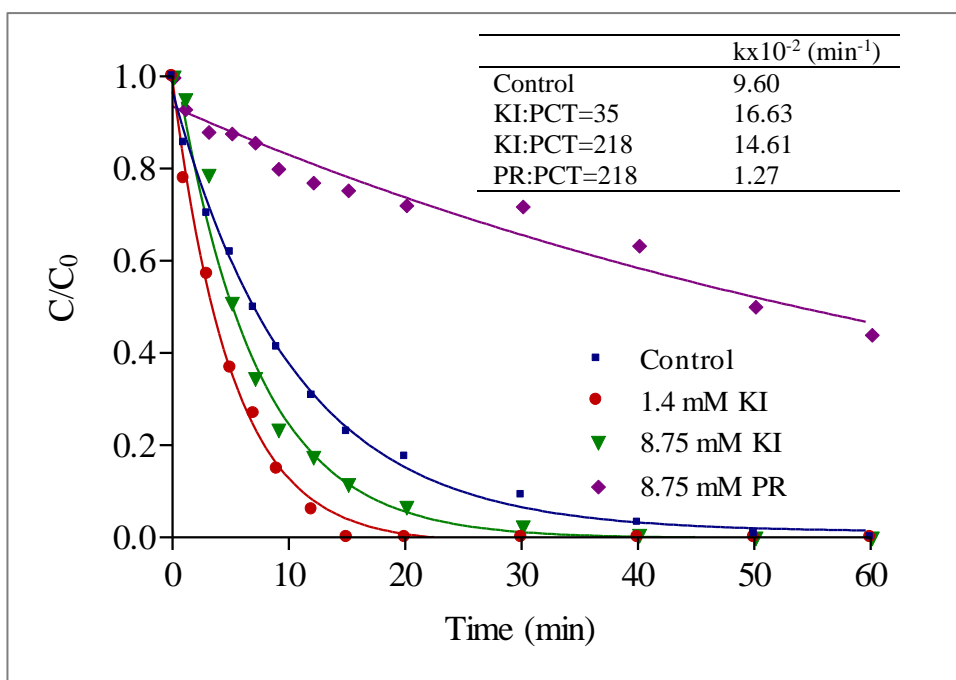


Figure 10.9. Relative rate of PCT elimination during sono-photocatalysis with Pt-TiO₂ (P4) in the presence of 2-propanol and potassium iodide. “Control” refers to the absence of scavengers.

A severe rate inhibition in the presence of 2-propanol indicates that the decomposition of PCT was highly $\bullet\text{OH}$ -dependent and proceeded mostly on the surface of the catalyst. The enhancement in the presence I⁻, which is not only a stronger scavenger of $\bullet\text{OH}$ but also of h^{+}_{vb} over the catalyst surface signifies the presence of other reactive species in solution and at the solid surface. The hypothesis is confirmed in the literature reporting the production of $\bullet\text{O}_2\text{H}$, $\bullet\text{OH}$, $\bullet\text{O}_2^{-}$ and O during sonolysis of iodide solutions (Hart and Henglein, 1985). Since iodide ion moves to the surface at $\text{pH} < \text{pK}_{\text{z}}$ of the semiconductor, the formation of these species also occurs at the catalyst surface. Peroxyl radicals ($\bullet\text{O}_2\text{H}$) are not reactive with I⁻ so that they are readily converted H₂O₂, which upon photolysis and direct reduction are transformed to $\bullet\text{OH}$. Hence, the enhancement in the rate of PCT decay at the low dosage of KI is due to compensation of the scavenging effect by the production of excess reactive species on the catalyst surface. This is justified in the literature, where a significant increase in $\bullet\text{OH}$ production was reported during photocatalytic decomposition of phenol in the presence of excess H₂O₂ (Hirakawa and Nosaka, 2002). Less significantly, the superoxide radicals ($\bullet\text{O}_2^{-}$) that form by sonolysis may have also contributed to the decomposition reaction since they are also non-reactive with I⁻. Moreover, the rate enhancement is a good indication of the insignificance of h^{+}_{vb} for the decomposition of PCT, as also reported in the

literature (Yang et al., 2009). Note that the degree of rate enhancement was considerably lower at the higher dose of I^- as a result of increased competition for $\bullet OH$.

We found that both scavengers hindered the mineralization reaction, as percentage of TOC decay in the presence of 2-propanol and KI were 0 %, 36 % (low dosage) and 1.3 % (high dosage), respectively; as opposed to 48 % in their absence. The data are presented in Figure 10.10 together with relative PCT decay to depict the different impacts of the scavenging agents on the elimination and mineralization reactions. Note that the data for PCT decay refers to 15-min reaction (because PCT was completely decomposed within 15-min), while those for TOC correspond to 60-min reaction.

It has been reported in the literature that the reaction byproducts of photocatalytic oxidation of PCT on TiO_2 are aromatics, carboxylic acids, nitrogen-containing straight chains and inorganics as ammonia and nitrate (Yang et al., 2009). The aromatics as the major products comprise of hydroquinone (HQ), benzoquinone (BQ), p-nitrophenol and p-aminophenol, which form subsequently upon $\bullet OH$ addition to the aromatic ring (Duprez et al., 1996; Moctezuma et al., 2012; Scheck, 1995). Yang et al (2009) found that relative to other intermediates, the three aromatic compounds, N-(3,4-dihydroxyphenyl)acetamide, N-(2,4-dihydroxyphenyl) acetamide, and hydroquinone, showed a higher concentration during photocatalytic oxidation of paracetamol. Early presence of hydroquinone was expected as it comprises the basic structure of paracetamol indicating that paracetamol undergoes photocatalytic oxidation initially through $\bullet OH$ addition onto the aromatic ring at ortho, meta, and para positions with respect to the -OH group of paracetamol (Yang et al., 2009). Hence, hydroxylation of ($\bullet OH$ reaction with) paracetamol can contribute to the significant concentrations and early presence of hydroquinone indicating that $\bullet OH$ addition may prefer the ortho position with respect to the -OH group of paracetamol (Yang et al., 2009). This may be driven by the nearby -OH, which serves as a stronger electron-donor group than the opposite-NHCOCH₃ in the benzene ring of paracetamol, making the ortho position more susceptible to attack by electrophilic $\bullet OH$ (Yang et al., 2009). Furthermore, cleavage of aromatic rings followed by further oxidation can yield the carboxylic acids (Yang et al., 2009). Following successive $\bullet OH$ oxidation of hydroquinone in aqueous environment takes place to produce p-benzoquinone, which is fairly unstable and tends to undergo ring rupture followed by further oxidation forming butenedioic acid (Duprez et al., 1996; Scheck, 1995).

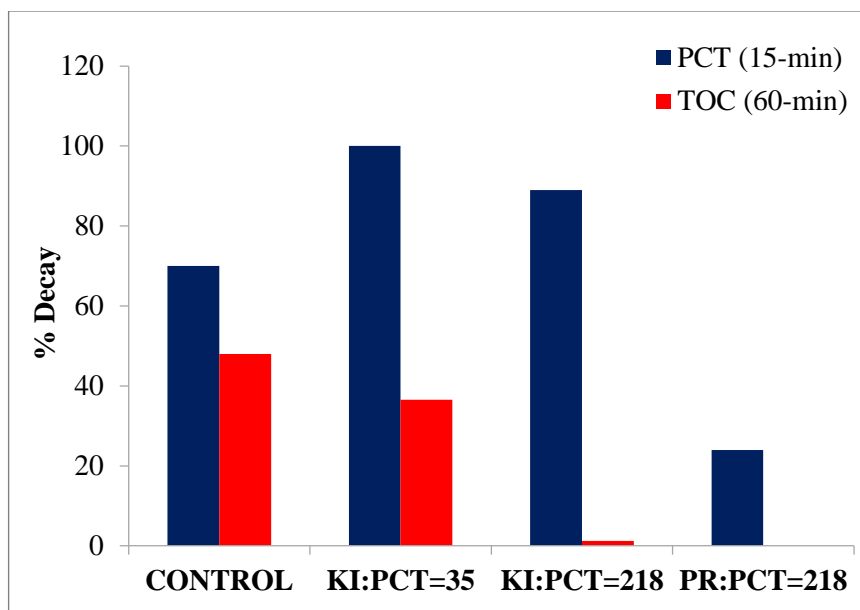


Figure 10.10. The impact of PR and two different doses of KI on the decomposition and carbon mineralization of PCT by sono-photocatalysis with P4. Control refers to the absence of scavengers.

As such, we monitored the evolution of HQ and BQ in the absence and presence of I^- to understand how and why the scavenger inhibited the mineralization process. We found that the formation of HQ was highly related to the abundance of h^+_{vb} on the surface of the catalyst, because there was no evidence of its formation in KI-added solutions, where they are rapidly consumed by I^- . The data as presented in Table 10.2 show that regardless of the catalyst structure, there is no HQ formation in I^- -spiked solutions, but a distinct evidence of BQ. As such, it is evident that the mineralization process was dependent largely on the formation of hydroquinone, because the efficiency was very poor despite the evidence of benzoquinone. The importance of HQ in the mineralization pathway was confirmed by the high efficiency of TOC decay when there was no I^- (47%) and when the amount of HQ was significantly high. It seems that in the iodide solution, the inhibition of HQ formation is not only due to the limited availability of h^+_{vb} on the catalyst surface, but also to the reductive decomposition of the compound at the semiconductor surface.

We further analyzed the concentration of nitrate in the samples to assess the degree of N-mineralization, and found that despite the poor efficiency of C-mineralization in the

presence of KI, 19% of organic N-was converted to NO_3^- -N during catalysis with P4 (as opposed to 100% conversion in its absence). However, there was no evidence of BQ formation throughout the reaction time, implying the contributions of other reaction pathways to the overall degradation process, such as those occurring on the active sites of n-Pt surfaces.

Table 10.2. Estimated concentrations of HQ and BQ, and the corresponding mineralization efficiency of the sonophoto process in the presence and absence of 8.75 mM KI and PR.

Catalyst/scavenger	HQ (μM)	BQ (μM)	% TOC decay	% N- decay
TiO ₂ -no scavenger	16	-	39.2	56.5
TiO ₂ -KI	-	1.18	0.12	na
P4 - no scavenger	20	-	47.9	100
P4-KI	-	1.81	1.26	19
P4-PR	-	-	< 1	2.3

10.4. Conclusions

Sonolytic immobilization of n-platinum on pristine TiO₂ is a viable method of enhancing the activity of the semiconductor under ultrasonic and UV-irradiation, as demonstrated by increased rate of PCT destruction by sono-, photo- and sono-photocatalysis in the presence of Pt-modified TiO₂. The effectiveness of the nanocomposite arises from its massive surface area promoting the formation of excess cavitation bubbles and the production of reactive oxygenated species on its activated reaction sites. It was found that increasing the Pt-loading enhanced the activity of the catalyst under ultrasonic irradiation (via production of excessive bubbles and $\bullet\text{OH}$), but reduced it under UV (via the growth of particle size upon agglomeration and the shadow they produced on the surface). Application of UV and US simultaneously was highly effective via the synergy of the latter for perfect mixing, for disaggregation of particle flocks and for polishing solid surfaces to prevent corrosion. Last but not least, the structure of P4-the nanocomposite with the highest Pt-loading was not deteriorated upon use, signifying its stability and easy recovery.

The study has also highlighted the role of $\bullet\text{OH}$ and h^+_{vb} , emphasizing $\bullet\text{OH}$ -dependence of decomposition and $\bullet\text{OH} / h^+_{\text{vb}}$ dependence of mineralization reactions. It was also demonstrated that the decay of PCT by sono-photocatalysis could be accelerated with the

addition of Γ , which is a strong scavenger of both $\bullet\text{OH}$ and h^+_{vb} , provided that it is not in excess so that the scavenging effect is compensated by the production of excess $\bullet\text{OH}$ during sonolysis of iodide solutions.

11. CATALYTIC OZONATION OF PARACETAMOL USING COMMERCIAL AND Pt-SUPPORTED NANOCOMPOSITES OF Al_2O_3 : THE IMPACT OF ULTRASOUND

The present chapter is a summary of the work published in *Ultrasonics Sonochemistry* (<http://dx.doi.org/10.1016/j.ultsonch.2017.02.017>) as “Catalytic ozonation of paracetamol using commercial and Pt-supported nanocomposites of Al_2O_3 : the impact of ultrasound”. This study is the assessment of commercial $\gamma\text{-Al}_2\text{O}_3$ and its sonolytically modified nanocomposite in catalytic ozonation of paracetamol (PCT), which is an emerging water contaminant and a highly reactive compound with ozone.

11.1. Introduction

Catalytic ozonation has lately emerged as a viable alternative to single ozonation, owing to benefits such as enhanced carbon mineralization, reduced selectivity and a wider range of pH applications. The challenge of the process lies on the selection and modification of the catalyst to assure sorption and decomposition of ozone on the surface. Still another challenge of catalytic ozonation processes is sustaining the decomposition of ozone to assure initiation, promotion and maintenance of radical chain reactions. Alumina (Al_2O_3) is a porous material that is capable of generating free radicals during ozonation via the interaction of hydroxyl groups on its surface with the adsorbed ozone (Vittenet et al., 2014). The phenomenon is based on the rapid adsorption and decomposition of ozone on the surface of the catalyst to yield ROS such as $\bullet\text{OH}$, superoxide anion radicals ($\bullet\text{O}_2^-/\bullet\text{O}_3^-$) and H_2O_2 (Ernst et al., 2004; Ikhlaq et al., 2013; Qi et al., 2013; Vittenet et al., 2014). Moreover, alumina is recognized with its stability against poisoning by ozone decomposition products, as the activity of the surface was found to be preserved even after several runs (Qi et al., 2013). Nevertheless, published research on catalytic ozonation of organic compounds with Al_2O_3 are controversial in that some have reported the high efficacy of the process, particularly at pH around the zero point charge of the metal oxide (Pocostales et al. 2011; Qi et al. 2013; Ikhlaq et al. 2013), while others claimed that the catalyst lacks activity and ineffective in decomposing ozone (Kasprzyk-Hordern et al., 2004; Kasprzyk-Hordern and Nawrocki, 2003;

Kasprzyk and Nawrocki, 2002; Lin et al., 2002; Pines and Reckhow, 2003). One common feature of all these studies is that alumina is more effective in mineralization of organic compounds and the activity of the catalyst is related to the strength of adsorption, which is inversely proportional to the hydrophilic nature of the pollutants (Ikhlaq et al., 2015).

There are also some studies reporting improved activity of alumina upon decoration of the surface with nano-sized noble metals (e.g. Pt, Ru, Rh, Pd, Cu, Ag) to increase the surface area and the number of active sites on it, while providing an additional redox medium via the presence of the co-catalyst (Lin et al., 2002). The aim of this study was to investigate the degradability of paracetamol by catalytic ozonation with commercial (γ) and surface-modified alumina, the latter obtained by decoration of the surface with nanoparticles of platinum. The emphasis of the study was on the operation parameters, the role of $\bullet\text{OH}$, and the impact of ultrasonic irradiation that was expected to improve the process efficiency via enhanced rate of mass transfer and excess $\bullet\text{OH}$ production.

11.2. Materials and Methods

Paracetamol sulfate potassium salt was used for making a standard solution of the compound. Sample solutions were prepared by dissolving commercial tablet pills of paracetamol in ultrapure water. The physical/environmental properties of the commercial product and the procedure for sample preparation are as given in Section 3.1.1. All reagent grade reagents were obtained from Merck (Istanbul), H_2PtCl_2 , γ -aluminum oxide- Al_2O_3 and polyethylene-glycol monostearate (PEG-MS) from Wako (Japan).

Preparation of the Catalysts. Platinum-supported nanocomposites of alumina ($\text{Pt-Al}_2\text{O}_3$) were prepared sonolytically following the procedure described in Section 3.3. Prior to catalytic experiments the nanocomposite was added to 20 mL water and pretreated by 20 kHz ultrasonic irradiation for 3-min to prevent floc formation or to disaggregate coagulated particles.

Adsorption Tests. Batch adsorption tests were carried out in a Julabo SW22 shaker with 2.5, 5 and 10 mg L^{-1} of Al_2O_3 and $\text{Pt-Al}_2\text{O}_3$ at pH 7.0, 9.0 and 12.0 for 6-h to determine the equilibrium conditions and to assess the contribution of adsorption on the elimination of

PCT. The effect of water matrix was tested by adding 2.5 mg L⁻¹, 5 mg L⁻¹ and 10 mg L⁻¹ of humic acid (HA) into the test solutions. The concentration of PCT and the rate of mixing were fixed at 35 μM and 250 rpm, respectively.

11.2.1. Experimental

Ozonation. Ozone was generated onsite using an Ozonolab-100 Model generator and dry pure oxygen flowing at 1.5 L min⁻¹. Preliminary experiments with ozone and PCT alone were carried out in 250 mL glass chambers at pH 7.0, 9.0 and 12 to assess the contribution of direct and indirect reactions of the compound with ozone. The gas flow rate was fixed at 3, 6 and 9 mg min⁻¹, which provided aqueous ozone concentrations of 2, 4 and 8 g m⁻³, respectively at t=0. The tests were repeated in the presence of HA and HCO₃⁻ to assess the effect of organic and inorganic constituents of natural waters.

Catalytic Ozonation. Catalytic ozonation of PCT (C₀=35 μM or 5 mg L⁻¹) with Al₂O₃ and Pt-Al₂O₃ was run in the presence of 5 mg L⁻¹ of the catalysts during 1-h ozonation at 4-6 mg min⁻¹ unless stated otherwise. The role of □OH scavengers was tested by adding various quantities of HA (2.5, 5 and 10 mg L⁻¹) and HCO₃⁻ (5, 50 and 100 mM) and running the experiments again in their presence. Ultrasound-assisted ozonation was carried out in a plate-type reactor, equipped with a 120 W generator and a piezo-electric transducer (22 cm²) that emitted at 572 kHz (Ultraschall/ Meinhardt, Germany). The ultrasonic power density during ozonation of the reactor in the presence of the catalysts was 0.23 W mL⁻¹.

11.2.2. Analytical

PCT, TOC, H₂O₂ was analyzed by filtering the samples through a 0.45 μm membrane. The concentration of residual ozone was determined by the indigo method (AWWA, 1998) followed by quenching of the remaining ozone with thiosulfate. The aqueous concentration of platinum and aluminum (due to potential leaching out of the element from the nanocomposites) was monitored by the method of inductively coupled plasma (ICP).

The structure, morphology and size of pristine and Pt-supported nanoparticles of alumina were analyzed by environmental scanning electron microscope (ESEM). Multi-

element mapping (EDX MEM/Line Scanning/Particle) and phase analyses were carried out to detect, characterize and classify the indefinite features under low/high vacuum conditions without limitation as described in Section 3.2.3.

11.3. Results and Discussion

11.3.1. Characterization of the Catalysts

SEM analysis of the catalyst surfaces for chemical layer characterization and homogeneity showed that particles of γ -alumina existed in aggregated form (Figure 11.1(a), while those of nPt-alumina were in form of very fine powders (Figure 11.1(b). Elemental mapping analysis (images depicted at the bottom of Figure 11.1(b) revealed that the nanoparticles were not concentrated in any specific area of the composite surface, signifying their uniform dispersion on the surface of the catalyst. Analysis of Al and Pt in solution during catalytic ozonation with and without ultrasound showed that metal leaching from the catalyst surface was insignificant (<1%), i.e. the nanocomposite was fairly stable.

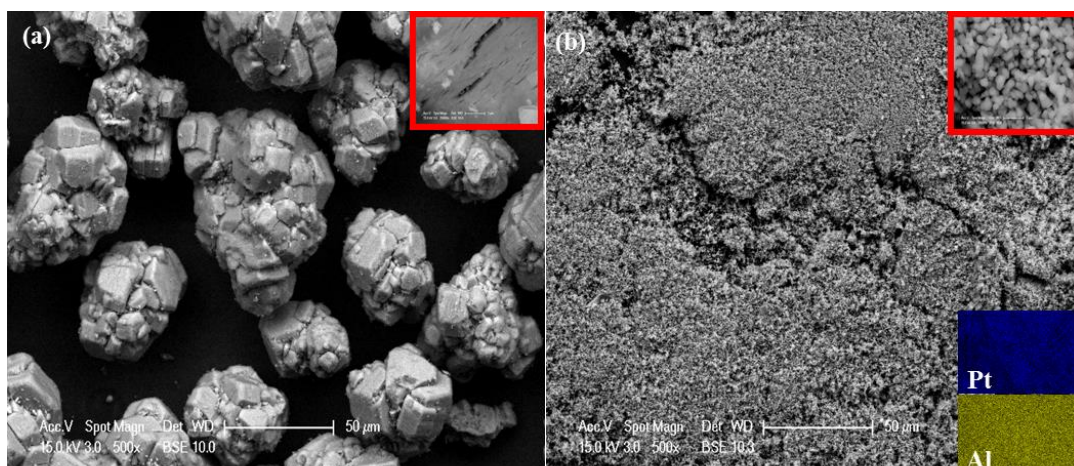


Figure 11.1. ESEM-EDX images of γ -Al₂O₃ (a) and nPt-Al₂O₃ (b) with multi elemental mapping. The regions at the top right of a, b corresponds to x20000 magnification.

11.3.2. Adsorption of PCT on Al₂O₃ and Pt-Al₂O₃: The Effect of Catalyst Dose and HA

Adsorption of organic compounds on hydrous Al₂O₃ follows a ligand exchange model, i.e. anions and organic acids replace the hydroxyl groups to form surface complexes, the concentration of which is related to pK_a of the solute, electrical properties of the surface and the affinity of alumina for the ligand (Ernst et al., 2004). We found that PCT was weakly adsorbed on both of the adsorbents, and the degree of adsorption was slightly enhanced by acidity (via population of the surface with positively charged OH). The adsorption isotherms obtained with the two forms of alumina are plotted in Figure 11.2 (a), which shows that at low solids concentrations (0-5 mg L⁻¹) the degree of adsorption increases with increased solids; but above 5 mg L⁻¹ of γ -Al₂O₃, adsorption sharply decreases, most likely via coagulation of the particles. No such curvilinear pattern was observed in the presence of the nanocomposite, signifying the stability of the particles for agglomeration. We also checked the effect of HA addition, based on the high affinity of humic substances for metallic oxide surfaces (Kasprzyk-Hordern, 2004) and found that the presence of the reagent did not significantly change the adsorption of PCT onto pristine or modified forms of Al₂O₃. The data as presented in Figure 11.2 (b) depict a curvilinear pattern of adsorption in the presence of γ -Al₂O₃ and a linear one in that of Pt-Al₂O₃. Nevertheless, the observed effects were insignificant compared to the initial mass of PCT (1.25 mg), because maximum reduction in the mass of the compound in the presence and absence of the reagent was 0.0092 mg and 0.0078 mg, respectively during adsorption on γ -Al₂O₃. Similarly, in the presence of Pt-Al₂O₃ maximum elimination of PCT was 0.0085 mg and 0.0047 mg without and with HA (10 mg L⁻¹), respectively. As a result, the adsorption of PCT on both forms of alumina was very poor and the presence of HA was insignificant within that context. As such, we concluded that adsorption will not contribute to the elimination of the compound during catalytic ozonation.

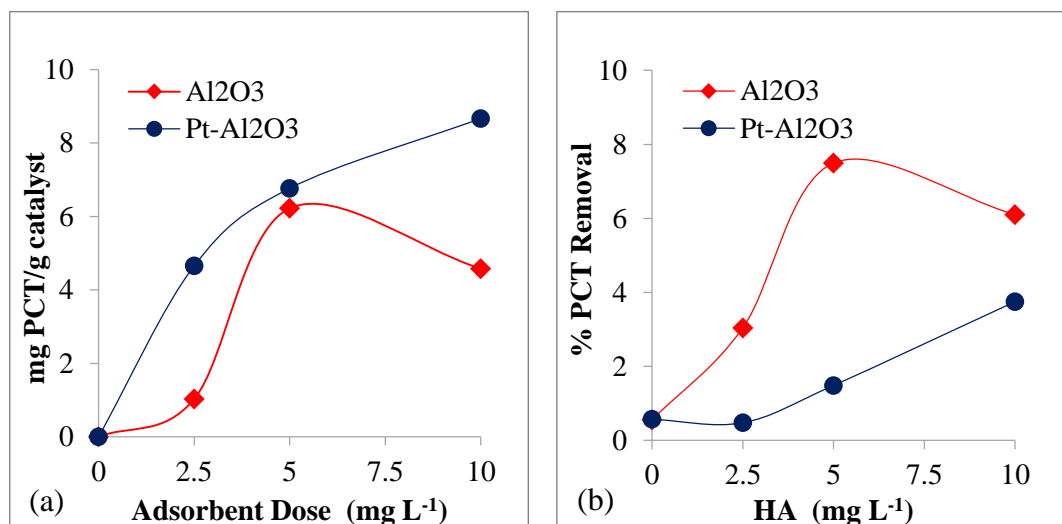


Figure 11.2. Adsorption isotherms of PCT (a) and adsorptive (or chemical) elimination of PCT in relation to humic acid concentration (b). Initial conditions were C_0 (PCT)= 35 μ M, pH 7.0, adsorbent dose in (b)=5 mg L⁻¹.

11.3.3. Ozonation: Selection of the Operating Parameters

The decomposition of PCT during ozonation alone at various gas flow rates is presented in Fig. 11.3 (a), which shows that the reaction was most rapid at a flow of 9 mg min⁻¹ ($k=1.25$ min⁻¹), slightly slower at 6 mg min⁻¹ ($k=0.97$ min⁻¹) and much slower at 3 mg min⁻¹ ($k=0.52$ min⁻¹). The overall degradation of the compound, represented by the decay of organic carbon after 1-h reaction and the corresponding rate of H₂O₂ formation at the three flow rates are depicted in Figure 11.3 (b). It was found that increasing the flow from 3 to 6 mg min⁻¹ made an insignificant contribution to mineralization; but the next increase to 9 mg min⁻¹ was effective via enhanced ozone decomposition, as verified by the excess H₂O₂ formation depicted in the inset of Figure 11.3 (b).

The effect of pH during ozonation is presented in Figure 11.4 in terms of the rate of PCT decay, H₂O₂ formation and C-mineralization at various pH. The data show that at alkaline and neutral pH, PCT was completely decomposed within the first seven and ten minutes, via indirect and direct/indirect reactions, respectively. We also monitored the formation and depletion of H₂O₂ based on the fact that it is the only stable active oxygen species produced by ozone decomposition. Moreover, H₂O₂ is generated as an end product

of direct reactions of ozone with organic compounds and depleted by decomposition and reaction with ozone.

It was found that the rate of peroxide formation was most rapid at pH 7.0 reaching a maximum at $t=10$ min and declining thereafter. At acidic pH, the H_2O_2 concentration was found to build up steadily throughout the reaction time as the evidence of direct reactions of PCT with ozone. Finally, we found that pH was highly stable when the reaction was initiated at acidic and alkaline levels, but dropped rapidly when initiated at the neutral level, signifying the formation of acidic intermediates. This is in agreement with the data of Andreozzi et al. 2003, who have detected oxalic, acetic and formic acid as the end products of direct reactions of PCT with ozone. Note also that carbon mineralization increased with increasing pH, showing the preference of the oxidation byproducts for indirect reactions with ozone.

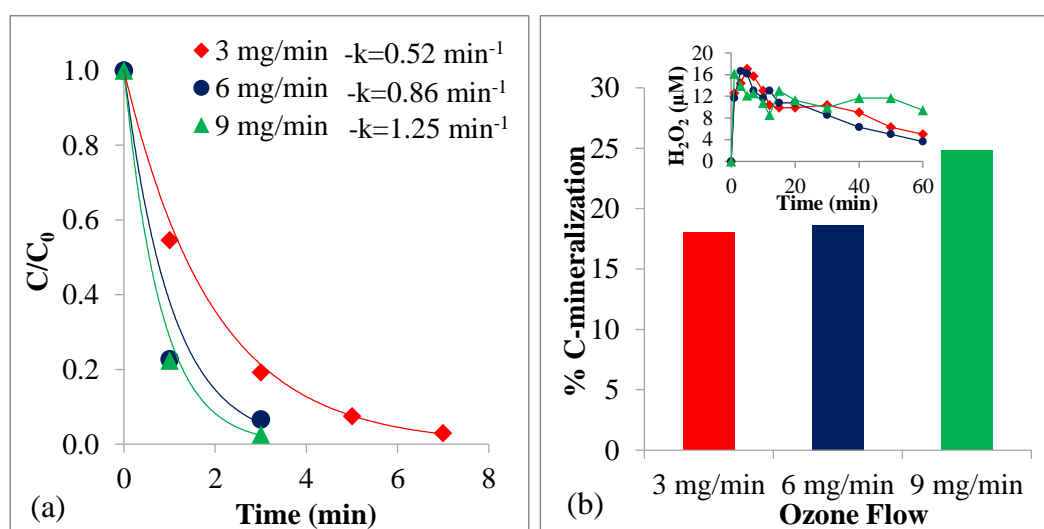


Figure 11.3. The impact of gas flow rate on the rate of PCT ($C_0=35 \mu M$) decay (a) and C-mineralization (b) by ozonation at pH 7.0. The inset on (b) shows the rate of H_2O_2 formation in relation to the ozone flow ($O_3=2, 4, 8 \text{ mg L}^{-1}$).

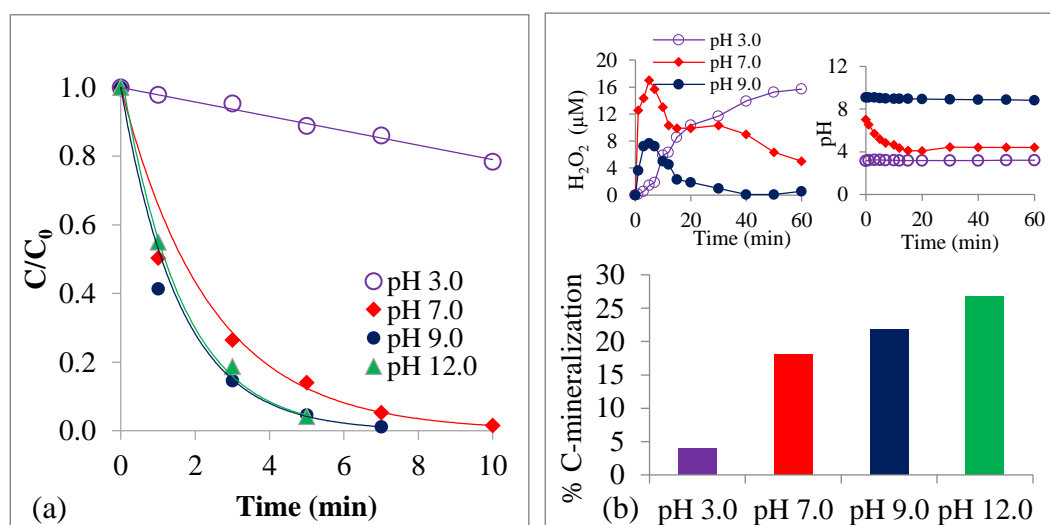


Figure 11.4. Variations in the rate of PCT decay ($C_0=35 \mu M$) (a), H_2O_2 formation and C-mineralization (b) with the solution pH during ozonation without catalysts at 6 mg min^{-1} ($O_3=4 \text{ mg L}^{-1}$).

Monitoring of the residual ozone concentration during ozonation of water (no PCT) in the absence and presence of the catalysts showed that at neutral pH and without catalysts it increased steadily with time, but when the catalysts were added it declined after 5-min as the evidence of decomposition on heterogeneous surfaces. In the presence of PCT we found that almost all of the ozone was rapidly depleted, as the evidence of direct reactions justified by the high rate constants reported for the reactions of neutral and anionic PCT with O_3 at pH 7.0 ($k=2.8-6.5 \times 10^6 \text{ M}^{-1}\text{s}^{-1}$ and $3.6-9.9 \times 10^8 \text{ M}^{-1} \text{ s}^{-1}$, respectively) (Andreozzi et al., 2003a; Najjar et al., 2014; Hoigné and Bader, 1983). The data are depicted in Figure 11.5.

11.3.4. Catalytic Ozonation with γ - and nPt-supported Al_2O_3

The efficiency of catalytic ozonation with metal oxides is directly related to the surface properties of the catalyst as well as the pH of the solution, which influences not only the character of surface active sites, but also the rate of ozone decomposition (Kasprzyk-Hordern, 2004). The pseudo-first order decay rate constants and the efficiency of mineralization by catalytic ozonation of PCT with γ - Al_2O_3 and nPt- Al_2O_3 are listed in Table 11.1 for various pH test levels.

The results show that γ -Al₂O₃ had either no or a negative contribution to the efficiency of PCT oxidation by ozonation alone (Control), while Pt-supported nanocomposites enhanced the oxidation of the compound at all pH levels. For the mineralization process, γ -Al₂O₃ was slightly effective at acidic pH (most likely due to the adsorption of the oxidation byproducts and the carboxylic end products on the surface of the catalyst), and ineffective at others; whereas the nanocomposite was effective at all pH with maximum activity at 9.0.

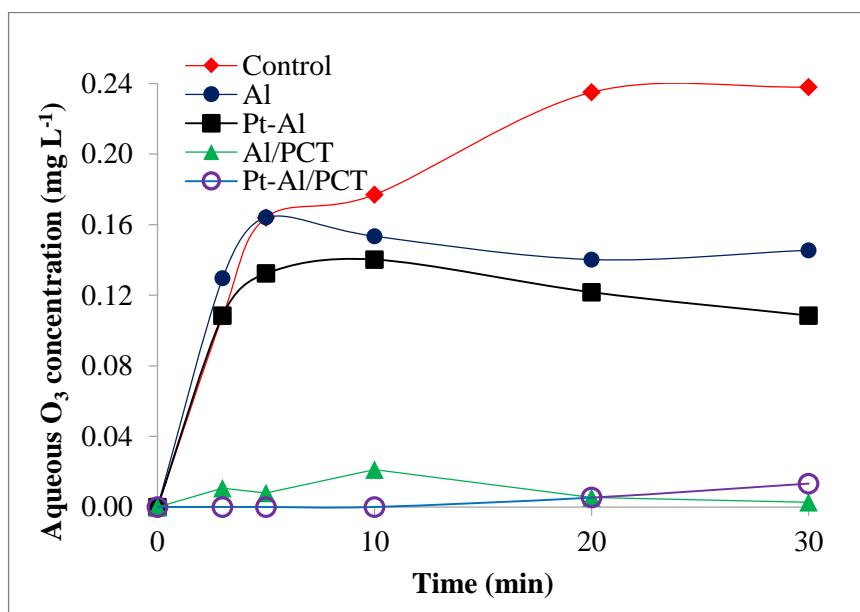


Figure 11.5. Accumulation/depletion of aqueous ozone with time in the presence of Al₂O₃, nPt-Al₂O₃ and PCT (O₃ flow=6 mg min⁻¹ (O₃= 4 mg L⁻¹). pH=7, catalyst dose=5 mg L⁻¹, PCT₀=35 μM). “Control” refers to ozonation alone.

Table 11.1. Relative effectiveness of γ -Al₂O₃ and nPt-Al₂O₃ in catalytic ozonation of PCT at various pH (k' and %TOC refer to 6-min and 60-min reaction times, respectively). Initial conditions were: C₀=35 μM, O₃ flow rate=3 mg min⁻¹ (O₃= 2 mg L⁻¹).

pH	k' (min ⁻¹)				%TOC decay			
	3.0	7.0	9.0	12.0	3.0	7.0	9.0	12.0
Control	0.02	0.42	0.53	0.63	4.00	18.01	21.78	26.72
γ-Al₂O₃	0.05	0.42	0.23	0.26	10.13	17.02	17.44	17.34
Pt-Al₂O₃	0.05	0.52	0.64	0.72	12.10	23.43	31.76	28.12

A very dramatic rate inhibition in the presence of γ - Al_2O_3 at pH 12 must be due to the absence of positively charged hydroxyl groups on the catalyst surface for initiating the decomposition of adsorbed ozone. As such, the ozone adsorbed on the catalyst surface was unused/wasted, so that the availability of radical species ($\text{HO}\cdot$, $\text{HO}_2\cdot$ and $\text{O}_2^-\cdot$) in solution (where PCT remained most of the time) was severely lower than that in ozonation alone under the same conditions. On the other hand, the catalyst was also poorly active at pH 9.0, which is inconsistent with some literature reporting very high activity of γ - Al_2O_3 at pH around the zero-point charge ($\text{pKz}=8.3\text{-}8.9$) due to the surplus of uncharged hydroxyl groups on the surface of the catalyst (Ikhlaiq et al., 2012; Qi et al., 2008). The inconsistency can be explained by: i) low reactivity of the test compounds with ozone; ii) low adsorption of PCT on alumina; and iii) non-reactivity of PCT with superoxide anion radicals ($\text{O}_2^-\cdot$), which are dominant products of ozone decomposition at $\text{pH}>8.0$. Moreover, an excess rate of superoxide radical production on the catalyst surface definitely restricts the formation of $\text{HO}\cdot$ leading to termination of the radical chain, which in turn results in the inhibition of oxidation reactions.

In summary, the literature reporting high efficacy of γ -alumina at pH around pKz is conditional, because it is not valid when the organic compound(s) under investigation adsorbs poorly on the catalyst surface; is very reactive with ozone and non-reactive with superoxide anion radicals. To assess the validity of this hypothesis we monitored the decay of another analgesic pharmaceutical-ibuprofen (that reacts poorly with molecular ozone) and found that the rate of elimination of the compound in the presence of γ - and Pt- Al_2O_3 was 43% and 87% faster and the extent of mineralization was 86% and 92% larger, respectively than those observed in ozonation alone.

On the other hand, we found that the poor activity of γ -alumina was substantially reversed (regardless of the pH level) by supporting it with nanoparticles of platinum at the surface. The result is the output of a massive surface area with increased number of active adsorption sites, and the ability of the co-catalyst to transfer electrons to the adsorbed O_3 for enhanced rate of $\cdot\text{OH}$ production.

11.3.5. The Effect of Water Matrix and/or •OH Scavengers

Natural organic matter (NOM) and carbonates are fundamental components of surface water and are recognized with their high reactivity with •OH. It is therefore of importance to elucidate their effect on catalytic ozonation of organic matter. Figure 11.6 shows the rate of decay and percentage of mineralization of PCT by catalytic ozonation in the absence and presence of humic acid (HA) that was selected as a surrogate of NOM. The rate of PCT decay in the presence of γ -Al₂O₃ and nPt-Al₂O₃ was found to decrease from 0.41 min⁻¹ to 0.08 min⁻¹, and 0.61 min⁻¹ to 0.13 min⁻¹, respectively by the addition of HA. Moreover, the fraction of C-mineralization dropped from 17% to 5% (γ -Al₂O₃), and 23% to 12% (Pt-Al₂O₃). The results clearly indicate a strong competition for •OH and the active adsorption sites on the catalyst surfaces. The adsorption of HA on alumina is supported by the information in the literature that at neutral pH, some of the phenolic and carboxylic moieties of the reagent are negatively charged and easily approach the positively charged catalyst surface (Ikhlaq et al., 2015). Note that the inhibition in the presence of Pt-Al₂O₃ was less dramatic, particularly for the mineralization process due to larger availability of •OH and larger number of adsorption sites. Figure 11.6 (b) shows that the inhibition increases with increasing doses of the reagent, which also leads to a considerable rate enhancement in the formation of H₂O₂ via increased consumption of ozone.

The degradation of PCT by catalytic ozonation was also retarded by HCO₃⁻ addition, as depicted in Fig. 11.7 (a-b), presented together with the effect of HA. The data show that the rate inhibition in the presence of HCO₃⁻ was slightly larger in the presence of Pt-alumina than in that of the pristine form, most likely due to a larger affinity of the anion to the modified surface. Nevertheless, we found that the influence of bicarbonate was less important in the mineralization process, most likely due to the affinity of the oxidation byproducts to the surface of the catalysts and their reactivity with carbonate radicals that form upon the reaction of bicarbonate with •OH.

We also monitored the absorption of two PCT solutions (spiked with one of the scavengers) at UV-220 and UV-254 during catalytic ozonation with Pt-Al₂O₃. The selection of these two wavelengths was based on the fact that an increase in absorption at 220 nm signifies the cleavage of complex aromatic structures (to form smaller molecular weight

compounds), while a decrease in 254 nm is the evidence of the depletion of aromatic/olefinic byproducts (Kasprzyk-Hordern et al., 2006). The data are presented in Figure 11.7 (c-d). A sharp increase in the absorbance of the control at 220 nm during early reaction is the sign of the cleavage of an aromatic ring, and the succeeding decrease shows the decomposition of the byproducts of this cleavage. Note that there was no such early increase at 220 nm in the presence of HA, and a relatively softer one in that of HCO_3^- . We also found that the decay of 254 nm absorbance, which practically represents mineralization of organic compounds, was more severely inhibited by the presence of the scavengers.

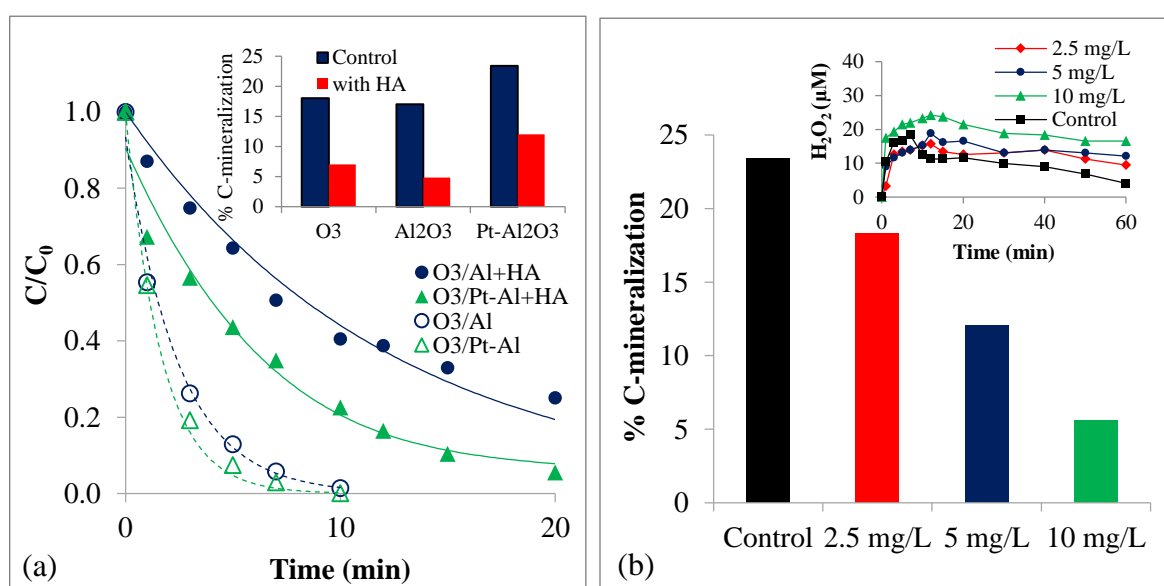


Figure 11.6. The impact of HA (5 mgL^{-1}) on the rate of oxidation and mineralization of PCT during and after catalytic ozonation with pristine and nPt- Al_2O_3 (a); the effect of HA dose on mineralization and H_2O_2 formation in the presence of nPt- Al_2O_3 (b). The reaction rate constants in (a) are 0.08 ($\text{Al}_2\text{O}_3/\text{HA}$), 0.13 (nPt- $\text{Al}_2\text{O}_3/\text{HA}$), 0.41 (Al_2O_3) and 0.61 min^{-1} (nPt- Al_2O_3). Initial conditions were pH 7.0, $\text{O}_{3(\text{aq})}=4 \text{ mg L}^{-1}$, $\text{PCT}_0=35 \text{ }\mu\text{M}$.

In summary and in the light of the data presented in Figure 11.7, it is obvious that $\bullet\text{OH}$ -mediated reaction mechanisms have a significant contribution to the oxidation and mineralization of PCT during catalytic ozonation with alumina and its modified nanocomposite.

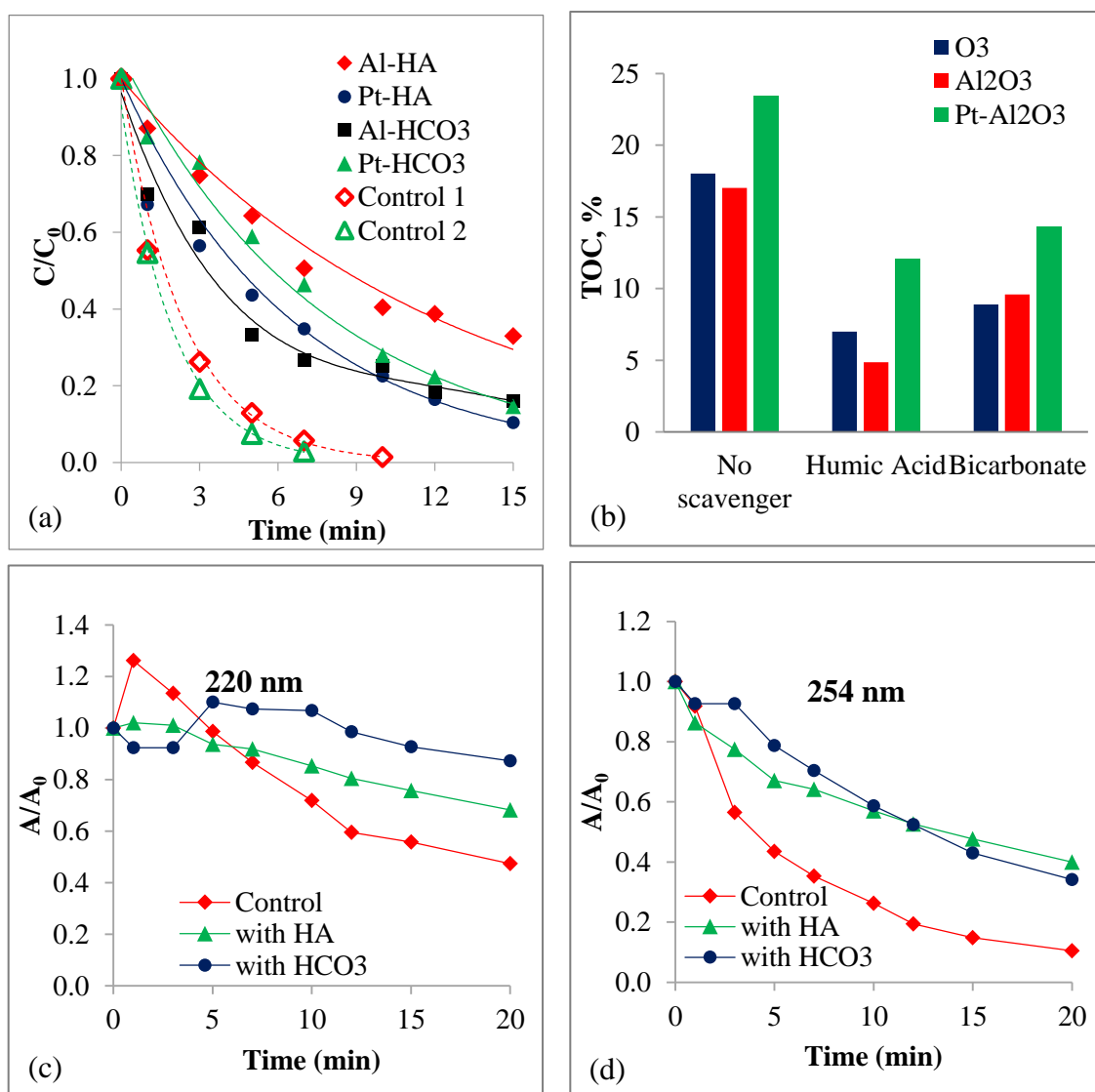


Figure 11.7. Impacts of HA and bicarbonate on the rate of decomposition/mineralization of PCT during ozonation with pristine and Pt-supported alumina (a-b); the rate of absorbance decay during ozonation of PCT with Pt-Al₂O₃ (c-d). Initial conditions were: O_{3(aq)}=4 mg L⁻¹, PCT₀=5 mg L⁻¹, catalyst dose=5 mg L⁻¹, HA=5 mg L⁻¹, HCO₃⁻=50 mM, pH=7.0. “Control” in a-b refers to the absence of scavengers; “Control1”, “Control2” in (c) refer respectively to catalysis with γ -Al₂O₃ and Pt-Al₂O₃ in the absence of the scavengers.

11.3.6. Can Ultrasound Improve the Activity of the Catalysts and the Efficiency of the Process?

In our earlier work related to the destruction of pharmaceuticals in water with TiO₂ and its metal-supported nanocomposites, we used ultrasound to enhance the rate of •OH formation and mass transfer to the catalyst surfaces (Ziylan-Yavas et al. 2015b; Ziylan-Yavas and Ince 2016). Based on the knowledge that ultrasound also increases dissolution and diffusion of gases, we carried out some of the experiments in the presence of ultrasonic cavitation to check if it is possible to improve the process efficiency via enhanced O₃ diffusion to the solution, enhanced •OH formation upon water pyrolysis and enhanced rate of mass transfer to the catalyst surfaces.

Contrary to our expectation we found that ultrasound slowed down the rate of PCT oxidation, while it was very effective in improving the efficiency mineralization reactions. The data are presented in Table 11.2 in terms of the fractions of PCT and TOC eliminated after 9-min and 1-h ozonation in the presence of the catalysts, respectively. The negative effect of ultrasound on the rate of PCT decomposition is a complicated issue, and in the following are two hypotheses that we believe are important in understanding and solving the complication:

- i) Molecules of gases such as ozone readily diffuse into acoustic cavity bubbles during sonication, and their existence in the bulk solution is unlikely for direct reactions with organic compounds. Although ozone undergoes thermal decomposition during the implosion of these bubbles, only some of the produced radicals can migrate to the bulk solution, since most of them rapidly recombine at the gas-liquid interface (Ince et al., 2001).
- ii) If the water contains solid particles as in our case, the bubbles form extensively on the solid surfaces. As such, the extreme conditions generated during the implosive collapse of these bubbles (e.g. T>2000 K, P>1000 atm) may temporarily damage the surface and its structural symmetry.

Table 11.2. The effect of ultrasound on the efficiency of PCT degradation by catalytic ozonation with alumina and Pt-supported alumina. Initial conditions were: $O_{3(aq)}=4 \text{ mg L}^{-1}$, $PCT_0=35 \text{ } \mu\text{M}$, $f=572 \text{ kHz}$, $P_{US}=0.21 \text{ W mL}^{-1}$, $\text{pH}=7.0$.

Ozonation	% PCT decay at t=9 min			% TOC decay at t=60 min		
	O_3 only	O_3/Alum	$O_3/\text{Pt-Alum}$	O_3 only	O_3/Alum	$O_3/\text{Pt-Alum}$
without US	98	98	100	18	17	24
with US	82	82	82	49	49	55

To verify the second hypothesis, we allowed an equal concentration (5 mg L^{-1}) of $\text{Pt-Al}_2\text{O}_3$ to contact with the same source of ultrasound for 40-min (in the absence of PCT and O_3), and then used it as the catalyst during ozonation (with $4 \text{ mg L}^{-1} O_3$) of PCT without ultrasound. The data as presented in Figure 11.8 show that the performance of $\text{Pt-Al}_2\text{O}_3$ (denoted as $\text{Pt-Al}_2\text{O}_3\text{-US}$) was not only poorer than that of the original catalyst ($\text{Pt-Al}_2\text{O}_3$), but also lower than the performance of non-modified alumina. Hence, it is true that ultrasound or the extreme conditions of cavitation collapse partially damaged the catalyst surfaces and this is one of the reasons why complete oxidation of PCT was four-times slower in the presence of ultrasound than in its absence.

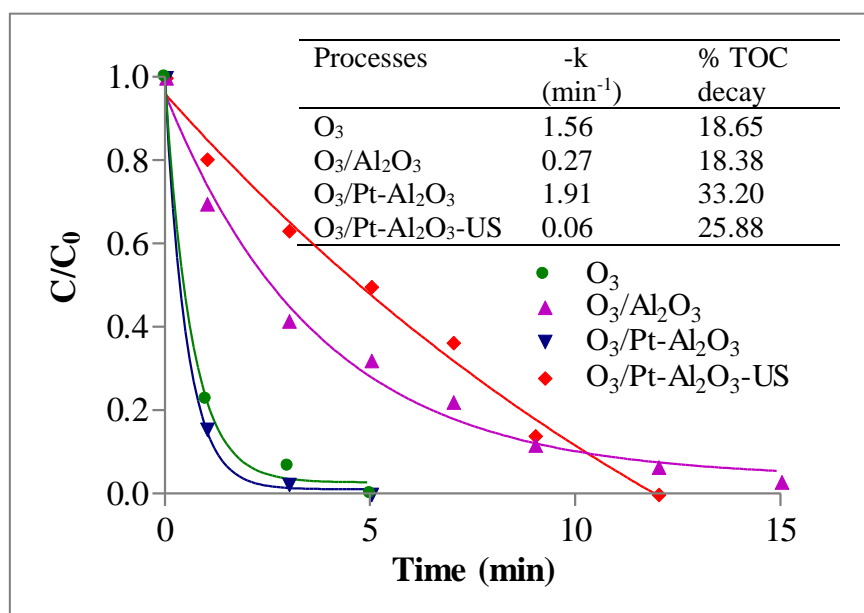


Figure 11.8. The impact of high-frequency ultrasonic irradiation on the activity of $\text{Pt-Al}_2\text{O}_3$ in ozonation. Initial conditions were: $O_{3(aq)}=6 \text{ mg L}^{-1}$, $PCT_0=35 \text{ } \mu\text{M}$, catalyst dose= 5 mg L^{-1} , $f=572 \text{ kHz}$.

Nevertheless as depicted in Table 11.2, sonication under the same conditions provided substantial improvement in the efficiency of mineralization. The paradox can be explained by the hydrophobic enrichment of the solution upon the formation of simpler intermediates and carboxylic end products via the oxidation process. These products are expected to migrate more easily to the solid surfaces (than the parent compound) and/or the gaseous cavity bubbles (if they are volatile), where they are rapidly destroyed by oxidation and thermal fragmentation. The potential damage on the surface of the catalyst due to extreme temperatures at this point is unimportant since ozone decomposition takes place predominantly inside the collapsing bubbles. The insignificance of the catalyst in terms of activity is verified by the considerable decrease in the efficiency of TOC decay when the reaction was catalyzed by the catalyst exposed to ultrasound (data presented in the inset of Figure 11.8). Hence, what improves the mineralization process in the presence of ultrasound despite the reduced activity of the catalyst, is the high abundance of $\bullet\text{OH}$ on the heterogeneous surfaces via the presence of cavities and their local collapse. What is more important is that most of the reactions take place at these surfaces and/or inside the gaseous bubbles, both of which are considerably more effective reaction sites than the bulk solution.

11.4. Conclusions

The study has highlighted the importance of solute properties over the solution pH in the activity of metallic oxides as catalysts during ozonation of organic compounds. The conclusion was based on the finding that commercial $\gamma\text{-Al}_2\text{O}_3$ either slowed down the degradation of the emerging water contaminant paracetamol (PCT) by ozonation (at alkaline pH), or was totally ineffective in it (at neutral and acidic pH) due to the following properties of the compound: i) poor adsorption affinity on the catalyst surface, ii) high reactivity with molecular ozone.

Although modification of the surface by supporting it with platinum nanoparticles provided a substantial improvement in the activity of the catalyst, ozonation alone was considerably sufficient for the early oxidation process. As such, modified alumina was meaningful as a catalyst only because ozonation alone was insufficient in the mineralization of the compound. Despite the significance of direct reactions in the early oxidation reactions, indirect reactions involving the OH radical were also very important, as verified by the

observed inhibition in the reaction rates upon the addition of humic acid and bicarbonate to the sample solutions.

Finally, sonication of the samples to enhance rates of mass transfer, ozone dissolution and $\bullet\text{OH}$ production was found to slow down the oxidation of the parent compound, but accelerate its mineralization. The hindrance was attributed to: i) the more likely decomposition of ozone inside the collapsing cavity bubbles than at the catalyst surfaces; ii) the damage on the catalyst surfaces caused by the extreme conditions of collapse. The positive contribution of ultrasound to the mineralization of organic carbon was explained by the hydrophobic enrichment of the solution that facilitated mass transfer to the solid surfaces and the cavity bubbles, both of which are very powerful reaction sites.

12. CONCLUSIONS AND RECOMMENDATIONS

The present dissertation is about the oxidative destruction and degradation of analgesic and anti-inflammatory pharmaceuticals by advanced oxidation processes using ultrasound and various catalysts either soluble such as Fe_2SO_4 , or insoluble such as goethite, micro- and nano-ZVI, graphite, TiO_2 (and its metal-supported nanocomposites) and alumina (and its Pt-supported nanocomposite). The modified forms of TiO_2 and Al_2O_3 , and nanoparticles of ZVI were synthesized in the laboratory using a novel sonolytic method. The major findings of the work are summarized in the following:

- 1) Ultrasonication is not only an effective tool of AOPs, but also an excellent method of enhancing mass transfer and chemical reaction rates, and reducing the consumption and generation of chemicals and hazardous sludge, respectively. Sonication alone was found viable for converting pharmaceuticals (diclofenac, ibuprofen and paracetamol) to simpler compounds and for detoxifying the reaction byproducts; but not for mineralization of organic carbon. Combined operation of double or multiple frequencies was found more effective than single-frequency applications provided that combinations and the mode of operation were well-selected.
- 2) Supporting of classical AOPs such as ozonation, UV-peroxide and TiO_2 -catalysis with ultrasound is an excellent option for achieving complete removal of the target chemicals and appreciable degrees of carbon mineralization.
- 3) The use of ZVI and metallic nanocomposites of TiO_2 is a very effective tool for enhancing the sonochemical and $\bullet\text{OH}$ -mediated oxidation of the test compounds, owing to accelerated rates of mass transfer to the gas-liquid and solid-liquid interfaces, and the massive surfaces with additional adsorption and reaction sites. It was found that even if the test compounds are highly water soluble as in our case, the reactions take place mostly at the heterogeneous surfaces.
- 4) Sonolytic modification of metallic oxides by decoration of their surface with noble metals is an excellent means of improving photolytic, sonolytic and sonophotolytic decomposition of analgesic and anti-inflammatory pharmaceuticals in water. Most importantly, the catalysts are highly stable and can be used in

multiple experiments without significant losses in catalytic activity. The use of noble metals as the co-catalysts is based on their unique properties to capture electrons, thus reducing the probability of e^-/h^+ combination reactions.

- 5) Sonolytically synthesized Pt-Al₂O₃ is a considerably more effective catalyst than commercial γ -Al₂O₃ in ozonation of paracetamol, due to the ability of the co-metal to facilitate charge transfer and decomposition of the adsorbed ozone. Low efficacy of the commercial form is due to the high reactivity of the test compound with ozone, which upon adsorption is less abundant for direct reactions. The catalytic activity was significantly enhanced via modification, but not further enhanced via the addition of ultrasound, which increased only the mineralization of the compound.
- 6) Integration of the ozonation unit of a typical water treatment plant with ultrasound seems to be a good solution as a pre-oxidation step to destroy pharmaceutical residues, the precursors of THMs and to facilitate the succeeding coagulation process.
- 7) In the light of the conclusions of the research, a list of recommendations for future work are proposed in the following:
 - Testing of less costly metals for modification of TiO₂ surface
 - Focusing more on Fe-based catalysts with magnetic properties
 - Improving the method of nanoparticle synthesis for allowing the production of nanotubes and films, which can be more easily separated (than powder forms) from solution after reaction.
 - Testing of real water and effluents (e.g. sewage treatment effluent) to shed light on the effect of water matrix on the efficiency of the applied processes.
 - Working with solar or UVA irradiation to enhance the activation of semiconductors and to reduce the cost of operation in sono-photocatalysis.
 - Investigation of the cost-efficiency of the proposed processes to shed light on their applicability in large scale operations.

13. REFERENCES

- Adewuyi, Y., 2001. Sonochemistry : Environmental science and engineering applications. *Journal of Industrial and Engineering Chemistry*, 40, 4681–4715.
- Adewuyi, Y.G., 2005. Sonochemistry in environmental remediation. 1. Combinative and hybrid sonophotocatalytic oxidation processes for the treatment of pollutants in water. *Environmental Science and Technology*, 39, 3409–3420.
- Agüera, A., Perez Estrada, L.A., Ferrer, I., Thurman, E.M., Malato, S., Fernandez-Alba, A.R., 2005. Application of time-of-flight mass spectrometry to the analysis of phototransformation products of diclofenac in water under natural sunlight. *Journal of Mass Spectrometry*, 40, 908–915.
- Ahmad, M., Teel, A.L., Watts, R.J., 2010. Persulfate activation by subsurface minerals. *The Journal of Contaminant Hydrology*, 115, 34–45.
- Ahmed, L.M., Ivanova, I., Hussein, F.H., Bahnemann, D.W., 2014. Role of platinum deposited on TiO₂ in photocatalytic methanol oxidation and dehydrogenation reactions. *International Journal of Photoenergy*, 1-9.
- Ameta, R., Kumar, A., Punjabi, P., Ameta, S.C., 2013. Advanced Oxidation Processes: Basics and Applications. In Rao, D., Senthilkumar, R., Byrne, J., Feroz, S. (Eds.), *Wastewater Treatment : Advanced Processes and Technologies*, 61-106, IWA Publishing, CRC Press Taylor and Francis Group, Boca Raton, FL, USA.
- Anderson, R., Bendell, D., Groundwater, P., 2004. *Organic Spectroscopic Analysis*, Tutorial Chemistry Texts, Royal Society of Chemistry, Cambridge.
- Andreozzi, R., Canterino, M., Marotta, R., Paxeus, N., 2005. Antibiotic removal from wastewaters: the ozonation of amoxicillin. *Journal of Hazardous Materials*, 122, 24350.

Andreozzi, R., Caprio, V., Marotta, R., Vogna, D., 2003a. Paracetamol oxidation from aqueous solutions by means of ozonation and H₂O₂/UV system. *Water Res.* 37, 993–1004.

Andreozzi, R., Raffaele, M., Nicklas, P., 2003b. Pharmaceuticals in STP effluents and their solar photodegradation in aquatic environment. *Chemosphere* 50, 1319–30.

APHA/AWWA/WPCP, 1998. *Standard Methods for the Examination of Water and Wastewater*. American Public Health Association, Washington DC.

Araujo, F.V.F., Yokoyama, L., Teixeira, L.A.C., Campos, J.C., 2011. Heterogeneous Fenton process using the mineral hematite for the discolouration of a reactive dye solution. *Brazilian Journal of Chemical Engineering*, 28, 605–616.

Asakura, Y., Nishida, T., Matsuoka, T., Koda, S., 2008. Effects of ultrasonic frequency and liquid height on sonochemical efficiency of large-scale sonochemical reactors. *Ultrasonics Sonochemistry*, 15, 244–250.

Ashokkumar, M., 2011. The characterization of acoustic cavitation bubbles - An overview. *Ultrasonics Sonochemistry*, 18, 864–872.

Ashokkumar, M., Grieser, F., 2002. Sonochemical preparation of colloids. *Encyclopedia of Surface and Colloid Science*, 4760-4774.

Ashokkumar, M., Lee, J., Kentish, S., Grieser, F., 2007. Bubbles in an acoustic field: an overview. *Ultrasonics Sonochemistry*, 14, 470–5.

Badawy, M., Gohary, F., Ghaly, M., Ali, M., 2009. Enhancement of olive mill wastewater biodegradation by homogeneous and heterogeneous photocatalytic oxidation. *Journal of Hazardous Materials*, 169, 673–679.

Badawy, M.I., Ghaly, M.Y., Ali, M.E.M., 2011. Photocatalytic hydrogen production over nanostructured mesoporous titania from olive mill wastewater. *Desalination*, 267, 250–255.

Badawy, M.I., Wahaab, R.A., El-Kalliny, A.S., 2009. Fenton-biological treatment processes for the removal of some pharmaceuticals from industrial wastewater. *Journal of Hazardous Materials*, 167, 567–574.

Bang, J.H., Suslick, K.S., 2010. Applications of ultrasound to the synthesis of nanostructured materials. *Advanced Materials*, 22, 1039-59.

Barbier, P.F., Petrier, C., 1996. Study of 20 kHz and 500 kHz of the ultrasound- ozone advanced oxidation system: 4-nitrophenol degradation. *Journal of Advanced Oxidation Technology*, 1, 154–159.

Barik, A.J., Gogate, P.R., 2016. Degradation of 4-chloro 2-aminophenol using combined strategies based on ultrasound, photolysis and ozone. *Ultrasonics Sonochemistry*, 28, 90–99.

Barrera-Salgado, K.E., Ramírez-Robledo, G., Álvarez-Gallegos, A., Pineda-Arellano, C.A., Sierra-Espinosa, F.Z., Hernández-Pérez, J.A., Silva-Martínez, S., 2016. Fenton Process Coupled to Ultrasound and UV Light Irradiation for the Oxidation of a Model Pollutant. *Journal of Chemistry*, 16-18.

Beckett, M., Hua, I., 2001. Impact of Ultrasonic Frequency on Aqueous Sonoluminescence and Sonochemistry. *The Journal of Physical Chemistry A*, 105, 3796–3802.

Bekbolet, M., 2011. Fundamentals of Advanced Oxidation Processes. In Belgiorno, V., Naddeo, Vincenzo, Rizzo, L. (Eds.), *Water, Wastewater and Soil Treatment by AOPs*, 13-22, SEED, Sanitary Environmental Engineering Division, Fisciano, Italy.

Beltran, F., Rivas, F., Monterodeespinosa, R., 2004. A TiO₂/Al₂O₃ catalyst to improve the ozonation of oxalic acid in water. *Applied Catalysis B Environ.* 47, 101–109.

Beltran, F.J., 2004. *Ozone Reaction Kinetics for Water and Wastewater Systems*. Lewis Publishers CRC Press LLC, Florida, USA.

Bendz, D., Paxéus, N.A., Ginn, T.R., Loge, F.J., 2005. Occurrence and fate of pharmaceutically active compounds in the environment, a case study: Høje River in Sweden. *Journal of Hazardous Materials*, 122, 195–204.

Benitez, F.J., Acero, J.L., Real, F.J., Roldan, G., Casas, F., 2011. Comparison of different chemical oxidation treatments for the removal of selected pharmaceuticals in water matrices. *Chemical Engineering Journal*, 168, 1149-1156.

Benotti, M.J., Trenholm, R. a, Vanderford, B.J., Holady, J.C., Stanford, B.D., Snyder, S. a, 2009. Pharmaceuticals and endocrine disrupting compounds in U.S. drinking water. *Environmental Science and Technology*, 43, 597-603.

Bose, P., Reckhow, D.A., 2007. The effect of ozonation on natural organic matter removal by alum coagulation. *Water Research*, 41, 1516–1524.

Boyd, G.R., Reemtsma, H., Grimm, D.A., Mitra, S., 2003. Pharmaceuticals and personal care products (PPCPs) in surface and treated waters of Louisiana, USA and Ontario, Canada. *Science of the Total Environment*, 311, 135–149. d

Boyd, G.R., Zhang, S., Grimm, D. A., 2005. Naproxen removal from water by chlorination and biofilm processes. *Water Research*, 39, 668–76.

Boynton, C., Dick, C., Mayor, G., 1988. NSAIDs: an overview. *The Journal of Clinical Pharmacology*, 28, 512–517.

Brotchie, A., Ashokkumar, M., Grieser, F., 2007. Effect of water-soluble solutes on sonoluminescence under dual-frequency sonication. *The Journal of Physical Chemistry C*, 111, 3066–3070.

Brotchie, A., Grieser, F., Ashokkumar, M., 2008. Sonochemistry and sonoluminescence under dual-frequency ultrasound irradiation in the presence of water-soluble solutes. *The Journal of Physical Chemistry C*, 112, 10247–10250.

Brun, G.L., Bernier, M., Losier, R., Doe, K., Jackman, P., Lee, H.B., 2006. Pharmaceutically active compounds in Atlantic Canadian sewage treatment plant effluents and receiving waters, and potential for environmental effects as measured by acute and chronic aquatic toxicity. *Environmental Toxicology and Chemistry*, 25, 2163-76.

Bui, T.X., Choi, H., 2010. Influence of ionic strength, anions, cations, and natural organic matter on the adsorption of pharmaceuticals to silica. *Chemosphere*, 80, 681–686.

Buser, H.R., Poiger, T., Mu, M.D., 1999. Occurrence and environmental behavior of the chiral pharmaceutical drug ibuprofen in surface waters and in wastewater. *Environmental Science and Technology*, 33, 15, 2529-2535.

Buser, H., Mu, M.D., Wa, C.-, 1998. Occurrence and fate of the pharmaceutical drug diclofenac in surface waters : rapid photodegradation in a lake. *Environmental Science and Technology*, 32, 22, 3449-3456.

Byrne, J., Fernandez-Ibanez, P., 2013. Solar Photocatalysis Treatment of Wastewater. In *Wastewater Treatment: Advanced Processes and Technologies*, 37-60, Taylor and Francis Group, LLC, CRC Press, Boca Raton, FL, USA.

Calza, P., Sakkas, V., Medana, C., Baiocchi, C., Dimou, A., Pelizzetti, E., Albanis, T., 2006. Photocatalytic degradation study of diclofenac over aqueous TiO₂ suspensions. *Applied Catalysis B: Environment*, 67, 197-205.

Camacho-Munoz, D., Martin, J., Santos, J.L., Aparicio, I., Alonso, E., 2010. Occurrence, temporal evolution and risk assessment of pharmaceutically active compounds in Doana Park (Spain). *Journal of Hazardous Materials*, 183, 602-608.

Canonica, S., Meunier, L., Gunten, U. Von, 2008. Phototransformation of selected pharmaceuticals during UV treatment of drinking water. *Water Research*, 42, 121-128.

Carballa, M., Omil, F., Lema, J.M., Llompart, M., García-Jares, C., Rodríguez, I., Gómez, M., Ternes, T., 2004. Behavior of pharmaceuticals, cosmetics and hormones in a sewage treatment plant. *Water Research*, 38, 2918–2926.

Caruso, R.A., Ashokkumar, M., Grieser, F., 2002. Sonochemical formation of gold sols. *Langmuir* 18, 7831-7836.

Centellas, F., Arias, C., Skoumal, M., Garrido, A., Brillas, E., Mari, R., 2006. Mineralization of paracetamol by ozonation catalyzed with. *Applied Catalysis B: Environment*, 66, 228-240.

Chakma, S., Moholkar, V.S., 2013. Physical Mechanism of Sono-Fenton Process. *AIChE Journal*, 59, 4303-4313.

Chan, J.Y.T., Ang, S.Y., Ye, E.Y., Sullivan, M., Zhang, J., Lin, M., 2015. Heterogeneous photo-Fenton reaction on hematite ($\alpha\text{-Fe}_2\text{O}_3$) {104}, {113} and {001} surface facets. *Chemical Physics*, 17, 25333-25341.

Chand, R., Ince, N.H., Gogate, P.R., Bremner, D.H., 2009. Phenol degradation using 20, 300 and 520 kHz ultrasonic reactors with hydrogen peroxide, ozone and zero valent metals. *Separation and Purification Technology*, 67, 103-109.

Chang, S.C., Wang, Y.F., You, S.J., Kuo, Y.M., Tsai, C.H., Wang, L.C., Hsu, P.Y., 2013. Toxicity evaluation of fly ash by Microtox®. *Aerosol and Air Quality Research*, 13, 1002-1008.

Choi, W., Termin, A., Hoffmann, M.R., 1994. The role of metal ion dopants in quantum-sized TiO_2 : correlation between photoreactivity and charge carrier recombination dynamics. *Journal of Physical Chemistry*, 98, 13669-13679.

Ciawi, E., Rae, J., Ashokkumar, M., Grieser, F., 2006. Determination of temperatures within acoustically generated bubbles in aqueous solutions at different ultrasound frequencies. *The Journal of Physical Chemistry*, 110, 27, 13656-13660.

Cleuvers, M., 2004. Mixture toxicity of the anti-inflammatory drugs diclofenac, ibuprofen, naproxen, and acetylsalicylic acid. *Ecotoxicology and Environmental Safety*, 59, 309-315.

Coelho, A.D., Sans, C., Agüera, A., Gómez, M.J., Esplugas, S., Dezotti, M., 2009. Effects of ozone pre-treatment on diclofenac: intermediates, biodegradability and toxicity assessment. *Science of the Total Environment*, 407, 3572-3578.

Cooper, C., Burch, R., 1999. An investigation of catalytic ozonation for the oxidation of halocarbons in drinking water preparation. *Water Research*. 33, 3695–3700.

Crum, L.A., Mason, T.J., Reisse, J.L., Suslick, K.S., 1999. *Sonochemistry and Sonoluminescence*, Nato ASI S., Kluwer Academic Publishers, Dordrecht, Netherlands.

Dantas, T.L.P., Mendonça, V.P., José, H.J., Rodrigues, A.E., Moreira, R.F.P.M., 2006. Treatment of textile wastewater by heterogeneous Fenton process using a new composite Fe₂O₃/carbon. *Chemical Engineering Journal*, 118, 77-82.

Daughton, C.G., Ternes, T.A., 1999. Pharmaceuticals and personal care products in the environment: agents of subtle change? *Environmental Health Perspectives*, 107, Suppl 6, 907-38.

De Laat, J., Truong Le, G., Legube, B., 2004. A comparative study of the effects of chloride, sulfate and nitrate ions on the rates of decomposition of H₂O₂ and organic compounds by Fe(II)/H₂O₂ and Fe(III)/H₂O₂. *Chemosphere*, 55, 715-723.

Deng, Y., Zhao, R., 2015. Advanced oxidation processes (AOPs) in wastewater treatment. *Journal of Industrial and Engineering Chemistry*, 1, 167-176.

Desale, A., Kamble, S.P., Deosarkar, M.P., 2013. Photocatalytic degradation of paracetamol using degussa TiO₂ photocatalyst 2, 140-148.

Dezhkunov, N. V, 2003. Investigation of sonoluminescence amplification under the interaction of ultrasonic fields widely differing in frequency. *The Journal of Engineering Physics and Thermophysics*, 76, 120-127.

Drzyzga, O., 2003. Diphenylamine and derivatives in the environment: A review. *Chemosphere*, 53, 809-818.

Duprez, D., Delanoë, F., Barbier, J., Isnard, P., Blanchard, G., 1996. Catalytic oxidation of organic compounds in aqueous media. *Catalysis Today*, 29, 317-322.

Edzwald, J.K., Tobiason, J.E., 1999. Enhanced coagulation: US requirements and a broader view. *Water Science and Technology*, 40, 63-70.

Encinas, S., Bosca, F., Miranda, M.A., 1998. Phototoxicity associated with diclofenac: A photophysical, photochemical, and photobiological study on the drug and its photoproducts. *Chemical Research in Toxicology*, 11, 946-952.

Entezari, M.H., Kruus, P., 1996. Effect of frequency on sonochemical reactions II. Temperature and intensity effects. *Ultrasonics Sonochemistry*, 3, 19-24.

Entezari, M.H., Kruus, P., Otson, R., 1997. The effect of frequency on sonochemical reactions III: dissociation of carbon disulfide. *Ultrasonics Sonochemistry*, 4, 49-54.

EPI Suit 4.0, EPA, 2008.

Eren, Z., Ince, N.H., 2010. Sonolytic and sonocatalytic degradation of azo dyes by low and high frequency ultrasound. *Journal of Hazardous Materials*, 177, 1019-24.

Ernst, M., Lurot, F., Schrotter, J.C., 2004. Catalytic ozonation of refractory organic model compounds in aqueous solution by aluminum oxide. *Applied Catalysis B: Environmental*, 47, 15-25.

EU Directive, 1993. Risk Assessment for new notified substances, 93/67/EEC.

F. H. Hussein and R. Rudham, 1984. Photocatalytic dehydrogenation of liquid propan-2-ol by olatinized anatase and other catalysts. *Journal of the Chemical Society, Faraday Transactions*, 80, 2817-2825.

Feng, R., Zhao, Y., Zhu, C., Mason, T.J., 2002. Enhancement of ultrasonic cavitation yield by multi-frequency sonication. *Ultrasonics Sonochemistry*, 9, 231-236.

Fent, K., Weston, A., Caminada, D., 2006. Ecotoxicology of human pharmaceuticals. *Aquatic Toxicology*, 76, 122-59.

Fernandez Rivas, D., Ashokkumar, M., Leong, T., Yasui, K., Tuiuti, T., Kentish, S., Loshe, D., Gardeniers, H.J., 2012. Sonoluminescence and sonochemiluminescence from a microreactor. *Ultrasonics Sonochemistry*, 19, 1252-1259.

Fu, Q., Wagner, T., Olliges, S., Carstanjen, H.D., 2005. Metal-oxide interfacial reactions: Encapsulation of Pd on TiO₂ (110). *Journal of Physical Chemistry B*, 109, 944-951.

Fuchs, B.F.J., Puskas, W.L., 2005. Application of Multiple Frequency Ultrasonics. *Cleaning Technologies Group, Blackstone-NEY Ultrasonics, Cincinnati, USA.*

Gagnon, C., Lajeunesse, A., Cejka, P., Gagné, F., Hausler, R., 2008. Degradation of selected acidic and neutral pharmaceutical products in a primary-treated wastewater by disinfection processes. *Ozone: Science and Engineering*, 30, 387-392.

Gayathri, P., Praveena Juliya Dorathi, R., Palanivelu, K., 2010. Sonochemical degradation of textile dyes in aqueous solution using sulphate radicals activated by immobilized cobalt ions. *Ultrasonics Sonochemistry*, 17, 566-71.

Gedanken, A., 2004. Using sonochemistry for the fabrication of nanomaterials. *Ultrasonics Sonochemistry*, 11, 47-55.

Ghauch, A., Tuqan, A.M., Kibbi, N., 2012. Ibuprofen removal by heated persulfate in aqueous solution: A kinetics study. *Chemical Engineering Journal*, 197, 483-492.

Gogate, P.R., Sutkar, V.S., Pandit, A.B., 2011. Sonochemical reactors: Important design and scale up considerations with a special emphasis on heterogeneous systems. *Chemical Engineering Journal*, 166, 1066-1082.

Gottschalk, C., Libra, J., Saupe, A., 2000. *Ozonation of water and waste water: A practical guide to understanding ozone and its application*. Wiley-VCH Verlag GmbH, Weinheim, Germany.

Gültekin, I., Ince, N.H., 2008. Ultrasonic destruction of bisphenol-A: The operating parameters. *Ultrasonics Sonochemistry*, 15, 524-529.

Gültekin, I., Ince, N.H., 2006. Degradation of aryl-azo-naphthol dyes by ultrasound, ozone and their combination: effect of alpha-substituents. *Ultrasonics Sonochemistry*, 13, 208-14.

Guo, Y., Yang, L., Wang, X., 2012. The application and reaction mechanism of catalytic ozonation in water treatment. *Journal of Environmental and Analytical Toxicology*, 2, 7, 1-6.

Gutierrez, M., Henglein, A., Ibanez, F., 1991. Radical Scavenging In the Sonolysis of Aqueous Solutions of I⁻, Br⁻, and N₃⁻. *Journal of Physical Chemistry*, 95, 6044-6047.

Jones, H.O., Voulvoulis, N., Lester, J.N., 2005. Human pharmaceuticals in wastewater treatment processes. *Critical Reviews in Environmental Science and Technology*, 35, 401-427.

Habibi, M.H., Vosooghian, H., 2005. Photocatalytic degradation of some organic sulfides as environmental pollutants using titanium dioxide suspension. *Journal of Photochemistry and Photobiology A: Chemistry*, 174, 45-52.

Hajibabania, S., Verliefde, A., McDonald, J.A., Khan, S.J., Le-Clech, P., 2011. Fate of trace organic compounds during treatment by nanofiltration. *The Journal of Membrane Science*, 373, 130-139.

Hamdi El Najjar, N., Touffet, A., Deborde, M., Journal, R., Karpel Vel Leitner, N., 2014. Kinetics of paracetamol oxidation by ozone and hydroxyl radicals, formation of transformation products and toxicity. *Separation and Purification Technology*, 136, 137-143.

Han, G.H., Hur, H.G., Kim, S.D., 2006. Ecotoxicological risk of pharmaceuticals from wastewater treatment plants in Korea: occurrence and toxicity to *Daphnia magna*. *Environmental Toxicology and Chemistry*, 25, 265-71.

Hao, F., Guo, W., Wang, A., Leng, Y., Li, H., 2014. Intensification of sonochemical degradation of ammonium perfluorooctanoate by persulfate oxidant. *Ultrasonics Sonochemistry*, 21, 554-558.

Harnagea-Theophilus, E., Gadd, S.L., Knight-Trent, H., DeGeorge, G.L., Miller, M.R., 1999. Acetaminophen-induced proliferation of breast cancer cells involves estrogen receptors. *Toxicology and Applied Pharmacology*, 155, 273-279.

Hart, E.J., Henglein, A., 1985. Free radical and free atom reactions in the sonolysis of aqueous iodide and formate solutions. *Journal of Physical Chemistry*, 89, 4342-4347.

Hartmann, J., Bartels, P., Mau, U., Witter, M., Tümpling, W. V, Hofmann, J., Nietzschmann, E., 2008. Degradation of the drug diclofenac in water by sonolysis in presence of catalysts. *Chemosphere*, 70, 453-61.

He, H., Zhong, Y., Liang, X., Tan, W., Zhu, J., Wang, C.Y., 2015. Natural Magnetite: an efficient catalyst for the degradation of organic contaminant. *Scientific Reports*, 5, 10139.

Heberer, T., 2002. Occurrence, fate, and removal of pharmaceutical residues in the aquatic environment: a review of recent research data. *Toxicol. Lett.* 131, 5-17.

Heberer, T., Verstraeten, I.M., Meyer, M.T., Mechlinski, A., Reddersen, K., 2000. Occurrence and fate of pharmaceuticals during bank filtration- preliminary results from investigations in Germany and The United States. *Journal of Contemporary Water Research and Education*, 120, 4-17.

Henschel, K.P., Wenzel, A, Diedrich, M., Fliedner, A, 1997. Environmental hazard assessment of pharmaceuticals. *Regulatory Toxicology and Pharmacology*, 25, 220-225.

Her, N., Park, J.-S., Yoon, Y., 2011. Sonochemical enhancement of hydrogen peroxide production by inert glass beads and TiO₂-coated glass beads in water. *Chemical Engineering Journal*, 166, 184-190.

Hirakawa, T., Nosaka, Y., 2002. Properties of O₂• and OH• Formed in TiO₂ Aqueous Suspensions by Photocatalytic Reaction and the Influence of H₂O₂ and Some Ions. *Langmuir* 18, 3247-3254.

Hofmann, J., Freier, U., Wecks, M., Hohmann, S., 2007. Degradation of diclofenac in water by heterogeneous catalytic oxidation with H₂O₂. *Applied Catalysis B: Environmental*, 70, 447-451.

Hoigné, J., Bader, H., 1983. Rate constants of reactions of ozone with organic and inorganic compounds in water-II: Dissociating organic compounds. *Water Research*, 17, 185-194.

Holm, J. V, Ruegge, K., Bjerg, P.L., Christensen, T.H., 1995. Occurrence and distribution of pharmaceutical organic compounds in the groundwater downgradient of a landfill (Grindsted, Denmark). *Environmental Science and Technology*, 29, 1415-1420.

Homlok, R., Takács, E., Wojnárovits, L., 2011. Elimination of diclofenac from water using irradiation technology. *Chemosphere*, 85, 603-8.

Hong, J., Chu, W., Chen, M., Wang, X., Zhang, T., 2007. Preparation of novel titania supported palladium catalysts for selective hydrogenation of acetylene to ethylene. *Catalysis Communications*, 8, 593-597.

Hori, H., Nagano, Y., Murayama, M., Koike, K., Kutsuna, S., 2012. Efficient decomposition of perfluoroether carboxylic acids in water with a combination of persulfate oxidant and ultrasonic irradiation. *Journal of Fluorine Chemistry*, 141, 5-10.

Hua, I., Hoffmann, M.R., 1997. Optimization of ultrasonic irradiation as an advanced oxidation technology. *Environmental Science and Technology*, 31, 2237-2243.

Huang, K., Couttenye, R.A., Hoag, G.E., 2002. Kinetics of heat-assisted persulfate oxidation of methyl tert -butyl ether (MTBE). *Chemosphere*, 49, 413-420.

Huang, W., 2012. Homogeneous and heterogeneous Fenton and photo-Fenton processes : impact of iron complexing agent ethylenediamine-N , N ' -disuccinic acid (EDDS), PhD Thesis, Universite Blaise Pascal.

Huber, M.M., Canonica, S., Park, G.-Y., von Gunten, U., 2003. Oxidation of pharmaceuticals during ozonation and advanced oxidation processes. *Environmental Science and Technology*, 37, 1016-24.

Huber, M.M., Göbel, A., Joss, A., Hermann, N., Löffler, D., McArdell, C.S., Ried, A., Siegrist, H., Ternes, T. a, von Gunten, U., 2005. Oxidation of pharmaceuticals during ozonation of municipal wastewater effluents: a pilot study. *Environmental Science and Technology*, 39, 4290-4299.

Hung, H.-M., Ling, F.H., Hoffmann, M.R., 1998. Kinetics and mechanism of the enhanced reductive degradation of nitrobenzene by elemental iron in the presence of ultrasound. *Environmental Science and Technology*, 34, 1758-1763.

Hutt, A.J., Caldwell, J., 1983. The metabolic chiral inversion of 2-arylpropionic acids - a novel route with pharmacological consequences. *The Journal of Pharmacy and Pharmacology*, 35, 693-704.

Ikehata, K., Jodeiri Naghashkar, N., Gamal El-Din, M., 2006. Degradation of aqueous pharmaceuticals by ozonation and advanced oxidation processes: A review. *Ozone: Science & Engineering*, 28, 353-414.

Ikhlaq, A., Brown, D.R., Kasprzyk-Hordern, B., 2015. Catalytic ozonation for the removal of organic contaminants in water on alumina. *Applied Catalysis B: Environmental*, 165, 408-418.

Ikhlaq, A., Brown, D.R., Kasprzyk-Hordern, B., 2013. Mechanisms of catalytic ozonation: An investigation into superoxide ion radical and hydrogen peroxide formation during catalytic ozonation on alumina and zeolites in water. *Applied Catalysis B: Environmental*, 129, 437-449.

Ikhlaq, A., Brown, D.R., Kasprzyk-Hordern, B., 2012. Mechanisms of catalytic ozonation on alumina and zeolites in water: Formation of hydroxyl radicals. *Applied Catalysis B: Environmental*, 123-124, 94-106.

Im, J.-K., Boateng, L.K., Flora, J.R.V., Her, N., Zoh, K.-D., Son, A., Yoon, Y., 2014. Enhanced ultrasonic degradation of acetaminophen and naproxen in the presence of powdered activated carbon and biochar adsorbents. *Separation and Purification Technology*, 123, 96-105.

Ince, N.H., 1999. Critical effect of hydrogen peroxide in Photochemical dye degradation. *Water Research*, 33, 1080-1084.

Ince, N.H., Apikyan, I.G., 2000. Combination of activated carbon adsorption with light-enhanced chemical oxidation via hydrogen peroxide. *Water Research*. 34, 4169-4176.

Ince, N.H., Gültekin, I., Tezcanli-Güyer, G., 2009. Sonochemical destruction of nonylphenol: effects of pH and hydroxyl radical scavengers. *Journal of Hazardous Materials*, 172, 739-743.

Ince, N.H., Tezcanli-Güyer, G., 2004. Impacts of pH and molecular structure on ultrasonic degradation of azo dyes. *Ultrasonics*, 42, 591-6.

Ince, N.H., Tezcanli, G., Belen, R.K., Apikyan, I., 2001. Ultrasound as a catalyzer of aqueous reaction systems: The state of the art and environmental applications. *Applied Catalysis B: Environmental*, 29, 167-176.

Ince, N.H., Tezcanlı, G., 2001. Reactive dyestuff degradation by combined sonolysis and ozonation. *Dyes and Pigments*, 49, 145-153.

Isariebel, Q., Carine, J., Ulises-javier, J., Anne-marie, W., Henri, D., 2009. Ultrasonics sonochemistry sonolysis of levodopa and paracetamol in aqueous solutions. *Ultrasonics Sonochemistry*, 16, 610-616.

Isidori, M., Lavorgna, M., Nardelli, A., Parrella, A., Previtera, L., Rubino, M., 2005. Ecotoxicity of naproxen and its phototransformation products. *Science of the Total Environment*, 348, 93-101.

Ismail, A.A., Bahnemann, D.W., Robben, L., Yarovy, V., Wark, M., 2010. Palladium doped porous titania photocatalysts: Impact of mesoporous order and crystallinity. *Chemistry of Materials*, 22, 108-116.

Jagannathan, M., Grieser, F., Ashokkumar, M., 2013. Sonophotocatalytic degradation of paracetamol using TiO₂ and Fe³⁺. *Separation and Purification Technology*, 103, 114-118.

Javier Benitez, F., Acero, J.L., Real, F.J., Roldán, G., 2009. Ozonation of pharmaceutical compounds: Rate constants and elimination in various water matrices. *Chemosphere* 77, 53-59.

Jin, L.-Y., Ma, R.-H., Lin, J.-J., Meng, L., Wang, Y.-J., Luo, M.-F., 2011. Bifunctional Pd/Cr₂O₃-ZrO₂ catalyst for the oxidation of volatile organic compounds. *Industrial and Engineering Chemistry Research*, 50, 10878-10882.

Johnson, K.A., Plumb, R., 2005. Investigating the human metabolism of acetaminophen using UPLC and exact mass oa-TOF MS. *Journal of Pharmaceutical and Biomedical Analysis*, 39, 805–810.

Joss, A., Keller, E., Alder, A.C., Göbel, A., McArdell, C.S., Ternes, T., Siegrist, H., 2005. Removal of pharmaceuticals and fragrances in biological wastewater treatment. *Water Research*, 39, 3139–3152.

Joss, A., Zabczynski, S., Göbel, A., Hoffmann, B., Löffler, D., McArdell, C.S., Ternes, T.A., Thomsen, A., Siegrist, H., 2006. Biological degradation of pharmaceuticals in municipal wastewater treatment: proposing a classification scheme. *Water Research*, 40, 1686-96.

Julien, F., Gueroux, B., Mazet, M., 1994. Comparison of organic compounds removal by coagulation-flocculation and by adsorption onto performed hydroxide floc. *Water Research*, 28, 2567-2574.

Kalathil, S., Khan, M.M., Banerjee, A.N., Lee, J., Cho, M.H., 2012. A simple biogenic route to rapid synthesis of Au@TiO₂ nanocomposites by electrochemically active biofilms. *The Journal of Nanoparticle Research*, 14, 1051.

Kamat, P. V., 2007. Meeting the clean energy demand: nanostructure architectures for solar energy conversion. *Journal of Physical Chemistry C*, 111, 2834-2860.

Kang, J.-W., Hung, H.-M., Lin, A., Hoffmann, M.R., 1999. Sonolytic destruction of methyl tert -butyl ether by ultrasonic. *Environmental Science and Technology*, 33, 3199-3205.

Kansal, S.K., Sood, S., Umar, A., Mehta, S.K., 2013. Photocatalytic degradation of Eriochrome Black T dye using well-crystalline anatase TiO₂ nanoparticles. *The Journal of Alloys and Compounds*, 581, 392-397.

Kasprzyk-Hordern, B., 2004. Chemistry of alumina, reactions in aqueous solution and its application in water treatment. *Advances in Colloid and Interface Science*, 110, 19-48.

Kasprzyk-Hordern, B., 2003. Catalytic ozonation and methods of enhancing molecular ozone reactions in water treatment. *Applied Catalysis B: Environmental*, 46, 639-669.

Kasprzyk-Hordern, B., Andrzejewski, P., Dabrowska, A., Czaczyk, K., Nawrocki, J., 2004. MTBE, DIPE, ETBE and TAME degradation in water using perfluorinated phases as catalysts for ozonation process. *Applied Catalysis B: Environmental*, 51, 51-66.

Kasprzyk-Hordern, B., Nawrocki, J., 2003. The feasibility of using a perfluorinated bonded alumina phase in the ozonation process. *Ozone: Science & Engineering*, 25, 185-197.

Kasprzyk-Hordern, B., Raczyk-Stanisławiak, U., Świetlik, J., Nawrocki, J., 2006. Catalytic ozonation of natural organic matter on alumina. *Applied Catalysis B: Environmental*, 62, 345-358.

Kasprzyk, B., Nawrocki, J., 2002. Preliminary results on ozonation enhancement by a perfluorinated bonded alumina phase. *Ozone: Science & Engineering*, 24, 63-68.

Katsumata, H., Sada, M., Kaneco, S., Suzuki, T., Ohta, K., Yobiko, Y., 2008. Humic acid degradation in aqueous solution by the photo-Fenton process. *Chemical Engineering Journal*, 137, 225-230.

Kenzo, H., 1967. *Handbook of Ultraviolet and Visible Absorption Spectra of Organic Compound*, Plenum Press Data Division, New York.

Keykavoos, R., Mankidy, R., Ma, H., Jones, P., Soltan, J., 2013. Mineralization of bisphenol A by catalytic ozonation over alumina. *Separation and Purification Technology*, 107, 310-317.

Kiassen, N. V., Marchington, D., McGowan, H.C.E., 1994. H_2O_2 determination by the I_3^- method and by KMO_4 Titration. *Analytical Chemistry*, 66, 2921-2925.

Kidak, R., Ince, N.H., 2006. Effects of operating parameters on sonochemical decomposition of phenol. *Journal of Hazardous Materials*, 137, 1453-7.

Kim, E., Cui, M., Jang, M., Park, B., Son, Y., Khim, J., 2014. Investigation of sonochemical activities at a frequency of 334 kHz: the effect of geometric parameters of sonoreactor. *Ultrasonics Sonochemistry*, 21, 1504-11.

Kim, I., Tanaka, H., 2009. Photodegradation characteristics of PPCPs in water with UV treatment. *Environment International*, 35, 793-802.

Kim, I., Yamashita, N., Tanaka, H., 2009. Performance of UV and UV/H₂O₂ processes for the removal of pharmaceuticals detected in secondary effluent of a sewage treatment plant in Japan. *Journal of Hazardous Materials*, 166, 1134-1140.

Kim, J.K., Martinez, F., Metcalfe, I.S., 2007. The beneficial role of use of ultrasound in heterogeneous Fenton-like system over supported copper catalysts for degradation of p-chlorophenol. *Catalysis Today* 124, 224-231.

Kim, S.D., Cho, J., Kim, I.S., Vanderford, B.J., Snyder, S.A., 2007. Occurrence and removal of pharmaceuticals and endocrine disruptors in South Korean surface, drinking, and waste waters. *Water Research*, 41, 1013-1021.

Kimura, T., Sakamoto, T., Leveque, J., Sohmiya, H., Fujita, M., Ikeda, S., Ando, T., 1996. Standardization of ultrasonic power for sonochemical reaction. *Ultrasonics Sonochemistry*, 3, S157-S161.

Klavarioti, M., Mantzavinos, D., Kassinos, D., 2009. Removal of residual pharmaceuticals from aqueous systems by advanced oxidation processes. *Environment International*, 35, 402-417.

Koltypin, Y., Perkas, N., Gedanken, A., 2004. Commercial edible oils as new solvents for ultrasonic synthesis of nanoparticles: the preparation of air stable nanocrystalline iron particles. *Journal of Materials Chemistry*, 14, 2975.

Kuang, Y., Wang, Q., Chen, Z., Megharaj, M., Naidu, R., 2013. Heterogeneous Fenton-like oxidation of monochlorobenzene using green synthesis of iron nanoparticles. *The Journal of Colloid and Interface Science*, 410, 67-73.

Kulik, N., Trapido, M., Goi, A., Veressinina, Y., Munter, R., 2008. Combined chemical treatment of pharmaceutical effluents from medical ointment production. *Chemosphere*, 70, 1525-31.

Kümmerer, K., 2001. Drugs in the environment: Emission of drugs, diagnostic aids and disinfectants into wastewater by hospitals in relation to other sources - A review. *Chemosphere*, 45, 957-969.

Lamsal, R., Walsh, M.E., Gagnon, G. a, 2011. Comparison of advanced oxidation processes for the removal of natural organic matter. *Water Research*, 45, 3263-3269.

Landi, M., Naddeo, V., 2011. AOPs Technologies: An Overview. In Belgiorno, V., Naddeo, V., Rizzo, L. (Eds.), *Water, Wastewater and Soil Treatment by AOP*, 23-40, SEED, Sanitary Environmental Engineering Division, Fisciano, Italy.

Laugier, F., Andriantsiferana, C., Wilhelm, A.M., Delmas, H., 2008. Ultrasonics Sonochemistry Ultrasound in gas – liquid systems : Effects on solubility and mass transfer. *Ultrasonics Sonochemistry*, 15, 965-972.

Lee, Y.-C., Lo, S.-L., Kuo, J., Lin, Y.-L., 2012. Persulfate oxidation of perfluorooctanoic acid under the temperatures of 20–40°C. *Chemical Engineering Journal*, 198-199, 27-32.

Leighton, T., 1995. Bubble population phenomena in acoustic cavitation. *Ultrasonics Sonochemistry*, 2, S123-S136.

Li, D., Qu, J., 2009. The progress of catalytic technologies in water purification: A review. *Journal of Environmental Sciences*, 21, 713-719.

Li, F.B., Li, X.Z., 2002. The enhancement of photodegradation efficiency using Pt-TiO₂ catalyst. *Chemosphere*, 48, 1103-1111.

Li, X., Elliott, D.W., Zhang, W., 2006. Zero-Valent iron nanoparticles for abatement of environmental pollutants: materials and engineering aspects. *Critical Reviews in Solid State and Materials Sciences*, 31, 111-122.

Lin, J., Kawai, A., Nakajima, T., 2002. Effective catalysts for decomposition of aqueous ozone. *Applied Catalysis B: Environmental*, 39, 157-165.

Lindqvist, N., Tuhkanen, T., Kronberg, L., 2005. Occurrence of acidic pharmaceuticals in raw and treated sewages and in receiving waters. *Water Research*, 39, 2219-28.

Lorimer, J.P., Mason, T.J., 1987. Sonochemistry part 1-The physical aspects. *Chemical Society Reviews*, 16, 239-274.

Madhavan, J., Grieser, F., Ashokkumar, M., 2010a. Combined advanced oxidation processes for the synergistic degradation of ibuprofen in aqueous environments. *Journal of Hazardous Materials*, 178, 202-208.

Madhavan, J., Kumar, P.S.S., Anandan, S., Zhou, M., Grieser, F., Ashokkumar, M., 2010b. Ultrasound assisted photocatalytic degradation of diclofenac in an aqueous environment. *Chemosphere*, 80, 747-52.

Mansoori, G.A., Bastami, T.R., Ahmadpour, A., Eshaghi, Z., 2008. Environmental application of nanotechnology. *Annual Review of Nano Research*, 2, 1-73.

Mark, G., Schuchmann, M., Schuchmann, H.P., Sonntag, C., 1990. A chemical actinometer for use in connection with UV treatment in drinking water processing. *Journal of Water Supply: Research and Technology*, 39, 309-313.

Martínez, C., Canle L., M., Fernández, M.I., Santaballa, J. a., Faria, J., 2011. Aqueous degradation of diclofenac by heterogeneous photocatalysis using nanostructured materials. *Applied Catalysis B: Environmental*, 107, 110-118.

Mason, T., Cobley, A., Graves, J., Morgan, D., 2011. New evidence for the inverse dependence of mechanical and chemical effects on the frequency of ultrasound. *Ultrasonics Sonochemistry*, 18, 226.

Mason, T.J., 2003. Sonochemistry and sonoprocessing: the link, the trends and (probably) the future. *Ultrasonics Sonochemistry*, 10, 175-179.

Mason, T.J., 1999. *Sonochemistry*, Oxford University Press Inc., New York.

Mason, T.J., Lorimer, J.P., 2002. *Applied Sonochemistry*. Wiley-VCH Verlag GmbH and Co. KGaA, Weinheim, Germany.

Mason, T.J., Peter, D., 2002. *Practical Sonochemistry, Second Edition: Power Ultrasound Uses and Applications*, Horwood Chemical Science Series.

Matilainen, A., Sillanpää, M., 2010. Removal of natural organic matter from drinking water by advanced oxidation processes. *Chemosphere*, 80, 351-365.

Matta, R., Hanna, K., Chiron, S., 2007. Fenton-like oxidation of 2,4,6-trinitrotoluene using different iron minerals. *Science of the Total Environment*, 385, 242-251.

Méndez-Arriaga, F., Torres-Palma, R. a, Pétrier, C., Esplugas, S., Gimenez, J., Pulgarin, C., 2009. Mineralization enhancement of a recalcitrant pharmaceutical pollutant in water by advanced oxidation hybrid processes. *Water Research*, 43, 3984-3991.

Méndez-Arriaga, F., Torres-Palma, R. a, Pétrier, C., Esplugas, S., Gimenez, J., Pulgarin, C., 2008. Ultrasonic treatment of water contaminated with ibuprofen. *Water Research*, 42, 4243-4238.

Miège, C., Choubert, J.M., Ribeiro, L., Eusèbe, M., Coquery, M., 2009. Fate of pharmaceuticals and personal care products in wastewater treatment plants - Conception of a database and first results. *Environmental Pollution*, 157, 1721-1726.

Mills, A., Lee, S.-K., 2004. Semiconductor Photocatalysis, in: Parsons, S. (Ed.), *Advanced Oxidation Processes for Water and Wastewater Treatment*, 137–166, IWA Publishing, TJ International, London, UK, pp..

Mizukoshi, Y., Makise, Y., Shuto, T., Hu, J., Tominaga, A., Shironita, S., Tanabe, S., 2007. Immobilization of noble metal nanoparticles on the surface of TiO₂ by the sonochemical method: photocatalytic production of hydrogen from an aqueous solution of ethanol. *Ultrasonics Sonochemistry*, 14, 387-392.

Mizukoshi, Y., Oshima, R., Maeda, Y., Nagata, Y., 1999. Preparation of Platinum Nanoparticles by Sonochemical Reduction of the Pt(II) Ion. *Langmuir* 15, 2733-2737.

Mizukoshi, Y., Sato, K., Konno, T.J., Masahashi, N., 2010. Dependence of photocatalytic activities upon the structures of Au/Pd bimetallic nanoparticles immobilized on TiO₂ surface. *Applied Catalysis B: Environmental*, 94, 248-253.

Moctezuma, E., Leyva, E., Aguilar, C.A., Luna, R.A., Montalvo, C., 2012. Photocatalytic degradation of paracetamol: Intermediates and total reaction mechanism. *Journal of Hazardous Materials*, 243, 130-138.

Mogyorósi, K., Kmetykó, Á., Czirbus, N., Veréb, G., Sipos, P., Dombi, A., 2009. Comparison of the substrate dependent performance of Pt-, Au- and Ag-doped TiO₂ photocatalysts in H₂-production and in decomposition of various organics. *Reaction Kinetics and Catalysis Letters*, 98, 215-225.

Moldovan, Z., 2006. Occurrences of pharmaceutical and personal care products as micropollutants in rivers from Romania. *Chemosphere*, 64, 1808-1817.

Molina, R., Martínez, F., Melero, J.A., Bremner, D.H., Chakinala, A.G., 2006. Mineralization of phenol by a heterogeneous ultrasound/Fe-SBA-15/H₂O₂ process: Multivariate study by factorial design of experiments. *Applied Catalysis B: Environmental*, 66, 198-207.

Mompelat, S., Le Bot, B., Thomas, O., 2009. Occurrence and fate of pharmaceutical products and by-products, from resource to drinking water. *Environment International*, 35, 803-814.

Munter, R., 2001. Advanced Oxidation Processes - Current Status and Prospect. *Proceedings of the Estonian Academy of Sciences: Chemistry*, 50, 59-80.

Naddeo, V., Belgiorno, V., Kassinos, D., Mantzavinos, D., Meric, S., 2010. Ultrasonic degradation, mineralization and detoxification of diclofenac in water: optimization of operating parameters. *Ultrasonics Sonochemistry*, 17, 179-185.

Naddeo, V., Belgiorno, V., Ricco, D., Kassinos, D., 2009a. Degradation of diclofenac during sonolysis, ozonation and their simultaneous application. *Ultrasonics Sonochemistry*, 16, 790-794.

Naddeo, V., Meriç, S., Kassinos, D., Belgiorno, V., Guida, M., 2009b. Fate of pharmaceuticals in contaminated urban wastewater effluent under ultrasonic irradiation. *Water Research*, 43, 4019-4027.

Nakada, N., Shinohara, H., Murata, A., Kiri, K., Managaki, S., Sato, N., Takada, H., 2007. Removal of selected pharmaceuticals and personal care products (PPCPs) and endocrine-disrupting chemicals (EDCs) during sand filtration and ozonation at a municipal sewage treatment plant. *Water Research*. 41, 4373-4382.

Newman, C.M.H., Bettinger, T., 2007. Gene therapy progress and prospects: Ultrasound for gene transfer. *Gene Therapy*, 14, 465-475.

Nikitenko, S.I., Koltypin, Y., Palchik, O., Felner, I., Xu, X.N., Gedanken, A., 2001. Synthesis of highly magnetic, air-stable iron-iron carbide nanocrystalline particles by using power ultrasound. *Angewandte Chemie International Edition*, 40, 23, 4447-4449.

Nikolaou, A., Meric, S., Fatta, D., 2007. Occurrence patterns of pharmaceuticals in water and wastewater environments. *Analytical and Bioanalytical Chemistry*, 387, 1225-1234.

O'Carroll, D., Sleep, B., Krol, M., Boparai, H., Kocur, C., 2013. Nanoscale zero valent iron and bimetallic particles for contaminated site remediation. *Advances in Water Resources*, 51, 104-122.

Okitsu, K., 2011. Sonochemical Synthesis of Metal Nanoparticles. In Pankaj, Ashokkumar, M. (Eds.), *Theoretical and Experimental Sonochemistry Involving Inorganic Systems*, 131-150, Springer Sciences Business Media, London.

Okitsu, K., Ashokkumar, M., Grieser, F., 2005. Sonochemical synthesis of gold nanoparticles: effects of ultrasound frequency. *The Journal of Physical Chemistry B*, 109, 20673-20675.

Ökte, A.N., Tuncel, D., Pekcan, A.H., Özden, T., 2014. Characteristics of iron-loaded TiO₂ supported montmorillonite catalysts: Naphthol degradation under UV-A irradiation. *Journal of Chemical Technology and Biotechnology*, 89, 1155-1167.

Onesios, K.M., Yu, J.T., Bouwer, E.J., 2009. Biodegradation and removal of pharmaceuticals and personal care products in treatment systems: A review. *Biodegradation* 20, 441-466.

Oppenlander, T., 2003. *Photochemical Purification of Water and Air Advanced Oxidation Processes: Principles, Reaction Mechanisms, Reactor Concepts*, Wiley-VCH Verlag GmbH and Co. KGaA, Weinheim, Germany.

Oyama, S.T., 2000. Chemical and Catalytic Properties of Ozone. *Catalysis Reviews*, 42, 279-322.

Packer, J.L., Werner, J.J., Latch, D.E., McNeill, K., Arnold, W.A., 2003. Photochemical fate of pharmaceuticals in the environment: Naproxen, diclofenac, clofibric acid, and ibuprofen. *Aquatic Sciences - Research Across Boundaries*, 65, 342-351.

Paje, M.L.F., Kuhlicke, U., Winkler, M., Neu, T.R., 2002. Inhibition of lotic biofilms by diclofenac. *Applied Microbiology and Biotechnology*, 59, 488-492.

Papadaki, M., Emery, R.J., Abu-Hassan, M.A., Díaz-Bustos, A., Metcalfe, I.S., Mantzavinos, D., 2004. Sonocatalytic oxidation processes for the removal of contaminants containing aromatic rings from aqueous effluents. *Separation and Purification Technology*, 34, 35-42.

Parsons, S., William, M., 2004. *Advanced Oxidation Processes for Water and Wastewater Treatment*, IWA Publishing, London.

Pavia, D., Lampman, G., Kriz, G., 2001. *Introduction to Spectroscopy*, Third Edit., Brooks/Cole Thomson Learning, Australia.

Pereira, V.J., Linden, K.G., Weinberg, H.S., 2007. Evaluation of UV irradiation for photolytic and oxidative degradation of pharmaceutical compounds in water. *Water Research*, 41, 4413-4423.

Pérez-Estrada, L. A., Maldonado, M.I., Gernjak, W., Agüera, A., Fernández-Alba, A. R., Ballesteros, M.M., Malato, S., 2005. Decomposition of diclofenac by solar driven photocatalysis at pilot plant scale. *Catalysis Today*, 101, 219-226.

Pérez-Estrada, L., Malato, S., Gernjak, W., Agüera, A., Thurman, E.M., Ferrer, I., Fernández-Alba, A.R., 2005. Photo-fenton degradation of diclofenac: identification of main intermediates and degradation pathway. *Environmental Science and Technology*, 39, 8300-8306.

Petrier, C., Casadonte, D., 2001. The Sonochemical Degradation of Aromatic and Chloroaromatic Contaminants. In Mason, T.J., Tiehm, A. (Eds.), *Advances in*

Sonochemistry: Ultrasound in Environmental Protection, 91–109, JAI Press Inc. Elsevier Science B.V., Connecticut, USA.

Petrier, C., Francony, A., 1997. Ultrasonic waste-water treatment : Incidence of ultrasonic frequency on the rate of phenol and carbon tetrachloride degradation. *Ultrasonics Sonochemistry*, 4, 295-300.

Petrier, C., Jeunet, A., Luche, J.-L., Reverdy, G., 1992. Unexpected frequency effects on the rate of oxidative processes induced by ultrasound. *Journal of American Chemical Society*, 114, 3148-3150.

Pines, D.S., Reckhow, D.A., 2003. Solid phase catalytic ozonation process for the destruction of a model pollutant. *Ozone: Science & Engineering*, 25, 25-39.

Pocostales, P., Álvarez, P., Beltrán, F.J., 2011. Catalytic ozonation promoted by alumina-based catalysts for the removal of some pharmaceutical compounds from water. *Chemical Engineering Journal*, 168, 1289-1295.

Pozdnyakov, I.P., Zhang, X., Maksimova, T. a., Yanshole, V. V., Wu, F., Grivin, V.P., Plyusnin, V.F., 2014. Wavelength-dependent photochemistry of acetaminophen in aqueous solutions. *Journal of Photochemistry and Photobiology A: Chemistry*, 274, 117-123.

Primo, A., Corma, A., García, H., 2011. Titania supported gold nanoparticles as photocatalyst. *Chemical Physics*, 13, 886-910.

Pupo, R.F., Agu, A., Trovo, A.G., 2012. Paracetamol degradation intermediates and toxicity during photo-Fenton treatment using different iron species. *Water Research*, 6, 3-9.

Qi, F., Chen, Z., Xu, B., Shen, J., Ma, J., Joll, C., Heitz, A., 2008. Influence of surface texture and acid-base properties on ozone decomposition catalyzed by aluminum (hydroxyl) oxides. *Applied Catalysis B: Environmental*, 84, 684-690.

Qi, F., Xu, B., Chen, Z., Feng, L., Zhang, L., Sun, D., 2013. Catalytic ozonation of 2-isopropyl-3-methoxypyrazine in water by γ -AlOOH and γ -Al₂O₃: Comparison of removal efficiency and mechanism. *Chemical Engineering Journal*, 219, 527-536.

Quintana, J.B., Weiss, S., Reemtsma, T., 2005. Pathways and metabolites of microbial degradation of selected acidic pharmaceutical and their occurrence in municipal wastewater treated by a membrane bioreactor. *Water Research*, 39, 2654-2664.

Ratpukdi, T., Siripattanakul, S., Khan, E., 2010. Mineralization and biodegradability enhancement of natural organic matter by ozone-VUV in comparison with ozone, VUV, ozone-UV, and UV: effects of pH and ozone dose. *Water Research*, 44, 3531-3543.

Ravina, M., Campanella, L., Kiwi, J., 2002. Accelerated mineralization of the drug Diclofenac via Fenton reactions in a concentric photo-reactor. *Water Research*, 36, 3553-3560.

Remberger, M., Wiklund, P., Woldegiorgis, A., Viktor, T., Kaj, L., Brorström-lundén, E., 2009. Anti-inflammatory and analgesic drugs in WWTP influent and effluent streams and the occurrence in the aquatic environment. No B1810, Swedish Research Institute.

Ricco, D., Naddeo, V., 2011. Emerging Contaminants Removal from Urban Wastewater by Ultrasonic based AOPs. In Belgiorno, V., Naddeo, V., Rizzo, L. (Eds.), *Water, Wastewater and Soil Treatment by AOPs*, 115–137, SEED, Sanitary Environmental Engineering Division, Fisciano, Italy.

Rizzo, L., Meric, S., Kassinos, D., Guida, M., Russo, F., Belgiorno, V., 2009. Degradation of diclofenac by TiO₂ photocatalysis: UV absorbance kinetics and process evaluation through a set of toxicity bioassays. *Water Research*. 43, 979-88.

Rodríguez-Gil, J.L., Catalá, M., Alonso, S.G., Maroto, R.R., Valcárcel, Y., Segura, Y., Molina, R., Melero, J.A, Martínez, F., 2010. Heterogeneous photo-Fenton treatment for the reduction of pharmaceutical contamination in Madrid rivers and ecotoxicological evaluation by a miniaturized fern spores bioassay. *Chemosphere*, 80, 381-388.

Rodriguez, S.M., Nikolaus, K., Alberola, I.O., Sierra, A.Z., 2013. Solar Photo-Fenton as Advanced Oxidation Technology for Water Remediation, in: Rao, D., Senthilkumar, R., Anthony Byrne, J., Feroz, S. (Eds.), *Wastewater Treatment: Advanced Processes and Technologies*, 11-35, IWA Publishing, CRC Press Taylor and Francis Group, Boca Raton, FL, USA.

Rooze, J., Rebrov, E. V., Schouten, J.C., Keurentjes, J.T.F., 2013. Dissolved gas and ultrasonic cavitation - A review. *Ultrasonics Sonochemistry*, 20, 1-11.

Rosal, R., Rodríguez, A., Gonzalo, M.S., García-Calvo, E., 2008. Catalytic ozonation of naproxen and carbamazepine on titanium dioxide. *Applied Catalysis B: Environmental*, 84, 48-57.

Rosseler, O., Shankar, M. V., Du, M.K. Le, Schmidlin, L., Keller, N., Keller, V., 2010. Solar light photocatalytic hydrogen production from water over Pt and Au/TiO₂ (anatase/rutile) photocatalysts: Influence of noble metal and porogen promotion. *Journal of Catalysis*, 269, 179-190.

Roth, J., Sullivan, D., 1981. Solubility of ozone in water. *Industrial and Engineering Chemistry Research*, 20, 137-140.

Rothenberger, G., Moser, J., Graetzel, M., Serpone, N., Sharma, D., 1985. Charge carrier trapping and recombination dynamics in small semiconductor particles. *Journal of American Chemical Society*, 107, 8054-8059.

Ryu, S.Y., Balcerski, W., Lee, T.K., Hoffmann, M.R., 2007. Photocatalytic production of hydrogen from water with visible light using hybrid catalysts of CdS attached to microporous and mesoporous silicas. *The Journal of Physical Chemistry C*, 111, 18195-18203.

Sakthivel, S., Shankar, M. V., Palanichamy, M., Arabindoo, B., Bahnemann, D.W., Murugesan, V., 2004. Enhancement of photocatalytic activity by metal deposition: Characterisation and photonic efficiency of Pt, Au and Pd deposited on TiO₂ catalyst. *Water Research*, 38, 3001-3008.

Salas, S.E., 2013. Photocatalytic Water Splitting using a Modified Pt- TiO₂, Kinetic Modeling and Hydrogen Production Efficiency. PhD Thesis, The University of Western Ontario.

San Sebastian Martinez, N., Figuls Fernandez, J., Font Segura, X., Sanchez Ferrer, A., 2003. Pre-oxidation of an extremely polluted industrial wastewater by the Fenton reagent. *Journal Hazardous Materials*, 101, 315-322.

Sathishkumar, P., Mangalaraja, R.V., Anandan, S., 2016. Review on the recent improvements in sonochemical and combined sonochemical oxidation processes – A powerful tool for destruction of environmental contaminants. *Renewable & Sustainable Energy Reviews*, 55, 426-454.

Sato, M., Itoh, H., Fujii, T., 2000. Frequency dependence of H₂O₂ generation from distilled water. *Ultrasonics*, 38, 312–315.

Scheck, C., 1995a. Degradation of phenol and salicylic acid by ultraviolet radiation/hydrogen peroxide/oxygen. *Water Research*, 29, 2346-2352.

Scheck, C., 1995b. Degradation of phenol and salicylic acid by ultraviolet radiation/hydrogen peroxide/oxygen. *Water Research*, 29, 2346-2352.

Scheytt, T., Mersmann, P., Lindstadt, R., Heberer, T., 2005a. 1-octanol / water partition coefficients of 5 pharmaceuticals from human medical care: carbamazepine, clofibric acid, diclofenac, ibuprofen, and propyphenazone. *Water, Air, & Soil Pollution*, 165, 3-11.

Scheytt, T., Mersmann, P., Lindstädt, R., Heberer, T., 2005b. Determination of sorption coefficients of pharmaceutically active substances carbamazepine, diclofenac, and ibuprofen, in sandy sediments. *Chemosphere*, 60, 245-253.

Schirmer, R., 1991. *Modern Methods of Pharmaceutical Analysis*, Second Ed., CRC Press, Florida, USA.

Schmitt-Jansen, M., Bartels, P., Adler, N., Altenburger, R., 2007. Phytotoxicity assessment of diclofenac and its phototransformation products. *Analytical and Bioanalytical Chemistry*, 387, 1389-1396.

Schwartz, Thomas; Kohnen, Wolfgang; Jansen, Brend; Obst, U., 2003. Detection of antibiotic-resistant bacteria and their resistance genes in wastewater, surface water, and drinking water biofilms. *FEMS Microbiology Ecology*, 43, 325-335.

Sclafani, A., Herrmann, J.-M., 1998. Influence of metallic silver and of platinum-silver bimetallic deposits on the photocatalytic activity of titania (anatase and rutile) in organic and aqueous media. *Journal of Photochemistry and Photobiology A: Chemistry*, 113, 181-188.

Sedlak, D.L., Pinkston, K.E., 2001. Factors affecting the concentrations of pharmaceuticals released to the aquatic environment, *Journal of Contemporary Water Research and Education*, 120, 1, 56-64.

Sein, M.M., Zedda, M., Tuerk, J., Schmidt, T.C., Golloch, A., Von Sonntag, C., 2008. Oxidation of diclofenac with ozone in aqueous solution. *Environmental Science and Technology*, 42, 6656-6662.

Servant, G., Laborde, J.L., Hita, A., Caltagirone, J.P., Gérard, A., 2003. On the interaction between ultrasound waves and bubble clouds in mono- and dual-frequency sonoreactors. *Ultrasonics Sonochemistry*, 10, 347-355.

Shimizu, N., Ogino, C., Dadjour, M.F., Murata, T., 2007. Sonocatalytic degradation of methylene blue with TiO₂ pellets in water. *Ultrasonics Sonochemistry*, 14, 184-190.

Sivakumar, M., Tatake, P.A., Pandit, A.B., 2002. Kinetics of p-nitrophenol degradation: Effect of reaction conditions and cavitation parameters for a multiple frequency system. *Chemical Engineering Journal*, 85, 327-338.

Sivasankar, T., Moholkar, V.S., 2010. Physical insight into the sonochemical degradation of 2,4-dichlorophenol. *Environmental Technology*, 31, 1483-1494.

Snyder, S.A., 2008. Occurrence, treatment, and toxicological relevance of EDCs and pharmaceuticals in water. *Ozone: Science and Engineering*, 30, 65-69.

Sochard, S., Wilhelm, A.M., Delmas, H., 1997. Modelling of free radicals production in a collapsing gas-vapour bubble. *Ultrasonics Sonochemistry*, 4, 2, 77-84.

Song, S., He, Z., Chen, J., 2007. US/O₃ combination degradation of aniline in aqueous solution. *Ultrasonics Sonochemistry*, 14, 84-88.

Soulet, B., Tauxe, A., Tarradellas, J., 2002. Analysis of acidic drugs in swiss wastewaters. *International Journal of Environmental Analytical Chemistry*, 82, 659-667.

Stefan, M., 2004. UV photolysis: Background. In Parsons, S. (Ed.), *Advanced Oxidation Processes for Water and Wastewater Treatment*, 7-43, IWA Publishing, TJ International, London, UK.

Stülten, D., Zühlke, S., Lamshöft, M., Spiteller, M., 2008. Occurrence of diclofenac and selected metabolites in sewage effluents. *Science of the Total Environment*, 405, 310-316.

Stumpf, M., Ternes, T.A, Wilken, R.D., Rodrigues, S.V, Baumann, W., 1999. Polar drug residues in sewage and natural waters in the state of Rio de Janeiro, Brazil. *Science of the Total Environment*, 225, 135-41.

Su, C.C., Bellotindos, L.M., Chang, A.T., Lu, M.C., 2013. Degradation of acetaminophen in an aerated Fenton reactor. *Journal of the Taiwan Institute of Chemical Engineers*, 44, 310-316.

Su, R., Tiruvalam, R., He, Q., Dimitratos, N., Kesavan, L., Hammond, C., Lopez-sanchez, J.A., Bechstein, R., Kiely, C.J., Hutchings, G.J., Besenbacher, F., 2012. Promotion of Phenol Photodecomposition over TiO₂ Using Au, Pd, and Au/Pd. *American Chemical Society:Nano*, 6, 6284-6292.

Su, S., Guo, W., Yi, C., Leng, Y., Ma, Z., 2012. Degradation of amoxicillin in aqueous solution using sulphate radicals under ultrasound irradiation. *Ultrasonics Sonochemistry*, 19, 469-474.

Suarez, S., Lema, J.M., Omil, F., 2009. Pre-treatment of hospital wastewater by coagulation-flocculation and flotation. *Bioresource Technology*, 100, 2138-2146.

Suslick, K., 1990. Sonochemistry. *Science* 247,80, 1349-1445.

Suslick, K., McNamara III, W., Didenko, Y., 1999. Hot Spot Conditions during Multi-Bubble Cavitation in Sonochemistry and Sonoluminescence, Kluwer Publishers, Dordrecht, Netherlands.

Suslick, K.S., 2001. Sonoluminescence and sonochemistry. In Meyers, RA (Eds.), *Encyclopedia of Physical Science and Technology*, 1-21, Academic Press, Inc., San Diego.

Suslick, K.S., Price, G.J., 1999. Applications of ultrasound to materials chemistry. *Annual Review of Materials Science*, 29, 295-326.

Szabo, L., Toth, T., Homlok, R., Takacs, E., Wojnarovits, L., 2012. Radiolysis of paracetamol in dilute aqueous solution. *Radiation Physics and Chemistry*, 81, 1503-1507.

Tauxe-Wuersch, A., De Alencastro, L.F., Grandjean, D., Tarradellas, J., 2005. Occurrence of several acidic drugs in sewage treatment plants in Switzerland and risk assessment. *Water Research*, 39, 1761-1772.

Tekin, H., Bilkay, O., Ataberk, S.S., Balta, T.H., Ceribasi, I.H., Sanin, F.D., Dilek, F.B., Yetis, U., 2006. Use of Fenton oxidation to improve the biodegradability of a pharmaceutical wastewater. *Journal of Hazardous Materials*, 136, 258-265.

Ternes, T., 1998. Occurrence of pharma in German sewage treatment plant and river. *Water Research*, 32, 11, 3245-3260.

Ternes, T., Meisenheimer, M., McDowell, D., Sacher, F., Brauch, H.-J., Haist-Gulde, B., Preuss, G., Wilme, U., Zulei-Seibert, N., 2002. Removal of pharmaceuticals during drinking water treatment. *Environmental Science and Technology*, 36, 3855-3863.

Ternes, T., Stüber, J., Herrmann, N., McDowell, D., Ried, A., Kampmann, M., Teiser, B., 2003. Ozonation: A tool for removal of pharmaceuticals, contrast media and musk fragrances from wastewater? *Water Research*, 37, 1976-1982.

Tezcanli-Güyer, G., Ince, N.H., 2004. Individual and combined effects of ultrasound, ozone and UV irradiation: a case study with textile dyes. *Ultrasonics*, 42, 603-609.

Tezcanlı-Güyer, G., Ince, N.H., 2011. Degradation of diclofenac in water by homogeneous and heterogeneous sonolysis. *Ultrasonics Sonochemistry*, 18, 114-119.

Thompson, L., Doraiswamy, L., 1999. Sonochemistry: science and engineering. *Industrial and Engineering Chemistry*, 38, 1215-1249.

Tian, Y., Tatsuma, T., 2005. Mechanisms and applications of plasmon-induced charge separation at TiO₂ films loaded with gold nanoparticles. *Journal of American Chemical Society*, 127, 7632-7637.

Tiehm, A., Krassnitzer, S., Koltypin, Y., Gedanken, A., 2009. Chloroethene dehalogenation with ultrasonically produced air-stable nano iron. *Ultrasonics Sonochemistry*, 16, 617-621.

Tixier, C., Heinz, P.S., Oellers, S., Müller, S.R., 2003. Occurrence and Fate of Carbamazepine, Clofibric Acid, Diclofenac, Ibuprofen, Ketoprofen, and Naproxen in Surface Waters. *Environmental Science and Technology*, 37, 1061-1068.

Triebkorn, R., Casper, H., Heyd, A., Eikemper, R., Köhler, H.-R., Schwaiger, J., 2004. Toxic effects of the non-steroidal anti-inflammatory drug diclofenac. Part II: cytological effects in liver, kidney, gills and intestine of rainbow trout (*Oncorhynchus mykiss*). *Aquatic Toxicology*, 68, 151-166.

Tronson, R., Ashokkumar, M., Grieser, F., 2002. Comparison of the effects of water-soluble solutes on multibubble sonoluminescence generated in aqueous solutions by 20- and 515-kHz pulsed ultrasound. *Journal of Physical Chemistry B*, 106, 11064-11068.

Tsitonaki, A., Petri, B., Crimi, M., Mosbæk, H., Siegrist, R.L., Bjerg, P.L., 2010. In situ chemical oxidation of contaminated soil and groundwater using persulfate: A review. *Critical Reviews in Environmental Science and Technology*, 40, 55-91.

Tuziuti, T., Yasui, K., Sivakumar, M., Iida, Y., Miyoshi, N., 2005. Correlation between acoustic cavitation noise and yield enhancement of sonochemical reaction by particle addition. *The Journal of Physical Chemistry A*, 109, 4869-4872.

Ullerstam, M., Langer, S., Ljungstro, E., 2000. Coefficients and activation energies for the reaction of butanal and 2-methyl- propanal with nitrate. *International Journal of Chemical Kinetics*, 32, 294-303.

Urase, T., Kikuta, T., 2005. Separate estimation of adsorption and degradation of pharmaceutical substances and estrogens in the activated sludge process. *Water Research*, 39, 1289-1300.

Valdez, H.C.A., Jiménez, G.G., Granados, S.G., León, C.P. De, 2012. Chemosphere Degradation of paracetamol by advance oxidation processes using modified reticulated vitreous carbon electrodes with TiO_2 and $\text{CuO} / \text{TiO}_2 / \text{Al}_2\text{O}_3$. *Chemosphere*, 89, 1195-1201.

Valentine, R.L., Wang, H.C.A., 1998. Iron oxide surface catalyzed oxidation of quinoline by hydrogen peroxide. *Journal of Environmental Engineering*, 124, 31-38.

Velichkova, F., Julcour-Lebigue, C., Koumanova, B., Delmas, H., 2013. Heterogeneous Fenton oxidation of paracetamol using iron oxide (nano)particles. *Journal of Environmental Chemical Engineering*, 1, 1214-1222.

Vieno, N., 2007. Occurrence of Pharmaceuticals in Finnish Sewage Treatment Plants, Surface Waters and Their Elimination in Drinking Water Treatment Processes. PhD Thesis, Tampere University of Technology.

Vieno, N., Tuhkanen, T., Kronberg, L., 2006. Removal of pharmaceuticals in drinking water treatment: effect of chemical coagulation. *Environmental Technology*, 27, 183-192.

Vieno, N.M., Härkki, H., Tuhkanen, T., Kronberg, L., 2007. Occurrence of pharmaceuticals in river water and their elimination in a pilot-scale drinking water treatment plant. *Environmental Science and Technology*, 41, 5077-5084.

Vieno, N.M., Tuhkanen, T., Kronberg, L., 2005. Seasonal variation in the occurrence of pharmaceuticals in effluents from a sewage treatment plant and in the recipient water seasonal variation in the occurrence of pharmaceuticals in effluents from a sewage treatment plant and in the recipient water. *Environmental Science and Technology*, 39, 8220-8226.

Vijayan, B.K., Dimitrijevic, N.M., Wu, J., Gray, K.A., 2010. The effects of Pt doping on the structure and visible light photoactivity of titania nanotubes. *The Journal of Physical Chemistry C*, 114, 21262-21269.

Villaroel, E., Silva-agredo, J., Petrier, C., Taborda, G., Torres-palma, R.A., 2014. Ultrasonic degradation of acetaminophen in water : Effect of sonochemical parameters and water matrix. *Ultrasonics Sonochemistry*, 21, 1763-1769.

Vittenet, J., Aboussaoud, W., Mendret, J., Pic, J.-S., Debellefontaine, H., Lesage, N., Faucher, K., Manero, M.-H., Thibault-Starzyk, F., Leclerc, H., Galarneau, A., Brosillon, S., 2014. Catalytic ozonation with γ -Al₂O₃ to enhance the degradation of refractory organics in water. *Applied Catalysis A General*, 1-14.

Vogna, D., Marotta, R., Napolitano, A., Andreozzi, R., 2004. Advanced oxidation of the pharmaceutical drug diclofenac with UV/H₂O₂ and ozone. *Water Research*, 38, 414-422.

von Gunten, U., 2003. Ozonation of drinking water: part I. Oxidation kinetics and product formation. *Water Research*, 37, 1443-1467.

Wadley, S., Waite, T., 2004. Fenton Process, in: Parsons, S. (Ed.), *Advanced Oxidation Processes for Water and Wastewater Treatment*, 111-136, IWA Publishing, London, UK,

Wang, J., Jiang, Z., Zhang, L., Kang, P., Xie, Y., Lv, Y., Xu, R., Zhang, X., 2009. Sonocatalytic degradation of some dyestuffs and comparison of catalytic activities of nano-sized TiO₂, nano-sized ZnO and composite TiO₂/ZnO powders under ultrasonic irradiation. *Ultrasonics Sonochemistry*, 16, 225-231.

Wang, X., Wang, L., Li, J., Qiu, J., Cai, C., Zhang, H., 2014. Degradation of Acid Orange 7 by persulfate activated with zero valent iron in the presence of ultrasonic irradiation. *Separation and Purification Technology*, 122, 41-46.

Wang, Y., Zhao, D.A.N., Ma, W., Chen, C., Zhao, J., 2008. Enhanced sonocatalytic degradation of azo dyes by Au/TiO₂. *Environmental Science and Technology*, 42, 6173-6178.

Watlington, K., 2005. *Emerging Nanotechnologies for Site Remediation and Wastewater Treatment*, Office of Solid Waste and Technology Innovation Technology Innovation and Field Services Division, U.S. Environmental Protection Agency, Washington, DC, USA.

Wayment, D.G., 1997. *Variable Frequency Sonochemistry*. PhD Thesis, Texas Technical University.

Weavers, L.K., 2001. Sonolytic Ozonation for the Remediation of Hazardous Pollutants. In Mason, T.J., Tiehm, A. (Eds.), *Advances in Sonochemistry: Ultrasound in Environmental Protection*, 111-137, JAI Press Inc., Elsevier Science B.V., Connecticut, USA.

Weavers, L.K., Hoffmann, M.R., 1998. Sonolytic decomposition of ozone in aqueous solution: mass transfer effects. *Environmental Science and Technology*, 32, 3941-3947.

Weavers, L.K., Ling, F.H., Hoffmann, M.R., 1998. Aromatic compound degradation in water using a combination of sonolysis and ozonolysis. *Environmental Science and Technology*, 32, 2727–2733.

Wei, L., Yi-zhong, W., 2004. Photodegradation mechanism of two dyes: The influence of adsorption behavior on the novel TiO₂ particles. *Journal of Environmental Sciences*, 16, 328-331.

Werner, J.J., McNeill, K., Arnold, W.A, 2005. Environmental photodegradation of mefenamic acid. *Chemosphere*, 58, 1339-1346.

Westerhoff, P., Yoon, Y., Snyder, S., Wert, E., 2005. Fate of endocrine-disruptor, pharmaceutical, and personal care product chemicals during simulated drinking water treatment processes. *Environmental Science and Technology*, 39, 6649-6663.

WILLIAM S., J., ROGIER, E.K., ACKERM, J., 1956. Steroid total synthesis-hydrochrysene approach. VI. catalytic hydrogenation of the aromatic nucleus. Synthesis of dl-3 β -acetoxy-14-iso-etioallohomobilianic acid. *Journal of American Chemical Society*, 78, 6322-6331.

Wold, A., 1993. Photocatalytic properties of TiO₂. *Chemistry of Materials*, 5, 280-283.

Xu, A.-W., Gao, Y., Liu, H.-Q., 2002. The preparation, characterization, and their photocatalytic activities of rare-earth-doped TiO₂ nanoparticles. *Journal of Catalysis*, 207, 151-157.

Xu, L.J., Chu, W., Graham, N., 2013. Sonophotolytic degradation of dimethyl phthalate without catalyst: Analysis of the synergistic effect and modeling. *Water Research*, 47, 1996-2004.

Xu, Z., Ma, C.Y., Xu, J.Y., Liu, X.J., 2009. Dynamical properties of iodine release in potassium iodide solution under combination of ultrasound and light irradiations. *Ultrasonics Sonochemistry*, 16, 475-480.

Xue, X., Hanna, K., Deng, N., 2009a. Fenton-like oxidation of Rhodamine B in the presence of two types of iron (II, III) oxide. *Journal of Hazardous Materials*, 166, 407-414.

Xue, X., Hanna, K., Despas, C., Wu, F., Deng, N., 2009b. Effect of chelating agent on the oxidation rate of PCP in the magnetite/H₂O₂ system at neutral pH. *Journal of Molecular Catalysis A: Chemical*, 311, 29-35.

Yang, L., Hu, C., Nie, Y., Qu, J., 2010. Surface acidity and reactivity of β -FeOOH/Al₂O₃ for pharmaceuticals degradation with ozone: In situ ATR-FTIR studies. *Applied Catalysis B: Environmental*, 97, 340-346.

Yang, L., Yu, L.E., Ray, M.B., 2009. Photocatalytic oxidation of paracetamol: dominant reactants, intermediates, and reaction mechanisms. *Environmental Science and Technology*, 43, 460-465.

Yang, L., Yu, L.E., Ray, M.B., 2008a. Degradation of paracetamol in aqueous solutions by TiO₂ photocatalysis. *Water Research*, 42, 3480-3488.

Yang, L., Yu, L.E., Ray, M.B., 2008b. Degradation of paracetamol in aqueous solutions by TiO₂ photocatalysis. *Water Research*, 42, 3480-3488.

Yang, S., He, H., Wu, D., Chen, D., Liang, X., Qin, Z., Fan, M., Zhu, J., Yuan, P., 2009. Decolorization of methylene blue by heterogeneous Fenton reaction using Fe_{3-x}Ti_xO₄ (0 ≤ x ≤ 0.78) at neutral pH values. *Applied Catalysis B: Environmental*, 89, 527-535.

Yi, H., Peng, T., Ke, D., Ke, D., Zan, L., Yan, C., 2008. Photocatalytic H₂ production from methanol aqueous solution over titania nanoparticles with mesostructures. *International Journal of Hydrogen Energy*, 33, 672-678.

Zhang, G., Zhang, P., Wang, B., Liu, H., 2006. Ultrasonic frequency effects on the removal of *Microcystis aeruginosa*. *Ultrasonic Sonochemistry*, 13, 446-450.

Zhang, X., Wu, F., Wu, X., Chen, P., Deng, N., 2008. Photodegradation of acetaminophen in TiO_2 suspended solution. *Journal of Hazardous Materials*, 157, 300-307.

Zhang, Y., Geissen, S.-U., Gal, C., 2008. Carbamazepine and diclofenac: removal in wastewater treatment plants and occurrence in water bodies. *Chemosphere*, 73, 1151-1161.

Zhou, D., Ding, L., Cui, H., An, H., Zhai, J., Li, Q., 2013. Fabrication of Pd/ TiO_2 -multiwall carbon nanotubes catalyst and investigation of its electrocatalytic activity for formic acid oxidation. *Journal of Power Sources*, 222, 510-517.

Zhou, T., Li, Y., Wong, F.S., Lu, X., 2008. Enhanced degradation of 2,4-dichlorophenol by ultrasound in a new Fenton like system (Fe/EDTA) at ambient circumstance. *Ultrasonics Sonochemistry*, 15, 782-790.

Ziylan-Yavas, A., Ince, N.H., 2016. Enhanced photo-degradation of paracetamol on n-platinum-loaded TiO_2 : The effect of ultrasound and OH/hole scavengers. *Chemosphere*, 162, 324-332.

Ziylan-Yavas, A., Mizukoshi, Y., Maeda, Y., Ince, N.H., 2015. Supporting of pristine TiO_2 with noble metals to enhance the oxidation and mineralization of paracetamol by sonolysis and sonophotolysis. *Applied Catalysis B: Environmental*, 172-173, 7-17.

Ziylan, A., Ince, N., 2013. Ozonation-based advanced oxidation for pre-treatment of water with residuals of anti-inflammatory medication. *Chemical Engineering Journal*, 220, 151-160.

Ziylan, A., Ince, N.H., 2014. Catalytic ozonation of ibuprofen with ultrasound and Fe-based catalysts. *Catalysis Today*, 240, 2-8.

Ziylan, A., Ince, N.H., 2013. Ozonation-based advanced oxidation for pre-treatment of water with residuals of anti-inflammatory medication. *Chemical Engineering Journal*, 220, 151-160.

Ziylan, A., Ince, N.H., 2011. The occurrence and fate of anti-inflammatory and analgesic pharmaceuticals in sewage and fresh water: treatability by conventional and non-conventional processes. *Journal of Hazardous Materials*, 187, 24-36.

Ziylan, A., Koltypin, Y., Gedanken, A., Ince, N.H., 2013. More on sonolytic and sonocatalytic decomposition of Diclofenac using zero-valent iron. *Ultrasonics Sonochemistry*, 20, 580-586.

Zwiener, C., Frimmel, F.H., 2000. Oxidative treatment of pharmaceuticals in water. *Water Research*, 34, 6, 1881-1885.

APPENDIX A: Supporting of pristine TiO_2 with noble metals to enhance the oxidation and mineralization of paracetamol by sonolysis and sonophotolysis

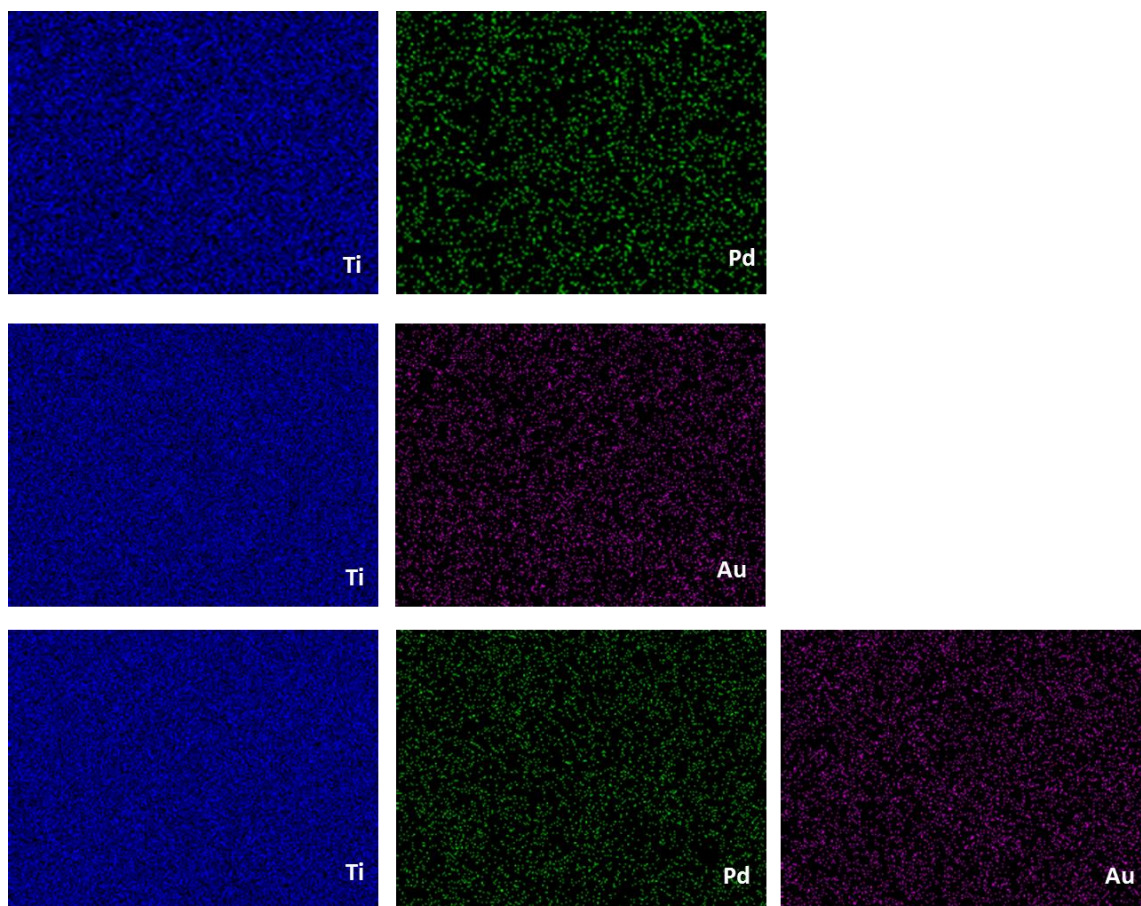


Figure A9.1 ESEM/EDX mapping of the elements (Pd, Au, Ti) in the composites of Pd-TiO₂, Au-TiO₂, Pd/Au-TiO₂.

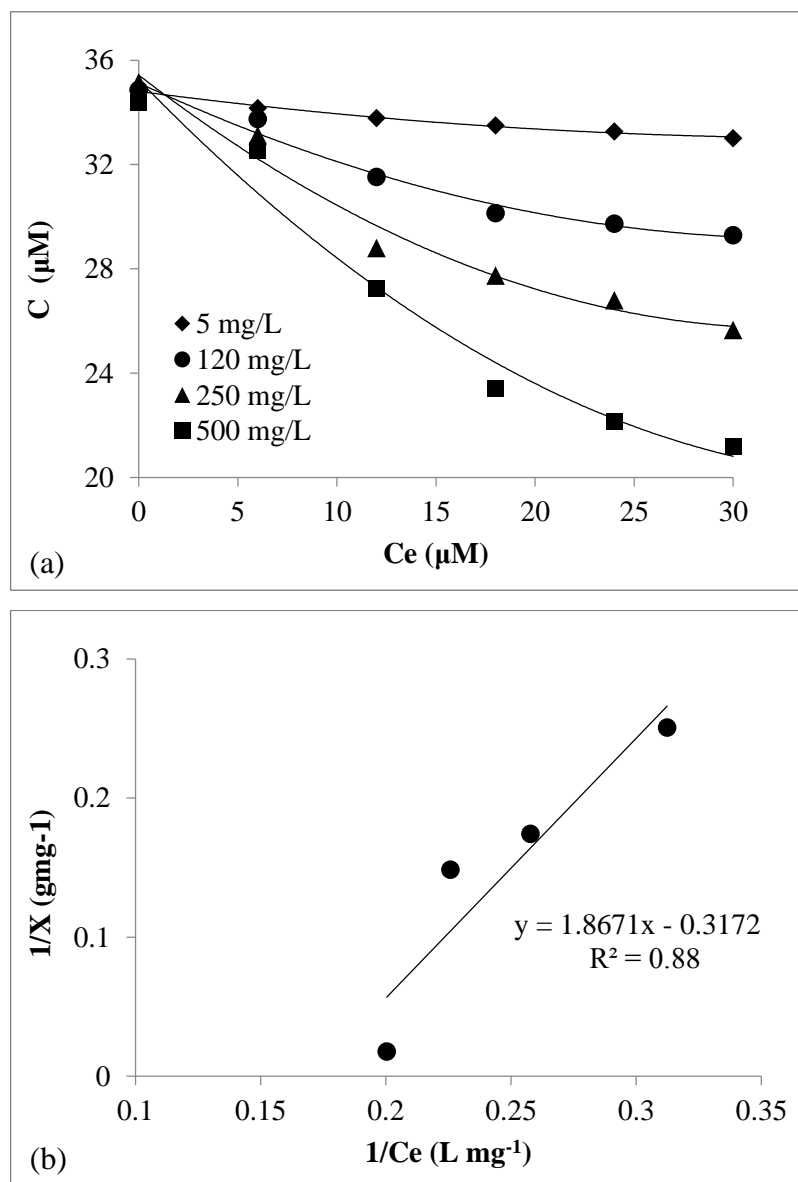


Figure A9.2. The adsorption of PCT ($C_0=35 \mu\text{M}$) on Pd-TiO₂ at varying concentrations of the catalyst during 6-h contact (a) and estimation of the Langmuir isotherm parameters (b).

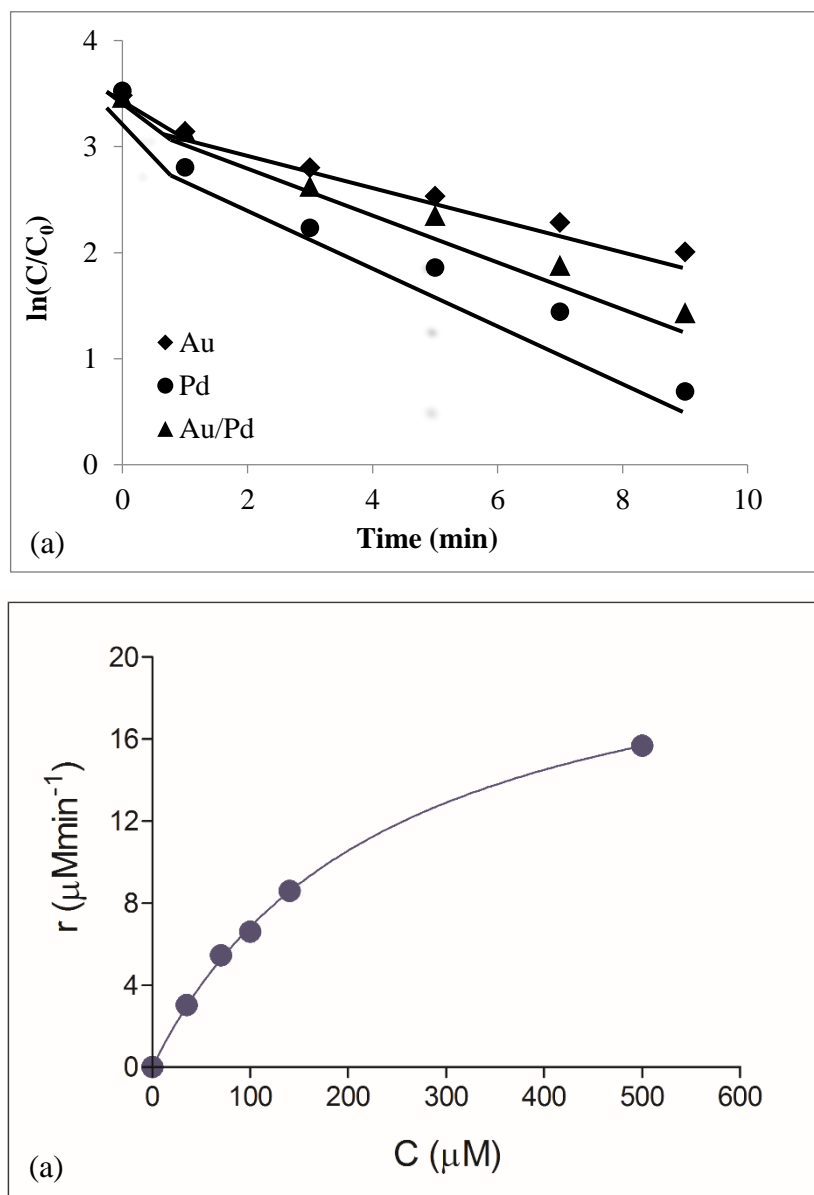


Figure A9.3. Deviation of PCT decay rate from pseudo-first order law during 10-min reaction of the compound in the presence of ultrasound and TiO_2 nanocomposites (initial conditions were $\text{TiO}_2 = 5 \text{ mg L}^{-1}$, $\text{PCT} = 35 \text{ }\mu\text{M}$, $\text{pH} = 6.5$ (a); the fit of Langmuir-Hinshelwood model to the observed rate data (estimated model parameters were: $r = 23.10 \text{ }\mu\text{M min}^{-1}$; $k_i = 0.19 \text{ min}^{-1}$; $K = 237.6 \text{ }\mu\text{M}$ (b)).

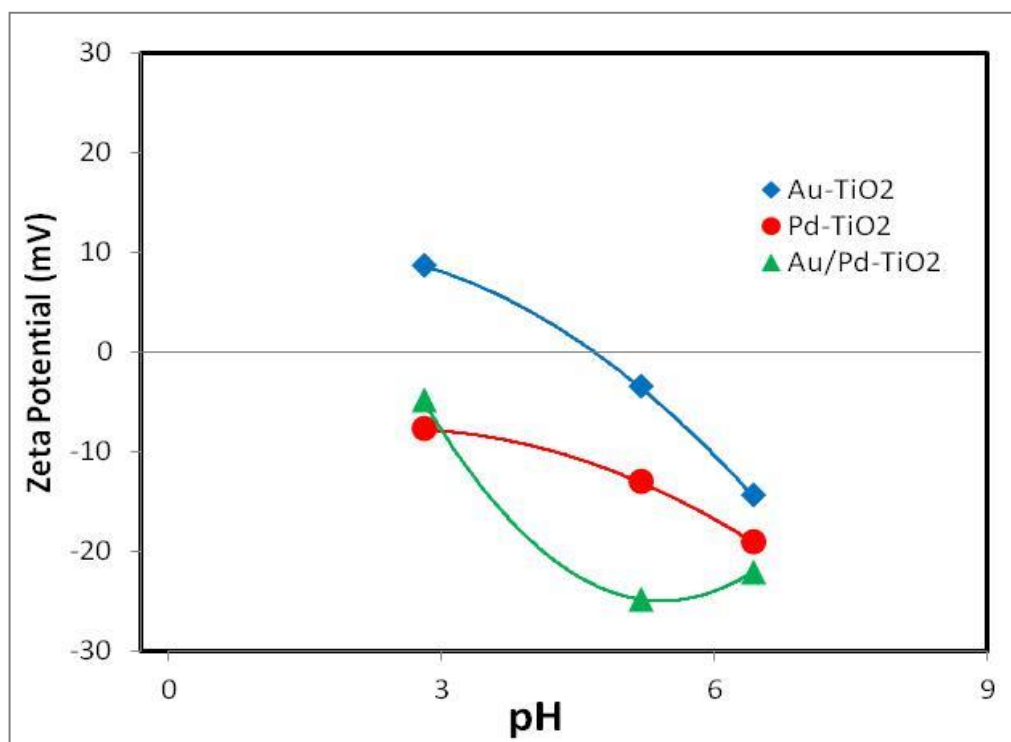


Figure A9.4. Variation of zeta potential of the nanocomposites with pH.

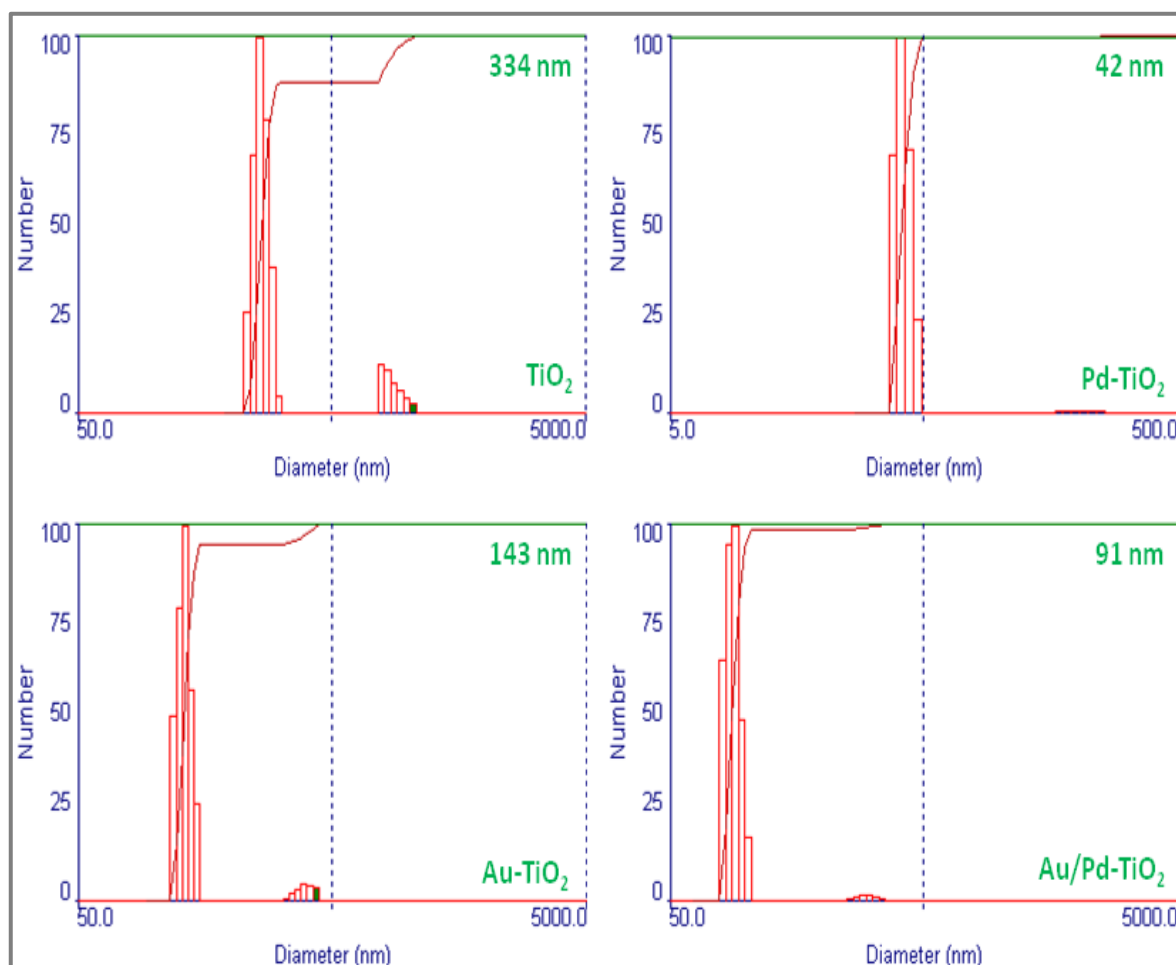


Figure A9.5. Hydrodynamic size and particle size distribution of solids in water (catalyst concentration = $0.0625 \text{ mg mL}^{-1}$).

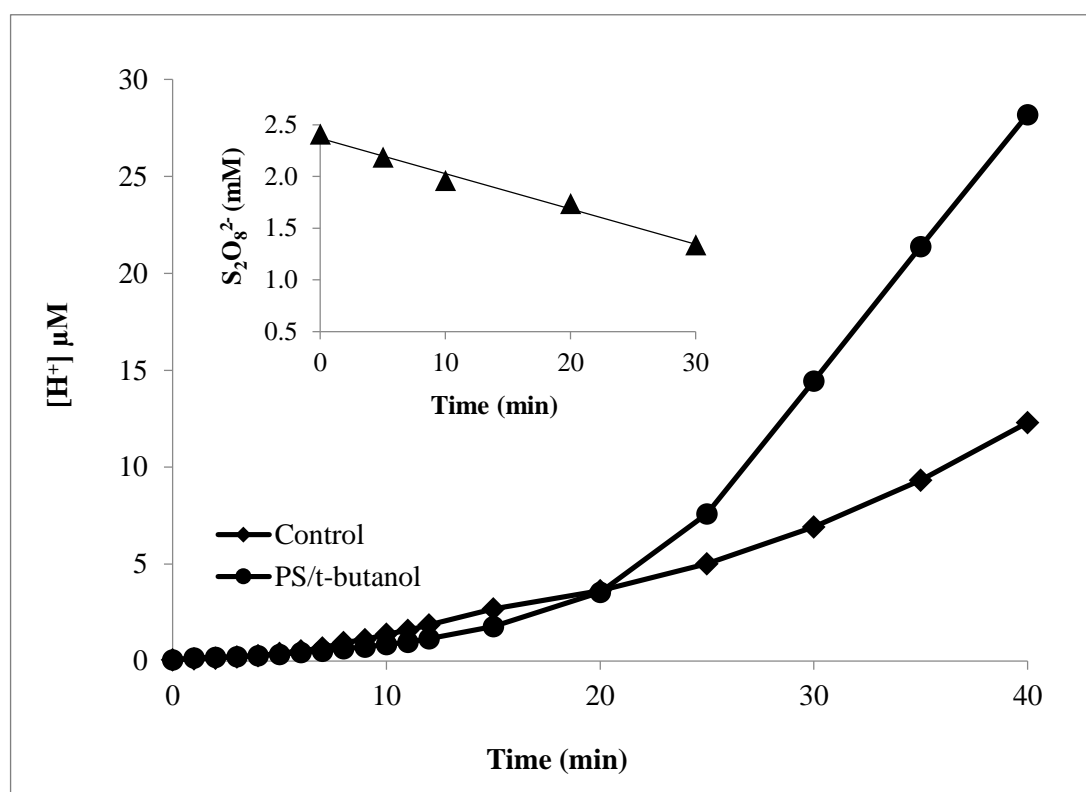


Figure A9.6. Evolution of H^+ during sonication of 2.5 mM $S_2O_8^{2-}$ (PS) in the presence of 2.5 mM t-butanol. “Control” refers to US and t-butanol only (no $S_2O_8^{2-}$). The inset shows the decay of PS ($C_0=2.5$ mM) during sonication of the reagent in the absence of t-butanol.

Table A9.1. Percent reduction in pH and TOC after 60-min reaction of PCT ($C_0=35$ μM , $pH_i=6.5$, $C_{cat}=5$ mgL^{-1}) under sonolysis, photolysis, sono-photolysis and sono-persulfate process.

Catalyst	Sonolysis		Photolysis		Sonophotolysis		Sono/persulfate	
	pH	TOC	pH	TOC	pH	TOC	pH	TOC
P-25	34.77	15.34	18.00	14.18	37.40	26.41	39.11	44.93
Au-	47.85	25.50	33.95	23.58	49.92	56.79	61.07	43.62
Pd-	49.07	37.19	35.43	27.32	51.31	58.74	50.69	52.37
Pd/Au-	47.71	44.51	31.38	16.53	46.40	61.02	58.15	47.24

APPENDIX B: Enhanced photo-degradation of paracetamol on n-platinum-modified TiO₂: the effect of ultrasound and •OH/hole scavengers

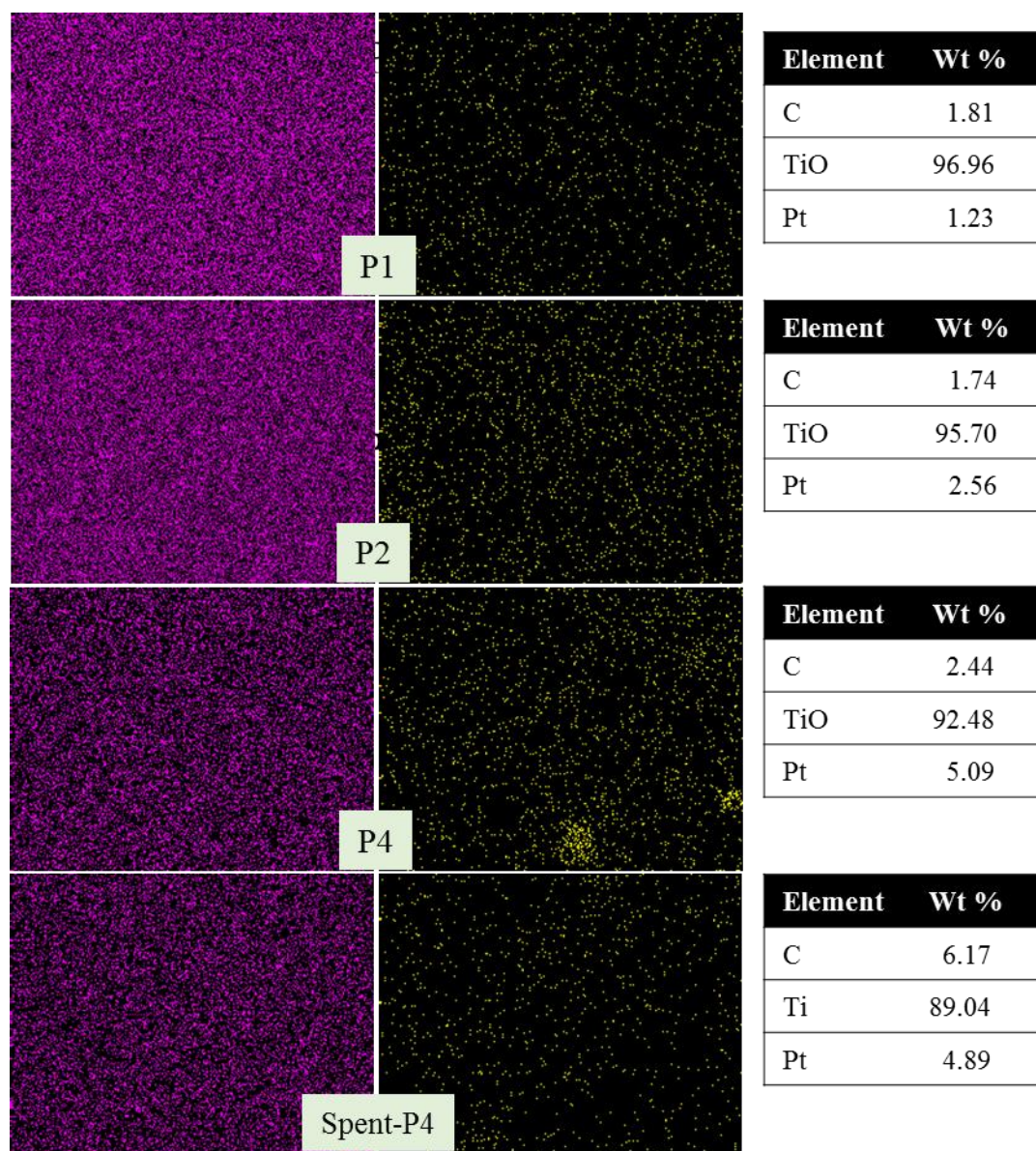


Figure B10.1. ESEM/EDX mapping of the elements in the composites of Pt-TiO₂ and weight distribution.

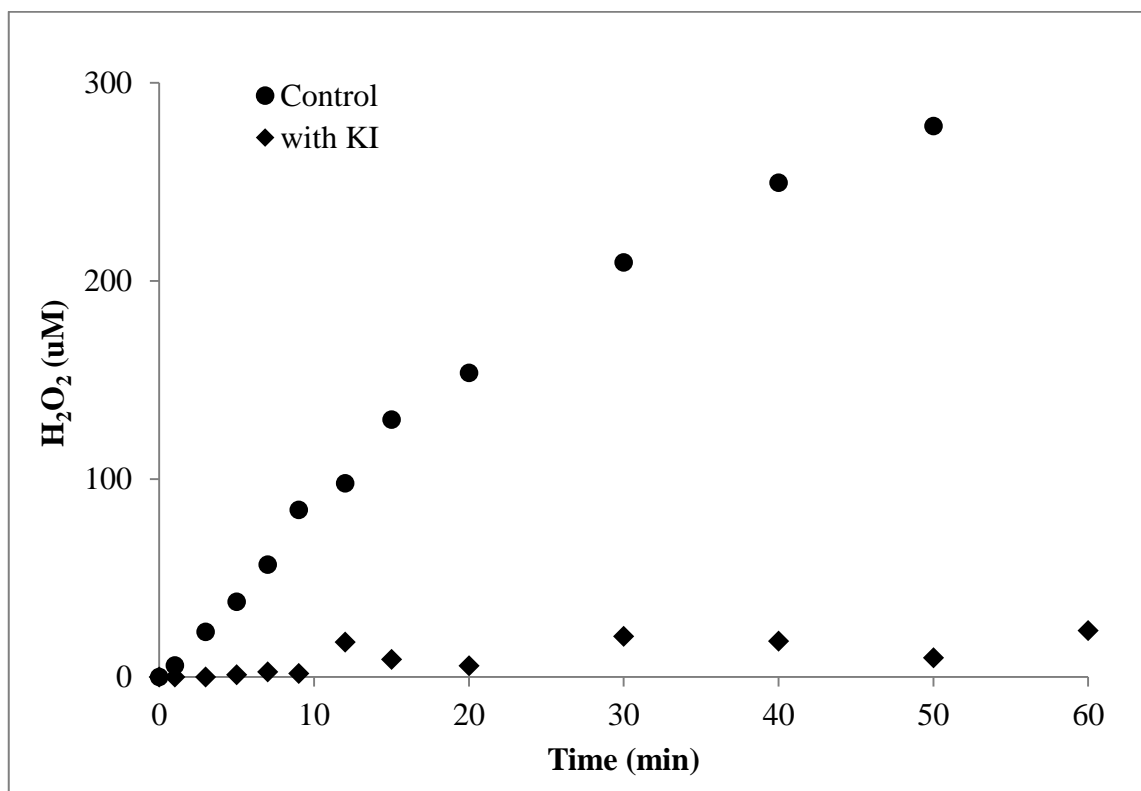


Figure B10.1. H_2O_2 generation by sonolysis of water in the presence and absence of KI.